O3M SAF VALIDATION REPORT

Validated products:

Identifier	Name	Acronym
O3M-02 O3M-50	Near-Real-Time Total NO_2 from GOME-2A&B	MAG-N-NO2 MBG-N-NO2
O3M-07 O3M-51	Offline Total NO_2 from GOME-2A&B	MAG-O-NO2 MBG-O-NO2
O3M-114	Reprocessed Total NO_2 from GOME-2A&B	MxG-RP1-NO2
O3M-36 O3M-52	Near-Real-Time Tropospheric NO_2 From GOME-2A&B	MAG-N-NO2TR MBG-N- NO2TR
O3M-37 O3M-53	Offline Tropospheric NO_2 from GOME-2A&B	MAG-O-NO2TR MBG-O-NO2TR
O3M-123	Reprocessed Tropospheric NO_2 from GOME-2A&B	MxG-RP1-NO2TR

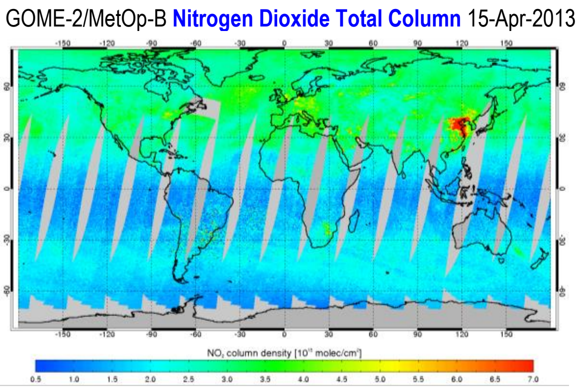

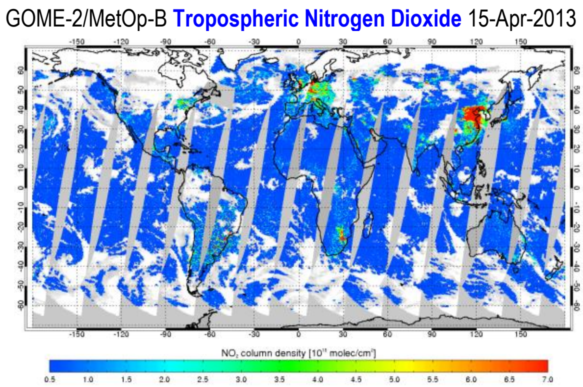

Authors:

Name	Institute
Gaia Pinardi	Belgian Institute for Space Aeronomy
Jean-Christopher Lambert	Belgian Institute for Space Aeronomy
Huan Yu	Belgian Institute for Space Aeronomy
Isabelle De Smedt	Belgian Institute for Space Aeronomy
José Granville	Belgian Institute for Space Aeronomy
Michel Van Roozendael	Belgian Institute for Space Aeronomy
Pieter Valks	German Aerospace Center

Reporting period: for GOME-2/MetOp-A, January 2007 – July 2015

for GOME-2/MetOp-B, January 2013 – July 2015

Input data versions: GOME-2 Level 1B version 5.3.0 until 17 June 2014

GOME-2 Level 1B version 6.0.0 since 17 June 2014

Data processor versions: GDP 4.8, UPAS version 1.3.9

authors / *auteurs*	G. Pinardi, J.-C. Lambert, J. Granville, H. Yu, I. De Smedt, M. van Roozendael, and P. Valks
edited by / *édité par*	G. Pinardi, BIRA-IASB, Brussels, Belgium
reference / *référence*	SAF/O3M/IASB/VR/NO2/TN-IASB-GOME2-O3MSAF-NO2-2015
document type / *type de document*	O3M-SAF Validation Report
issue / *edition*	1
revision / *revision*	0
date of issue / *date d'édition*	29 October 2015
products / *produits*	MAG-N-NO2, MBG-N-NO2, MAG-O-NO2, MBG-O-NO2, MxG-RP1-NO2, MAG-N-NO2TR, MBG-N-NO2TR, MAG-O-NO2TR, MBG-O-NO2TR, MXG-RP1-NO2TR
identifier / *identificateur*	O3M-02, O3M-50, O3M-07, O3M-51, O3M-114, O3M-36, O3M-52, O3M-37, O3M-53, O3M-123
product version / *version des données*	level-0-to-1 v5.3, and 6.0; level-1-to-2 GDP v4.8

distribution / *distribution*

Function	***Organisation***
O3M-SAF	EUMETSAT, BIRA-IASB, DLR, DMI, DWD, FMI, HNMS/AUTH, KNMI, LATMOS, RMI
GOME Team	DLR, ESA/ESRIN, BIRA-IASB, RTS, various
UPAS Team	DLR-IMF, DLR-DFD
NDACC UVVIS Working Group	BAS-NERC, BIRA-IASB, CAO, CNRS/IPSL/LATMOS, DMI, FMI-ARC, IFE/IUP, INTA, IPMet/UNESP, KSNU, NIWA, U. Manchester, U. Réunion/LACy, U. Wales

external contributors / *contributions externes au SAF*

NDACC teams contributing ground-based correlative measurements

Acronym	*Organisation*	*Country*
BAS-NERC	British Antarctic Survey – National Environment Research Council	United Kingdom
BIRA-IASB	Belgian Institute for Space Aeronomy	Belgium
CAO	Central Aerological Observatory	Russia
CNRS/LATMOS	CNRS / Laboratoire Atmosphère, Milieux, Observations Spatiales	France
DMI	Danish Meteorological Institute	Denmark
FMI-ARC	Finnish Meteorological Institute – Arctic Research Centre	Finland
IFE/IUP	Institut für Umweltphysik/Fernerkundung, University of Bremen	Germany
INTA	Instituto Nacional de Técnica Aeroespacial	Spain
IPMet/UNESP	Instituto de Pesquisas Meteorológicas, Universidade Estadual Paulista	Brazil
KSNU	Geophysical Laboratory, Kyrgyz State National University	Kyrgyzstan
NIWA	National Institute of Water and Atmospheric Research	New Zealand
U. Manchester	University of Manchester and University of Wales	United Kingdom
U. Réunion/LACY	Université de la Réunion	France

other teams contributing ground-based correlative measurements

Acronym	*Organisation*	*Country*
BIRA-IASB	Belgian Institute for Space Aeronomy	Belgium
AUTH	Aristotle University of Thessaloniki	Greece
JAMSTEC	Research Institute for Global Change	Japan
Chiba University	Center for Environmental Remote Sensing	Japan
IUP-Bremen	Institut für Umweltphysik	Germany
IUP-Heidelberg	Institut für Umweltphysik	Germany
MPIC-Mainz	Max Planck Institute for Chemistry	Germany
TU-Delft	Department of Geosciences & Remote Sensing	The Netherlands
KNMI	Royal Netherlands Meteorological Institute	The Netherlands
DLR	German Aerospace Center	Germany
LuftBlick	LuftBlick, Kreith	Austria
U. of Innsbruck	Institute of Meteorology and Geophysics	Austria
U. of Maryland	Joint Center for Earth Systems Technology, Baltimore	USA
DWD	German Weather Service, Hohenpeissenberg	Germany
FMI	Finnish Meteorological Institute	Finland
GIST	Gwangju Institute of Science and Technology	Korea
IAP/RAS	Institute of Atmospheric Physics, Russian Academy of Sciences	Russia
CAMS	Chinese Academy of Meteorological Sciences	China
NASA	NASA/Goddard Space Flight Center, GSFC	USA

document change record / *historique du document*

Issue	*Rev.*	*Date*	*Section*	*Description of Change*
1	0	11.08.2015	all	Creation of this document
1	1	30.11.2015		Small changes after ORR RIDs

Validation report of NRT, offline and reprocessed GOME-2 GDP 4.8 NO_2 column data for MetOp-A and -B Operational Readiness Review

CONTENTS

ACRONYMS AND ABBREVIATIONS

AMF	Air Mass Factor, or optical enhancement factor
BIRA-IASB	Belgian Institute for Space Aeronomy
CNRS/LATMOS	Laboratoire Atmosphère, Milieux, Observations Spatiales du CNRS
DLR	German Aerospace Centre
DOAS	Differential Optical Absorption Spectroscopy
Envisat	Environmental Satellite
ESA	European Space Agency
EUMETSAT	European Organisation for the Exploitation of Meteorological Satellites
FMI-ARC	Finnish Meteorological Institute – Arctic Research Centre
GDOAS/SDOAS	GOME/SCIAMACHY WinDOAS prototype processor
GDP	GOME Data Processor
GOME	Global Ozone Monitoring Experiment
IASB	Institut d’Aéronomie Spatiale de Belgique
IFE/IUP	Institut für Fernerkundung/Institut für Umweltphysik
IMF	Remote Sensing Technology Institute
LOS	Line Of Sight
NDACC	Network for the Detection of Atmospheric Composition Change
NDSC	Network for the Detection of Stratospheric Change
NO_2	nitrogen dioxide
O_3	ozone
O3M-SAF	Ozone and Atmospheric Chemistry Monitoring Satellite Application Facility
OCRA	Optical Cloud Recognition Algorithm
OMI	Ozone Monitoring Instrument
ROCINN	Retrieval of Cloud Information using Neural Networks
RRS	Rotational Raman Scattering
RTS	RT Solutions Inc.
SAOZ	Système d’Analyse par Observation Zénithale
SCD	Slant Column Density
SCIAMACHY	Scanning Imaging Absorption spectroMeter for Atmospheric CHartography
SNR	Signal to Noise Ratio
STS	Stratosphere Troposphere Separation
SZA	Solar Zenith Angle
TEMIS	Tropospheric Emission Monitoring Internet Service
UPAS	Universal Processor for UV/VIS Atmospheric Spectrometers
UVVIS	ground-based DOAS ultraviolet-visible spectrometer
VCD	Vertical Column Density

DATA DISCLAIMER

In the framework of EUMETSAT's Satellite Application Facility on Ozone and Atmospheric Chemistry Monitoring (O3M-SAF), nitrogen dioxide (NO_2) total column and tropospheric column data products, as well as associated cloud parameters, are generated at DLR from MetOp-A and B GOME-2 measurements using the UPAS level-1-to-2 GDP 4.8 DOAS retrieval processor (see [ATBD] and [PUM]). BIRA-IASB, DLR and RMI ensure detailed quality assessment of algorithm upgrades and continuous monitoring of GOME-2 NO_2 data quality with a recurring geophysical validation using correlative measurements from the NDACC and others MAXDOAS and DirectSun ground-based network and from other satellites, modelling support, and independent retrievals.

This report present verification and validation results of MetOp-A and -B reprocessed, off-line and NRT GOME-2 NO_2 total and tropospheric data by comparisons of GDP 4.8 data to previous GDP 4.7 results and to availables ground-based correlative data. These include (1) the verification of the consistency to GDP 4.7 GOME-2 NO_2 column retrievals, (2) the evaluation of the stratospheric contribution to the NO_2 total column against ground-based observations provided by near-real-time DOAS UV-Visible spectrometers of the NDACC network, (3) comparisons of tropospheric NO_2 column data against ground-based MAX-DOAS measurements at around 20 stations worldwide, and (4) comparisons of total NO_2 columns against Directsun instruments from the Pandora network.

In the following, the abbreviations GOME-2A and GOME-2B are used as short names for MetOp-A GOME-2 and MetOp-B GOME-2. When used alone, the terms MetOp or GOME-2 stand for MetOp-A and MetOp-B, or GOME-2A and GOME-2B.

The following main conclusions can be drawn:

- The two version of NO_2 slant columns from DOAS retrievals have a very good agreement. The standard deviation of NO_2 columns and the RMS of DOAS are very similar between two processor as well. Compared to the previous version, the GDP 4.8 NO_2 slant columns are slightly larger over south hemisphere, with slightly smaller RMS, thanks to the improvement of NO_2 cross section in the DOAS fits, and this effect is more significant for GOME-2B than GOME-2A. The difference is zonally homogeneous, with slightly larger differences found for GOME-2B results over the very polluted area of Eastern China region. This is probably linked to the different temperature of the used cross sections.
- The maps of the stratospheric SCDs difference between the two processor versions is highly consistent with the maps of the SCD differences. The systematic bias on the slant columns is almost transferred to the stratospheric vertical columns.
- GDP 4.8 tropospheric NO_2 VCD are slightly smaller than previous GDP 4.7 for most regions (significant differences can be found over East Asia, North America, and Europe). The main change in the GDP 4.8 tropospheric NO_2 retrieval is due to the cloud product, that affects the calculation of the tropospheric AMF. Cloud free AMFs are identical between GDP 4.7 and GDP 4.8, since albedo, a-prioir profiles, and surface elevation maps have not been updated. Comparing the difference between AMF_{tropo} and AMF_{clear}, we highlighted the limitations of the previous version (no significant effect on AMF due to cloud correction for GDP 4.7, the cloud algorithm was not sensitive to cloud in the nearly cloudy-free scenes). The new cloud correction (used for GDP 4.8) leads to about ±20% difference in the AMF. Positive and negative effect are found over the polluted regions over North Hemisphere, while a positive effect is found over tropical biomass burning regions, where high clouds are present (and that were not seen in GDP 4.7). A better consistency of the cloud correction effect on NO_2 retrieval is found for GDP 4.8 between GOME-2A 2013 and GOME-2B 2013.
- The stratospheric NO_2 differences (due to slant column changes) and tropospheric NO_2 differences (due to cloud correction changes) are combined and transferred to the total NO_2 GDP 4.8 columns.

- With respect to 20 NDACC ZLS-DOAS UV-visible spectrometers, the MetOp-A GOME-2A and MetOp-B GOME-2B NO_2 column data sets processed with both GDP 4.7 and GDP 4.8, offer the same level of consistency. Variations of the stratospheric NO_2 column, from day-to-day fluctuations and to the annual cycle, are captured consistently by all measurement systems.
- In most of the cases, and for both GDP 4.7 and 4.8 processors, GOME-2B reports NO_2 column values slightly lower than GOME-2A, by about 1-3·10^{14} molec.cm^{-2}, which is close to the combined uncertainty of ground-based NDACC measurements and of the comparison method.
- In most of the cases, GDP 4.8 reports NO_2 column values slightly higher than GDP 4.7, by about 1-3 10^{14} molec.cm^{-2}, which is again close to the combined uncertainty of ground-based NDACC measurements and of the comparison method.
- Over the middle latitudes of the Northern Hemisphere (Aberystwyth, Jungfraujoch, O.H.P.), at low latitude stations like Izaña (Tenerife) and Saint-Denis (Reunion Island), and at both Arctic and Antarctic stations when only twilight GOME-2 data are considered, both satellites and both processor versions offer, with respect to NDACC ZLS-DOAS data, a comparable good agreement of a few 10^{14} molec.cm^{-2} on a monthly median basis.
- Over the Southern Hemisphere both GOME-2 instruments and both GDP processor versions report lower values than NDACC ZLS-DOAS spectrometers, this systematic bias starting at the Brazilian station of Bauru (22°S), propagating at four contributing middle latitude stations in the Pacific (New Zealand, Kerguelen, Macquarie) and in Argentina (Rio Galegos), and vanishing at Antarctic stations: within combined uncertainties.
- GOME-2 GDP 4.8 data are able to measure total and tropospheric NO_2 columns and it temporal evolution very well, especially in sub-urban and remote conditions, while larger under-estimation is found with respect to ground-based MAXDOAS and DirectSun measurements performed in urban environment. This is partially inherent to the large GOME-2 pixel size (40 x 80 km^2), not representative of the local urban NO_2 pattern sampled by the ground-based instruments (sensitivity within ~10 km in the pointing direction) and partially due to the a priori NO_2 profile shape used to calculate GOME-2 AMF.
- The use of GOME-2 GDP 4.8 averaging kernels to smooth the MAXDOAS NO_2 profiles (in order to take into account the different sensitivity of the two instruments) is generally giving better comparisons results. The bias is generally improved, but not the correlation coefficient.
- Validation results for GOME-2A and B are generally very similar, with comparable mean biases (with and without smoothing the MAXDOAS profiles), even if the regression parameters can be slightly different.
- Differences in the tropopsheric NO_2 validation results due to GOME-2 GDP 4.8 version instead of GDP 4.7 are minimal in locations such as OHP, Beijing or Bujumbura and can be up to a factor 10% to 20% smaller in Xianghe and Uccle. These differences are mostly due to change in the estimation of the cloud parameters themselves, that have a strong effect on tropospheric NO_2 columns estimation. Possibles compensating errors due to the cloud correction are likely to explain the better validation results with the previous version, that are now more visible thanks to the improved cloud estimation and the more homogeneous approach between GOME-2A and B in the DOAS fit.
- Except the large differences with the MAXDOAS instruments found in urban cases (Bujumbura, Beijing, Uccle), the validation results in sub-urban conditions (Xianghe) are within the target accuracy of 30% for tropospheric NO_2. Impact of the a-priori profile shape is of about 10% around Uccle, 20% to 26% in Xianghe and Beijing and up to 35% in Bujumbura.
- Differences in the total NO_2 validation results due to GOME-2 GDP 4.8 version instead of GDP 4.7 are small (a few percents in Xianghe).

In summary, the transition to the new GDP 4.8 algorithm is recommended as it is more homogeneous between GOME-2A and B DOAS settings, and as the cloud product seems to better handle the scenes only slightly contaminated by clouds. Further improvements on surface albedo, stratospheric content estimation and model for the a-priori profile shapes for AMF calculation are recommended for a future release.

A. INTRODUCTION

A.1. Scope of this document

The present document reports on the verification and geophysical validation of reprocessed, off-line and NRT GOME-2 NO_2 total and tropospheric column data produced by the GOME Data Processor (GDP) version 4.8 operated at DLR in the framework of the EUMETSAT Satellite Application Facility on Ozone and Atmospheric Chemistry Monitoring (O3M-SAF). Based on an end-to-end validation approach, this report addresses the quality of individual components of the data processing chain, starting with DOAS spectral fitting results. The report is based on the comparisons of GDP 4.8 data to previous versions GDP 4.7, and on comparisons of GOME-2 final data products with correlative observations acquired by independent ground-based DOAS spectrometers in several geometries: zenith-sky instruments to sampel the stratosphere, MAXDOAS instruments for the troposphere and Direct-sun instruments for the total column.

A.2. Preliminary remarks

Ground-based validations rely on the early delivery of provisional data by NDACC/UVVIS network affiliates. This early delivery is the result of individual agreements arranged in the framework of the joint ESA/EUMETSAT RAO on the Calibration and Validation of EPS/MetOp data. Results relying on early-delivery data must always be considered as preliminary. Consolidated data from all ground-based stations and with official NDACC endorsement will be available via the NDACC Data Host Facility (see http://www.ndacc.org) within two years after acquisition, in accordance with NDACC Data Protocols. For tropospheric columns from MAXDOAS instruments, measurements and analysis are performed by BIRA-IASB at the OHP, Beijing, Bujumbura, Uccle and Xianghe sites, and automated analysis (with one month delay) have been developed within specific projects (NORS, QA4ECV) and this benefits to the O3M SAF validation. Since 2014 a large effort of data collection has been initiated by BIRA-IASB, collecting ad-hoc MAXDOAS andDirect-Sun data from scientific partners, and also used for the validation.

A.3. Plan of this document

After presentation of the GOME-2 Data Disclaimer for NO_2 column products, this document is divided into the following sections:

- **A.** This introduction,
- **B.** Validation protocol presenting the end-to-end method and the reference data used,
- **C.** Step by step verification: GOME-2A&B NO_2 retrievals (GDP 4.7 against GDP 4.8). Results of the verification of individual components of the DOAS analysis: slant column densities and fit residuals, stratospheric, tropospheric and total columns,
- **D.** Time-series of these parameters above several emissions regions
- **E.** The evaluation of the NO_2 columns, by comparison with correlative ground-based measurements
- **F.** Conclusions
- **G.** References

B. VALIDATION PROTOCOL

B.1. Rationale and method

Retrieval principles of GOME-2 NO_2 data are described in the Algorithm Theoretical Basis Document [ATBD] and the Product User Manual [PUM] available via the O3M-SAF web site (http://o3msaf.fmi.fi). The previous version 4.7 of the GOME Data Processor (GDP) for NO_2 is also described and illustrated for its application on Metop-A in Valks et al. (2011). The main algorithm changes compared to GDP 4.7 are described in the next section.

The NO_2 column data are retrieved from the GOME-2 Earthshine backscattered radiance and solar irradiance spectra by several modules calculating intermediate parameters: the apparent slant column density along the optical path (SCD), the fractional cover (CF) and top pressure (CTP) of clouds interfering with the measurement scene, their optical thickness (COT) and albedo (CTA), the geometrical enhancement factor (AMF) needed to convert slant into vertical columns (VCD), and the stratospheric NO_2 reference that must be subtracted from the total column to obtain the tropospheric column. Those intermediate parameters are assembled to derive the final column data products: the total and the tropospheric column data. A sketch of the different steps of the retrieval is presented in Figure B.1.

To ensure that the final product of such a complex production chain is validated meaningfully, validations cannot be limited to comparisons with correlative measurements of the final total column data. An end-to-end validation of critical individual components of the level-1-to-2 retrieval chain has been set up, e.g. to detect uncertainties affecting intermediate parameters but possibly cancelling each other in the final data product.

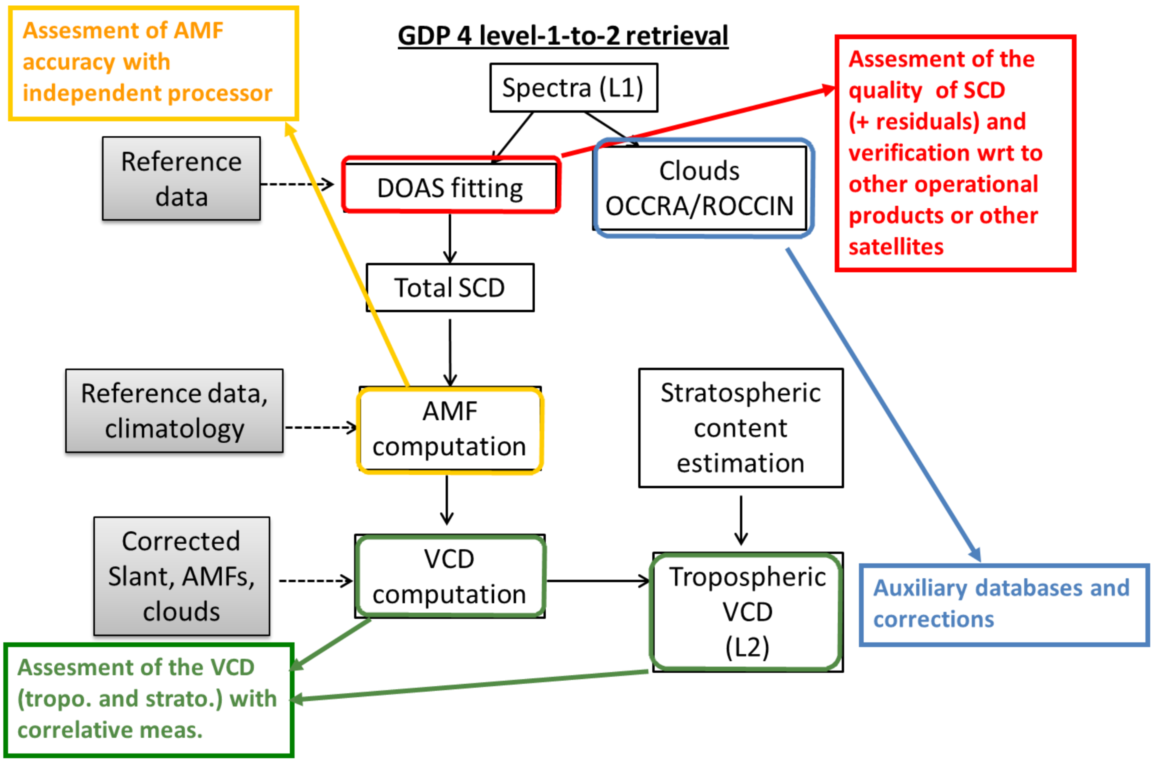

Figure B.1. Sketch of the GDP 4.8 L1 to L2 retrieval chain for total and tropospheric NO_2 VCD and the intermediary steps of the validation approach.

The end-to-end validation approach adopted in this document consists in: (a) an assessment of the quality of GOME-2 DOAS analysis results, by confrontation of GDP 4.8 and GDP 4. 7 retrievals performed respectively on GOME-2A and GOME-2B spectra, both on an orbit-to-orbit base and time-series comparisons (b) an assessment of the geophysical validity of stratospheric column measurements by comparison with stratospheric column measurements provided by zenith-sky DOAS UV-visible spectrometers affiliated with the Network for the Detection of Atmospheric Composition Change (NDACC); (c) an assessment of the validity of the GOME-2 tropospheric NO_2 column data, with respect to MAX-DOAS observations performed by BIRA-IASB and by external parteners (up to 20 stations), and (d) an assessment of the validity ot the GOME-2 total NO_2 column data by comparisons with around 20 direct-sun stations from the Pandora NASA network and a few scientific instruments.

The end-to-end approach to GOME-2 validation is detailed in the MetOp-A validation report (NO_2 O3MSAF VR 2011) and in Valks et al. (2011), where the validation protocol has been described and illustrated at the OHP pilot station. This protocol describes the reference measurements used as validation source, their quality and usability for satellite NO_2 validation, and how to handle key issues like the photochemical diurnal cycle of nitrogen oxides and the difference in sensitivity to tropospheric NO_2.

The overarching principles of the Quality Assurance Framework for Earth Observation (QA4EO), which establishes the data quality strategy for the Global Earth Observation System of Systems (GEOSS) and as such applies directly to GMES/Copernicus, are also followed:

- All data and derived products have associated with them a documented and fully traceable quality indicator (QI).
- A quality indicator shall provide sufficient information to allow all users to readily evaluate the “fitness for purpose” of the data or derived product.
- A quality indicator shall be based on a documented and quantifiable assessment of evidence demonstrating the level of traceability to internationally agreed (where possible SI) reference standards.

B.2. Data description

B.2.1. GOME-2 NO_2 retrieval: algorithm description and changes relative to GDP 4.7

The operational GDP 4.8 NO_2 retrieval algorithm for GOME-2 is fully described in the corresponding Algorithm Theoretical Basis Document [ATBD]. The previous version of this algorihm, GDP 4.7 is described in Valks et al. (2011). Details on the differences between GDP 4.7 and GDP 4.8 are summarized below in brief:

DOAS algorithms

- Improved Kurucz Solar reference spectrum (SAO2010) for wavelength calibration
- Use of consistent NO2 cross-sections for both platforms (Vandaele et al., 2002) instead of the GOME-2 FM/CATGAS cross-sections (because of quality issues with the FM NO2 cross-sections for GOME-2B).

Cloud treatment

- Using new cloud (version 3.0) algorithms:
- OCRA: PMD degradation correction + new cloud-free map based on GOME-2A data (see Lutz et al., 2015)
- ROCINN: New Tikhonov inversion + updated RTM (spectroscopy, a-priori surface albedo, etc)

Averaging Kernels

- Provision of Averaging Kernels for the tropospheric NO_2 column

Flag reporting/data selection

- In GDP 4.7, for cloud-free GOME-2 pixels (CRF < 50%) with a retrieved negative trop. NO_2 column, the VCD_{tropo} value is set to zero in the L2 product. In GDP 4.8, the negative VCD_{tropo} value is reported in the L2 product (instead of zero) and a NO_2 quality flag is set.
- For cloudy GOME-2 pixels (CRF > 50%), the trop. NO_2 column is not provided in in the GDP 4.7 (because of the large uncertainty). In the GDP 4.8, the trop. NO_2 column is provided also for cloudy pixels, and a NO_2 quality flag is set.

Table B.1 DOAS settings used for the GOME-2 NO_2 retrieval GDP 4.8.

Fitting interval	425-450 nm
Sun reference	Sun irradiance for GOME-2 L1 product
Wavelength calibration	Wavelength calibration of sun reference optimized by NLLS adjustment on convolved Chance and Spurr solar lines atlas
Absorption cross-sections	
- NO_2	Vandaele et al., 2002 at 240K
- O_3	GOME-2 FM/CATGAS cross-sections
- O_2-O_2	Greenblatt et al., 1990
- H_2O	HITRAN (Rothman et al., 2003)
- Ring effect	Additive Fraunhofer Ring spectrum

All these algorithm changes are expected to affect the NO_2 slant columns (and its coherence between the 2 platforms), the AMF calculation (via the cloud corrections) and the number of tropospheric NO_2 data, and to be transferred to all the steps of the retrievals, needing thus a detailed validation (sections C and E).

B.2.2. Correlative datasets

Zenith-sky twilight measurements from the NDACC network mostly sensitive to stratospheric NO_2, are used to assess the stratospheric contribution on the global scale (Lambert et al. 2004, Lambert 2006, Ionov et al. 2008, Celarier et al. 2008) in Section E.1.

MAXDOAS instruments are increasingly exploited to validate satellite tropospheric NO_2 columns (Brinksma et al. 2008, Celarier et al. 2008, Irie et al. 2008, Ma et al., 2013, Kanaya et al., 2014, Pinardi et al., 2014). So far, most of the studies were focusing on one or a few sites, and long time-series (several years) were very rare. In this report, we extended the number of MAXDOAS stations, from stations operated by BIRA-IASB at Observatoire de Haute Provence (background site, 44°N, 5.7°E) in South of France, Beijing and Xianghe (urban and sub-urban polluted site, 40°N, 116.3°E and 39.7°N, 117°E) in China, Uccle (sub-urban site, 50.8°N, 4.3°E) in Belgium and Bujumbura (3°E,29°E) in Burundi, central Africa, to stations operated by scientific partners all over the globe. A series of ~20 MAXDOAS datasets have been collected, in order to extend the representativeness of the ground-based stations.

Moreover, for this report, the tropospheric NO_2 columns from BIRA MAXDOAS instruments are retrieved with the optimal estimation profiling technique (Clémer et al., 2010, Hendrick et al., 2014) instead of the geometrical approximation (Brinksma et al. 2008, Pinardi et al. 2008) previously used in MetOp-A and MetOp-B report (GOME-2A validation report 2011, GOME-2B validation report 2013). This allows us to obtain low tropospheric NO_2 profiles, that can be integrated to get tropospheric VCD (and compared directly to the satellites columns, Section E.2.1), but that can also be smoothed by the satellite averaging kernels in order to take into account the difference in vertical sensitivity between the two measurements types (Section E.2.2). A few other MAXDOAS stations are retrieving profiles, as described in section E.2.

Ground-based direct-sun data from the Pandora network (hosted at NASA) have also been collected for the Pinardi et al (2014) study and an update of that dataset (~20 stations) is used in this report, to focus on the total NO_2 column comparisons (Section E.3).

C. VERIFICATION OF INDIVIDUAL COMPONENTS OF THE GOME-2 PROCESSING CHAIN: GDP 4.8 AGAINST GDP 4.7

C.1. Verification of Slant Column Density

To verify the improvements of GDP v4.8 against v4.7, the results of two processor versions are compared along a single orbit of GOME-2A in 2007 (Figure C.1) and GOME-2B in 2013 (Figure C.2). Both retrieved SCD and the DOAS fit residuals (RMS) are shown in the figures. Monthly averaged differences are displayed here as well. Figure C.3 presents two maps with the monthly averaged NO_2 slant column differences (GDP 4.7 minus GDP 4.8), from GOME-2A in February 2007 and GOME-2B in February 2013.

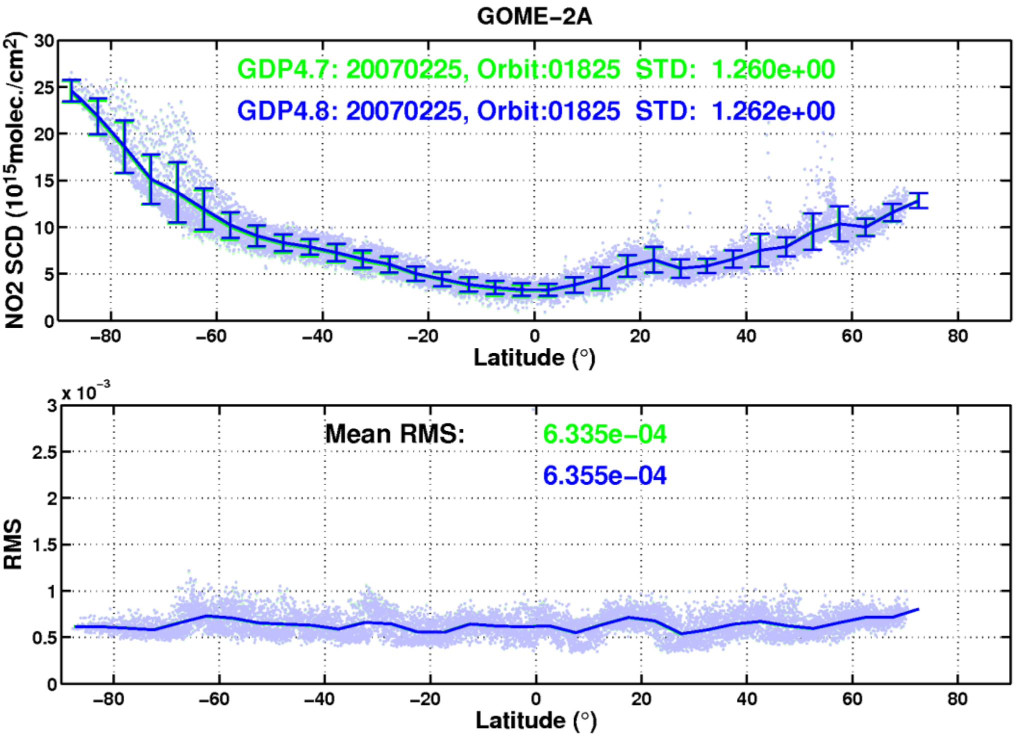

Figure C.1: GDP 4.7 (in green) vesus GDP 4.8 (in blue) NO_2 retrievals for one orbit of GOME-2 on METOP-A in 2007 (25/02/2007, orbit nb. 1825). Dots are individual measurements; lines are averages within 5° latitude-bands. First panel: slant columns and standard deviation of the slant columns within the 5° latitude-bands (STD), second panel: residuals of the fit (RMS).

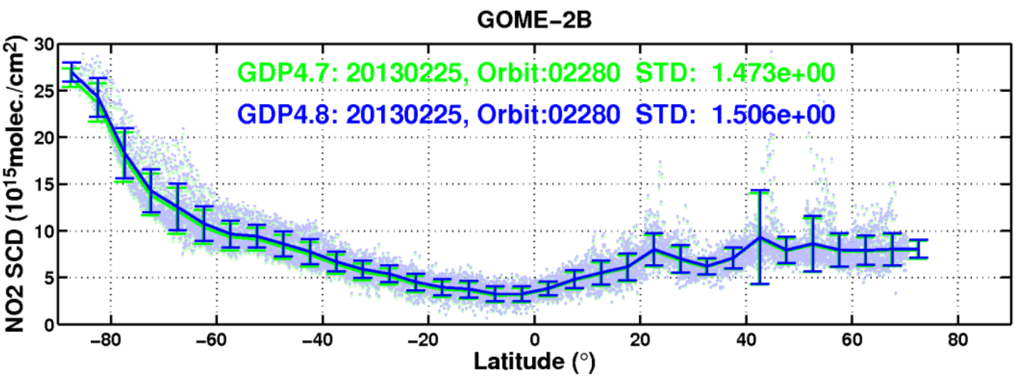

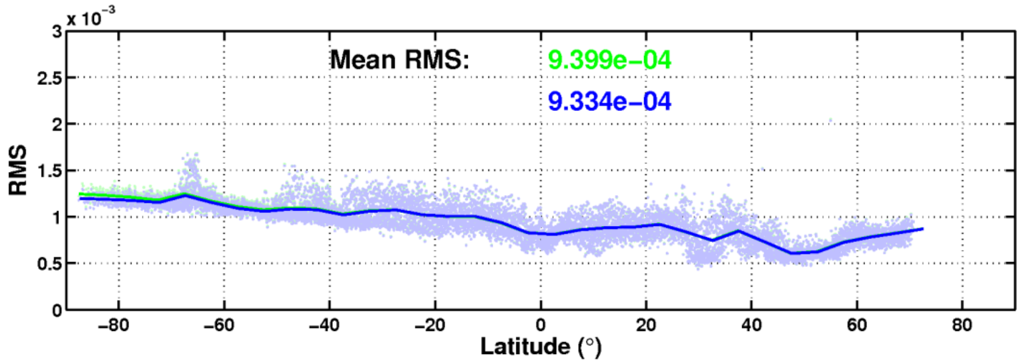

Figure C.2: GDP 4.7 (in green) vesus GDP 4.8 (in blue) NO_2 retrievals for one orbit of GOME-2 on METOP-B in 2013 (25/02/2013, orbit nb. 2280). Dots are individual measurements; lines are averages within 5° latitude-bands. First panel: slant columns and standard deviation of the slant columns within the 5° latitude-bands (STD), second panel: residuals of the fit (RMS).

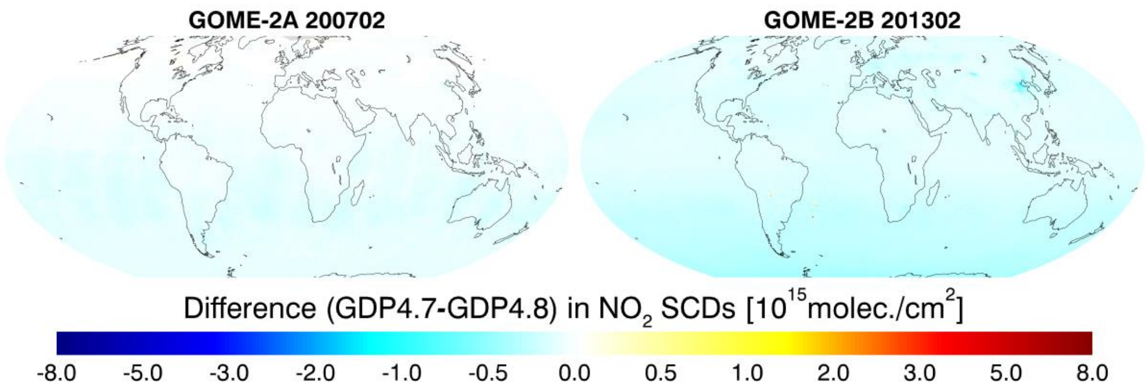

Figure C.3: Map of monthly averaged NO_2 slant column differences (GDP 4.7 minus GDP 4.8), from GOME-2A in February 2007 and GOME-2B in February 2013.

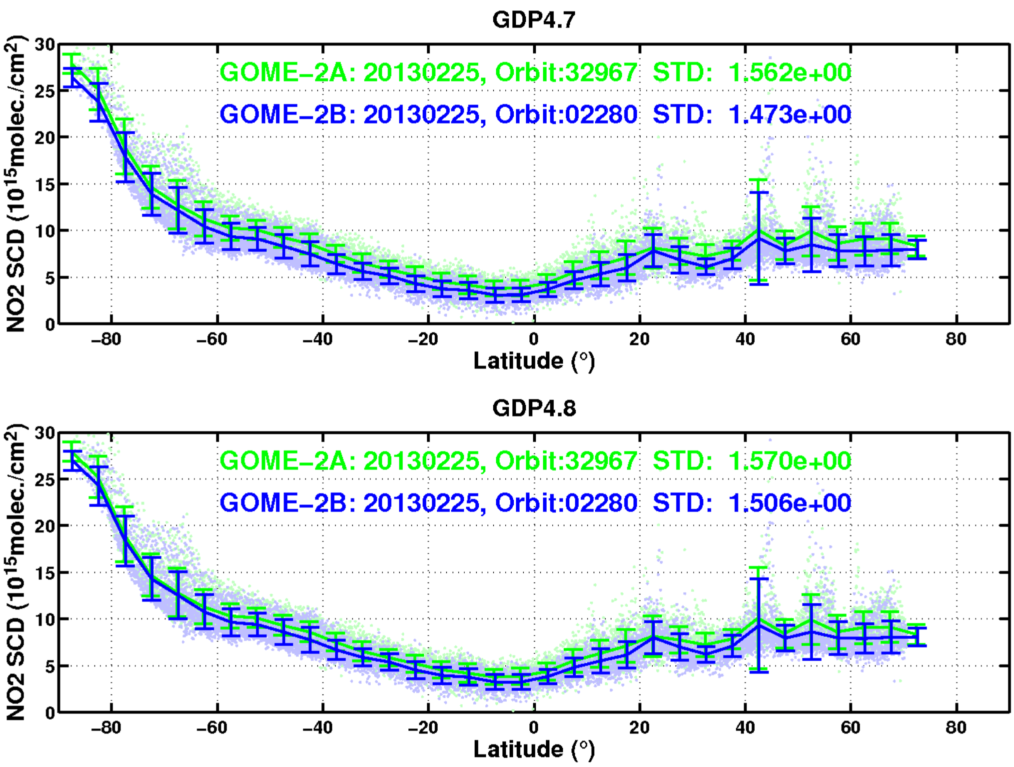

Figure C. 4: Comparison of NO_2 retrievals between one orbit of GOME-2 on METOP-A in 2013 (red, 25/02/2013, orbit nb. 32977) and METOP-B in 2013 (blue, 25/02/2013, orbit nb. 2290) for GDP4.7 (top) and GDP4.8 (bottom). Dots are individual measurements; lines are averages within 5° latitude-bands.

From inspection of Figure C.1 - 4 we conclude the following:

- The two version of NO_2 slant columns from DOAS retrievals have a very good agreement. The standard deviation of NO2 columns and the RMS of DOAS are very similar between two processor as well.
- Compared to the previous GDP 4.7 version, the GDP 4.8 NO_2 slant columns are slightly larger over the Southern Hemisphere, with slightly smaller RMS, thanks to the improvement of NO_2 cross section in the DOAS fits (see Sect. B.2.1), and this effect is more significant for GOME-2B than GOME-2A. The new version of the slant columns almost compensate the discrepancy between GDP and TEMIS product as shown in previous reports (NO_2 O3MSAF GOME-2B VR 2013).
- The maps of monthly averaged differences show results similar to those illustrated with one orbit of measurements, highlighting that the difference is zonally homogeneous, with slightly larger differences found for GOME-2B results over the very polluted area of Eastern China region. This is probably linked to the different temperature of the used cross sections (240 K for Vandaele in GDP 4.8 vs. 243 K for GOME-2 FM cross section in GDP 4.7).
- Owing to use of the consistent NO_2 cross-sections (Vandaele, 1998 at 240K), GDP4.8 shows the slightly better agreement between GOME-2A and B than GDP4.7, but the bias is still not recovered.

C.2 Verification of Stratospheric Column Density

The GDP 4.8 stratospheric columns are compared to GDP 4.7 and Figure C.5 shows one month of observations from GOME-2A (February 2007) and GOME-2B (February 2013). The difference in the residual tropospheric slant column, i.e. when the stratospheric component is subtracted from total slant column, is also presented in the Figure C.4.

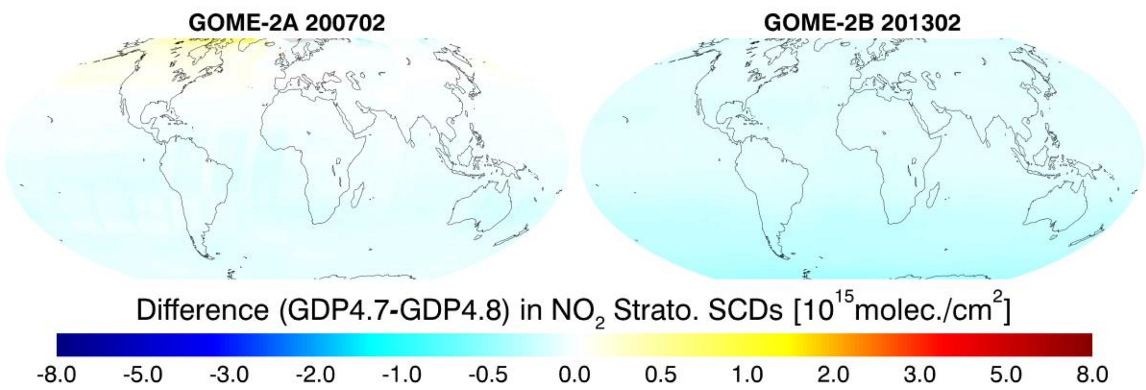

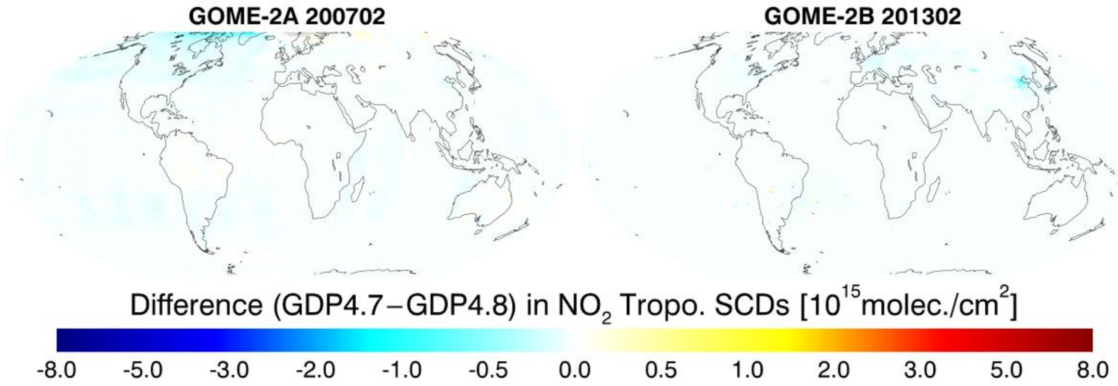

Figure C.5: Maps of monthly difference of stratospheric slant columns (top) and residual tropospheric slant columns (bottom) between GDP 4.7 and GDP 4.8 for GOME-2A in February 2007 and for GOME-2B in February 2013.

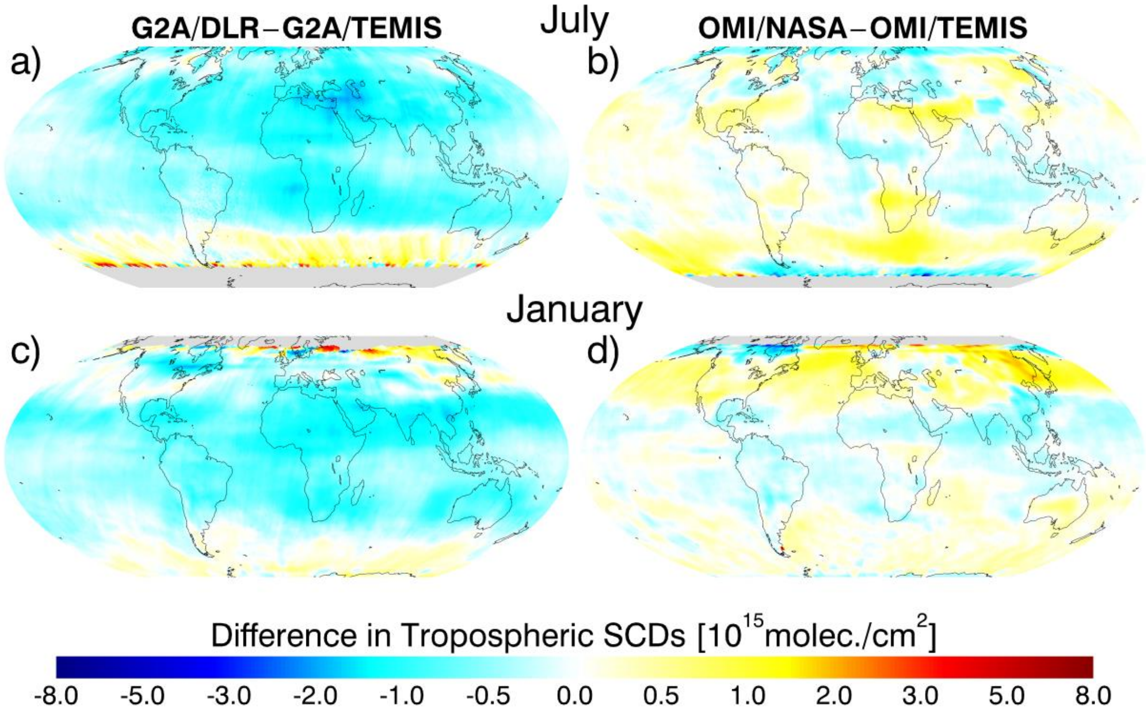

Figure C. 6: Monthly mean differences in residual tropospheric slant columns for July 2007 and January 2008. G2A/DLR: GDP4.8 NO_2 for GOME-2A; G2A/TEMIS: NO_2 retrieval from TEMIS (TM4NO2A V2.3) for GOME-2A; OMI/NASA: operational OMI NO_2 product (V2.1); OMI/TEMIS: DOMINO NO_2 product (V2.0). The stratospheric correction for two TEMIS products are based on the same approach (so-called assimilation approach).

Main conclusion on stratospheric columns:

- The maps of the difference of stratospheric SCDs between GDP 4.7 and GDP 4.8 is highly consistent with the maps of the SCD differences between the two processor versions.
- The systematic bias on the slant columns is almost transferred to the stratospheric vertical columns. The residual tropospheric slant columns between GDP 4.7 and GDP 4.8 are therefore equivalent, with only slightly lower (within $1{\cdot}10^{15}$ molec/cm²) tropospheric values for GDP 4.7 over high laititude regions for GOME-2A in February 2007 and over Eastern China for GOME-2B in February 2013.
- Compared to other independent stratospheric correction approaches, the residual tropospheric slant columns based on GDP retrieval are systematic lower ($\sim 1{\cdot}10^{15}$ molec/cm²) over most of the regions.

C.3 Verification of Tropospheric Vertical Column Density

To verify the improvements of GDP v4.8 against v4.7, the tropospheric NO_2 VCD results of the two processor versions are first compared along a single orbit of GOME-2A in 2007 (Figure C.7). For the verification, three parameters are compared: the tropospheric NO_2 VCD, the corresponding tropospheric AMF, and the AMF without cloud correction (i.e., the tropospheric AMF for clear scenes). Figure C.7 illustrates the comparisons for GOME-2A in 2007, and the same conclusions can be drawn for GOME-2A and GOME-2B in 2013 (not shown here). Figure C.8 shows both GDP 4.7 and GDP 4.8 monthly averaged tropospheric NO_2 vertical columns for GOME-2A in February 2007 and 2013 and GOME-2B in February 2013, and Figure C.9 give their differences between two processor versions.

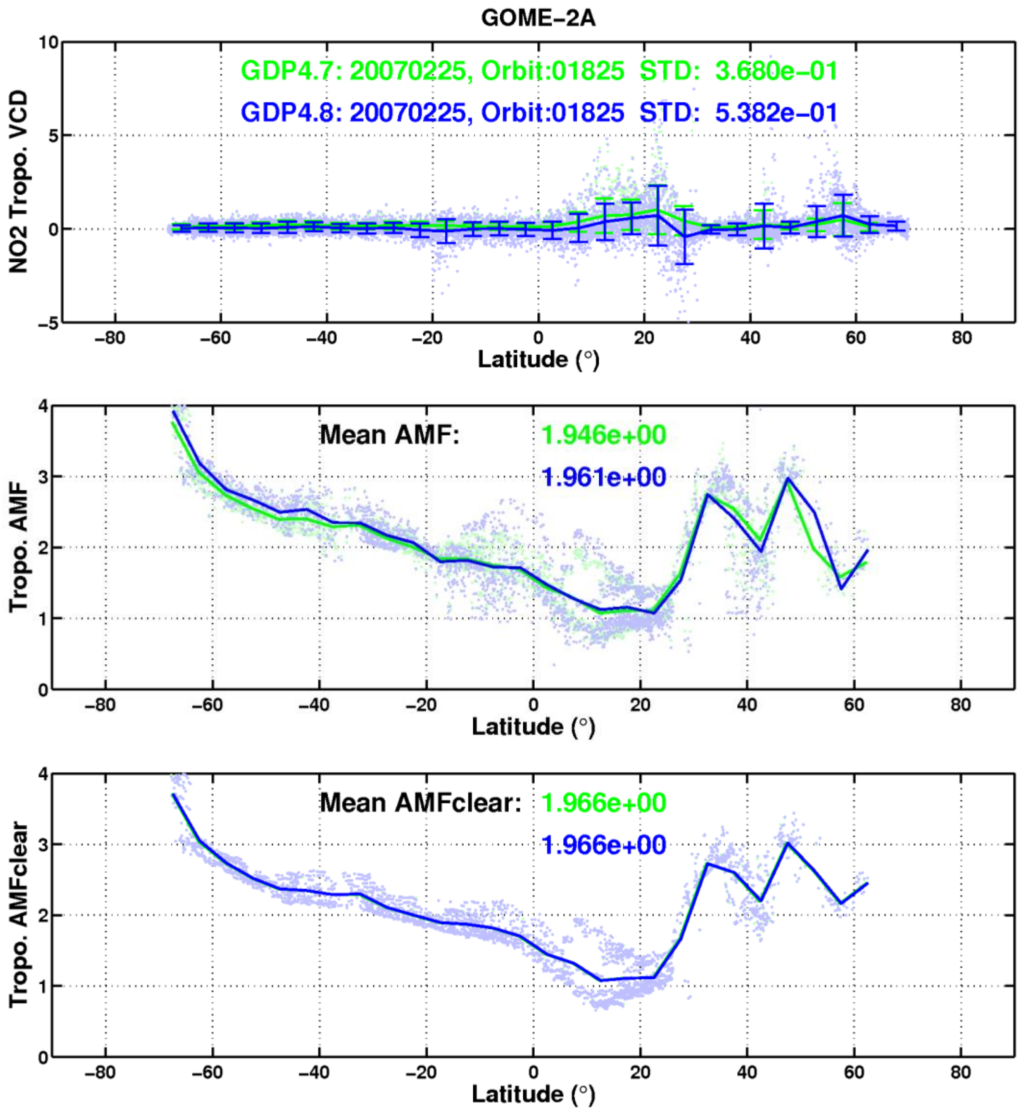

Figure C.7: GDP 4.7 (in green) versus GDP 4.8 (in blue) tropospheric NO_2 vertical columns, with the corresponding tropospheric AMF, for one orbit of GOME-2 on Metop-A (25/02/2007, orbit number 1835). Only pixels with the corresponding cloud radiance fraction less than 50% are used for the figures (NO_2 VCDs and Tropo. AMF), and only data where both GDP 4.7 and GDP 4.8 have retrieved tropospheric NO_2 VCD (that have meaningfull AMF values) are shown in the AMF_{clear} figure (bottom).

GDP 4.7 **GDP 4.8**

GOME-2A 2007

GOME-2A 2013

GOME-2B 2013

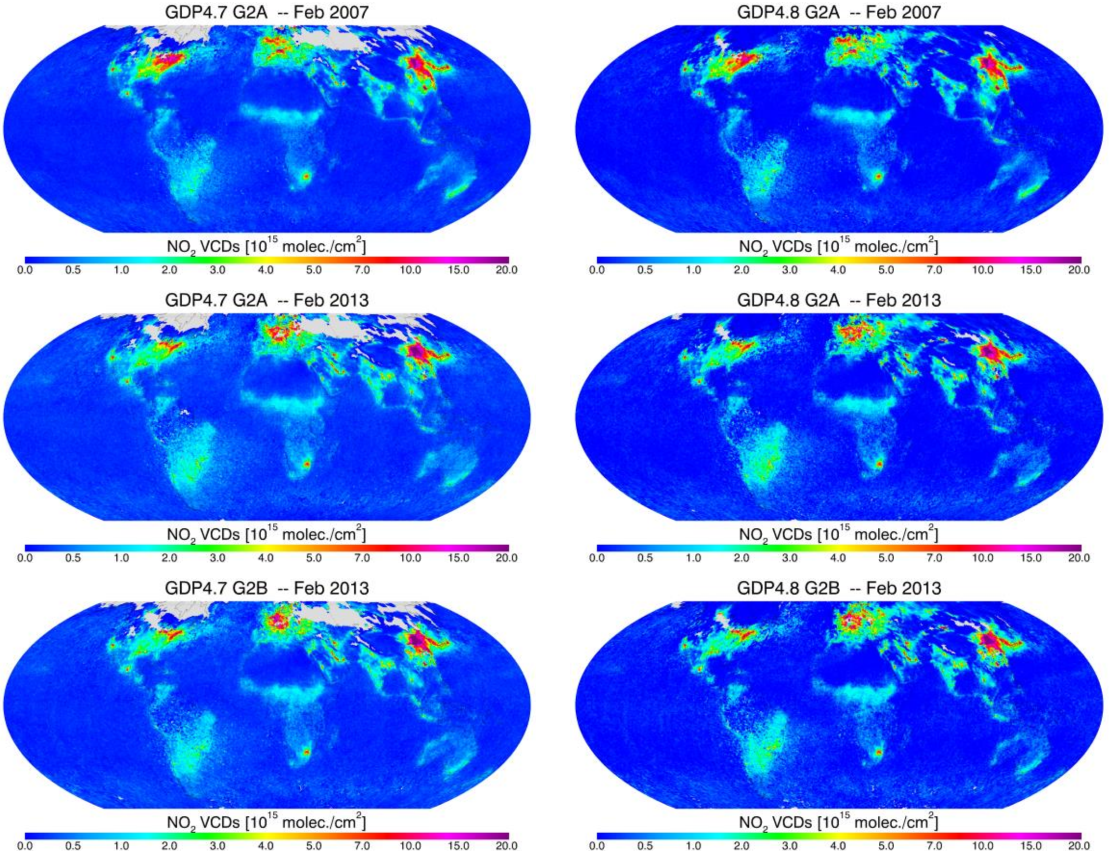

Figure C.8: GOME-2 monthly averaged tropospheric NO_2 vertical columns (CRF<50%) for GOME-2A in February 2007 & 2013 and GOME-2B in February 2013.

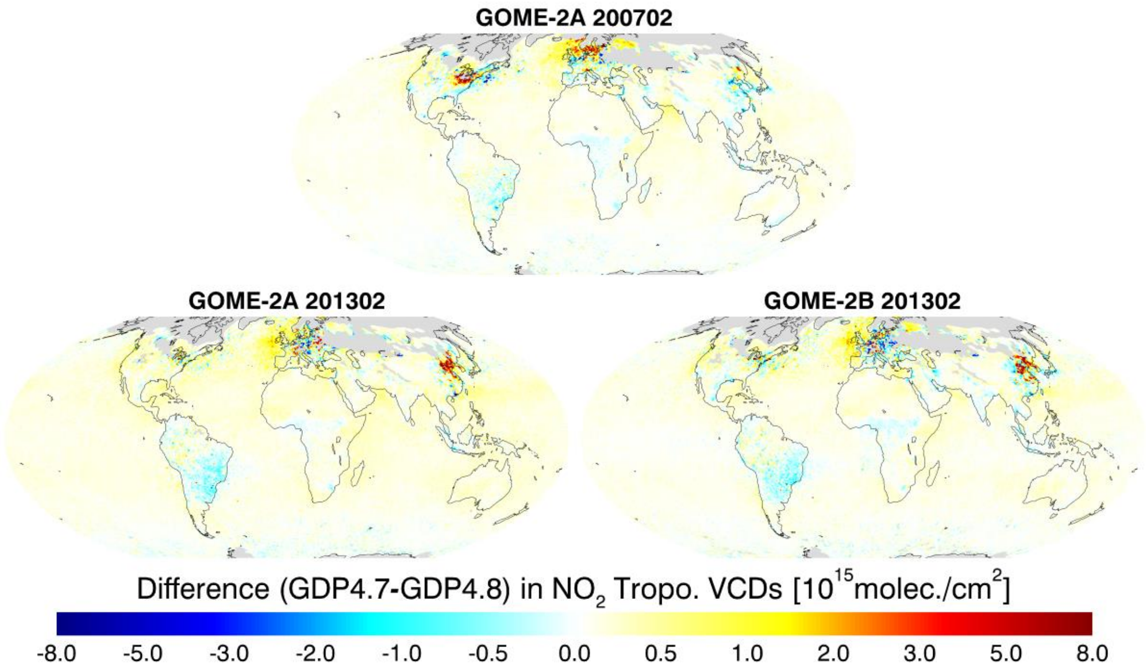

Figure C.9: Maps of monthly averaged tropospheric NO_2 vertical column differences between GDP 4.7 and GDP 4.8 for GOME-2A 2007 and 2013 and GOME-2B 2013. Only measurements with CRF<50% and forward scan pixels are used in the analysis.

From inspection of Figure C.7 and Figure C.9, we conclude the following:

- GDP 4.7 NO_2 tropospheric VCD are slightly higher than those of GDP 4.8 for most of regions.
- The standard deviation (STD) of the NO_2 VCD_{trop} is higher in GDP 4.8 than in GDP 4.7. This is a result of clipping negative tropospheric residuals in the GDP 4.7 and the inclusion of negative VCD_{trop} valuses in the GDP 4.8 L2 NO2 product. See next section.
- Cloud free AMFs are identical between GDP 4.7 and GDP 4.8, since albedo, a-prioir profiles, and surface elevation maps have not been updated.The main difference in the AMFs is from the change of cloud product.
- Comparing the difference between AMF_{tropo} and AMF_{clear}, there is no significant effect on AMF due to cloud correction for GDP 4.7, since the previous version of cloud algorithm is not sensitive to cloud in the nearly cloudy-free scenes, and there is a large number of GOME-2 pixels with a CF of 0, and only few pixels with a small CF value. Cloud correction based on GDP 4.8 cloud product leads to about ±20% difference in AMF.
- From the global maps, significant differences can be found over East Asia, North America, and Europe. The details of effects of the individual changes on AMF will be further discussed in the following section.

C.3.1 Effect of individual changes on tropospheric NO_2 retrieval

The main change in the GDP 4.8 tropospheric NO_2 retrieval is from cloud product (Lutz et al., 2015) for the calculation of the tropospheric AMF. Here, we investigate the effect of individual changes on tropospheric NO_2 retrieval (Figure C.8 and Figure C.9). Effect of cloud on NO_2 retrieval have been investigated in two steps: effect of cloud correction on AMF calculation, and effect of the sampling of cloud free GOME-2 measurements (CRF < 50%). This is done by comparing the differences of using a tropospheric AMF including cloud correction ($AMF_{tropo} = AMF_{clear} \cdot (1\text{-}CRF) + AMF_{cloud} \cdot CRF$) or a AMF without cloud correction (i.e. AMF_{clear}). As GDP 4.7 and 4.8 have several differences in the retrieval algorithm, the differences seen in Figure C.8 are only related to the cloud correction itself.

The effect of the sampling of GOME-2 measurements with CRF < 50% in the GDP 4.7 and 4.8 is investigated based on the residual tropospheric slant columns , the results display in Figure C.8 as well.

Another change in the GDP 4.8 data product is that all the retrieved tropospheric NO_2 columns are included (i.e. also for cloudy pixels, and negative residual tropospheric columns). In satellite NO_2 retrieval, tropospheric NO_2 columns can be positive and negative due to instrumental random error, and in the GDP 4.7, the retrieved tropospheric NO_2 column is clipped to zero (i.e. if the residual tropospheric NO_2 slant column is less than zero, then the measurement is flagged as unpolluted background conditions, and NO_2 VCD_{tropo} set as zero). In the GDP 4.8, negative residual tropospheric columns are not clipped to zero. The effect of this change is shown in Figure C.9.

	GDP 4.7	**GDP 4.8**
Effect of cloud correction	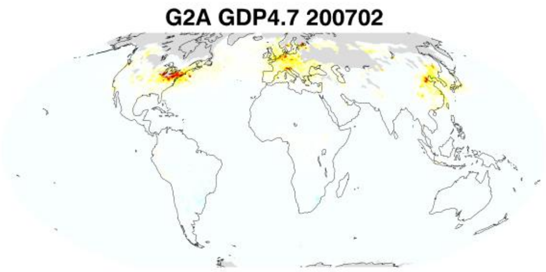	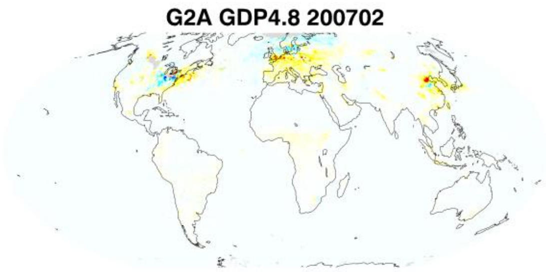

Effect of cloud-free sampling

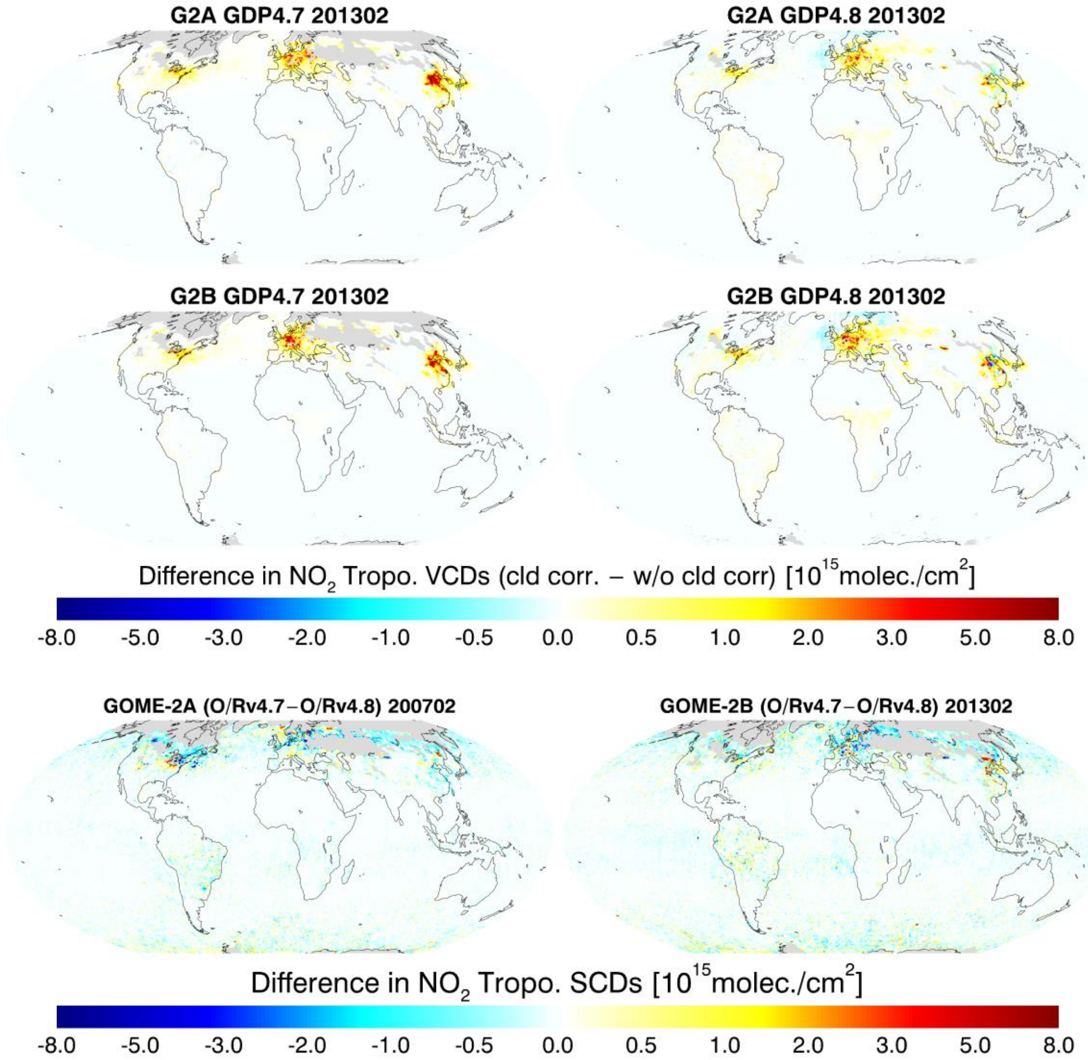

Figure C.10: Effect of the new cloud product on NO_2 retrieval. Row 1-3: comparison of NO_2 retrieval using tropospheric AMF including cloud correction ($AMF_{tropo} = AMF_{clear} \cdot (1\text{-}CRF) + AMF_{cloud} \cdot CRF$) and the AMF without cloud correction (i.e. AMF_{clear}) for GOME-2A February 2007&2013 and GOME-2B February 2013. Row 4: comparison of monthly mean residual tropospheric slant columns, from GOME-2 measurements with CRF(from GDP 4.7) and CRF(from GDP 4.8) < 50%, for GOME-2A February 2007 (left) and GOME-2B February 2013 (right).

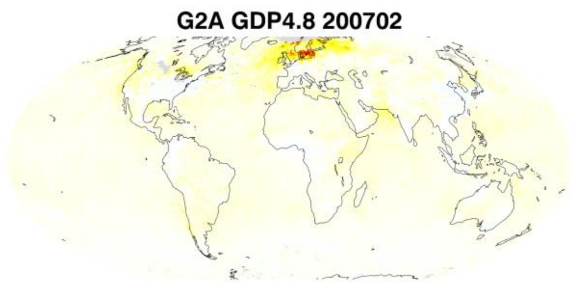

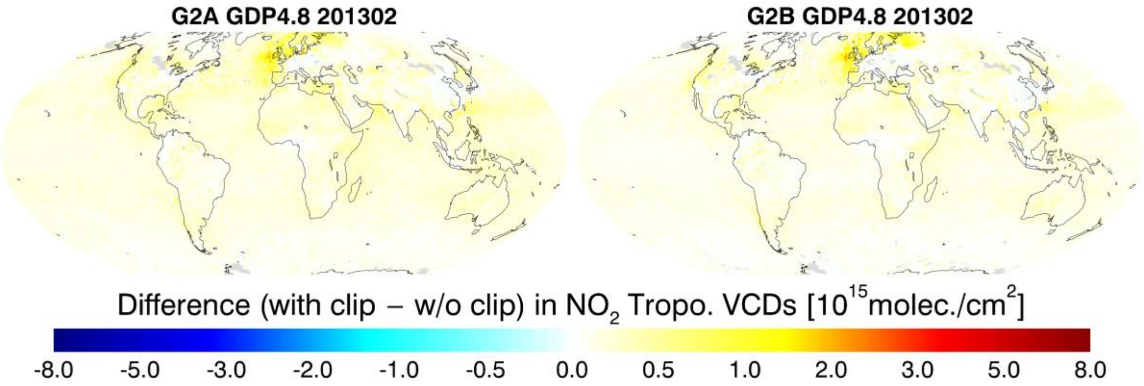

Figure C.11: Effect of 'clipping' negative residual tropospheric columns to zero: Monthly average of tropospheric NO_2 columns from GDP 4.8 without clipping compared to the average calculated with negative residual tropospheric columns clipped to zero.

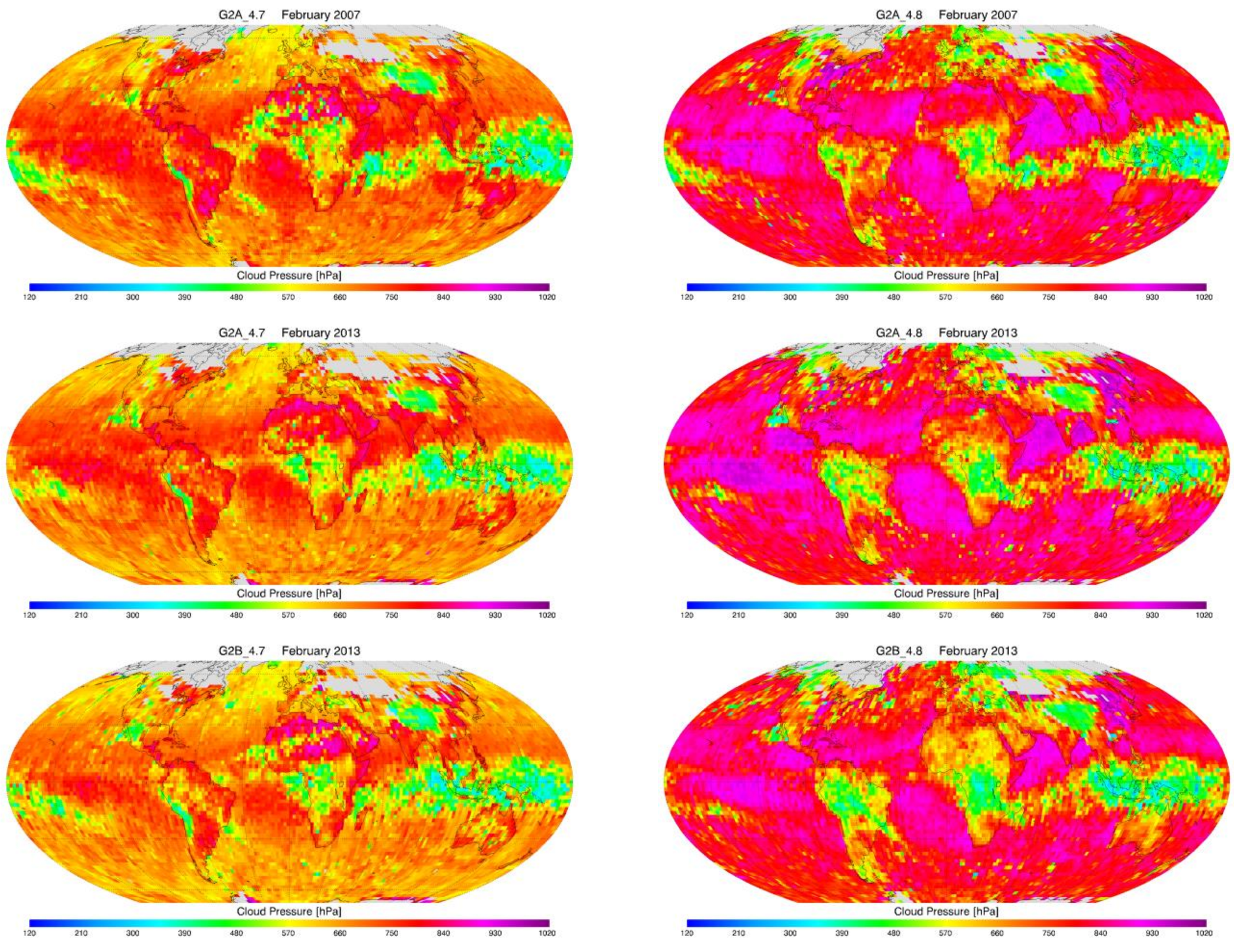

Figure C. 12: Comparison of monthly median cloud pressure over the nearly cloud-free pixels Statistic is based on one month of observations with intensity-weighted cloud fraction between 10% and 50% over 1°×1° cell.

<u>Effect of cloud correction:</u>

- Almost only positive cloud correction effects on NO_2 retrieval for GDP 4.7, and both positive and negative effects can be found for GDP 4.8 over the polluted regions over North Hemisphere. The larger cloud correction effects in the GDP 4.7 over polluted regions in winter are mainly a results of quality issues with the OCRA cloud fractions in the GDP 4.7 for larger solar zenith angles.

- The huge difference in NO_2 columns due to cloud correction are linked to the difference in the cloud retrievals (see Figure C. 12). For the nearly cloud-free pixels, cloud pressure from GDP4.8 is systematically higher that from GDP4.7, especially for low cloud (high cloud pressure) cases. Low cloud often occurs over the polluted regions (such as Eastern China), and change of cloud pressure significantly affects the NO_2 retrieval for those cases.
- GDP 4.8 also present a positive effect over tropical biomass burning regions, where high clouds are present, not seen in GDP 4.7 maps.

Effect of cloud-free sampling:

There is no obvious difference due to the cloud-free sampling, except some regions over high latitude or tropical land regions, that are always covered by cloud and/or snow, and only few cloud-free observation are present over the whole month. Although the previous version of cloud product was underestimating the cloud fraction for the nearly cloud-free scenes, both products distinguish well cloud-free and cloudy pixels.

Effect of ‘clipping’ negative residual tropospheric columns:

This effect mainly affect the retrieval over background regions. This effect is much significant over Northwest European water area, probably due to the overestimation of stratospheric correction over high latitude polar vortex areas. In this area, strong stratospheric gradients are present, that current stratospheric estimation scheme can not account for, leading to a significant underestimation of tropospheric NO_2 columns, and thus negetive NO_2 values often occurr over this area (see also Valks et al., 2011). This effect is stronger for GOME-2A retrieval in 2013 than in 2007, probably due to effect of the instrumental degradation, and the increased random error in the NO_2 slant columns. An improved Stratosphere-Troposphere Separation (STS) algorithm is currently being developed for GOME-2 in the framework of a VS project by MPI-Mainz (Beirle et al., 2015), and will be implemented in a future version of the GDP.

C.3.2 Verification of Total Vertical Column Density

To vertify the improvements of GDP v4.8 against v4.7 total vertical columns (VCD_{corr}), the results of the two processor versions are compared for the monthly average of GOME-2A measurements in 2007 and 2013 and GOME-2B in 2013 in Figure C.10.

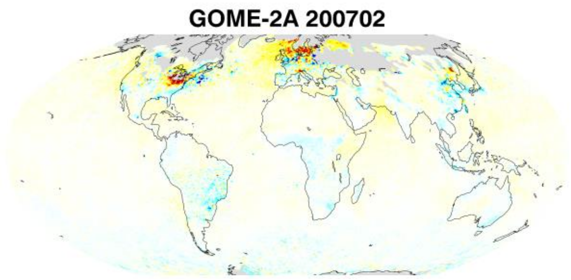

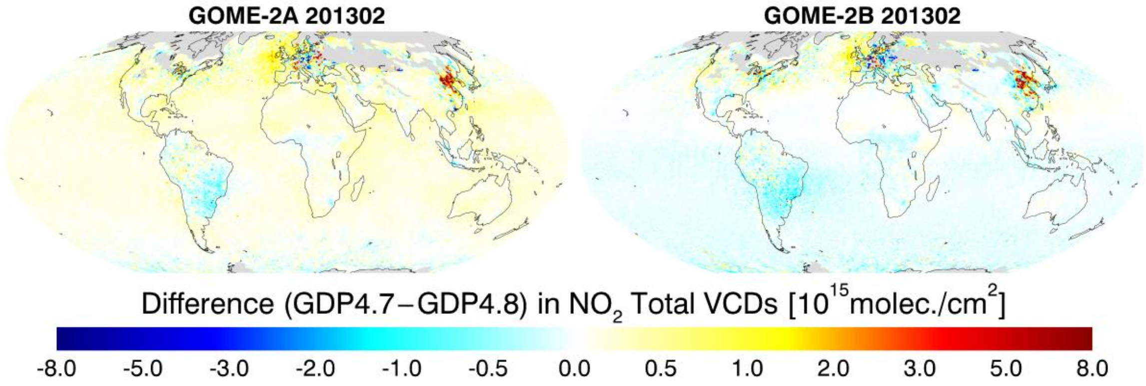

Figure C.13: Maps of monthly averaged differences in total NO2 columns between GDP 4.7 and GDP 4.8, obtained from GOME-2A in February 2007 & 2013 and GOME-2B in February 2013.

Main conclusions on the tropospheric and total vertical columns:

There is a general good agreement, and the effects of individual change on NO_2 retrieval are clearly shown in the figures. Compared to GDP 4.7, GDP 4.8 NO_2 VCDs have a systematically negative bias, mainly due to the effect of 'clipping' negative residual tropospheric columns in GDP 4.7 processor. The difference in GOME-2A is larger in 2013 than in 2007, which is the result of the clipping and instrumental degradation. The difference in the tropospheric and total columns over the polluted areas are mainly due to changes in the calculation of tropospheric AMF. The total vertical columns from GOME-2B shows a positive offset over the Southern Hemisphere because of the change in the NO_2 cross section in the DOAS fit in the GDP 4.8.

D. VERIFICATION OF INDIVIDUAL COMPONENTS OF PROCESSING CHAINS: TIME-SERIES ABOVE EMISSION REGIONS

In order to explore the overall consistency of the new GDP 4.8 product, end-to-end time-series plots of the different contributions of the operational processing chain of both Metop-A and Metop-B are presented for several emission regions, and compared to GDP 4.7 values. The individual components of the NO_2 VCD processing chain are compared separately, in order to investigate possible compensating errors. We focus on:

- Total slant columns (SCD_{tot}) coming from the DOAS fit
- Tropopsheric slant columns (SCD_{tropo}) that are the residual content after having estimated the stratospheric contribution
- Stratospheric vertical columns (VCD_{strato})
- Tropopsheric air-mass factors (AMF_{tropo}) used to convert SCD_{tropo} into the final tropospheric vertical column (VCD_{tropo})
- Tropopsheric and Total vertical columns (VCD_{tropo}, VCD_{tot})

Monthly mean averages of cloud free pixels are performed for the whole time-series, around specific sites where ground-based correlative instruments exist and that will be further used for the validation (Section E).

Different pollution levels are studied by looking to data around several Northern Hemisphere stations: from background/remote site (OHP, South of France), to European pollution levels (around Uccle, Belgium) and to higher levels of pollution in China (around Beijing) (Figures D.1 to D.3). Data around Bujumbura (Burundi, 3°S,) are also showed to explore evolution in the Southern Hemisphere (Figure D.4).

Figures D.1 to D.4 present the full GOME-2A and GOME-2B time-series, showing the temporal evolutions of the different component of the retrieval. As presented in Section C, differences between GDP 4.8 and 4.7 exist in all the different steps of the retrieval chain, affecting differently GOME-2A and GOME-2B in different regions of the world (see maps in Figures C.3, C.4, C.7 and C.10 for SCD_{tot}, SCD_{tropo}, VCD_{tropo} and VCD_{tot} respectively). Here, part of the differences between GDP 4.8 and GDP 4.7 are reduced by keeping only GOME-2 measurements with CRF < 50% and positive tropospheric VCD data in the 4.8 dataset (i.e. elimination the effect of clipping negative residual tropospheric columns, see Figure C.9). Remaining differences are essentially due to the improved cloud correction scheme in GDP 4.8 (affecting AMF_{tropo} and thus VCD_{tropo} and VCD_{tot}) and slant columns improvements (affecting SCD_{tot} and propagating to all the other retrieval steps) .

Quantification of the differences can be better seen in Figures D.1b to D.4b, where only the GOME-2A and GOME-2B common period (since 2013) are shown, as well as the absolute differences of GDP 4.8 and 4.7 for both platforms and the absolute difference between the platforms, for both products.

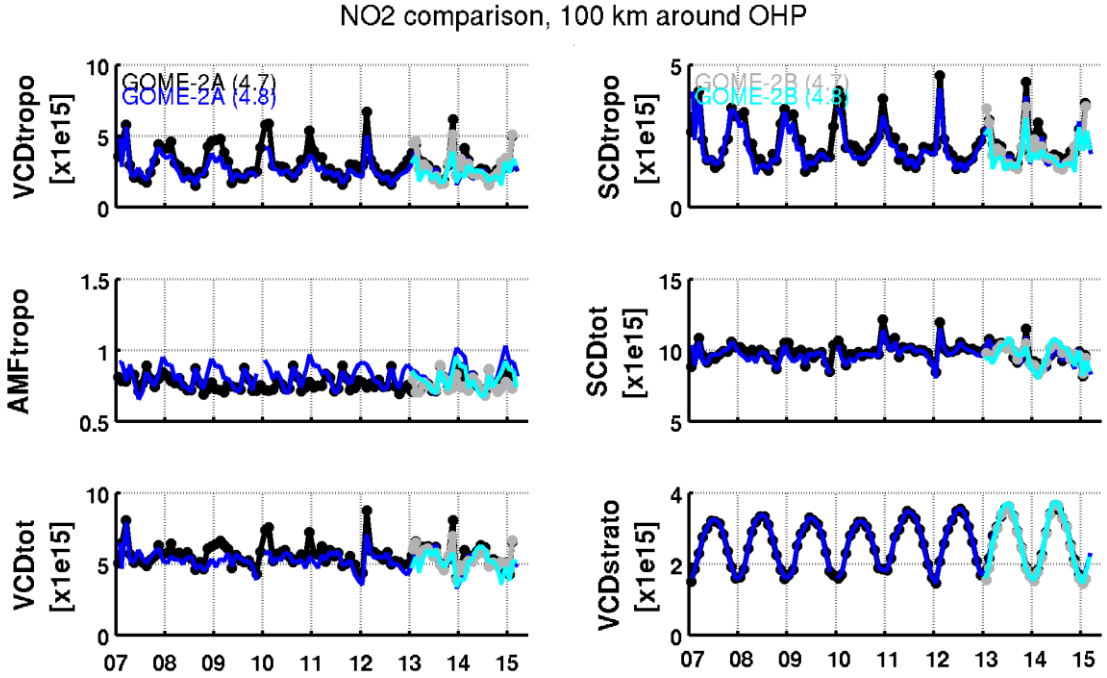

Figure D.1 End-to-end comparison between GOME-2A (in black and blue) and GOME-2B (in grey and cyan) monthly mean averages in a region of 100 km around OHP, south of France. The different contributions of the NO_2 retrieval are investigated: tropospheric VCD, total VCD, total SCD, tropopsheric SCD, stratospheric VCD and tropospheric AMF.

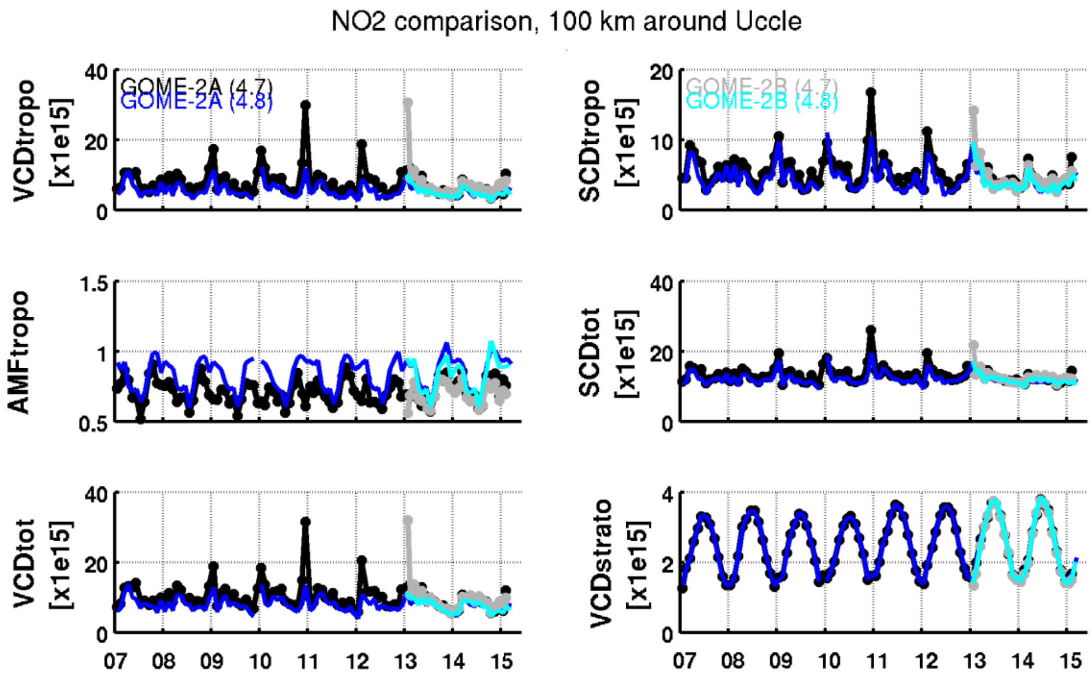

Figure D.2 as Figure D.1 but around Uccle, Belgium.

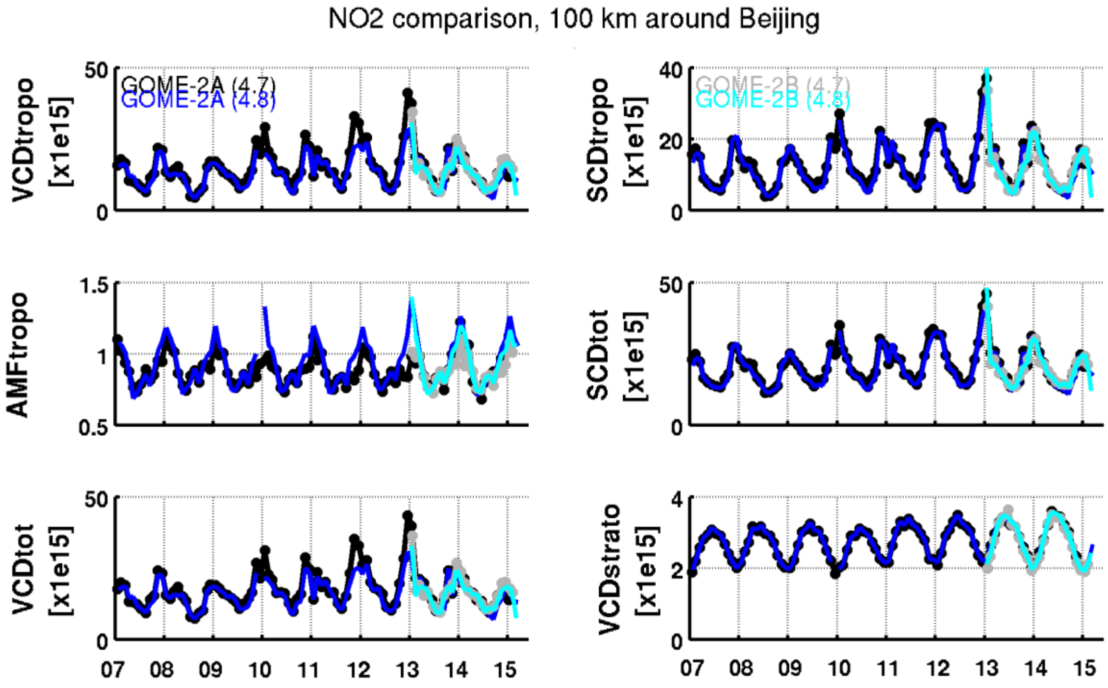

Figure D.3 as Figure D.1 but around Beijing, China.

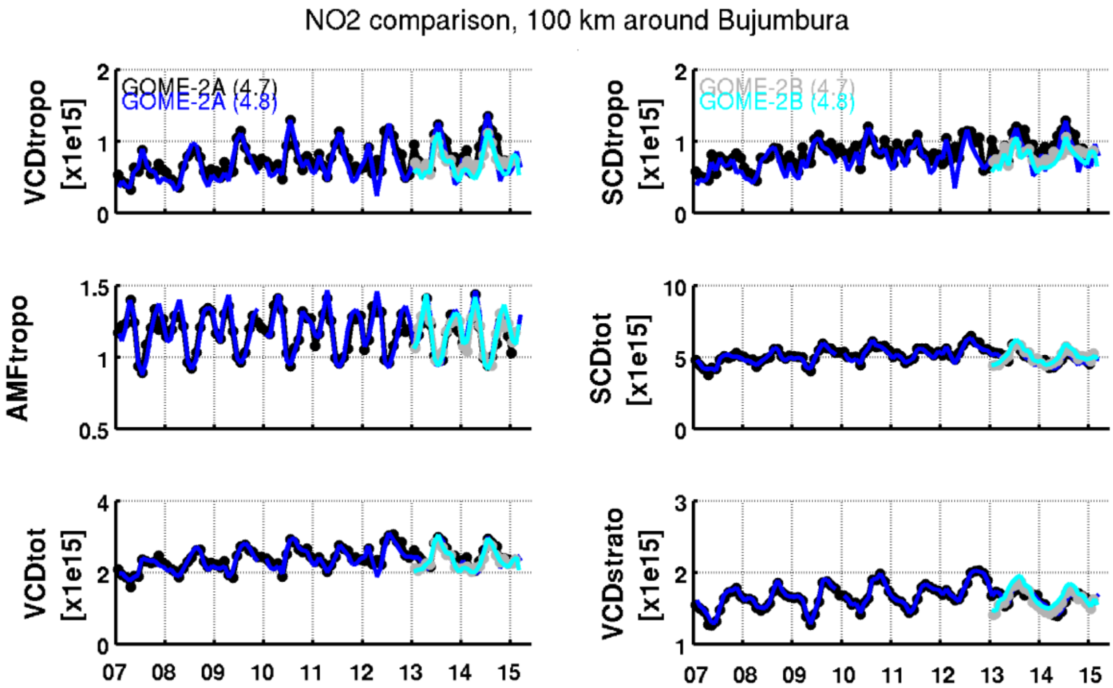

Figure D.4 as Figure D.1 but around Bujumbura, Burundi (Central Africa).

From Figures D.1 to D.4 we can conclude on a good consistency of the temporal evolution of the different parameters for both products and both platforms. More particularly, differences in SCD_{tropo}, VCD_{tropo} and VCD_{tot} between the two versions is seen with GDP 4.8 being generally smaller than 4.7 (of about $0.5x10^{15}$ molec/cm²). The stratospheric columns seems to agree very well between the 2 instruments and the 2 versions, with some larger differences between GOME-2A and GOME-2B in the case of Bujumbura, in the Southern Hemisphere. This is to be expected when recalling the hemispheric differences between GOME-2A and GOME-2B total SCD exist (highlighted in Section C.1, maps of Figure C.3) that are transferred to the stratospheric component (Figure C.4).

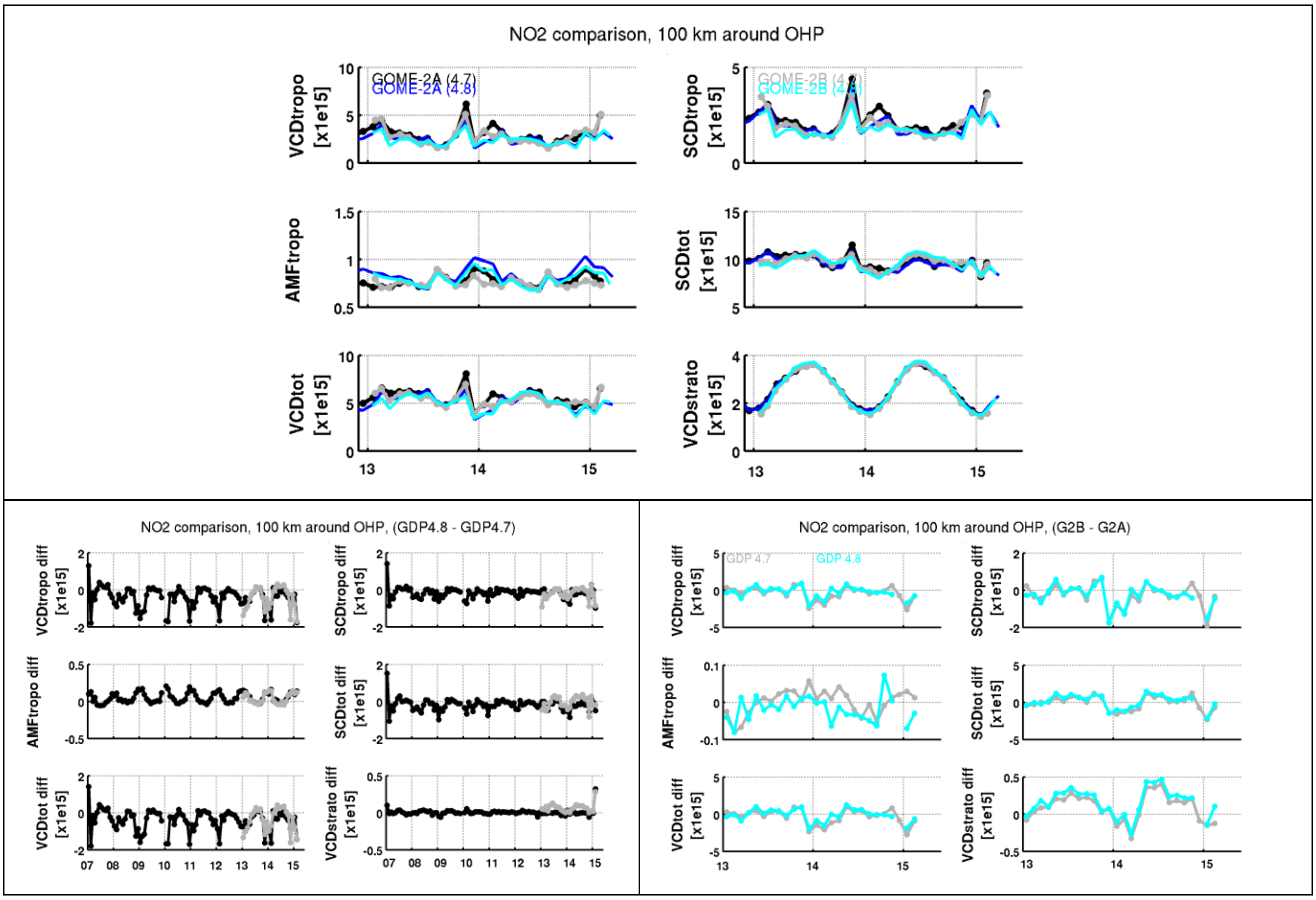

Figure D.1b (upper panel): same as Figure D.1 but zooming on the common time-period of Metop-A and –B (January 2013 to 2015). (lower panel): absolute differences of the different pairs of products and platforms: (left panel) GDP 4.8-GDP 4.7 for GOME-2A (black) and GOME-2B (grey) ; (right panel) GOME-2B- GOME-2A for GDP 4.7 (grey) and GDP 4.8 (cyan).

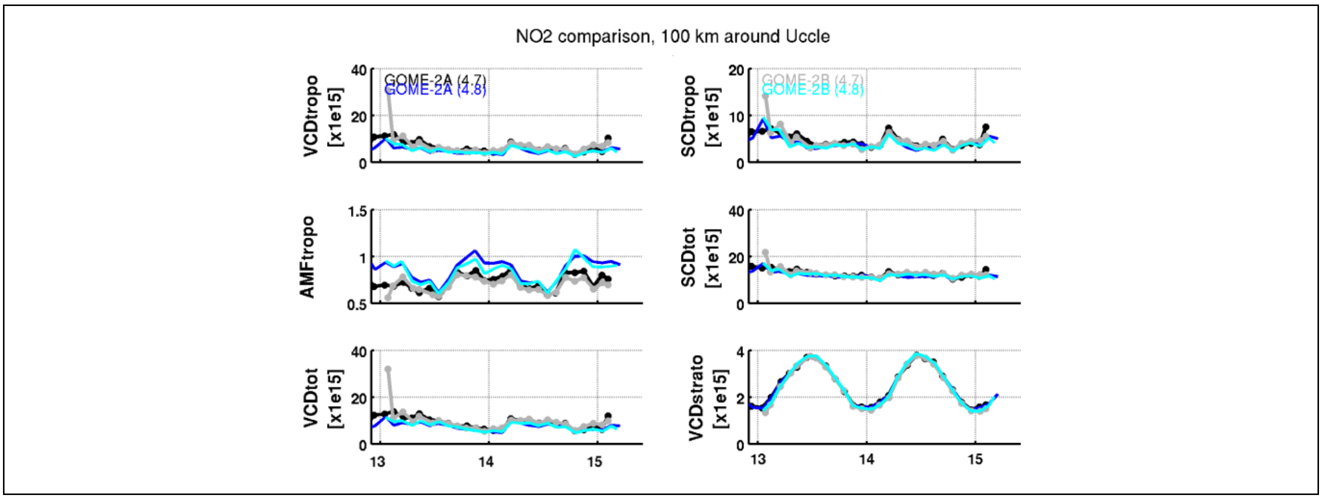

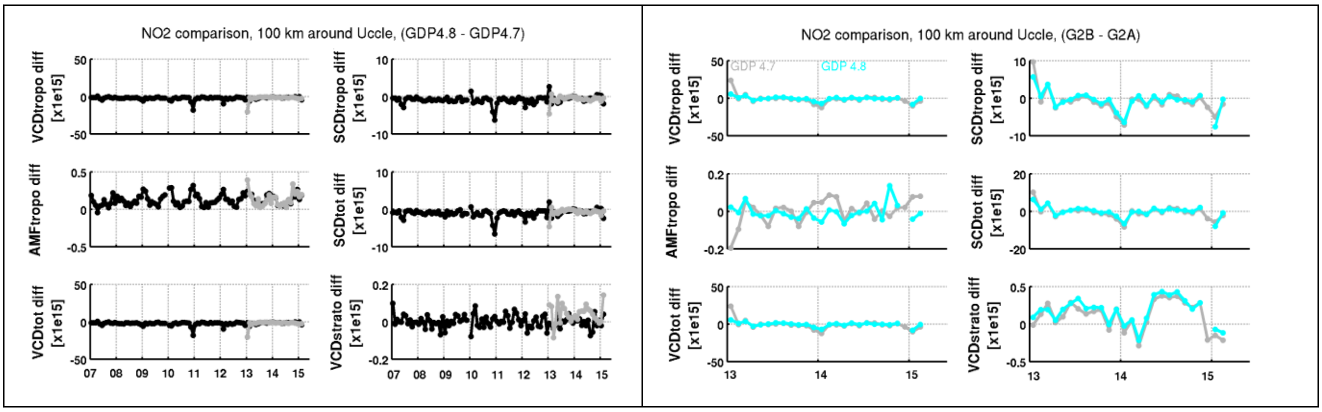

Figure D.2b as Figure D.1b, but for Uccle.

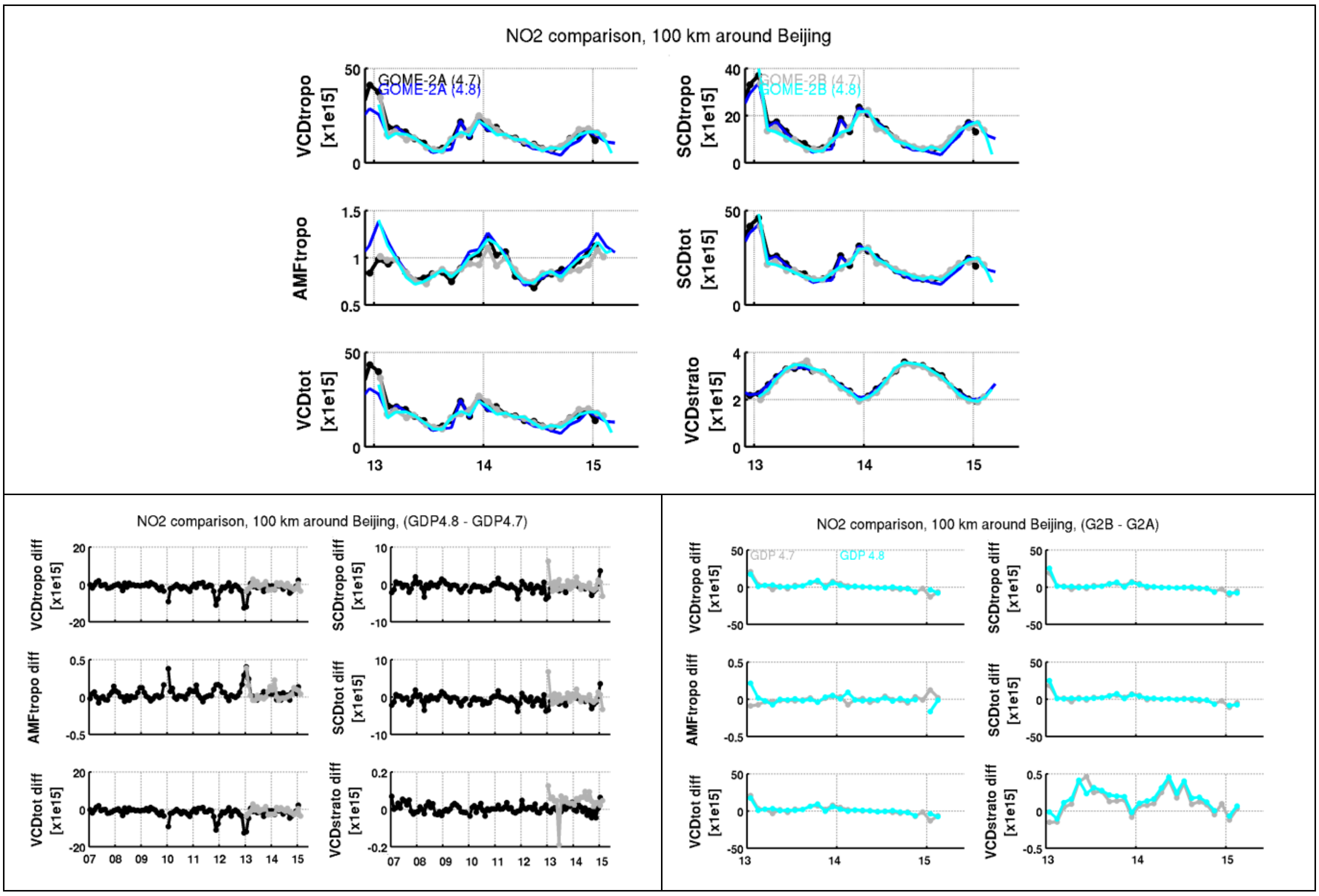

Figure D.3b as Figure D.1b, but for Beijing.

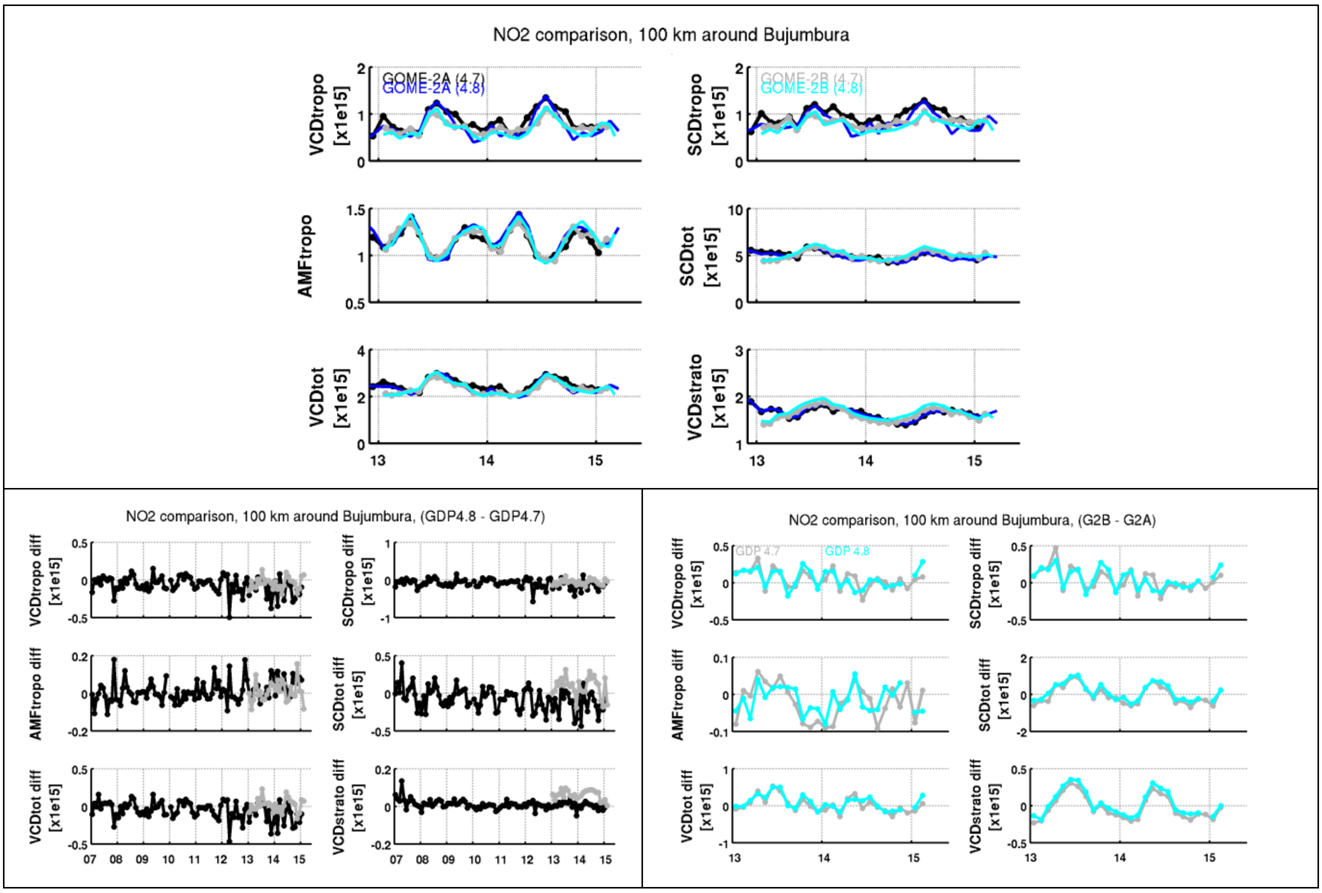

Figure D.4b as Figure D.1b, but for Bujumbura.

From Figures D.1b to D.4b we can distinguish the relative importance between platform differences and version differences. E.g., around Bujumbura, the differences in VCDstrato between the 2 instruments are more important than the differences between the versions (less than ~0.1×10^{15} molec/cm²), and these differences present a seasonal variation of about 0.5×10^{15} molec/cm², mostly present in GOME-2B. This pattern is also present in the other stations shown here, and should be focused in more details.

E. EVALUATION OF THE NO_2 COLUMN DATA PRODUCTS

E.1. Stratospheric Vertical Column

E.1.1 Comparison against ground-based zenith-sky DOAS data

This chapter reports on comparisons of two versions (GDP 4.7 and GDP 4.8) of GOME-2A/B stratospheric NO_2 column data against ground-based reference measurements acquired routinely at twilight by zenith-sky looking UV-visible spectrometers (ZLS-DOAS). All considered ZLS-DOAS instruments perform network operation in the context of NDACC, with due certification of their measurement protocol and quality control of their data. NDACC stations having provided data for this GOME-2 validation study of GDP upgrade from version 4.6/4.7 to 4.8, are highlighted in red in Figure E.1.1. Comparison results are shown for both GOME-2A and GOME-2B, and also for both GDP 4.8 (in red in the statisctical graphs at the end of the section) and GDP 4.7 (in green). Due to the photochemical diurnal cycle of the nitrogen oxides family, a bias can appear between twilight measurements acquired by definition between 86° and 91° SZA, and GOME-2 measurements acquired at a solar local time linked to the orbit of the MetOp platforms: usually in the mid-morning, but also at larger SZAs in polar areas, and at various SZAs in case of multiple daily overpasses during polar day. To avoid this bias, in this study only twilight GOME-2 data (hereafter beyond 75° SZA) are to be considered during polar day, and only sunrise ZLS-DOAS measurements (blue curves) are to be considered elsewhere (at low and middle latitudes sunrise NO_2 differ from mid-morning NO_2 by only a few 10^{14} molec.cm^{-2}). At twilight the zenith-sky viewing geometry becomes sensitive mainly to stratospheric absorbers like NO_2, which makes it particularly suitable for stratospheric validations.

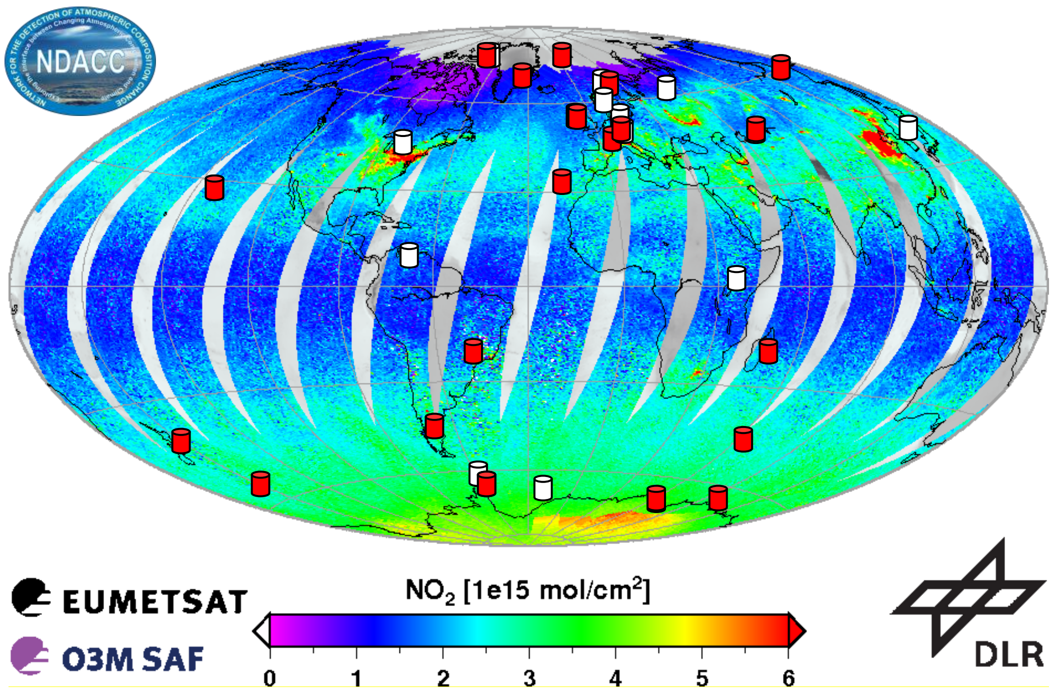

Figure E.1.1 Geographical distribution of NDACC UVVIS spectrometers measuring the NO_2 total column at twilight. Stations having provided data for this GOME-2 validation study are highlighted in red. Stations are displayed on top of the global NO_2 field measured by GOME-2A on February 10, 2011.

Hereafter comparison results are reported from the Arctic (Section E.1.1.1) to the Antarctic (E.1.1.5), and summarized in Section E.1.1.6, at 14 to 20 stations representative of the following observational conditions:

- Southern middle latitude stations, combining negligible tropospheric pollution, easy-to-handle diurnal cycle of stratospheric NO_2 (sunrise values close to mid-morning values), and large NO_2 SNR.
- Clean Northern middle latitude sites surrounded by large polluted areas, where pollution episodes have been filtered out for fractional cloud covers below 25%.
- Polar stations, with polar day exhibiting a particular diurnal cycle sampled several times a day by GOME-2, and polar wintertime with low NO_2 columns and SNR and large relative variability.
- Tropical stations, with low NO_2 columns observed under small SZA, which result in poor SNR.

E.1.1.1 Stratospheric NO_2 column over the Arctic

Figures E1.2 to E1.5 present comparisons at four NDACC stations distributed around the Arctic circle: Ny-Ålesund on Spitsbergen, Scoresbysund in Greenland, Sodankylä in Finland and Zhigansk in Eastern Siberia. Statistics on absolute differences presented in the bottom plots are based on monthly medians and interpercentile values rather than means and standard deviations, to avoid unwanted overweight of exceptional outliers. At all stations GOME-2A GDP 4.8, GOME-2B GDP 4.8 and NDACC ZLS-DOAS instruments capture similarly the seasonal cycle of stratospheric NO_2, as well as monthly and day-to-day changes in stratospheric NO_2. Quantitatively, from fall to springtime both GOME-2A and GOME-2B agree with ground-based measurements by about a few 10^{14} molec.cm^{-2}, that is, within the uncertainty bar of the comparison method. During polar day statistical results seem to conclude to an underestimation of NDACC data by the satellites, however, this underestimation can be attributed mainly to imperfect correction of diurnal cycle effects. Indeed, the photochemical correction used here works at best for GOME-2 data acquitted at the largest SZAs on the orbit. Figure E.1.4 (bis) shows that the same results as plotted in Figure Figure E.1.4 but plotted now as a function of GOME-2 solar zenith angle and separated by season, conclude to a better agreement to within $2\text{-}5\cdot10^{14}$ molec.cm^{-2} if we consider only measurements coincident in time, that is at twilight SZAs. The agreement is even better in the 55°-65° SZA range, where the photochelical correction works also well.

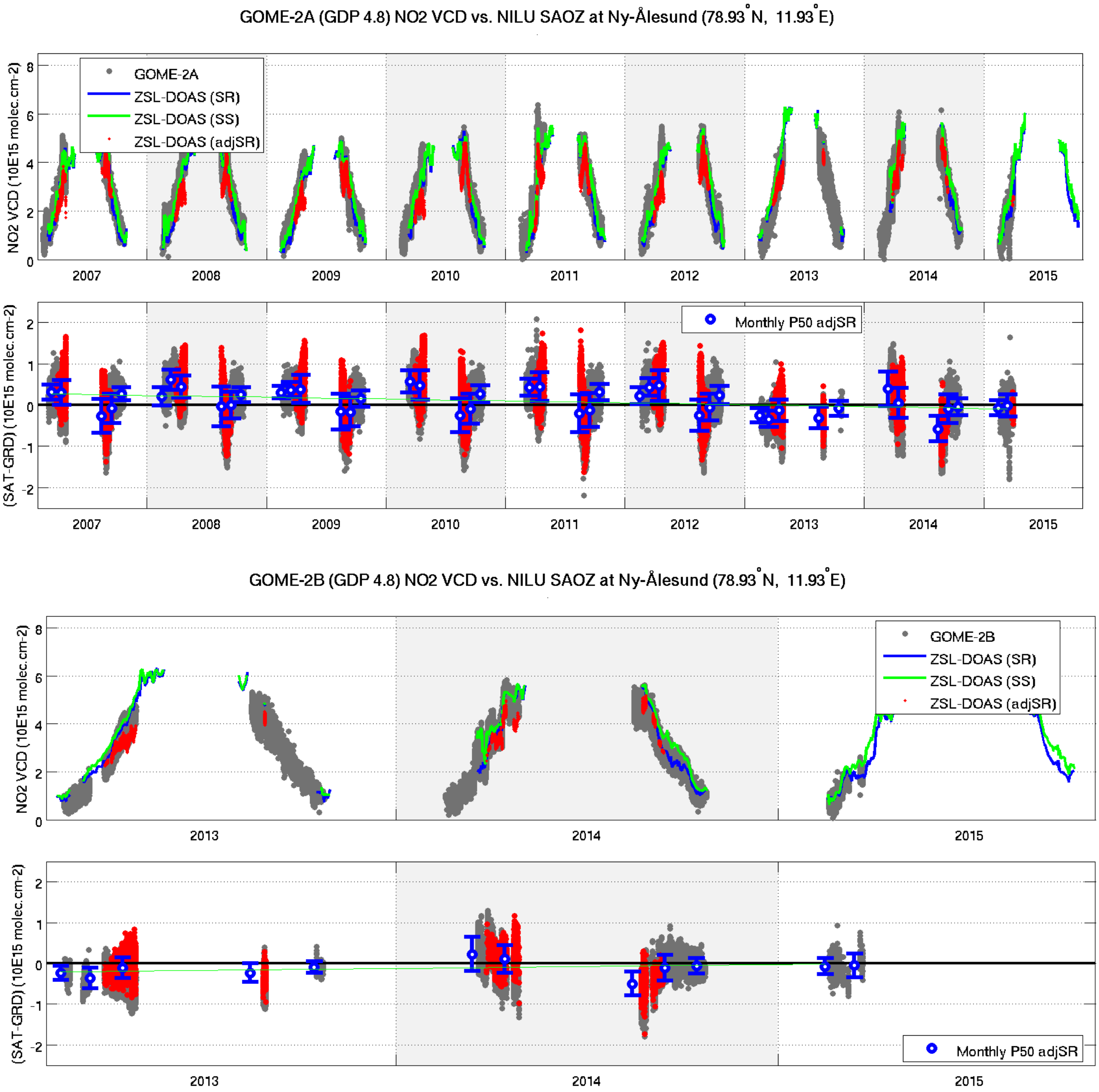

Figure E.1.2 Comparison of NO_2 total column measured at the NDACC station of the Ny-Ålesund (Spitsbergen) by GOME-2-A/B (GDP 4.8) and by the SAOZ UVVIS spectrometer operated by NILU (LATMOS V3 reprocessing). Top panel: GOME-2A results; bottom panel: GOME-2B results. In every panel, top graph: NO_2 column time series; bottom graph: absolute difference between GOME-2A and SAOZ UVVIS. Monthly medians (P50) and corresponding 68% interpercentile (error bars) are based on all GOME-2 data and on sunrise (blue curve) SAOZ data only.

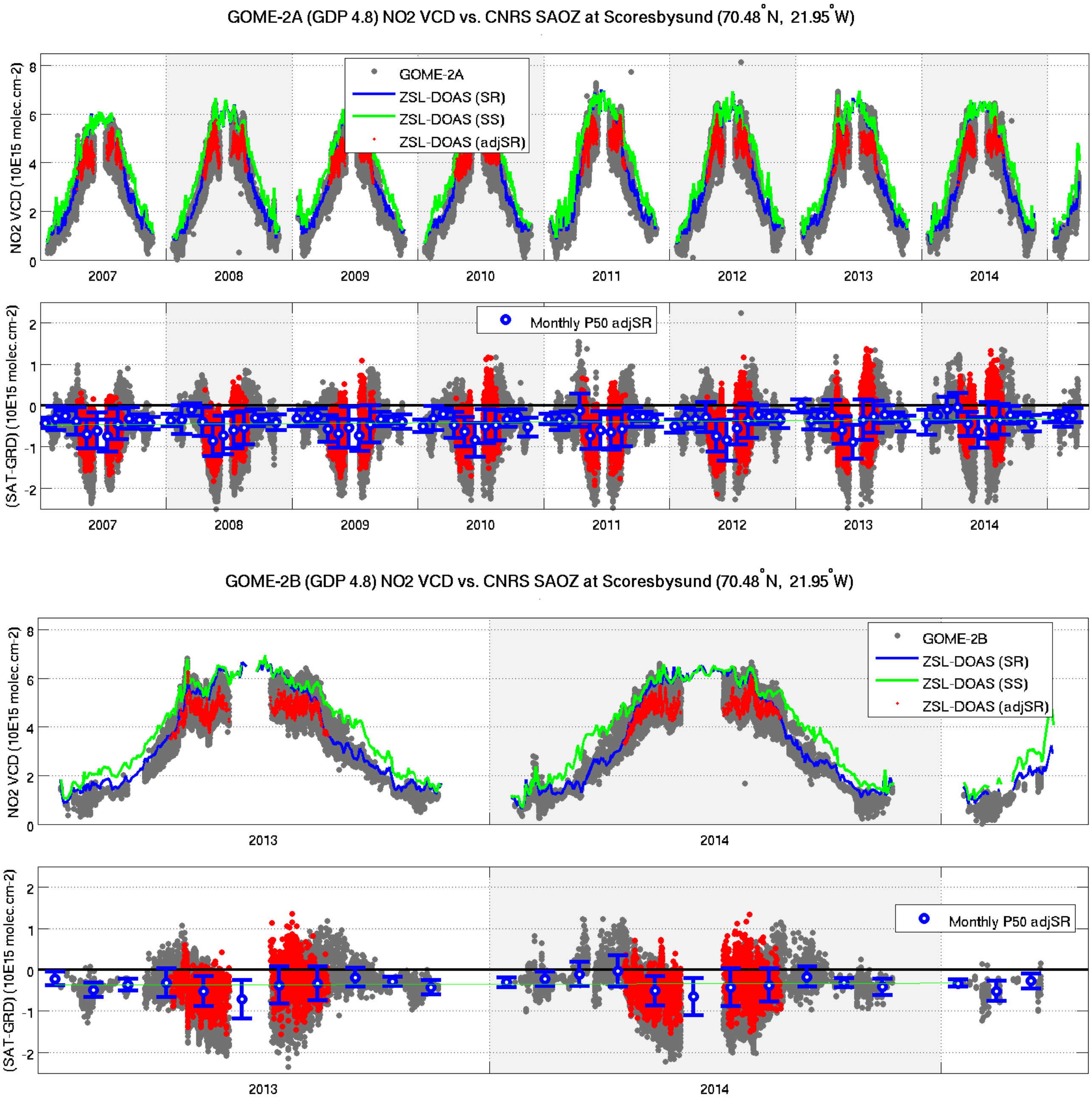

Figure E.1.3 Same as Figure E.1.2 but over the NDACC station of Scoresbysund (Eastern Greenland), measured by GOME-2A and GOME-2B (GDP 4.8) and by the SAOZ UVVIS spectrometer (LATMOS V3 reprocessing) operated by CNRS/DMI.

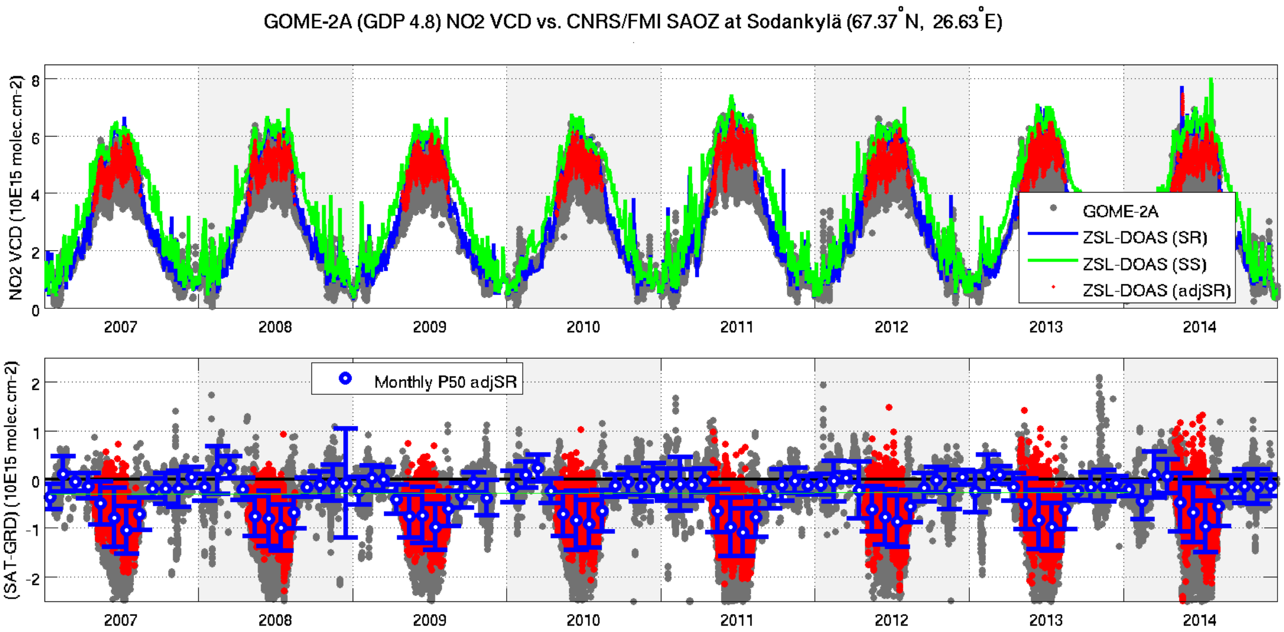

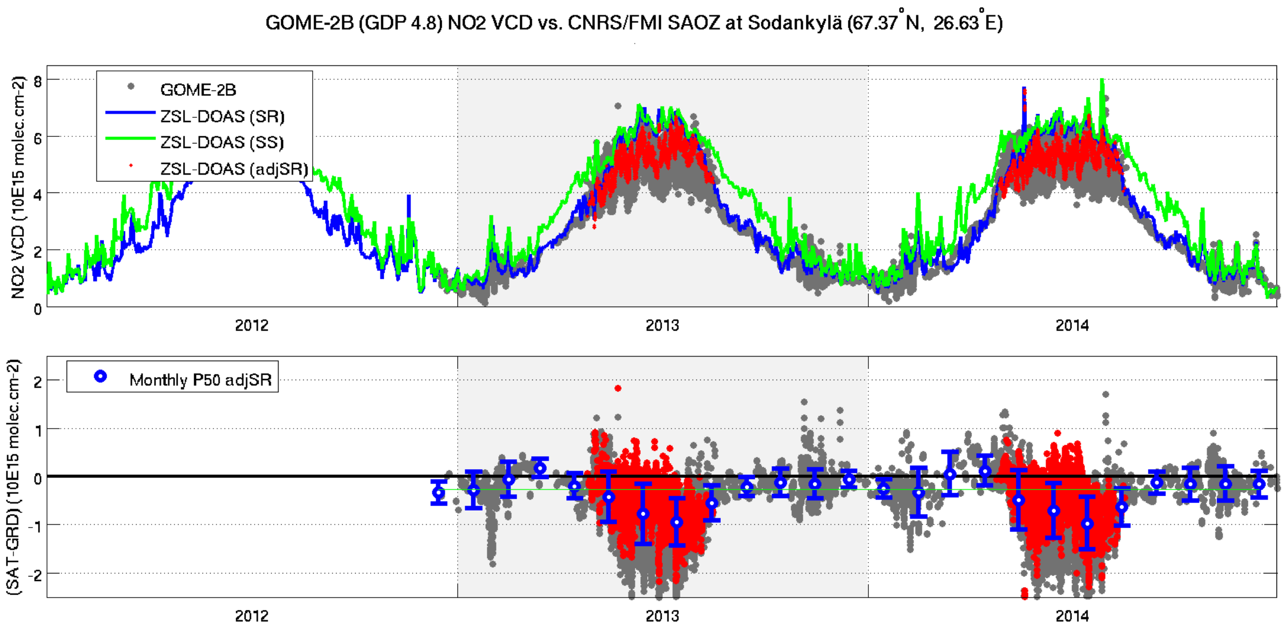

Figure E.1.4 Same as Figure E.1.2 but over the NDACC station of Sodankylä (Finland), measured by GOME-2A and GOME-2B (GDP 4.8) and by the SAOZ UVVIS spectrometer (LATMOS V3 reprocessing) operated by CNRS/FMI-ARC.

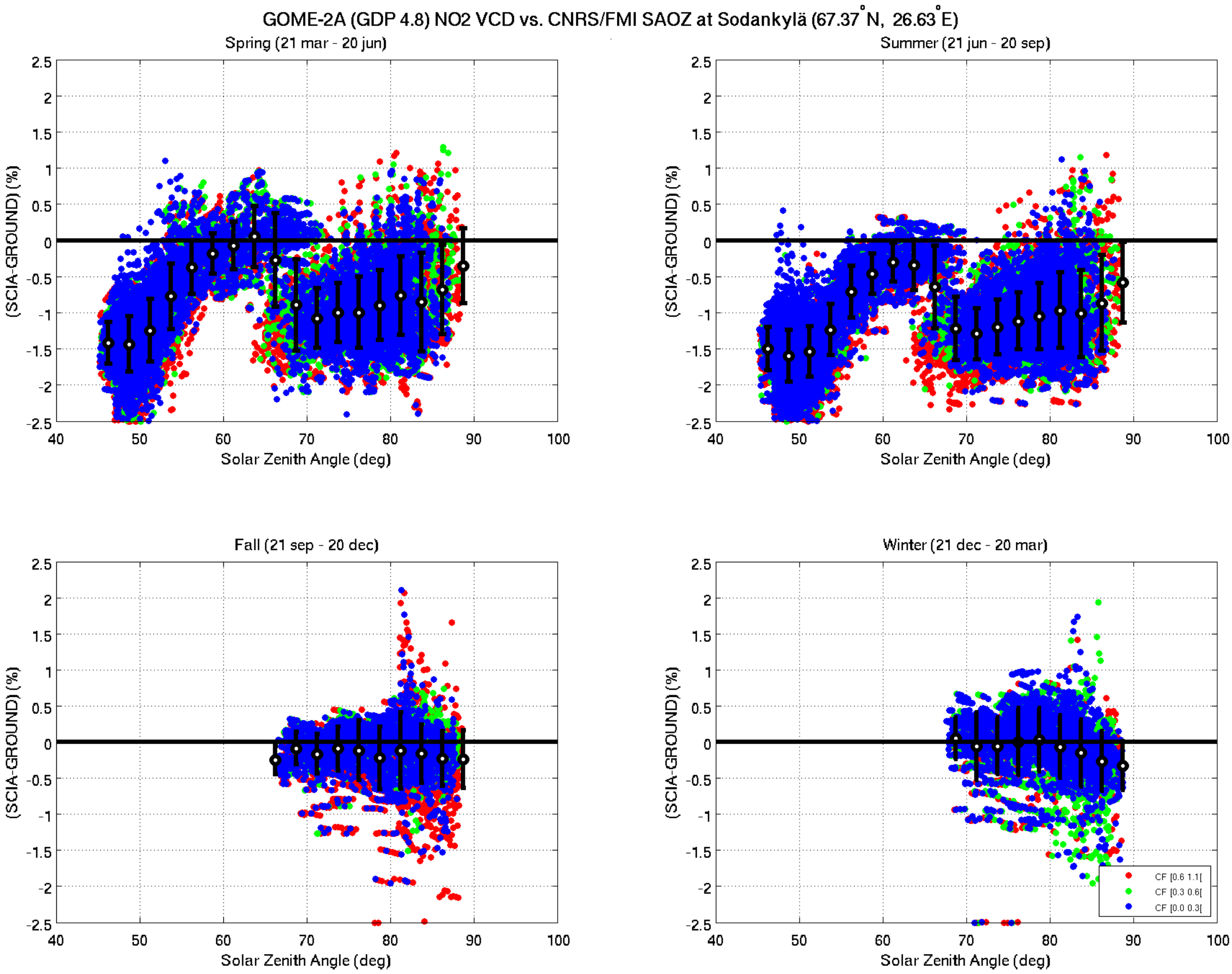

Figure E.1.4 (bis) Same GOME-2A results as in Figure E.1.4, but plotted as a function of GOME-2A solar zenith angle and separated by season.

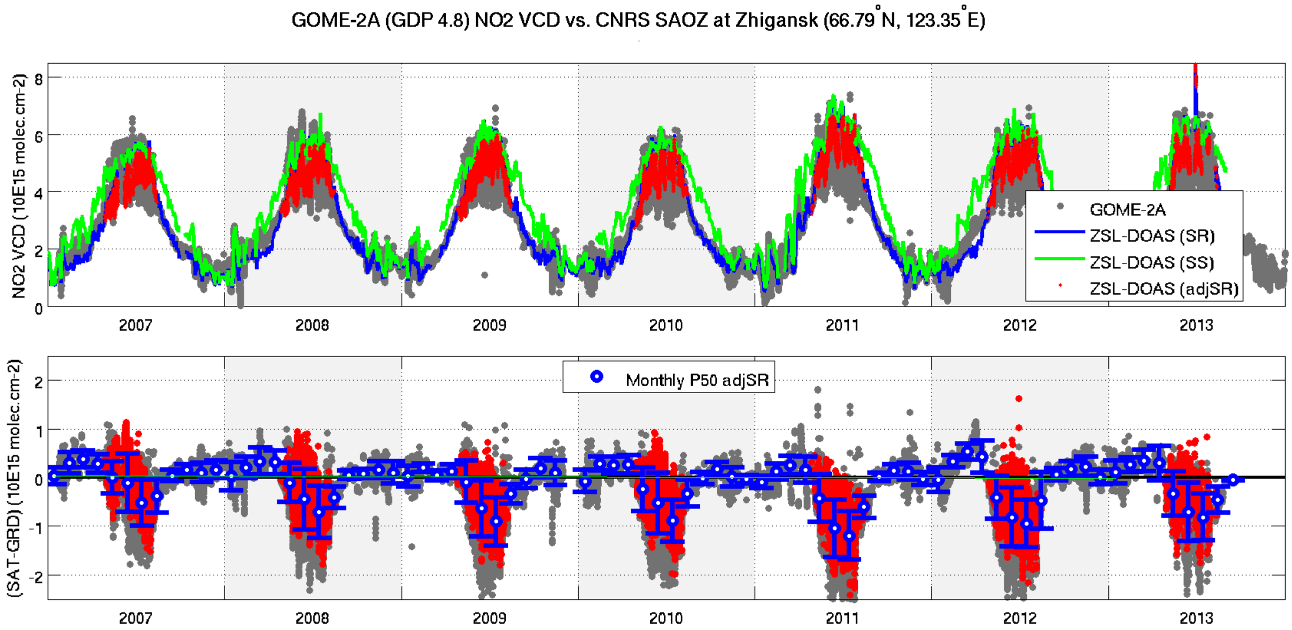

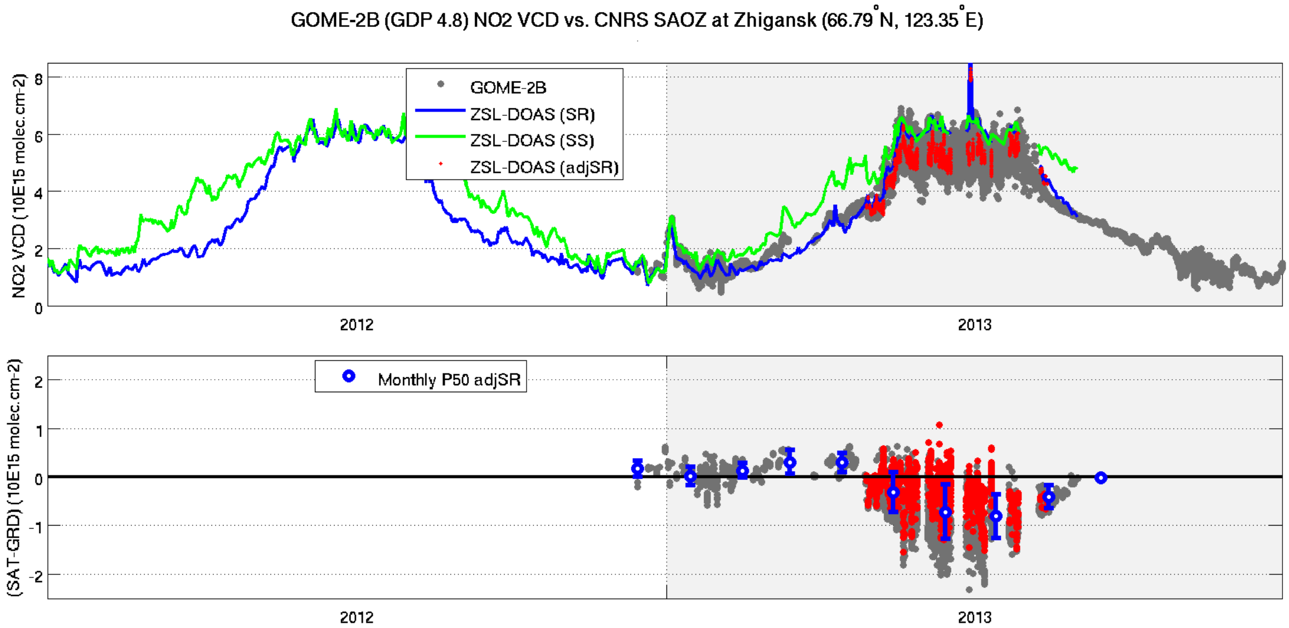

Figure E.1.5 Same as Figure E.1.2 but over the NDACC station of Zhigansk (Eastern Siberia), measured by GOME-2A and GOME-2B (GDP 4.8) and by the SAOZ UVVIS spectrometer (LATMOS V3 reprocessing) operated by CNRS/CAO.

E.1.1.2 Stratospheric NO_2 column in Northern middle latitudes

Figures E.1.6 and E.1.7 present comparisons at two NDACC middle latitude stations: Jungfraujoch (Switzerland), and O.H.P. (Southern France). These two stations are considered as background stations, only episodically affected by tropospheric pollution. The day-to-day and seasonal agreement between the satellite and NDACC data sets is remarkable, of the order of a few 10^{14} molec.cm^{-2}.

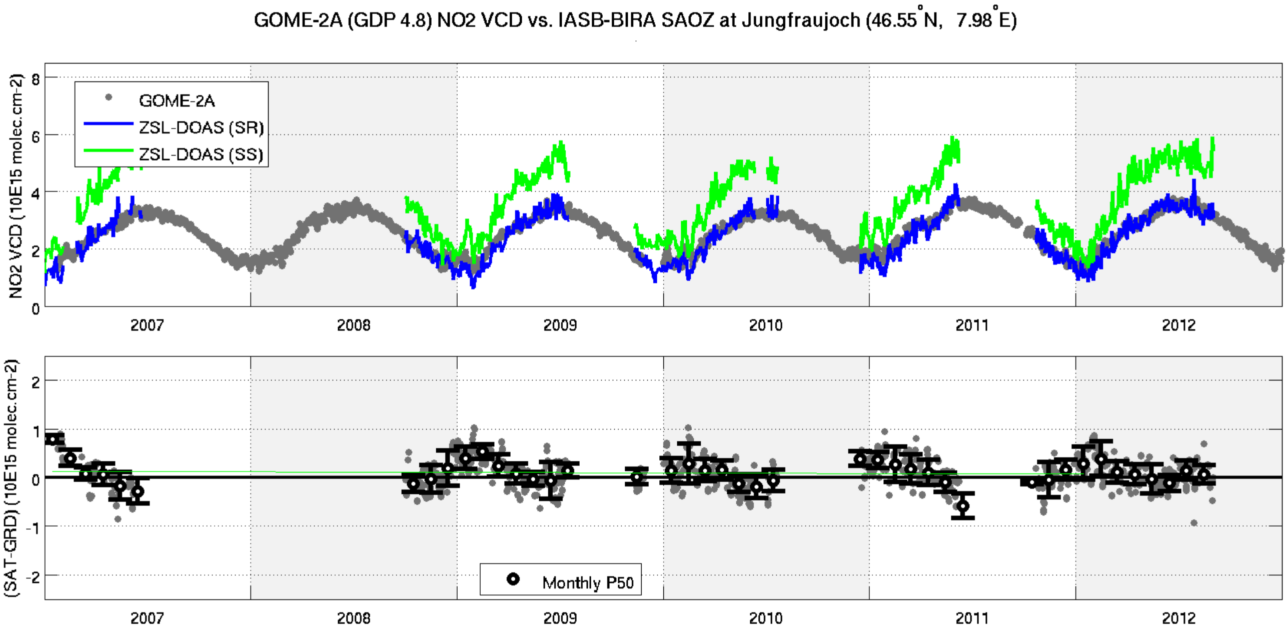

Figure E.1.6 Same as Figure E.1.2 but over the NDACC station of Jungfraujoch (Switzerland), measured by GOME-2A (GDP 4.8) and by the SAOZ UVVIS spectrometer (BIRA-IASB reprocessing) operated by BIRA-IASB. No Jungfraujoch SAOZ data available in the GOME-2B timeframe.

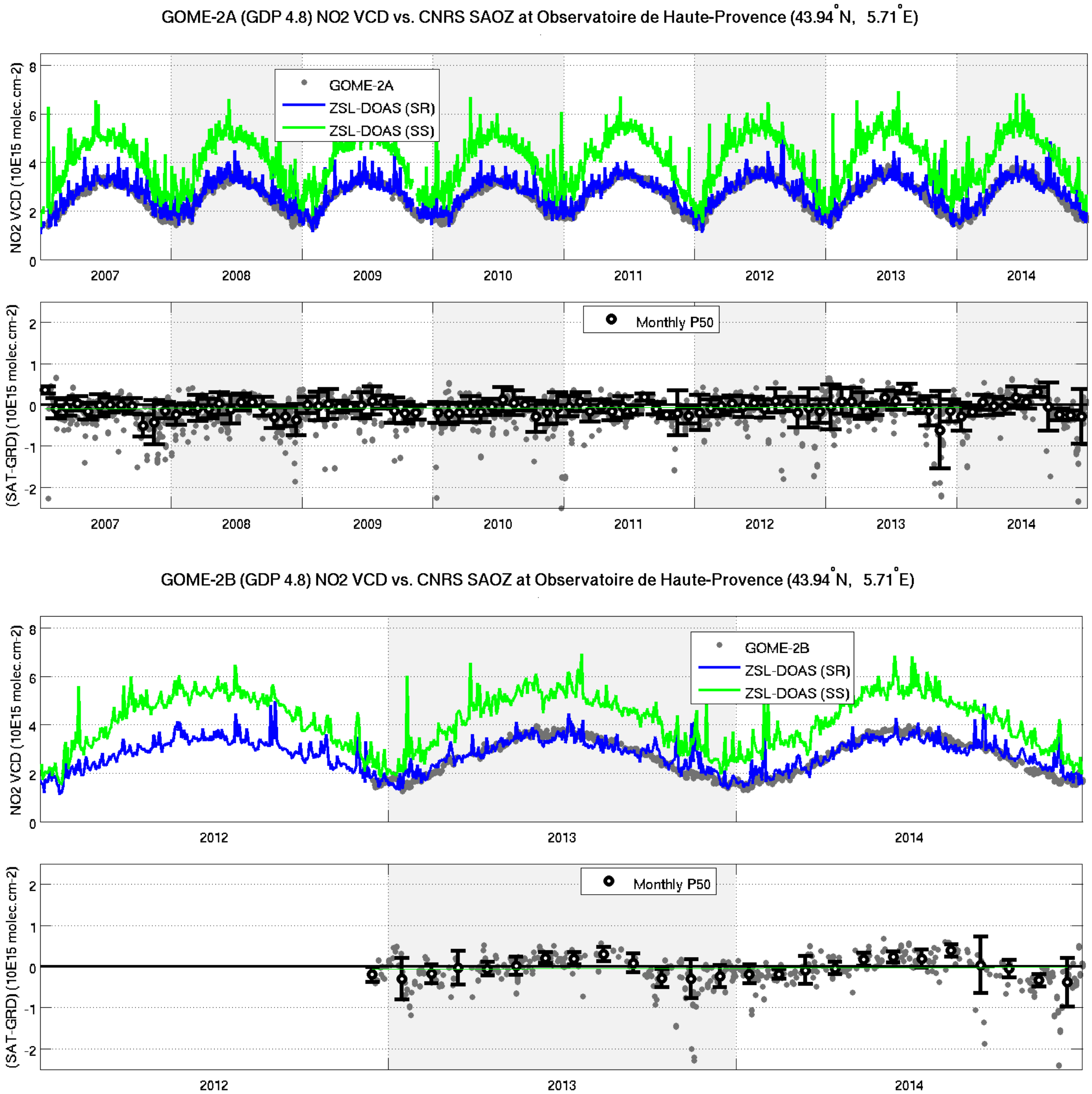

Figure E.1.7 Same as Figure E.1.2 but over the NDACC station of Observatoire de Haute Provence (O.H.P., Southern France), measured by GOME-2A and GOME-2B (GDP 4.8) and by the SAOZ UVVIS spectrometer (LATMOS V3 reprocessing) operated by CNRS/LATMOS.

E.1.1.3 Stratospheric NO_2 column in the tropics

Figures E.1.8 to E.1.10 present comparisons at three tropical stations, where only GOME-2 data with a fractional cloud cover of at least 25% have been taken into account as a first-order mask of pollution events. At Izaña (Tenerife Island, Figure E.1.8) and Saint Denis (Reunion Island, Figure E.1.9) the monthly median agreement between the two GOME-2 and the NDACC DOAS UVVIS NO_2 column data is within a few 10^{14} molec.cm^{-2}. The three instruments capture also similarly the day-to-day fluctuations. At the Brazilian station of Bauru (Figure E.1.10) a systematic low bias of $11 \cdot 10^{14}$ molec.cm^{-2} appear between the satellite and ground-based data. This bias will be observed also at all stations of the Southern middle latitudes (see next sub-section).

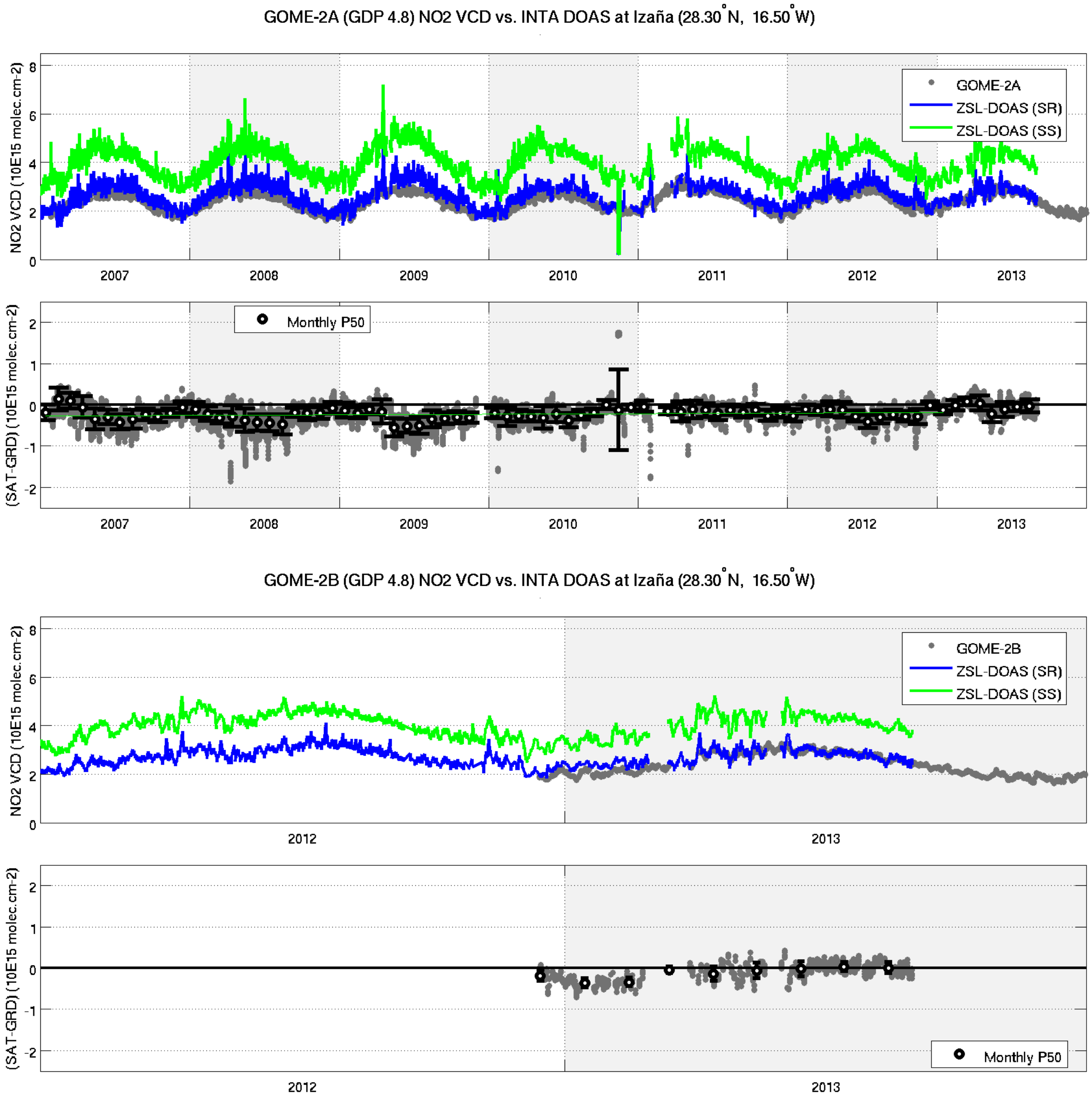

Figure E.1.8 Same as Figure E.1.2 but over the NDACC station of Izaña (Tenerife, Canary Islands), measured by GOME-2A and GOME-2B (GDP 4.8) and by the ZLS-DOAS UVVIS spectrometer operated by INTA.

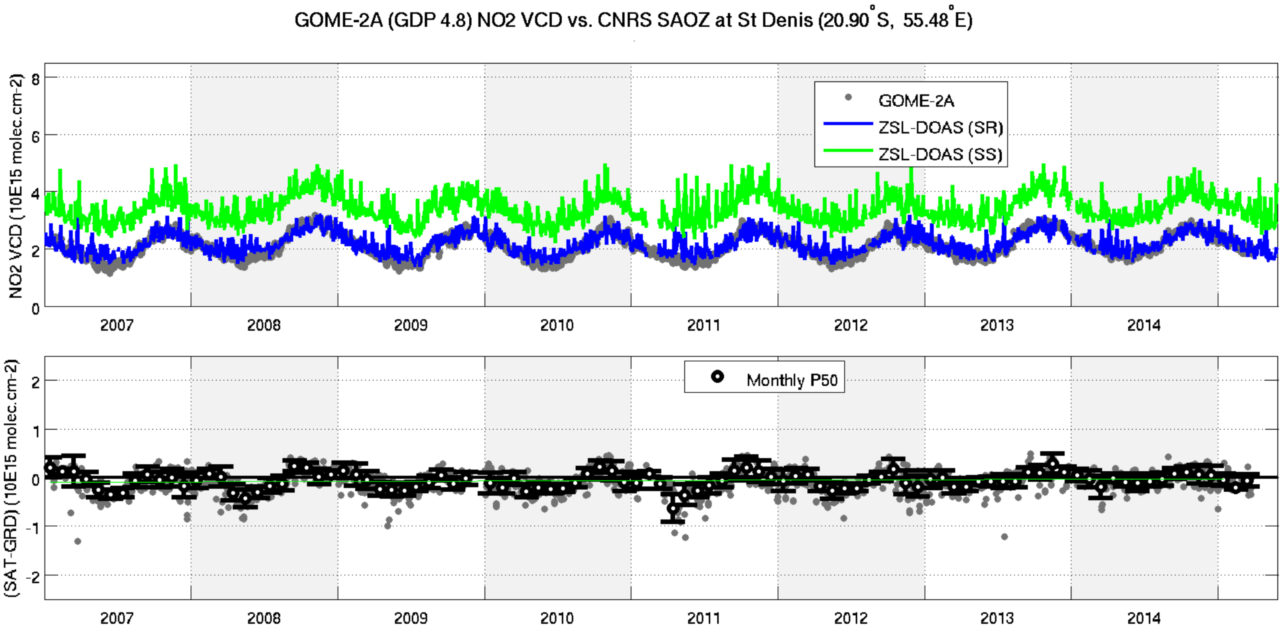

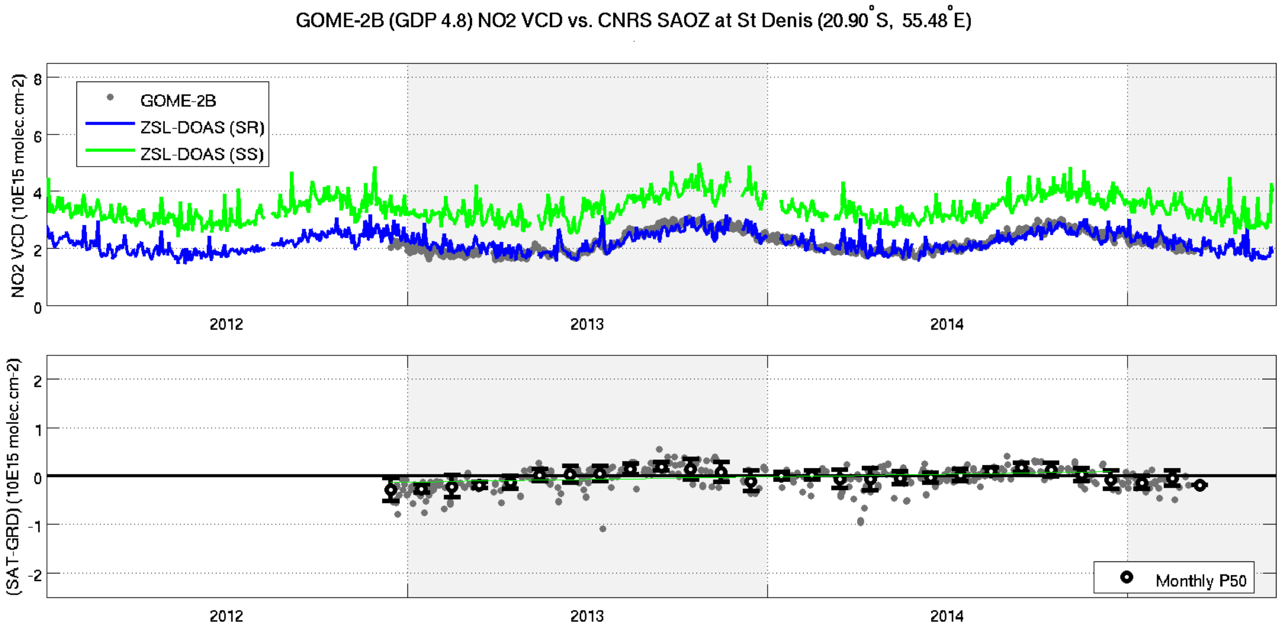

Figure E.1.9 Same as Figure E.1.2 but over the NDACC station of Saint Denis (Reunion Island), measured by GOME-2A and GOME-2B (GDP 4.8) and by the SAOZ UVVIS spectrometer (LATMOS V3 reprocessing) operated by CNRS/LACy.

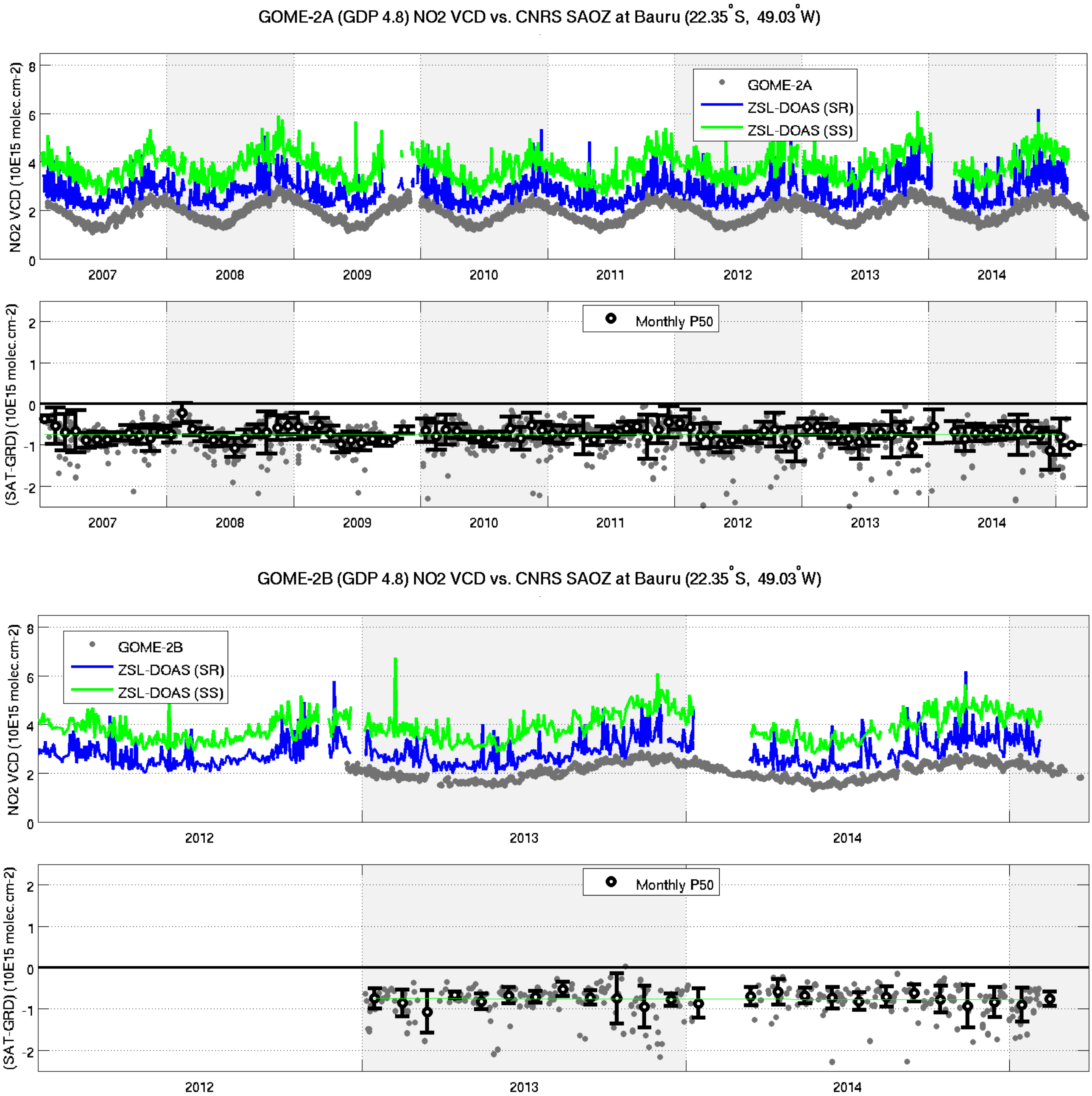

Figure E.1.10 Same as Figure E.1.2 but over the NDACC station of Bauru (Brazil), measured by GOME-2A and GOME-2B (GDP 4.7) and by the SAOZ UVVIS spectrometer (LATMOS V3 reprocessing) operated by CNRS/UNESP.

E.1.1.4 Stratospheric NO_2 column in the Southern middle latitudes

Figures E.1.11 to E.1.13 present comparisons at three NDACC stations distributed around the Southern middle latitudes (between 45° and 52°S): Lauder in New Zealand, Kerguelen in the Indian Ocean, and Rio Gallegos in Argentina. Those stations are, if never, at least rarely affected by tropospheric pollution. GOME-2A, GOME-2B and NDACC ZLS-DOAS instruments capture similarly the seasonal cycle of stratospheric NO_2, as well as monthly and day-to-day changes in stratospheric NO_2. But quantitatively, both GOME-2A and GOME-2B underestimate ground-based values by 6 to $14 \cdot 10^{14}$ molec.cm^{-2}, GOME-2B reporting slightly higher values than GOME-2A by about $1\text{-}3 \cdot 10^{14}$ molec.cm^{-2}.

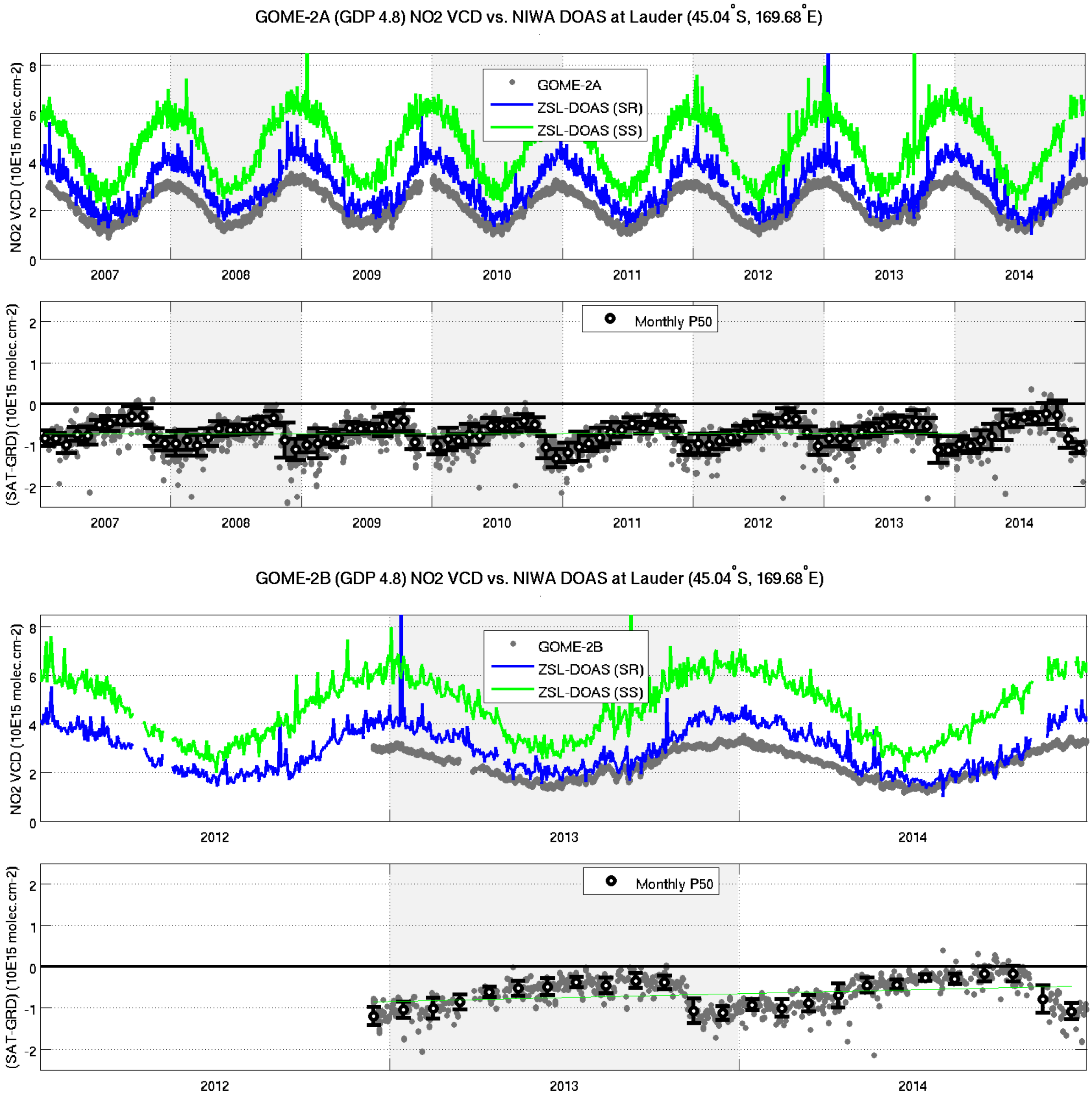

Figure E.1.11 Same as Figure E.1.2 but over the NDACC station of Lauder (New Zealand), measured by GOME-2A and GOME-2B (GDP 4.8) and by the ZLS-DOAS UVVIS spectrometer operated by NIWA.

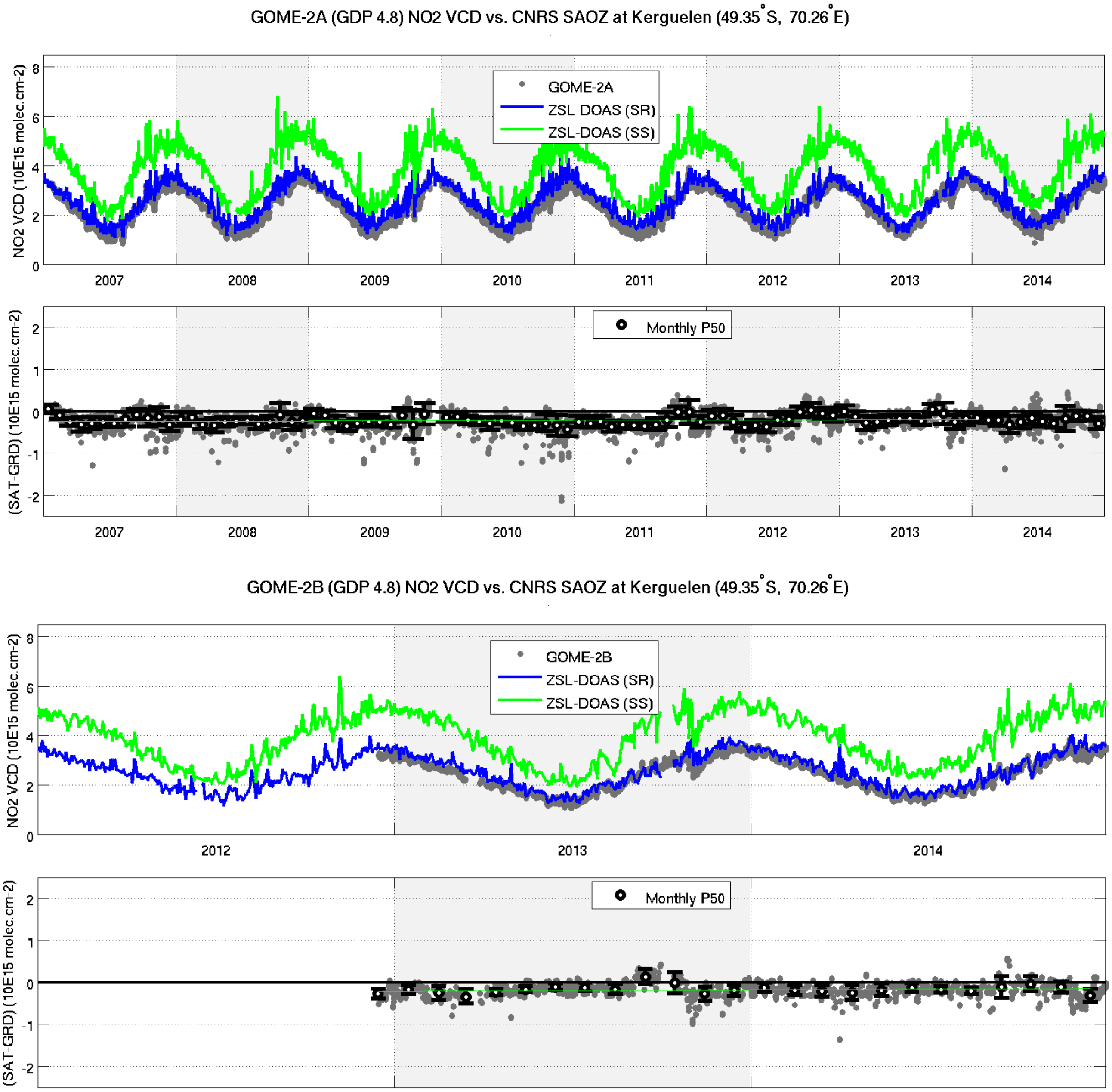

Figure E.1.12 Same as Figure E.1.2 but over the NDACC station of Kerguelen Islands (Indian Ocean), measured by GOME-2A and GOME-2B (GDP 4.8) and by the SAOZ UVVIS spectrometer (LATMOS V3 reprocessing) operated by CNRS/LATMOS.

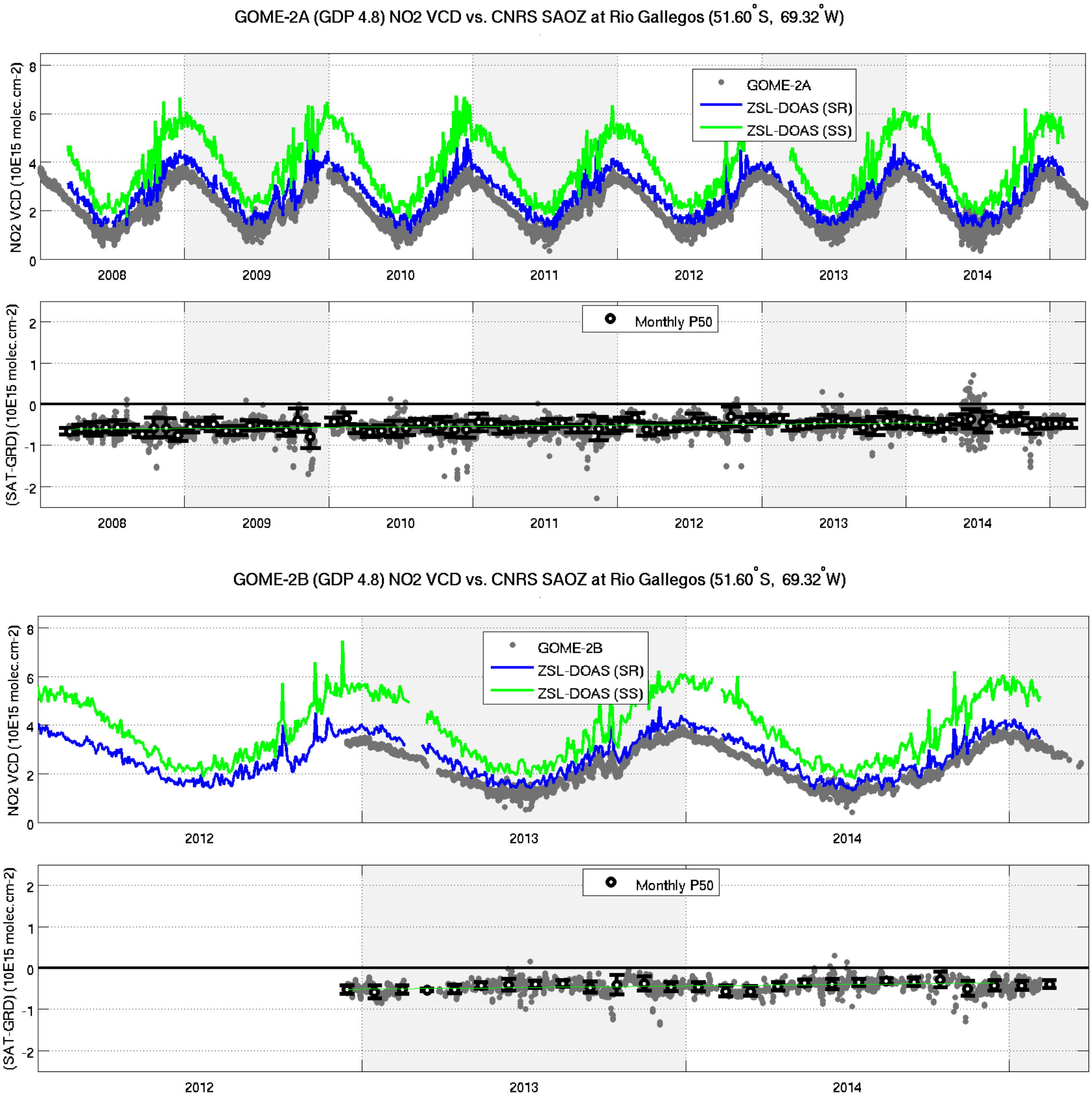

Figure E.1.13 Same as Figure E.1.2 but over the NDACC station of Rio Gallegos (Argentina), measured by GOME-2A and GOME-2B (GDP 4.8) and by the SAOZ UVVIS spectrometer (LATMOS V3 reprocessing) operated by CNRS/LATMOS.

E.1.1.5 Stratospheric NO_2 column in Antarctica

Figures E.1.14 reports comparisons at the NDACC Antarctic station of Dome Concorde. This station is free of any tropospheric pollution. During polar day, GOME-2 data are distributed in two tracks: one orbit of GOME-2 data acquired in the mid-morning, under moderate SZA, and a scond orbit of GOME-2 data closer to midnight sun conditions, acquired at larger SZA. At the end of summer the midnight sun track disappears and the solar local time difference between mid-morning GOME-2 data and twilight ground-based data is too large to avoid unbiased comparisons. In fall this local time difference vanishes progressively. To avoid interferences of diurnal cycle effects with the comparison results, only GOME-2 data acquired at SZA larger than 75° have been selected here to draw statistical conclusions. Figure E.1.15 shows that at such large SZAs the agreement between the satellites and the NDACC data falls to within 0 to $-5 \cdot 10^{14}$ molec.cm^{-2}. This slight negative bias remains small in comparison with the larger systematic bias observed at Southern middle latitudes. Looking only at short term and seasonal signatures and not at the bias, Figure E.1.14 shows that the two satellites and the ground-based spectrometer capture similarly day-to-day fluctuations in stratospheric NO_2 and its annual cycle.

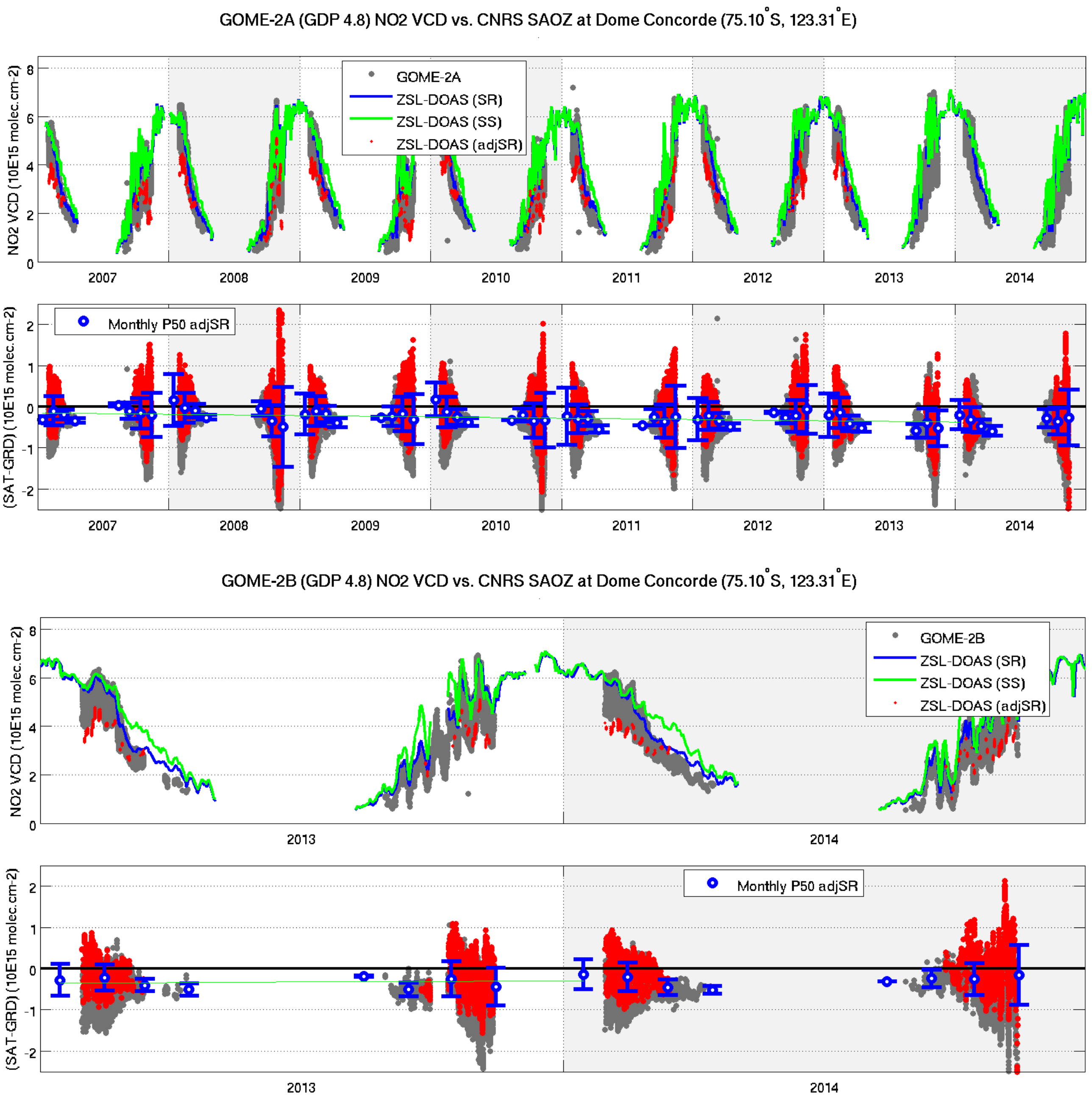

Figure E.1.14 Same as Figure E.1.2 but over the NDACC station of Dome Concorde (Antarctica), measured by GOME-2A and GOME-2B (GDP 4.8) and by the SAOZ UVVIS spectrometer (LATMOS V3 reprocessing) operated by CNRS/LATMOS.

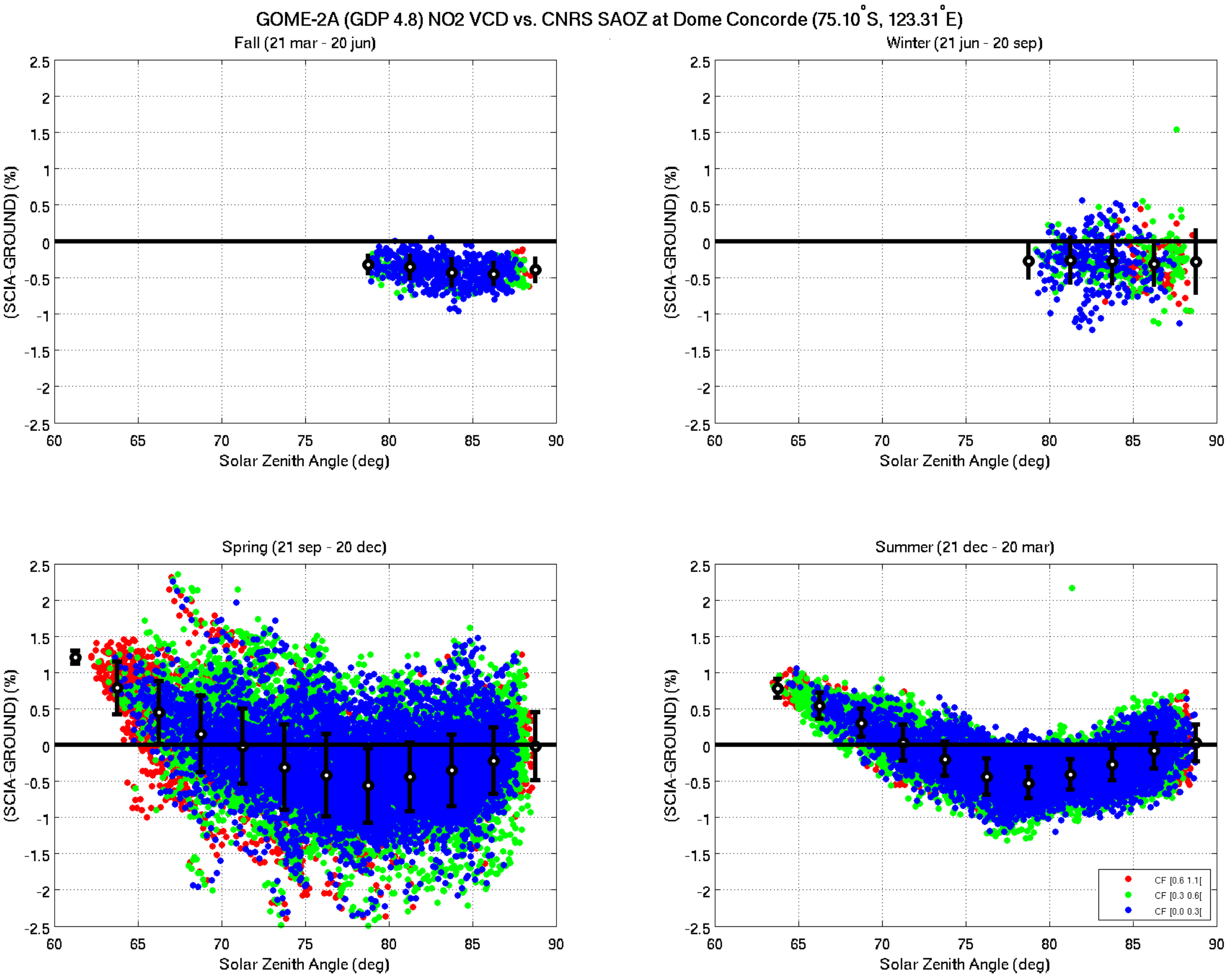

Figure E.1.15 Absolute difference between GOME-2A (GDP 4.8) and ground-based ZLS-DOAS SAOZ (LATMOS V3 processing) NO_2 column data at the NDACC Antarctic station of Dome Concorde, sorted now by season and displayed as a function of GOME-2 solar zenith angle.

E.1.2 Stratospheric comparisons summary

Based on the data filtering and selection described in the previous sub-sections (application or not of cloud mask, selection on SZA at polar stations etc.) the comparison results can be synthesized as in Figures E.1.16 to E.1.19. Figure E.1.16 shows the interannual median difference of the GOME-2A (upper plot) and GOME-2B (lower plot) minus ground-based zenith-sky column data, as a function of the latitude of the station. GDP 4.8 results are shown in red, while GDP 4.7 results are shown in green. Uncertainty estimates are repsented as areas (grey area for GDP 4.8, red contour for NDACC/UVVIS ZLS). Figures E.1.17 to E.1.19 show, for three latitude zones, the same results but as a function of GOME-2A/B cloud fraction (upper graph), and also as a function of GOME-2A/B solar zenith angle and separated by season (four graphs). From these summary plots and those reported in previous sub-sections it can be concluded that:

- With respect to 20 NDACC ZLS-DOAS UV-visible spectrometers, the MetOp-A GOME-2A and MetOp-B GOME-2B NO_2 column data set available at present time, processed with both GDP 4.7 and GDP 4.8, offer the same level of consistency. Variations of the stratospheric NO_2 column, from day-to-day fluctuations and to the annual cycle, are captured consistently by all measurement systems. The agreement between satellite data and network data does not depend significantly on GOME-2 solar zenith angle and fractional cloud cover.

- In most of the cases, and for both GDP 4.7 and 4.8 processors, GOME-2B reports NO_2 column values slightly lower than GOME-2A, by about $1\text{-}3\cdot10^{14}$ molec.cm^{-2}, which is close to the combined uncertainty of ground-based NDACC measurements and of the comparison method.
- In most of the cases, GDP 4.8 reports NO_2 column values slightly higher than GDP 4.7, by about $1\text{-}3\cdot10^{14}$ molec.cm^{-2}, which is again close to the combined uncertainty of ground-based NDACC measurements and of the comparison method.
- Over the middle latitudes of the Northern Hemisphere (Aberystwyth, Jungfraujoch, O.H.P.), both satellites and both processor versions offer, with respect to NDACC ZLS-DOAS data, a comparable good agreement of a few 10^{14} molec.cm^{-2} on a monthly median basis.
- Over the Southern Hemisphere both GOME-2 instruments and both GDP processor versions report lower values than NDACC ZLS-DOAS spectrometers, this systematic bias starting at the Brazilian station of Bauru (22°S), propagating at four contributing middle latitude stations in the Pacific (New Zealand, Kerguelen, Macquarie) and in Argentina (Rio Galegos), and vanishing at Antarctic stations: within combined uncertainties at Dumont d'Urville, Dome Concorde, Rothera and Arrival Heights.

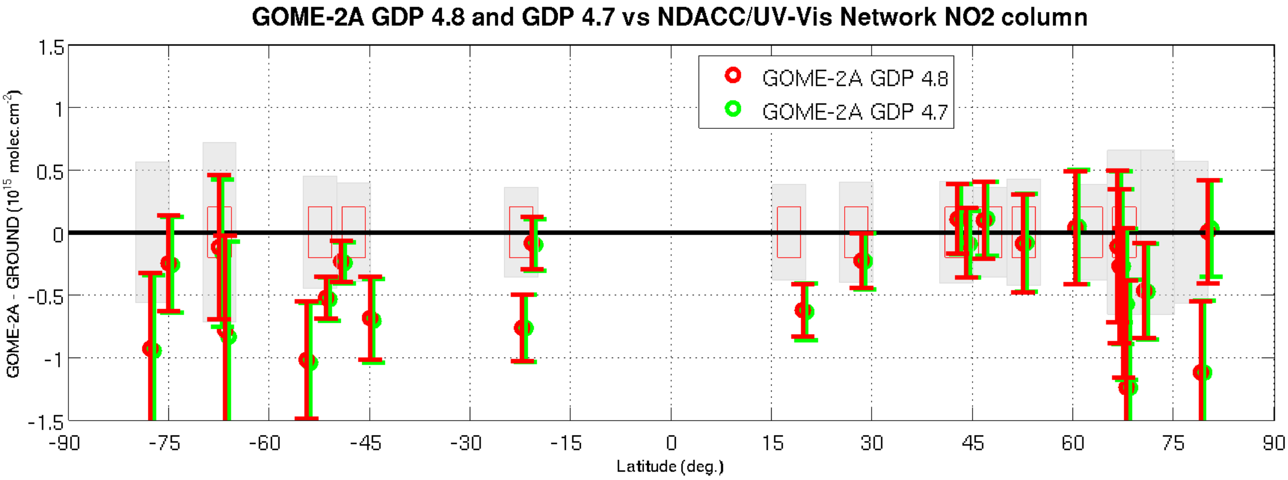

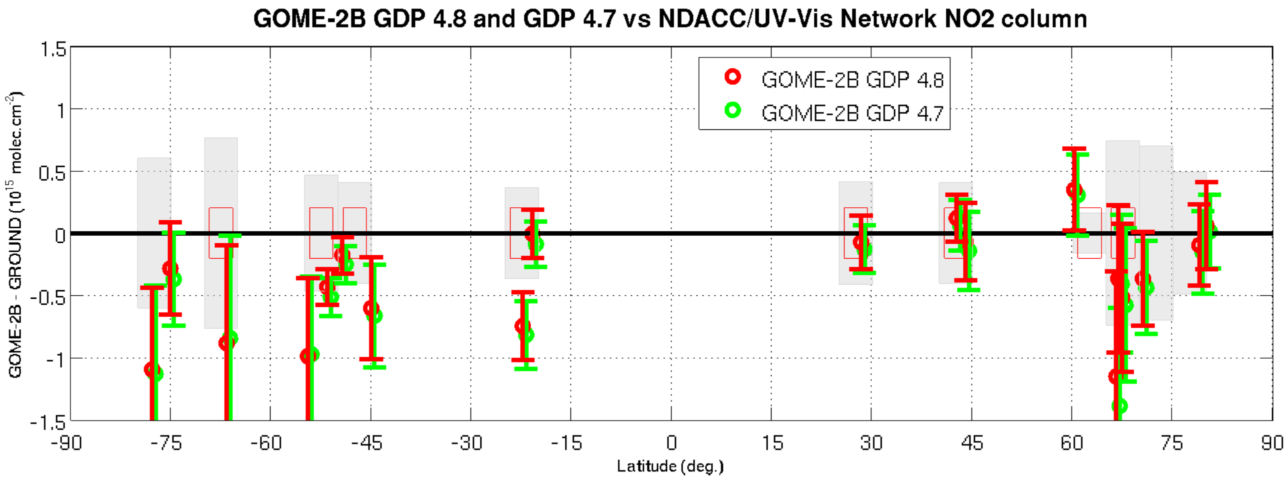

Figure E.1.16 Pole-to-pole overview of the median absolute difference at each station between NO_2 column data reported by GOME-2A/B (GDP 4.7 and 4.8) and by 20 NDACC ground-based ZLS-DOAS spectrometers. Grey areas show a median estimate of the GOME-2 uncertainty reported in GDP 4.8 data files; red rectangles show a median estimate of the NDACC NO_2 column data uncertainty.

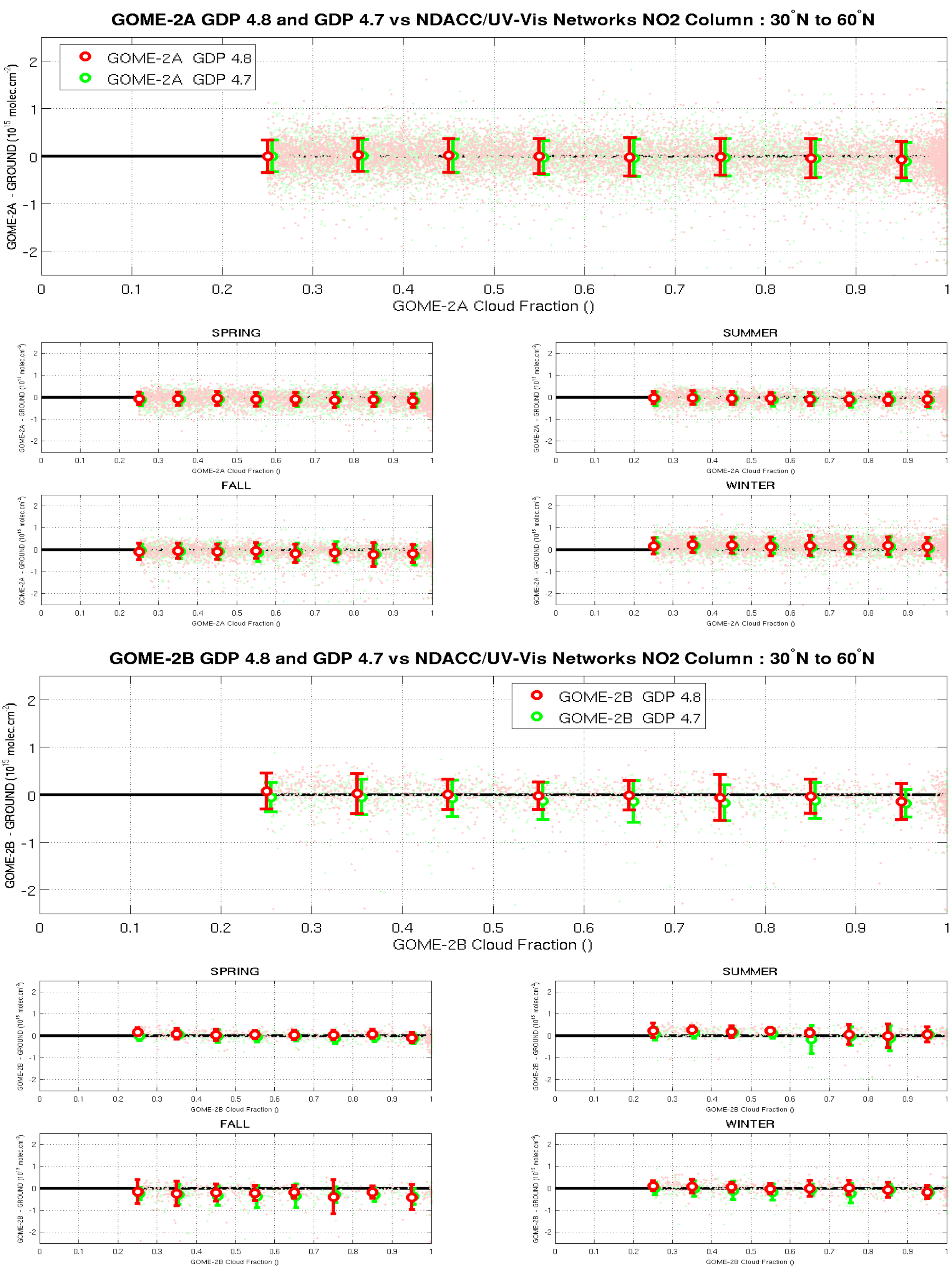

Figure E.1.17 Cloud fraction and solar zenith angle dependence of the absolute difference between NO_2 column data reported by GOME-2A/B (GDP 4.8 and 4.7) and by NDACC ground-based ZLS-DOAS spectrometers in the Northern middle latitudes (30°N – 60°N). Top pannel: GOME-2A vs. NDACC/UVVIS; bottom pannel: GOME-2B vs. NDACC/UVVIS.

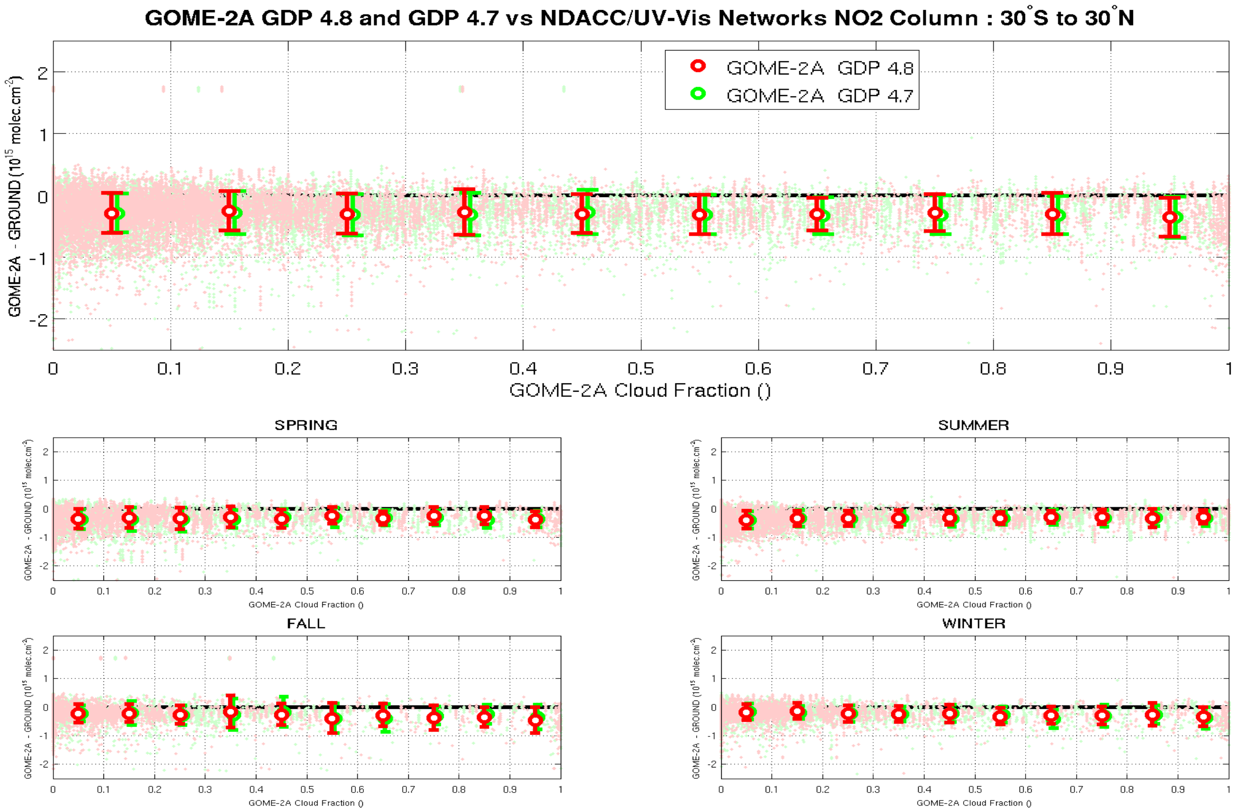

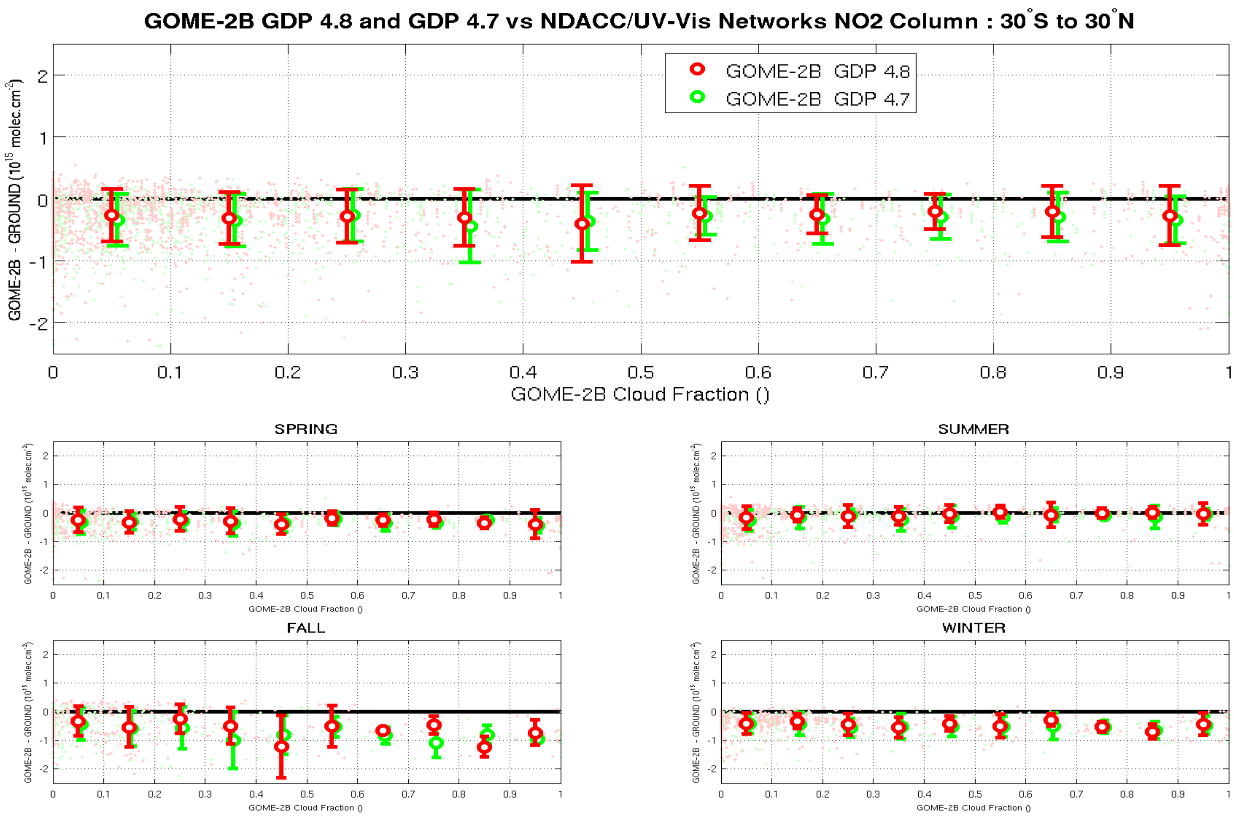

Figure E.1.18 Same as Figure E.1.17, but at low latitudes (30°N – 30°S).

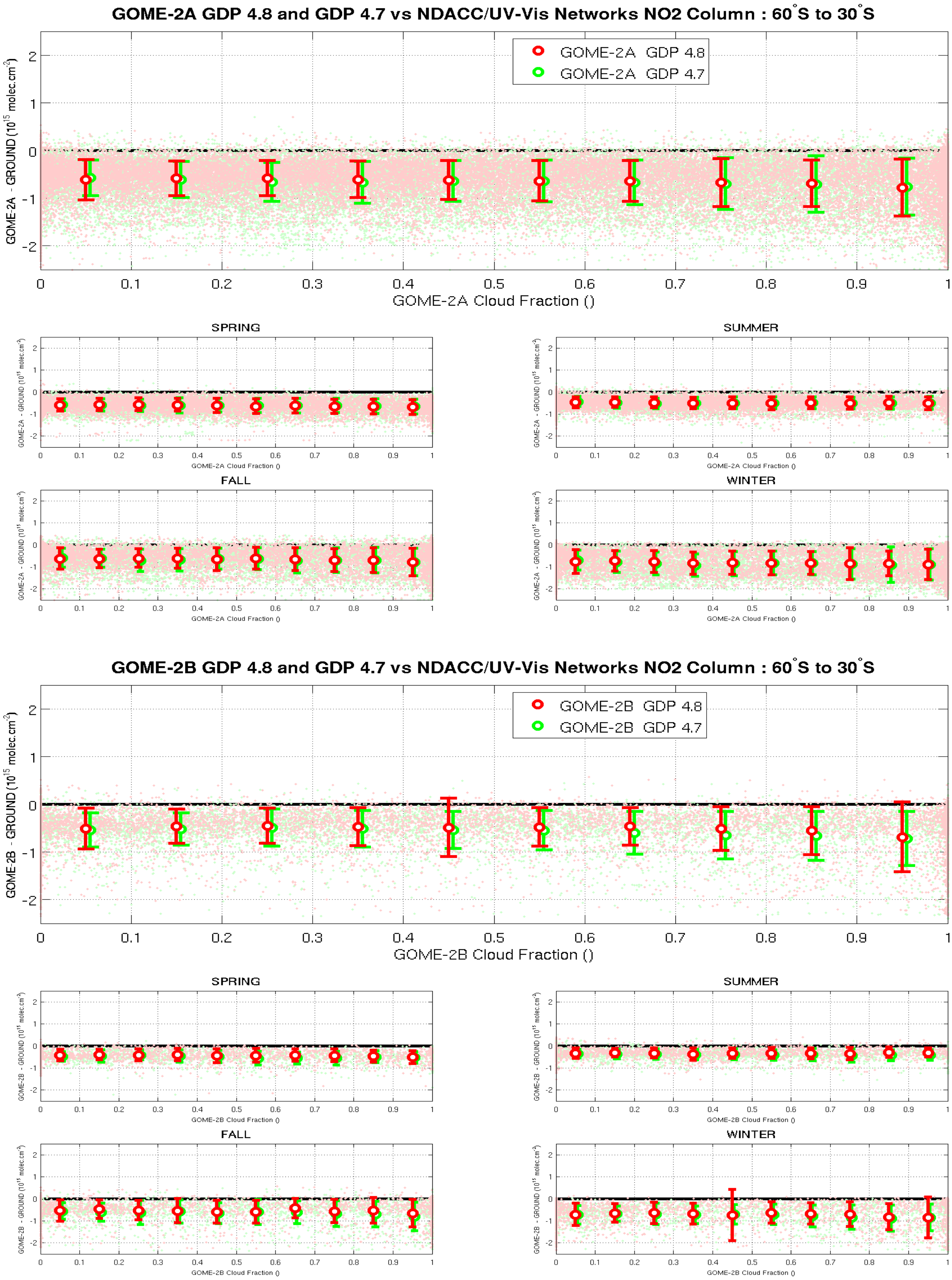

Figure E.1.19 Same as Figure E.1.17 and Figure E.1.18, but at southern middle latitudes (30°S – 60°S).

E.2. Tropospheric Vertical Column

The direct comparison of GOME-2 tropospheric NO_2 with correlative sources is the last step of this validation exercice. The methodology and the techniques for the comparison with ground-based MAXDOAS correlative data have been developed for Metop-A and presented in details in the Metop-A validation report (NO_2 O3MSAF GOME-2A VR 2011) and applied to MetOp-B data (NO_2 O3MSAF GOME-2B VR 2013). Since then, the comparisons are continuously updated in time and by increasing the number of MAXDOAS stations. In 2014 a large validation exercice was initiated by BIRA with the collection of more than 20 MAXDOAS datasets from partners all over the world (AUTH, BIRA-IASB, Chiba University, IUP-Bremen, IUP-Heidelberg, JAMSTEC, KNMI and Mainz), sampling very different pollution conditions, and the results were presentated at the EUMETSAT conference and summarized in a proceeding (Pinardi et al., 2014). The update of such a comparison, with the reprocessed GDP 4.8 dataset is presented in the following section.

Moreover, the different figures for BIRA MAXDOAS stations are also grouped in Annex H.1, showing in more details the results for OHP, Uccle, Bujumbura, Xianghe and Beijing stations for both GDP 4.8 and 4.7. Figures with the daily and monthly time-series and corresponding scatter plots, as well as absolute and relative differences between GOME-2 A and B datasets and MAXDOAS ground-based data are shown in the annex and results are summarized in Table E.2.

E.2.1 Comparison against ground-based MAX-DOAS columns data

MAXDOAS datasets

Multi-axis DOAS instruments (MAXDOAS) measure scattered sunlight under different viewing elevations from the horizon to the zenith. The observed light travels a long path in the lower troposphere (the lower the elevation angle, the longer is the path) and the different elevations of one scan have the same path in the stratosphere. The stratospheric contribution can thus be removed by taking the difference in SCD between an off-axis elevation and a zenith reference. Tropospheric absorbers are measured all day long generally up to 85° of solar zenith angle (SZA). In addition, MAXDOAS instruments can provide low resolution vertical profiles (degrees of freedom DOF <3) of NO_2 and aerosol in the lowermost troposphere (Friess et al., 2006; Clemer et al., 2010; Wagner et al., 2011; Irie et al., 2011; Hendrick et al., 2014).

In the past decade, MAXDOAS instruments have been deployed worldwide as part of small research networks, such as the BIRA-IASB (http://uv-vis.aeronomie.be/groundbased/), BREDOM (http://www.doas-bremen.de/groundbased_data.htm), Heidelberg, Mainz and MADRAS (MAX-DOAS instruments in Russia and ASia) networks (Kanaya et al., 2014).

During the EC FP6 GEOMON (Global Earth Observation and Monitoring of the atmosphere), the EC FP7 NORS (Demonstration Network Of ground-based Remote Sensing Observations in support of the GMES Atmospheric Service, http://nors.aeronomie.be/) and the EC FP7 QA4ECV (http://www.qa4ecv.eu/) projects, a strong focus has been put on tropospheric NO_2 column and profile data product characterization and harmonization, for a limited number of pilot stations. Recent efforts have also been made to intercompare MAXDOAS instruments, in particular during the CINDI campaign (Piters et al., 2012), and to formulate recommendations for SCD retrieval (Roscoe et al., 2010). The inclusion of MAXDOAS instruments in the NDACC network is under progress, following efforts recently done in the NORS project to harmonize and automatize data processing, and continued within the QA4ECV framework.

The accuracy of the MAXDOAS technique depends on the SCD retrieval noise, the uncertainty on the NO_2 absorption cross-sections and most importantly on the uncertainty of the tropospheric AMF calculation. A summary of all the contributing error sources can be found in Haze et al. (2013). The estimated total error on NO_2 VCD is of the order of 7-17% in polluted conditions (e.g. Irie et al., 2008; Wagner et al., 2011; Hendrick et al., 2014; Kanaya et al., 2014), including both random (around 3 to 10% depending on the instruments) and systematic (11 to 14%) contributions.

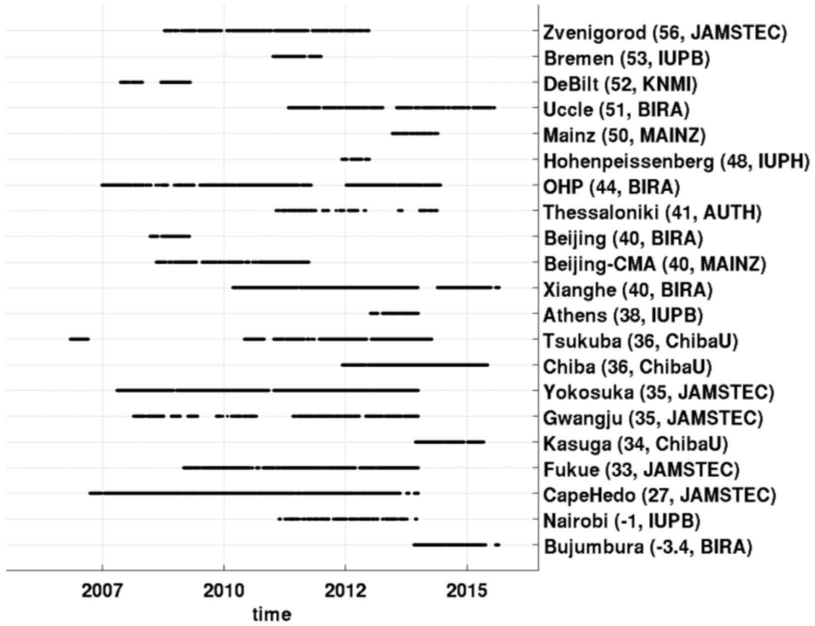

Figure E.2.1 List of MAXDOAS instruments used in this study and their temporal coverage.

The different MAXDOAS instruments used in this study are presented in Figure E.2.1. With this dataset, a good temporal coverage is assured, with stations measuring from one year to almost the whole Metop-A time length. A good coverage of the Northern Hemisphere is also assured, with several stations in Europe and Asia, but only 2 stations measured in the Southern Hemisphere: Bujumbura and Nairobi. However, as briefly described in Table E.1, this dataset is so far only an aggregate of national/project-based networks, and there is no “real” harmonized yet. While recommendations defined during the CINDI campaign for the SCD retrieval (Roscoe et al., 2010) have generally been followed by the data-providers, vertical columns and/or profiles have been obtained using a combination of different approaches. These range from the simple geometrical approximation used to determine vertical columns (Honninger et al., 2004, Brinksma et al., 2008, Ma et al., 2013) to more elaborated profiling algorithms exploiting the full information content of the MAXDOAS technique. Generally speaking, two families of MAXDOAS algorithms coexist currently: (1) vertical profile inversion algorithms using optimal estimation methods (Friess et al., 2006, Clémer et al 2010, Hendrick et al., 2014), and (2) algorithms based on a parameterization of the vertical profile using analytical functions constrained by a few parameters (Irie et al., 2008, Vlemmix et al., 2010, Wagner et al., 2011). Both approaches provide vertical profiles in the 0-4 km altitude range with a DOF between 1.5 and 3. Intercomparison studies are currently ongoing (e.g. Vlemmix et al., 2015 and Friess et al. in prep., Wittrock et al. in prep.) showing that both approaches lead to consistent results in term of vertical columns but also to differences in terms of profile shapes, stability and information content extraction (Vlemmix et al., 2015).

Table E.1: Description of the different MAXDOAS ground-based NO_2 datasets used in this study and adopted retrieval strategies.

MAXDOAS Group and stations	**Retrieval type**	**Reference**
AUTH: Thessaloniki	Tropospheric NO_2 VCD with geom. approx.	Kouremeti et al., 2013
BIRA-IASB: Beijing, Bujumbura, Xianghe, Uccle, OHP	Tropospheric NO_2 VCD and profiles with optimal estimation profiling	Clémer et al., 2010; Hendrick et al., 2014
ChibaU: Chiba, Kasuga, Tsukuba	Tropospheric NO_2 VCD and profiles with parameterized profiles	Irie et al., 2011; Irie et al., 2012
IUPB: Athens, Nairobi	Tropospheric NO_2 VCD with geom. approx.	Wittrock et al. 2004
Bremen	Tropospheric NO_2 VCD and profiles with optimal estimation profiling	Peters et al. 2012
IUPH: Hohenpeissenberg	Tropospheric NO_2 VCD and profiles with optimal estimation profiling	Yilmaz 2012
JAMSTEC: Cape Hedo, Fukue, Gwangju, Yokosuka, Zvernigorod	Tropospheric NO_2 VCD and profiles with parameterized profiles	Kanaya et al., 2014 http://ebcrpa.jamstec.go.jp/maxdoashp/
KNMI: De Bilt	Tropospheric NO_2 VCD with fixed profile shape	Vlemmix et al., 2010
MAINZ: Beijing-CMA, Mainz	Tropospheric NO_2 VCD with geom. approx.	Ma et al., 2013

Tropopsheric NO_2 comparisons

For the comparison, the GOME-2 GDP 4.8 data are extracted within 50 km of the different stations listed in Figure E.2.1 and only cloud free pixels (cloud fraction < 20%) and positive VCD_{topo} are selected. The mean value is then calculated for each day. For the ground-based MAXDOAS data, an optional filtering is performed following partners recommendations (on error, cloud flags, color index, etc.) before interpolation at the satellite overpass time. Daily and monthly comparisons are performed, and an overview of the time-series of tropospheric NO_2 columns from GOME-2 GDP 4.8 and MAXDOAS for most of the stations is presented in Figure E.2.2.

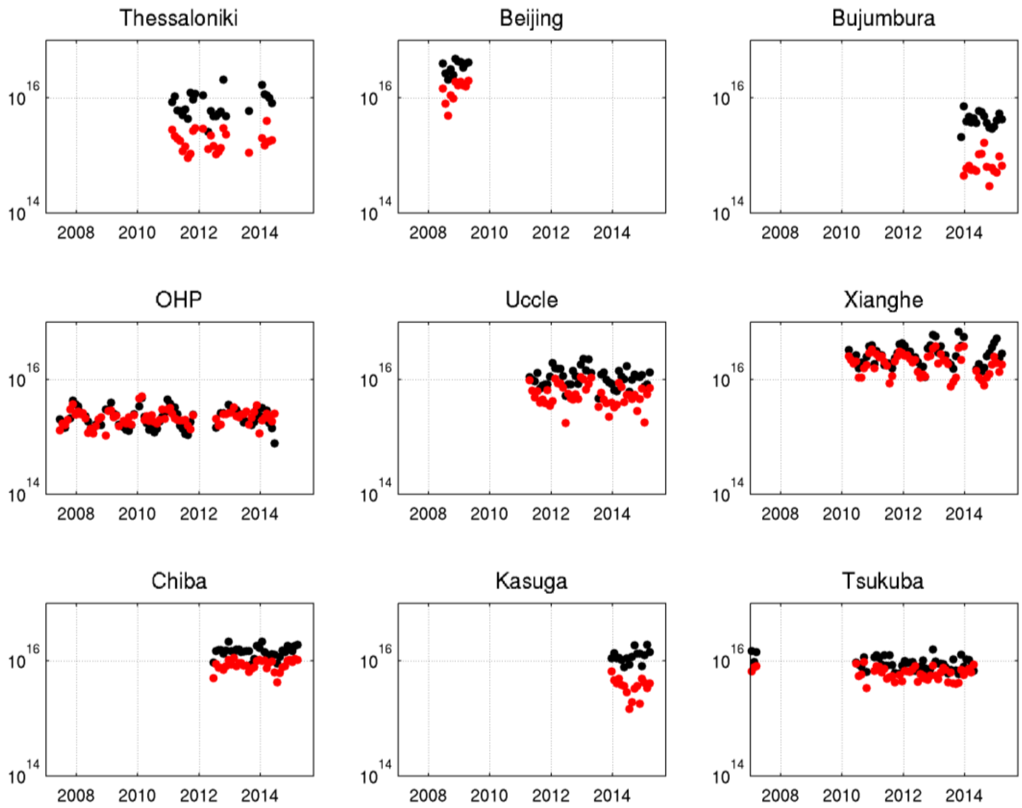

Figure E.2.2 Tropospheric NO_2 column time series comparison GOME-2 GDP 4.8 (red) and the ground-based MAXDOAS data (black), between January 2007 and August 2015. The y-axis (the same for every subplot) is a logarithmic scale from 1×10^{14} to 1×10^{17} molec/cm².

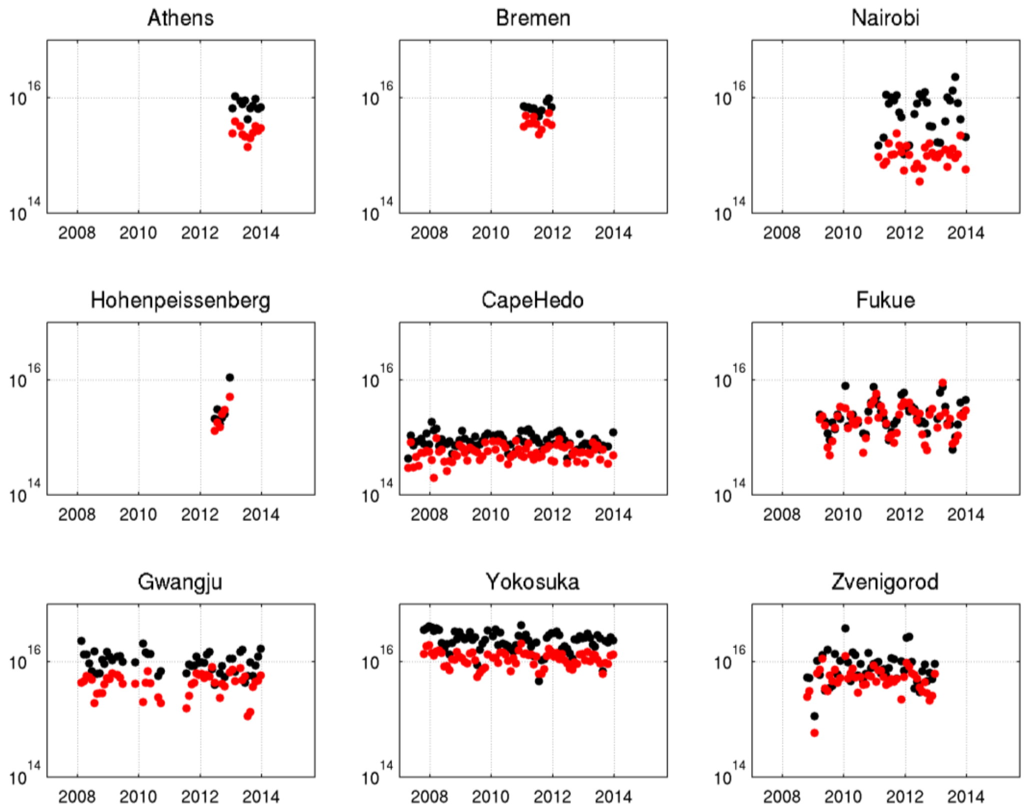

Figure E.2.2 cont.

As for comparisons performed in Pinardi et al. (2014) for GDP 4.7 data, pollution episodes are generally well captured by GOME-2 and the monthly averaged comparisons show consistent seasonal variations, with high NO_2 in winter and low NO_2 in summer. Results depend strongly on the location: excellent agreement is obtained for some stations (e.g., Xianghe, OHP, Uccle, Fukue, Kasuga, De Bilt), while larger differences show up at other stations (e.g., Beijing, Yokosuka, Gwangju, Thessaloniki). In such cases, GOME-2 tend to systematically display smaller columns than ground-based MAXDOAS measurements. The same conclusion can be drawn when inspecting correlation plots representing GOME-2 data against MAXDOAS values for all twenty stations (see Figure E.2.3). A global correlation coefficient of 0.84 is obtained from this comparison, and a slope of about 0.45. Note that these numbers can not be compared directly to results of Pinardi et al. (2014) performed on GDP 4.7, because of updated ground-based time-series covering 2014 and 2015 and inclusion of some additional stations in this exercise.

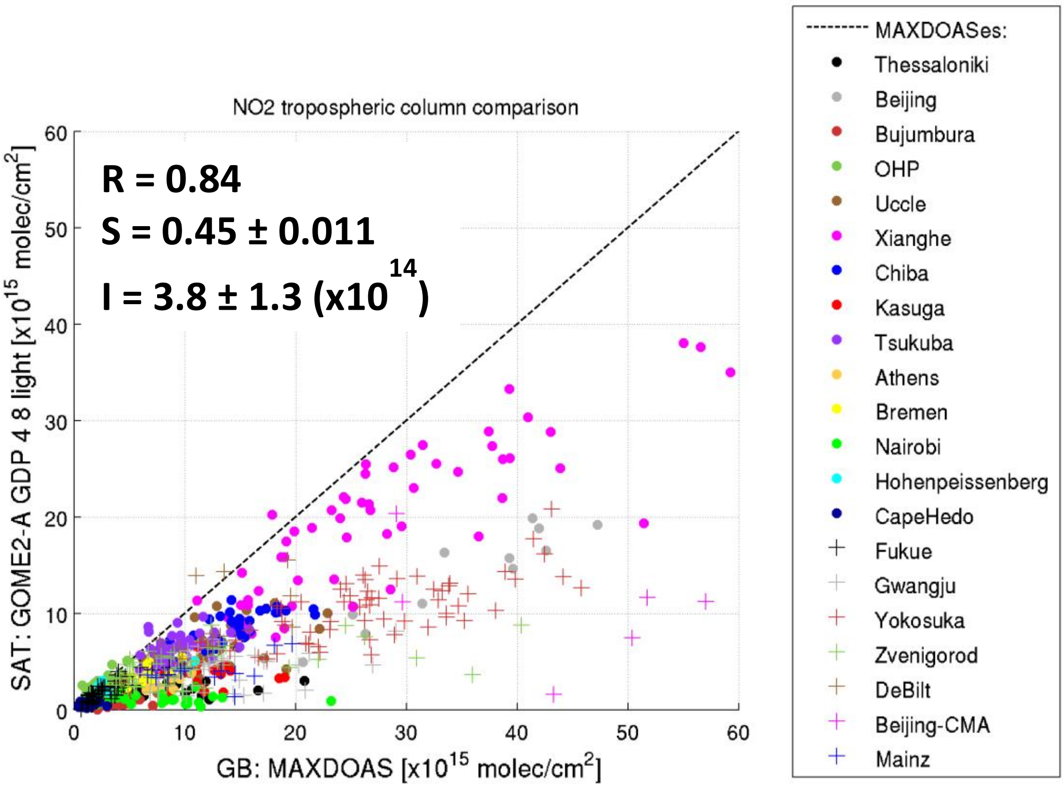

Figure E.2.3 Tropospheric NO_2 VCD scatter plot between GOME-2A GDP 4.8 satellite data and MAXDOAS ground-based data at the 20 stations included in the study.

A closer examination of the results indicates that largest differences are obtained at highly populated urban sites, likely due to the effect of strong local NO_2 emissions seen by ground-based instruments but smeared out at the coarse resolution of the GOME-2 observations (40x80 km^2). In Figure E.2.4, the stations have been categorized in rural/background, suburban and urban sites and the comparisons are shown separately. Good agreement is found in suburban and background stations, with slopes around 0.66 (e.g., Xianghe, Chiba, Tsukuba, Kasuga, Uccle, De Bilt, Hohenpeissenberg, OHP and Cape Hedo) while in urban conditions (Beijing, Yokosuka, Gwangju, Mainz) the MAXDOAS columns are generally much higher than GOME-2 ones. In such cases, the slope of the regression is close to 0.4 in average.

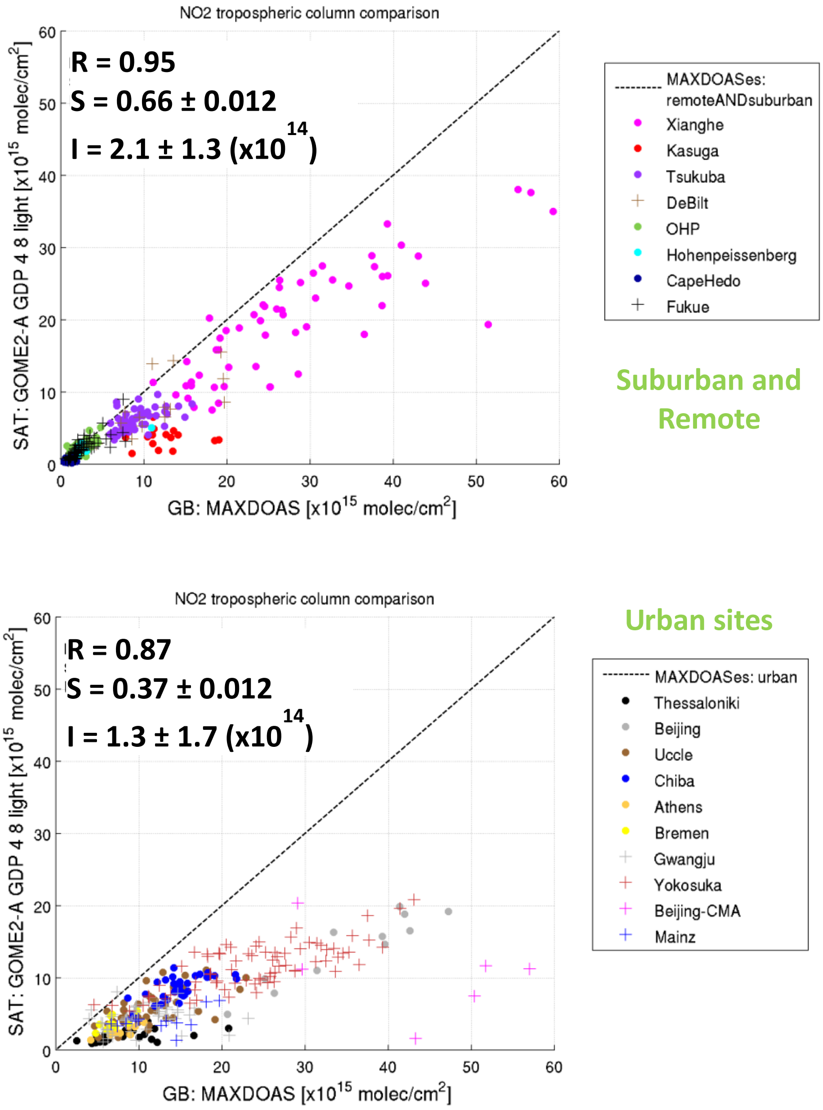

Figure E.2.4 Same as Figure E.2.3 but dividing into (a) **s**uburban and remote, (b) urban sites.

In addition to the expected smearing effect of GOME-2 measurements in urban locations characterized by strong local emissions (also seen in the total NO_2 comparisons performed in Section E.3 with direct-sun data), other possible impacts are due to the uncertainties in the applied satellite retrieval assumptions (such as the choices of the a-priori NO_2 profiles, the albedo, the cloud treatment, …). The impact of the different vertical sensitivities of the ground-based and satellite measurements can be assessed through application of the averaging kernels available from both datasets at those stations where NO_2 vertical profiles are retrieved (see Table E.1 for details). This is performed in the next Section (E.2.2).

The impact of the choice of the satellite a-priori NO_2 profiles or the impact of horizontal smearing due to the large GOME-2 pixel size (40x80km²), can be assessed by extending this comparison to other satellites datasets, such as the TEMIS GOME-2 NO_2 product (to see the impact of the a-priori choice importance), or such as SCIAMACHY (60x30km² pixel size) and OMI (13x24km²) satellites. This is however out of the scope of this report.

E.2.2 Comparison against ground-based MAX-DOAS profiles data

Some of the stations presented in section E.2, in addition to the tropospheric VCD, also retrieved low tropospheric profiles, giving the opportunity to test the use of GOME-2 NO_2 averaging kernels. Figure E.2.5 show these stations and their time-series.

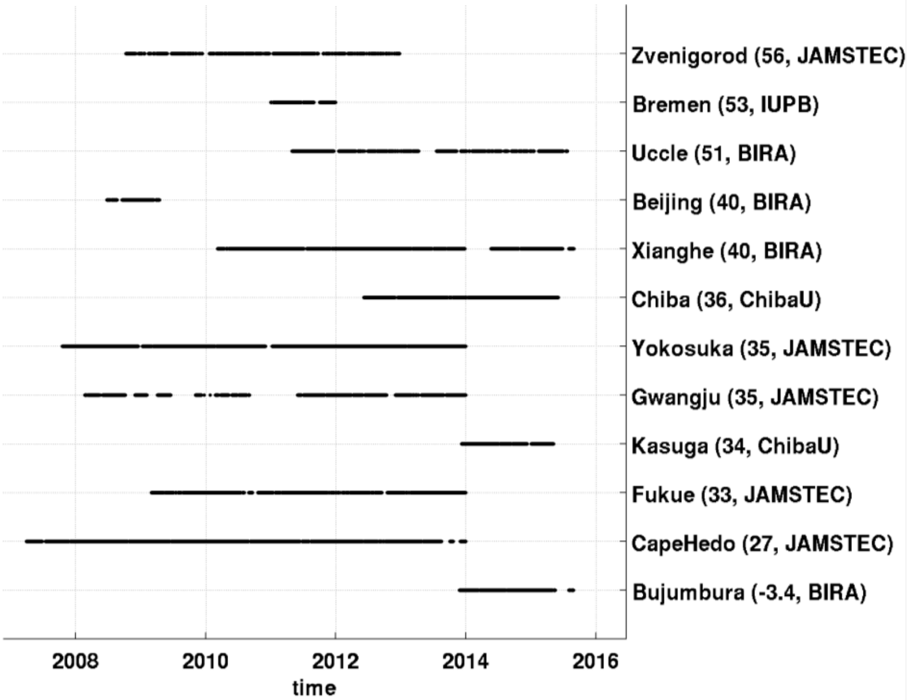

Figure E.2.5 List of MAXDOAS instruments retrieving low tropospheric NO_2 profiles and their temporal coverage.

The difference in vertical sensitivity between GOME-2 and the MAXDOAS measurements can be taken into account either by using the retrieved MAX-DOAS profile shapes as a priori for the calculation of satellite air mass factors or by applying the satellite column averaging kernels to the MAX-DOAS NO_2 profiles. This latter option is selected, and smoothed MAXDOAS NO_2 VCD are calculated from every MAXDOAS profiles ($\mathbf{x}_{MAXDOAS}$) and the monthly mean cloud free averaging kernel (AK_{sat}) coming from the GOME-2 GDP 4.8 dataset:

$$VCD_{MAXDOAS,smoothed} = AK_{sat} * \boldsymbol{x}_{MAXDOAS} \quad (1)$$

If the first altitude level of the satellite column averaging kernel is above the altitude of the station, then the averaging kernel is extrapolated down to the altitude of the station.

An example of the AK_{sat} around Beijing are shown in Figure E.2.6, while the MAXDOAS profiles are shown in Figure E.2.7. Examples of the impact of this approach on the comparison are presented in Figures E.2.8 to E.2.10, where time-series and correlation plots (and statistics) for Xianghe, Beijing and Bujumbura stations are shown for the original comparisons (as done in Section E.2.1) and when smoothing the MAXDOAS profiles as described in Equation (1).

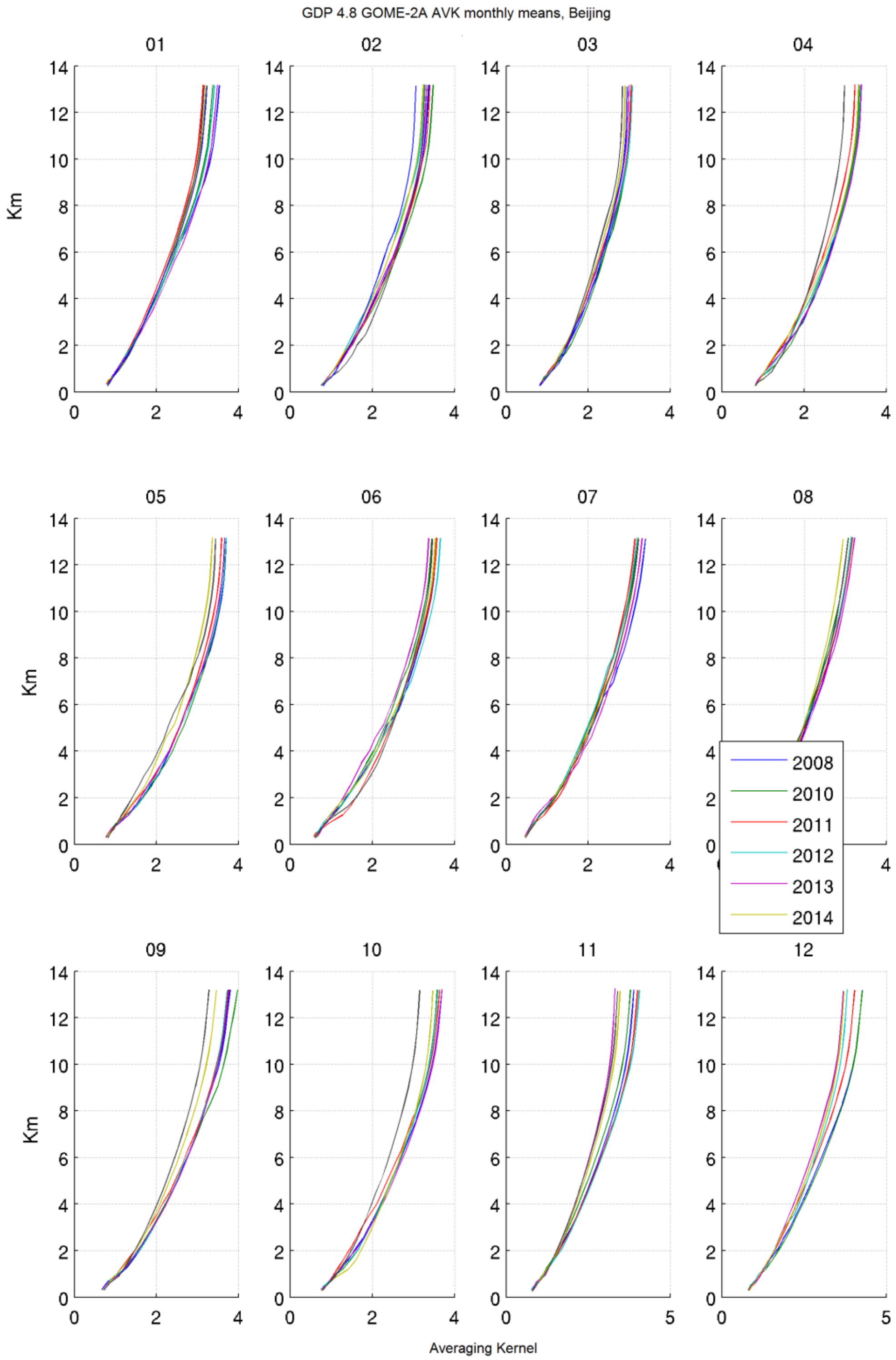

Figure E.2.6 Example of GOME-2A GDP 4.8 monthly mean cloud free averaging kernels around Beijing.

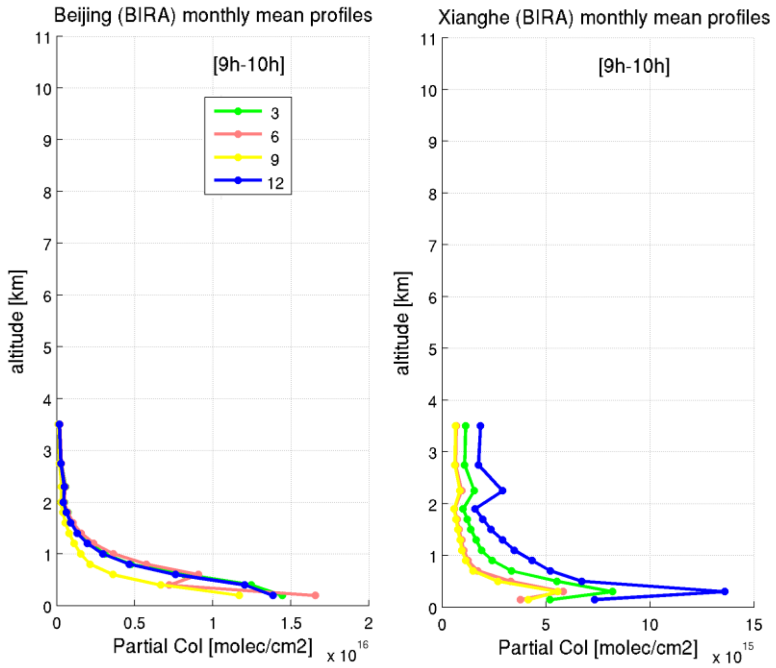

Figure E.2.7 Examples of monthly mean NO_2 profiles from MAXDOAS measurements in Beijing and in Xianghe, between 9h and 10h local time. The different colors are different months of the year (March, June, September and December).

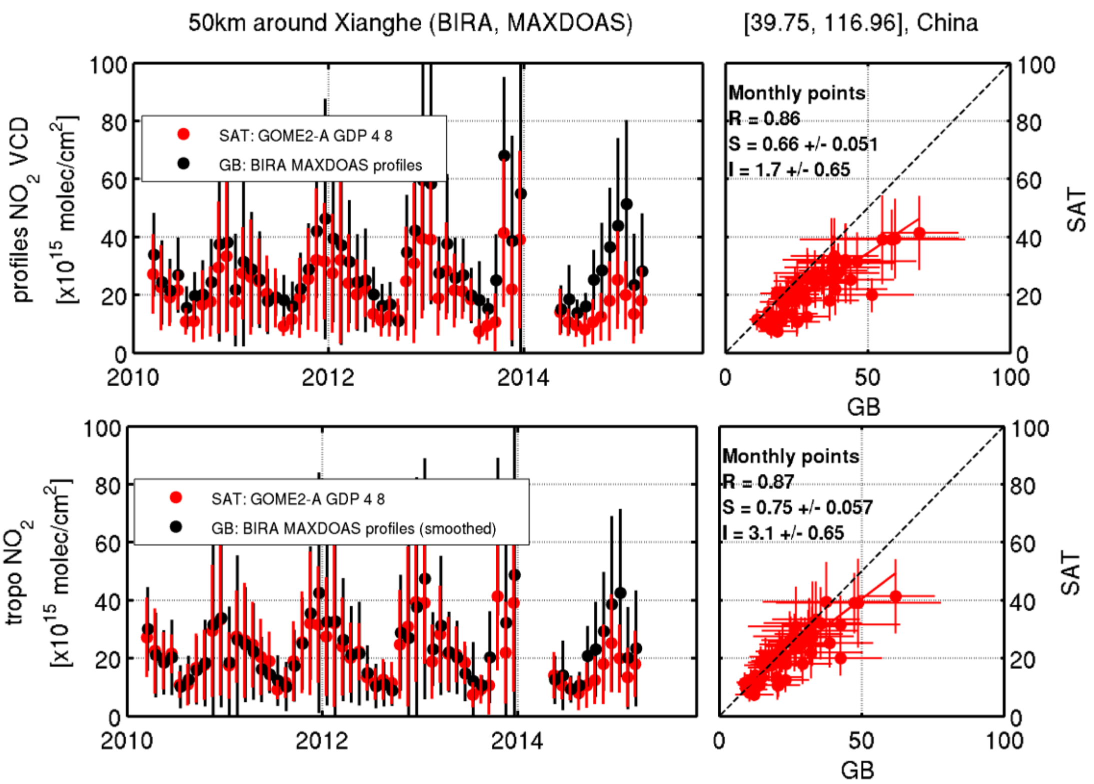

Figure E.2.8 Monthly mean comparisons between GOME-2A GDP 4.8 tropopsheric VCD and MAXDOAS columns in Xianghe (upper panels) original comparisons as in Section E.2.1; (lower panels) when smoothing the MAXDOAS profiles with the satellite averaging kernels as described in Eq. 1.

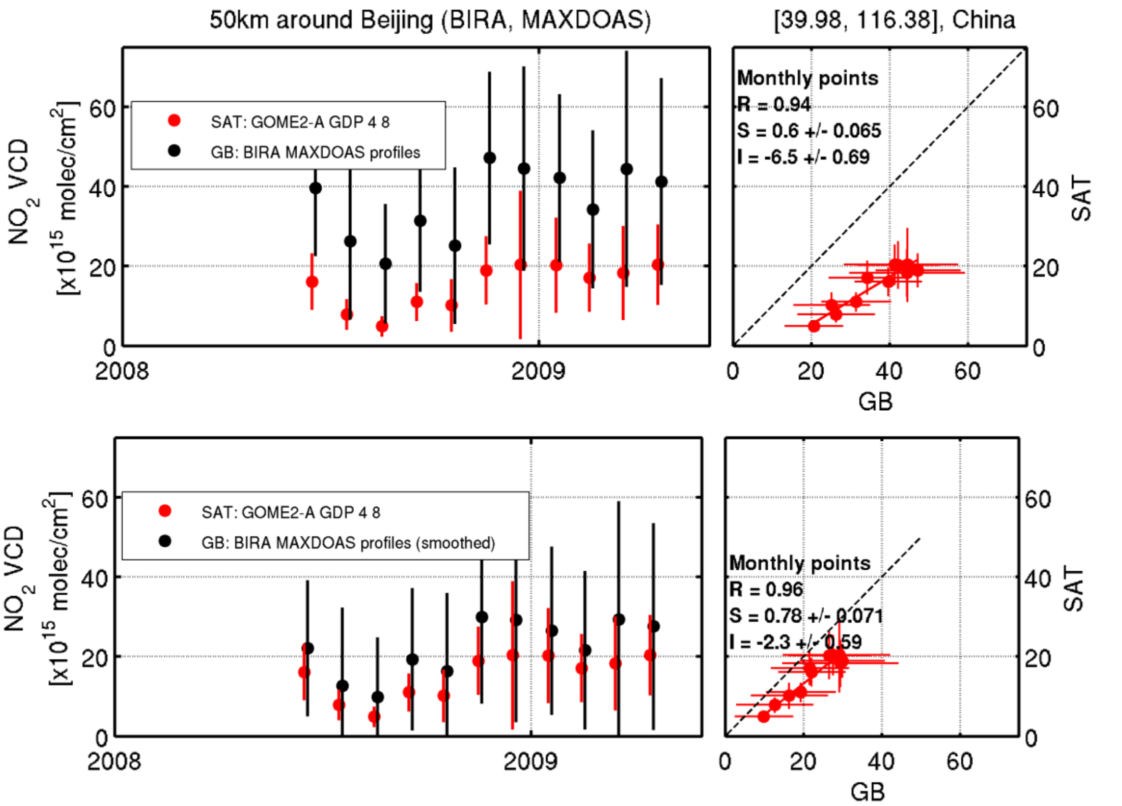

Figure E.2.9 same as Figure E.2.8, but for Beijing station.

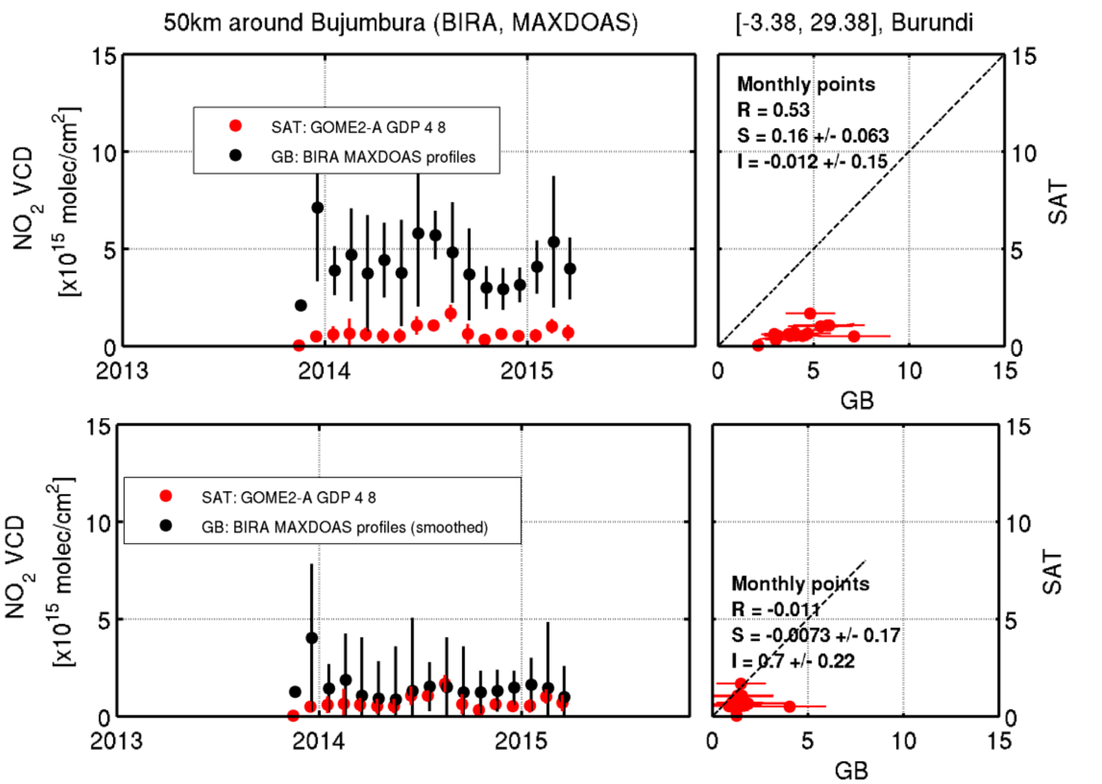

Figure E.2.10 same as Figure E.2.8, but for Bujumbura station.

As can be seen in Figures E.2.8 to E.2.10, the smoothing of the MAXDOAS profiles at BIRA-IASB Xianghe, Beijing and Bujumbura stations is generally reducing the ground-based columns, while conserving the seasonal patterns. This lead to a better agreement with the satellites columns, basically by excluding the highest values of lower layers of the ground-based profiles (see Figure E.2.7), where the GOME-2 instrument has a smaller sensitivity (see Figure E.2.6). This allows to take into account difference in vertical sensitivity between GOME-2 and the MAXDOAS measurements, but is somehow corrupting the ground-based measurements, which should be considered as the “truth” values. A way around would be to recalculate the satellite AMF_{tropo} by using as a-priori profile shape the MAXDOAS profiles instead of the MOZART model profiles. This would have as an impact to increase the satellite VCD_{tropo} data, but mathematically the comparisons results should be the same, and this is out of the scope of the current exercise.

The smoothing of the MAXDOAS profiles has been performed at the 12 stations where the MAXDOAS profiles are availables, and the results are summarized in Figure E.2.11, where scatter plots of the results are presented for both GOME-2A and GOME-2B data, with the original MAXDOAS columns and when smoothing them.

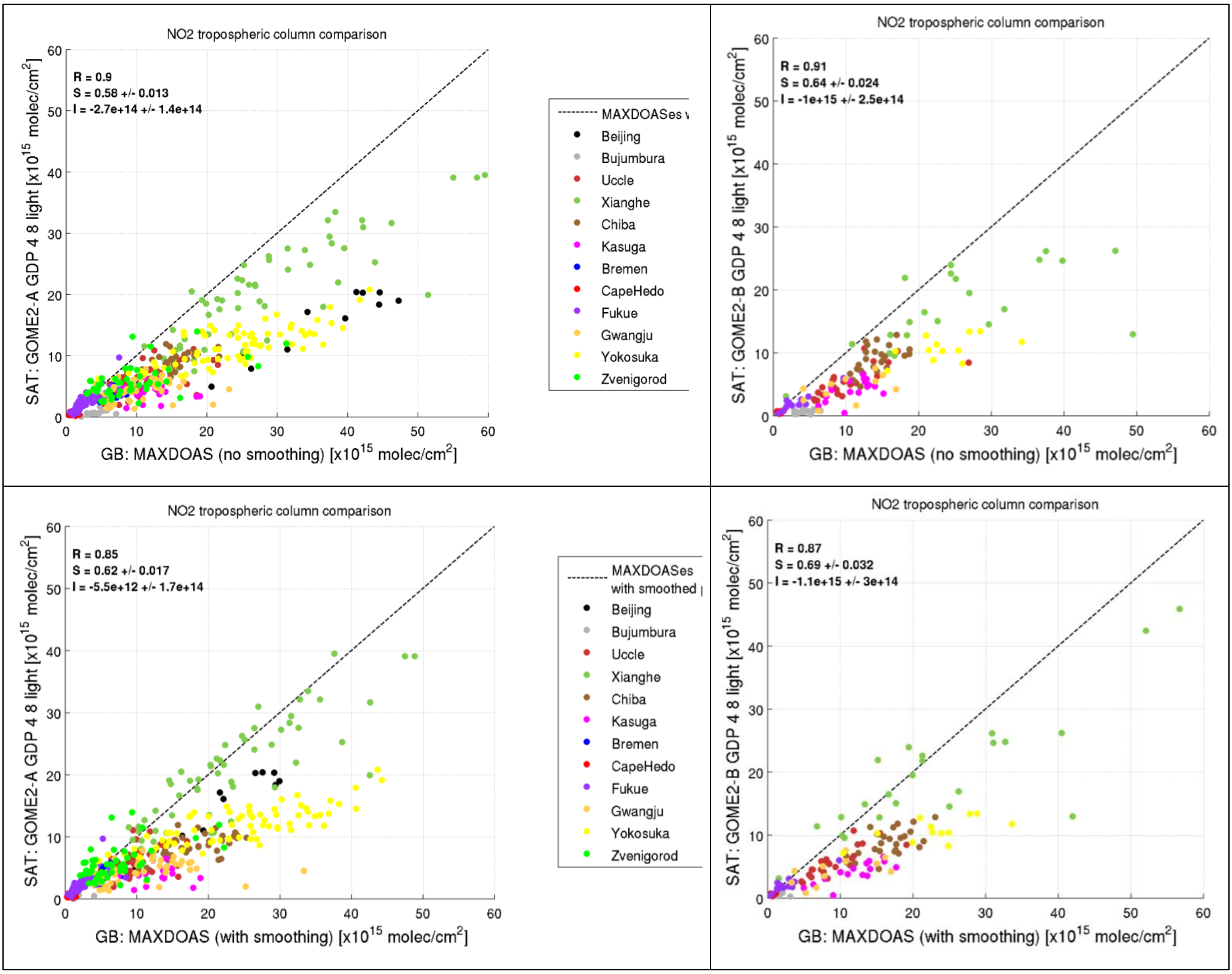

Figure E.2.11 Scatter plot of the GOME-2A and B (left panels for A, and right panels for B) tropospheric VCD with respect to MAXDOAS columns for 12 stations. Upper panels show the comparisons with the original MAXDOAS columns, while lower panels show the comparisons with the smoothed MAXDOAS profiles. Statistics such as correlation R, slope S and intercept I of the regression are given as an insert on every plot.

As can be seen from Figure E.2.11, at some of the stations (such as Beijing, Xianghe and Bujumbura) the comparisons results are much better when the MAXDOAS profiles have been smoothed (results closer to the 1:1 line), but this is not the case at all the stations, leading to less striking statistical improvement than what seen in Figure E.2.8 and E.2.9. This could be explained by the different impact of the difference in shape between the MAXDOAS retrieved profiles and the MOZART model used as a-priori value in the AMF_{tropo} calculation at each station. The individual station comparisons should be further studied in order to eventually recommend an improved model/solution for a more representative satellite's AMF calculation.

To conclude on the validation of tropospheric NO_2 columns from GDP 4.8 version, an overview table grouping the statistical results at the BIRA-IASB stations for both GOME-2A and B is presented in Table E.2. This table also includes values obtained when smoothing MAXDOAS profiles and when performing the comparisons with the previous GDP 4.7 data (figures provided in Annex H.1). Only values from the comparisons at the BIRA-IASB stations are presented in Table E.2, because altought the main outcome of the comparison at around 20 stations are considered valid and representative of the overall GOME-2 behaviour (and consistent with results of the total NO_2 comparisons shown in the next section), these MAXDOAS data are not harmonized among them yet and this could affect the estimation of bias due to the possible lack of consistency between the MAXDOAS stations. The BIRA-IASB MAXDOAS stations on the other hand are well-known by the authors, and except the OHP station, are all similar scientific grade instruments using the same approach for profile retrievals and are thus assumed to be an homogeneous mini-network.

In order to give a feeling of how much the cloud product has changed between the 2 versions, an overview of the number of almost cloud free pixels (CF<0.2) and their respective cloud pressure values are gathered in figure E.2.12 and E.2.13 for GDP 4.7 and 4.8 respectively. As an example, all the pixels of the year 2014 within 50 km of OHP, Uccle, Xianghe and Bujumbura stations are considered. In GDP files, when the pixel is completely cloud free (CF=0), the values of the cloud pressure are set to -1, which explain the large bar in the first bin of the histograms.

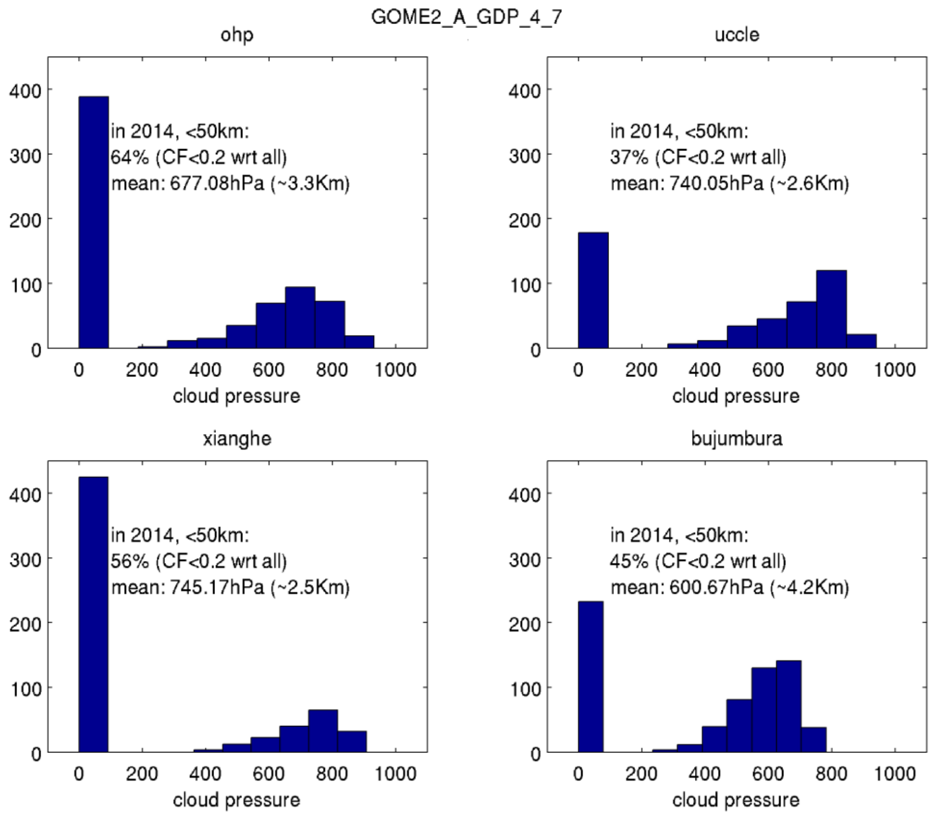

Figure E.2.12 Histogram of the cloud pressure distribution for almost cloud free pixels (CF<0.2) of GOME-2A GDP4.7 in 2014, within 50 km of 4 BIRA-IASB stations. As an insert, the number of almost cloud free pixels

(CF<0.2) with respect to the total number of pixels is given in percent, as well as the mean value of the cloud pressure and its estimation in Km.

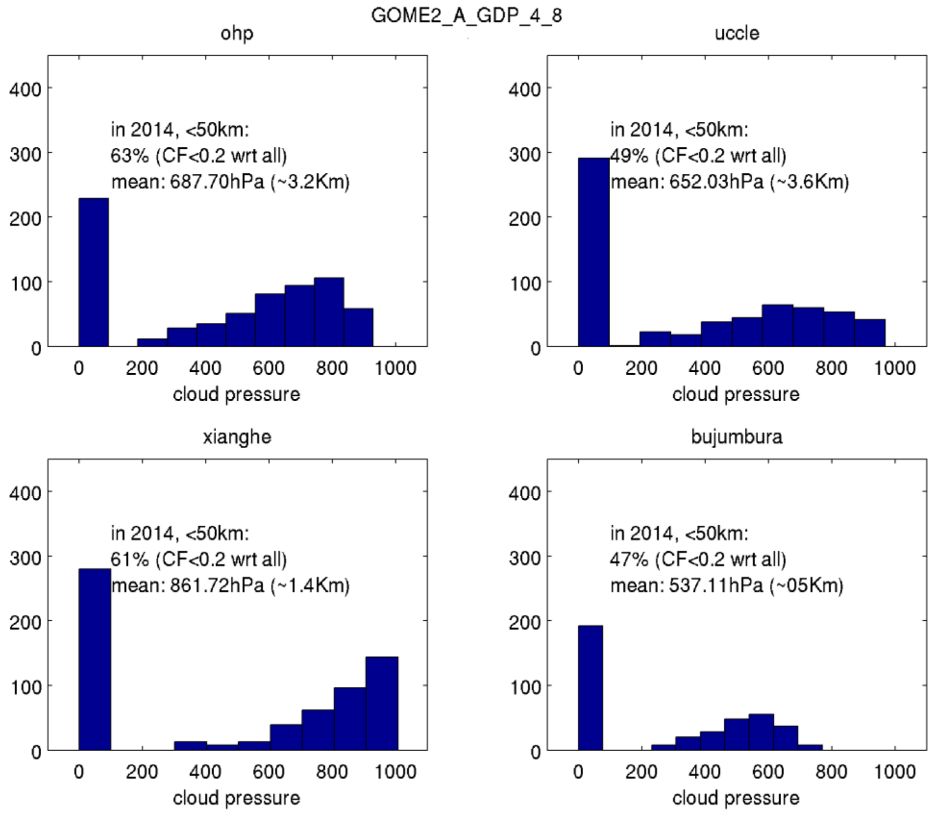

Figure E.2.13 Histogram of the cloud pressure distribution for almost cloud free pixels (CF<0.2) of GOME-2A GDP4.7 in 2014, within 50 km of 4 BIRA-IASB stations. As an insert, the number of almost cloud free pixels (CF<0.2) with respect to the total number of pixels is given in percent, as well as the mean value of the cloud pressure and its estimation in Km.

From figure E.2.12 and E.2.13 we can see that:

- For both cloud product versions, OHP is the station with the largest number of clear-sky cases (~63%); for the other stations, the number of almost cloud free (CF<0.2) pixels and their cloud pressure is different between GDP 4.7 and 4.8, especially in the case of Uccle (37% to 49%) and Xianghe (56% to 61%). Differences in cloud pressure can be larger than 100 hPa, i.e. clouds height change up to ~1 Km;
- Except for Uccle, the number of completely cloud free pixels (CF=0 and CTP=-1) is reduced in GDP 4.8; in GDP 4.7 the region around Uccle was very strongly affected by clouds (only 37% of pixels with CF<0.2) while in GDP 4.8 around half of the pixels are clear-sky (CF<0.2).

These changes in the cloud presence and height are the main change in the GDP NO_2 update, and (can) have large impact in the comparisons with the ground-based data.

The validation results at each BIRA MAXDOAS stations are reported in table E.2, but every station has different characteristics, and should thus considered differently when looking to the validation results and the numbers in the table. Some stations are background stations, with relatively small variability in the measured NO_2, and in these cases the mean bias is considered as the best indicator of the validation results. Other stations are in urban situation, and (as seen in the previous section) the NO_2 levels seen by the ground-based instruments are local peaks, averaged out in the GOME-2 pixel. In this case, the correlation coefficient R is a good indication of the linearity/coherence of the satellite and ground-based dataset, but a large difference in term of slope (closer to 0.5 than to 1) and of mean bias is expected. The best stations for the comparisons with the satellite data are those in sub-urban conditions, where the variability is large enough and where the ground-based measurements are not in the middle of the pollution hot-spot and are thus more representative of what seen by the satellite.

For those MAXDOAS instruments that allow for tropospheric profile retrievals (see table E.2), the impact of the a-priori profile used in the satellite retrieval can be removed through application of the satellite averaging kernel to the MAXDOAS profiles resulting in a physically more robust comparison.

Table E.2: Summary of the regression parameters and bias values (mean (GOME2-MAXDOAS) differences ± standart deviations) between GOME-2A and B and MAXDOAS tropospheric NO_2 VCDs at BIRA-IASB stations.

Monthly mean comparisons	**MetOp-A**		**MetOp-B**	
	GDP 4.7	**GDP 4.8**	**GDP 4.7**	**GDP 4.8**
OHP (44°N, 5.7°E, background)	**06/2007-06/2014**		**01/2013-06/2014**	
Regression parameters	R = 0.75 S = 0.87±0.09 I = 0.29±0.16	R = 0.66 S = 0.71±0.09 I = 0.62±0.16	R = 0.54 S = 1.3±0.46 I = -0.51±0.72	R = 0,35 S = 0.7 ±0.43 I = 0.61±0.69
Differences [molec/cm²]	Mean: 2.9×10^{13} Median: 8.4×10^{14} **[7±30 %]**	Mean: -0.46×10^{13} Median: -0.36×10^{14} **[7±30 %]**	Mean: 6.1×10^{13} Median: -0.99×10^{14} **[9±29 %]**	Mean: -8.5×10^{13} Median: -1.3×10^{14} **[8±35 %]**
Uccle (50.8°N, 4.3°E, urban)	**03/2011-03/2015**		**01/2013-03/2015**	
Regression parameters	R = 0.73 S = 0.76±0.11 I = -0.69±0.58	R = 0.64 S = 0.46±0.08 I = 0.71±0.4	R = 0.66 S = 2.8±0.65 I = -18 ± 2.5	R = 0.75 S = 0.41±0.07 I = 1.2 ±0.4
Differences [molec/cm²]	Mean: -3.28×10^{15} Median: -2.3×10^{15} **[-29±31 %]**	Mean: -5.33×10^{15} Median: $- 4 \times 10^{15}$ **[-47±27 %]**	Mean: -2.6×10^{15} Median: -2.02×10^{15} **[-21±69 %]**	Mean: -4.9×10^{15} Median: -3.53×10^{15} **[-46±32 %]**
-With smoothing		R = 0.6 S = 0.53±0.11 I = 0.63±0.44 **[-38±28 %]**		R = 0.83 S = 0.61±0.08 I = 0.03±0.35 **[-39±23 %]**
Xianghe (39.7°N, 117.0°E, sub-urban)	**03/2010-03/2015**		**01/2013-03/2015**	
Regression parameters	R = 0.87 S = 0.77±0.06 I = 2.1±0.7	R = 0.86 S = 0.66±0.06 I = 1.7 ±0.65	R = 0.95 S = 0.84 ±0.06 I = -2.1±0.82	R = 0.84 S = 0.58 ±0.08 I = 3.1±1.2
Differences [molec/cm²]	Mean: -3.9×10^{15} Median: -2.18×10^{15} **[-14±22 %]**	Mean: -7.3×10^{15} Median: -3.4×10^{15} **[-27±23 %]**	Mean: -6.6×10^{15} Median: -3.8×10^{15} **[-23±16 %]**	Mean: -9.8×10^{15} Median: -4.5×10^{15} **[-23±32 %]**
-With smoothing		R = 0.87 S = 0.75±0.06 I = 3.1 ±0.65 **[-8±24 %]**		R = 0.84 S = 0.66±0.09 I = 4.3 ±1.2 **[-2±34 %]**
Beijing (40°N, 116.4°E, urban)	**06/2008-04/2009**			

Regression parameters	R = 0.91 S = 0.52±0.07 I = -3.5±0.8	R = 0.94 S = 0.6±0.065 I = -6.5±0.69	na	na
Differences [molec/cm²]	Mean: -2.1×10^{16} Median: -1.6×10^{16} **[-59±16 %]**	Mean: -2.1×10^{16} Median: -1.8×10^{16} **[-60±12 %]**	na	na
-With smoothing		R = 0.96 S = 0.78±0.07 I = -2.3±0.59 **[-34±11 %]**	na	na
Bujumbura (3.0°S, 29.0°E, background but in the city)	**11/2013-03/2015**		**11/2013-03/2015**	
Regression parameters	R = 0.46 S = 0.07±0.04 I = 0.47±0.11	R = 0.53 S = 0.16±0.06 I = -0.01±0.15	R = 0.19 S = 0.05±0.06 I = 0.55±0.13	R = 0.36 S = 0.09±0.06 I = 0.28±0.14
Differences [molec/cm²]	Mean: -3.6×10^{15} Median: -3×10^{15} **[-82±38 %]**	Mean: -3.6×10^{15} Median: -3.2×10^{15} **[-84±26 %]**	Mean: -3.26×10^{15} Median: -2.8×10^{15} **[-81±23 %]**	Mean: -3.4×10^{15} Median: -3.05×10^{15} **[-84±25 %]**
-With smoothing		R = -0.011 S = -0.007.±0.17 I = 0.7±0.22 **[-49±54 %]**		R = -0.16 S = -0.09.±0.15 I = 0.79±0.19 **[-52±44 %]**

OHP is a background mid-latitude station, very sunny and not very impacted by clouds. The instrument location is away from local NO_2 sources and mainly affected by transport of NO_2, and the station is considered representative of the area sampled by the satellite. The NO_2 levels are quite small (see figure H.1.1 to H.1.4), with monthly mean values between 0 and 7×10^{15} molec/cm², and maximum daily peaks up to 25-30 $\times 10^{15}$ molec/cm². Validation results for GDP 4.7 and 4.8 are very similar for the mean bias (~7±30%) which is consistent with the small impact of clouds in this comparisons. The correlation coefficient and the slopes vary more, and can be worst for GDP 4.8 compared to GDP 4.7, but considering the small NO_2 variability, these parameters are not considered the best estimates for this comparison. A similar comment is true also for the other background station, Bujumbura, in the southern hemisphere. The NO_2 maximum daily peaks measured by the MAXDOAS are up to 15×10^{15} molec/cm², while GOME-2 maximum values are of about 3 $\times 10^{15}$ molec/cm² (see H.1.15 to H.1.18) . It should be noted that although the instrument allow for profile retrieval, the MAXDOAS to satellite comparison is complicated by the orography: the instrument is situated within the Bujumbura city at around 800m and the city is surrounded by a lake and mountains, while the satellite pixels mean height (from a surface model) is higher than the MAXDOAS instrument location. Moreover, the station is affected by local pollution peaks not well sampled by the large GOME-2 pixel. The statistics analysis on correlation and slopes are thus considered less meaningfull, and altought increased for GDP 4.8, they are very small. The mean bias is significant (around -80% for both products and both platforms) but when the MAXDOAS profiles are smoothed with the averaging kernels, it is reduced down to ~-50%. Around 30% of the differences are thus due to the satellite a-priori profile shapes not representative of the local Bujumbura measurements.

A similar effect is present in the Beijing case, with a MAXDOAS instrument in the city center, and local NO_2 peaks up to 100×10^{15} molec/cm², while GOME-2 maximum values are about half of them (see H.1.13 and H.1.14). With this large NO_2 range, the correlation and slopes values are good indicators, showing very good correlation (larger than 0.9) and slopes between 0.52 and 0.6 for both versions, highlighting a large bias between the 2 datasets. The median difference is of about -60% for both GDP versions, and when we remove the contribution from the a-priori profile shape (~26%), it drops to -34%. To avoid the large impact of the city pollution on the comparisons, the instrument that was in Beijing was then moved in Xianghe in March 2010, a suburban location at around 60km from Beijing. This zone is much more representative of what the

GOME-2 pixels measures. This station, with its several years of measurements, the important NO_2 signal and the possibility to retrieve tropospheric profiles, is considered our best station for satellite validation. In Xianghe, the comparisons statistics show very coherent correlations values between both GDP versions (0.87 and 0.86) but slopes reduced from 0.77 to 0.66 for GDP 4.8. In addition, the mean bias is also worst: from -14% for GDP 4.7 to -27% for GDP 4.8. Both these values are within the target accuracy for polluted regions, of 30%. Moreover, when we remove the contribution from the a-priori profile shape (~19%), the mean bias with GDP 4.8 drops down to -8% (-3.8×10^{15}molec/cm²).

The MAXDOAS in Uccle is situated in the south-west of Brussels city, and can be strongly affected by clouds. The comparisons results are quite different for both versions, which is to expected, due to the large importance of the cloud parameters change over Uccle (see figures E.2.12 and E.2.13). The number of coincident daily points is also strongly increased when using GDP 4.8 (see H.1.5a and H.1.6a for GOME-2A) due to the larger number of cloud-free pixels.The comparison of the statistical correlation and slopes values is thus hampered by the different number of points beeing used for the monthly comparison. Moreover, for GOME-2B, some outliers would need to be removed from the statistical analysis, due to the limited number of points in the monthly mean (one or two days only – e.g., see figure H.1.7a). If considering the mean bias, we can see a difference of about 20% between the 2 versions, with differences around -29% to -21% for GDP 4.7 and up to around -47% for GDP 4.8. This is coherent with the reduction of cloud fraction in the new version (see E.2.13), that will lead to increased AMF, and thus reduced vertical columns. When removing the contribution from the a-priori profile shape (up to ~9%), the mean bias with GDP 4.8 drops down to -38%.

Main conclusions on tropospheric vertical columns validation with MAXDOAS instruments:

- GOME-2 GDP 4.8 data are able to measure tropospheric NO_2 columns and it temporal evolution very well, especially in sub-urban and remote conditions, while larger under-estimation is found with respect to ground-based MAXDOAS measurements performed in urban environment. This is partially inherent to the large GOME-2 pixel size (40 x 80 km²), not representative of the local urban NO_2 pattern sampled by the ground-based instruments (sensitivity within ~10 km in the pointing direction) and partially due to the a-priori NO_2 profile shape used to calculate GOME-2 AMF.
- The use of GOME-2 GDP 4.8 averaging kernels to smooth the MAXDOAS NO_2 profiles (in order to take into account the different sensitivity of the two instruments) is generally giving better comparisons results. The bias is generally improved, but not the correlation coefficient. This is true for BIRA-IASB stations (see Table E.2), but not for all the other 12 stations. The importance of the different shape of the model profiles used by the satellite in the AMF calculations with respect to the MADOAS retrieved profiles should be further assessed at each station.
- Validation results for GOME-2A and B are generally very similar, with comparable mean biases (with and without smoothing the MAXDOAS profiles), even if the regression parameters can be slightly different.
- Larger differences of the new GDP version are found for Uccle and Xianghe stations (from 10 to 20% smaller columns), while in OHP, Beijing and Bujumbura the comparisons are of the same order of magnitude than with GDP 4.7. These differences are mostly due to change in the estimation of the cloud parameters themselves. Another reasons for the larger differences in GDP 4.8 is the possibility of hidden differences in the previous version, related to error compensations by the cloud correction. One hint in this direction is given in figure C.6 where the residual tropospheric slant column of GDP4.8 (and 4.7) and of the TEMIS product are compared. The difference between the 2 stratospheric estimation approaches (a systematic bias of about 1×10^{15} molec/cm²) is compared to the result of similar approaches applied to OMI instrument, resulting in smaller differences. This larger stratospheric correction in GDP would lead to smaller tropospheric SCD, that transfers to the tropospheric VCD (considering a tropospheric AMF between 0.5 to 1 around Uccle, 0.8 to 1.2 for Beijing area, see figures in section D) from 0.5 to 1.2 $\times 10^{15}$ molec/cm². The stratosphere/troposphere separation is one of next thing to focus on in future versions of GDP.

- Very large differences with the MAXDOAS instruments are found in urban cases (Bujumbura, Beijing, Uccle) while in sub-urban conditions (Xianghe) the difference is within the target accuracy of 30%. Impact of the a-priori profile shape is of about 10% around Uccle, 20% to 26% in Xianghe and Beijing and up to 35% in Bujumbura.

E.3. Total Vertical Column

The direct comparison of GOME-2 total NO_2 with correlative sources is possible by comparing the satellite dataset to direct-sun instruments, as performed with scientific direct-sun mode DOAS instruments and Pandora network in Pinardi et al. (2014) for GDP 4.7. As for the previous section, validation figures for the BIRA ground-based dataset are also presented individually in H.2 for both GDP 4.8 and GDP 4.7 datasets to better conclude on the evolution of the product version.

E.3.1 Comparison against ground-based Directsun columns data

Direct-sun datasets

Direct-sun instruments measure direct sun (ir)radiance during daytime. The light travels through the whole atmosphere and the measurement is equally sensitive to both troposphere and stratosphere. These instruments therefore provide accurate total column measurements with a minimum of a-priori assumptions.

Although direct-sun measurements have occasionally been performed by MAXDOAS instruments (e.g., BIRA-IASB (Clémer et al., 2008) or AUTH (Kouremeti et al., 2013)), systematic large scale direct-sun observations are currently mostly available from the network of standardized Pandora sun-photometers recently set-up by NASA (Herman et al., 2009, Tzortziou et al., 2013). These instruments have been deployed in about 60 different locations and the network continues to grow. The Pandora spectrometer provides NO_2 vertical column observations with a random uncertainty of about 2.7×10^{14}molec/cm² and a systematic uncertainty of 2.7×10^{15} molec/cm² (Herman et al., 2009). NO_2 column retrievals from Pandora have been compared to direct-sun multifunction DOAS (MF-DOAS) and Fourier transform ultraviolet spectrometer (UVFTS) data and have been found to agree to within 12 % (Piters et al., 2012; Wang et al., 2010; Herman et al., 2009).

The different direct-sun instruments used in this study are represented in Figure E.3.1. These include 16 systems mainly located in polluted areas, most of them being Pandora systems operated by NASA. Only Pandora stations having at least 3 months of data have been considered in this study.

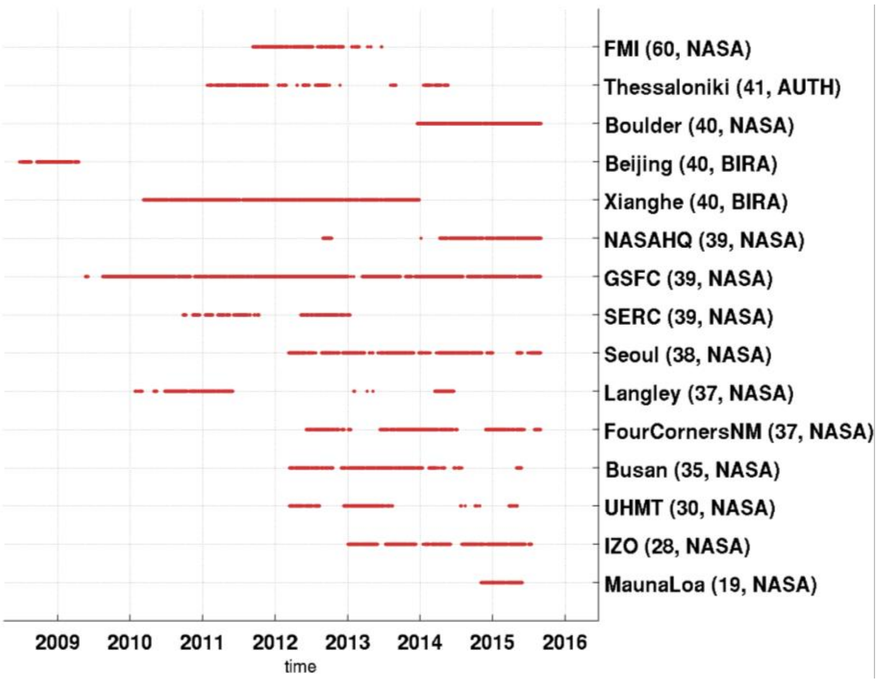

Figure E.3.1 List of Directsun instruments used in this study and their temporal coverage.

Total NO_2 comparisons

For the comparison, the GOME-2 GDP 4.8 data are extracted within 50 km of the different stations and only cloud free pixels (satellite cloud fraction < 20%) are selected. For the ground-based direct-sun data, a filtering on error, cloud flags, color index, etc. is performed following recommendations formulated by the Pandora team. The resulting data are interpolated at the satellite overpass time for further comparison. Total columns from the satellites are stratospheric plus tropospheric values.

As for MAXDOAS instruments, the agreement between GOME-2 and ground-based direct-sun measurements is found to be good at the suburban site of Xianghe while larger differences are obtained at the urban sites (e.g., Beijing, Busan, Seoul). This can be seen in the time-series of Figure E.3.2 and in the scatter plot of Figure E.3.3. and E.3.4.

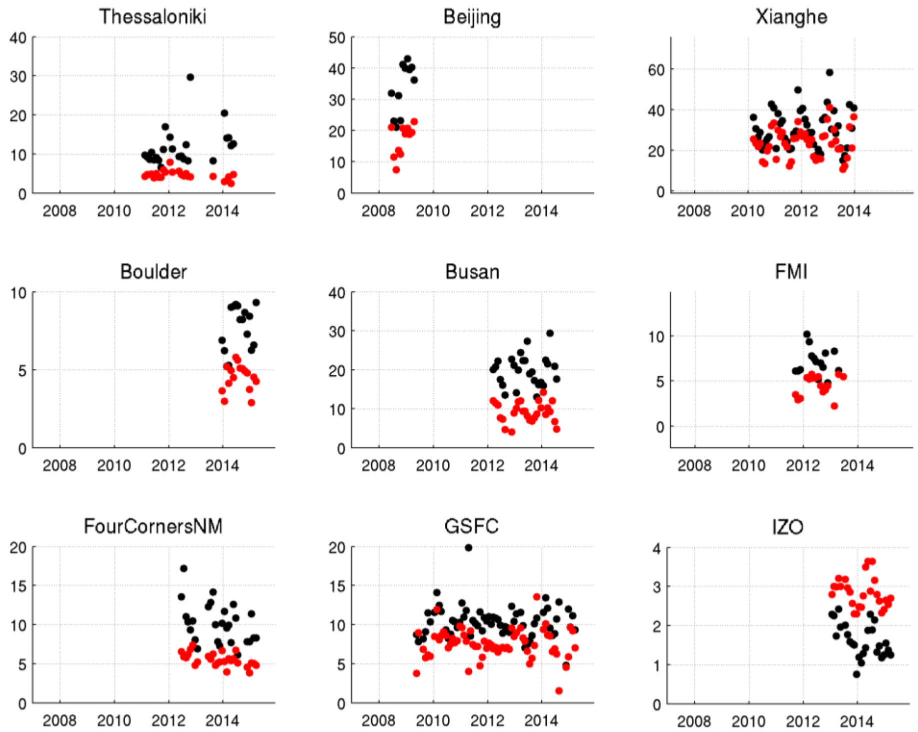

Figure E.3.2 NO_2 total column time series of GOME-2 GDP 4.8 (red) and the ground-based direct-sun data (black), between January 2007 and August 2015.

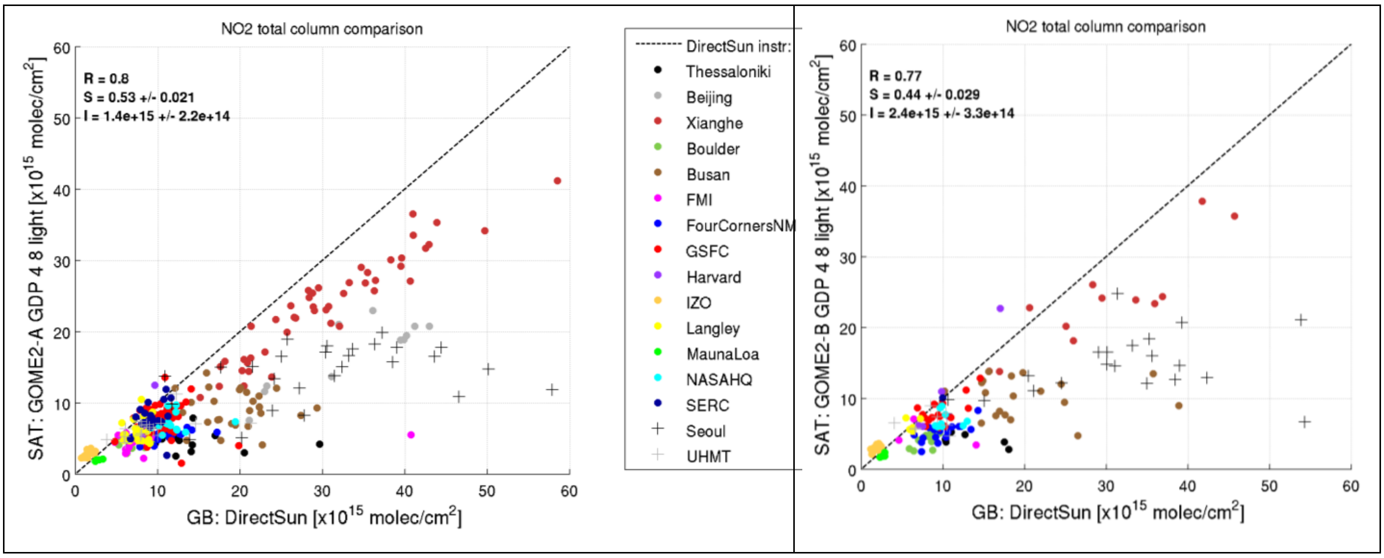

Figure E.3.3 Total NO_2 VCD scatter plot between GOME-2 GDP 4.8 satellite data and direct-sun ground-based data at the 16 stations included in the study.

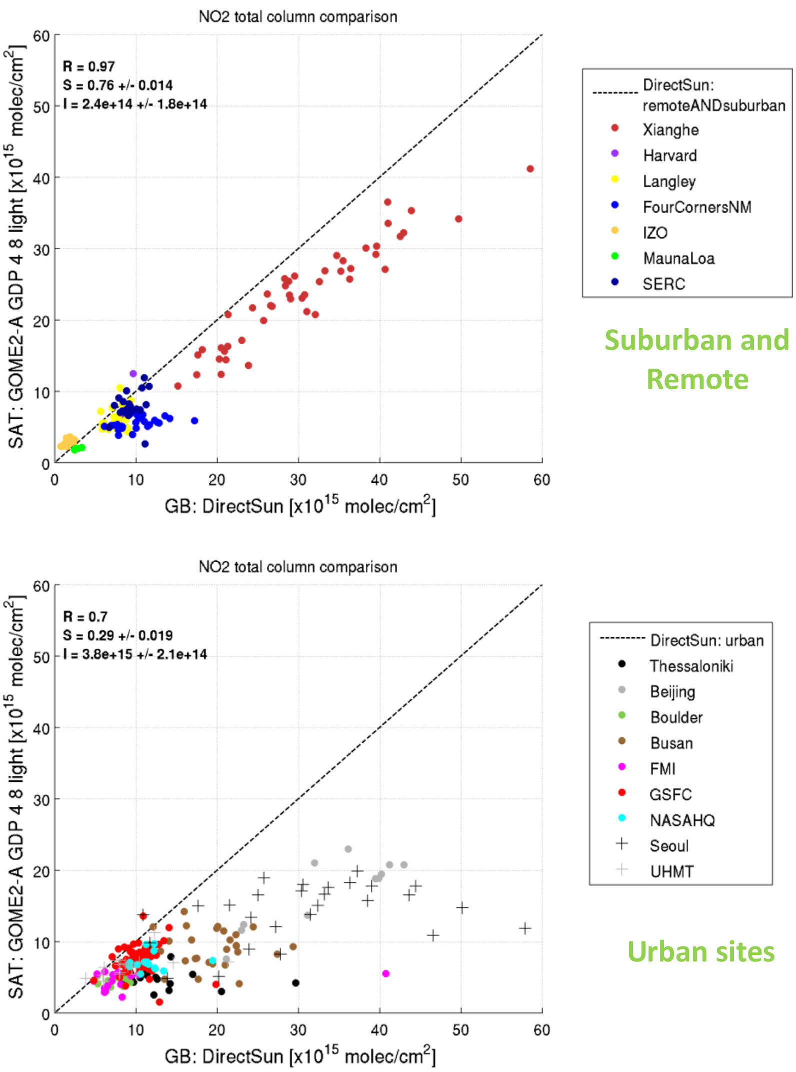

Figure E.3.4 Same as Fig. E.3.3 but dividing comparisons for GOME-2A into (a) suburban and remote, (b) urban sites.

As for the MAXDOAS, the correlation coefficients R drops from more than 0.9 to around 0.7/0.8 when focusing only on suburan or remote location to urban locations, while the slope S of the regression ft drops from around 0.7/0.6 to 0.3/0.4, even if the stations are not the same. This is also visible when looking to stations where both MAXDOAS and direct-sun data were operated (Beijing, Xianghe, Thessaloniki): a good coherence between the tropospheric and total NO_2 results is found.

Furthermore, the coherence of the results for megacities is impressive. Very similar results are indeed obtained e.g. for Beijing and Seoul data (see Figure E.3.4).

As for Section E.2, numerical results and comparison to previous version is only reported

Table E.3.1: Summary of the regression parameters and bias values (mean (GOME2-MAXDOAS) differences ± standart deviations) between GOME-2A and B and DirectSun total NO_2 VCDs at BIRA-IASB stations.

Monthly means	**MetOp-A**		**MetOp-B**	
	GDP 4.7	**GDP 4.8**	**GDP 4.7**	**GDP 4.8**
Xianghe	**03/2010-12/2013**		**01/2013-12/2013**	
Regression parameters	R = 0.93 S = 0.94±0.06 I = -2.6±0.55	R = 0.95 S = 0.78±0.04 I = 0.16±0.42	R = 0.91 S = 1±0.13 I = -4.5±1.7	R = 0.91 S = 0.74±0.09 I = 2.6±1.1
Differences [molec/cm²]	Mean: -4.8×10^{15} Median: -3.65×10^{15} **[-15±11 %]**	Mean: -6.6×10^{15} Median: -3.9×10^{15} **[-21±11 %]**	Mean: -4.01×10^{15} Median: -3.14×10^{15} **[-14±17 %]**	Mean: -5.43×10^{15} Median: -3.2×10^{15} **[-16±15 %]**
Beijing				
Regression parameters	R = 0.92 S = 0.55±0.07 I = -1.6±0.75	R = 0.85 S = 0.59±0.11 I = -2.1±1.1	na	na
Differences [molec/cm²]	Mean: -17.8×10^{15} Median: -13.5×10^{15} **[-50±14 %]**	Mean: -17.5×10^{15} Median: -13.5×10^{15} **[-47±15 %]**	na	na

Main conclusions on total vertical columns validation with DirectSun instruments:

- As for tropospheric columns, GOME-2 GDP 4.8 data are able to measure total NO_2 columns and their temporal evolution very well, especially in sub-urban and remote conditions, while larger under-estimation is found with respect to ground-based measurements performed in urban environment. This is partially inherent to the large GOME-2 pixel size (40 x 80 km²), not representative of the local urban NO_2 pattern sampled by the ground-based.
- Validation results for GOME-2A and B are generally very similar, with comparable mean biases, even if the regression parameters can be slightly different.
- Differences in the total NO_2 validation results due to GOME-2 GDP 4.8 version instead of GDP 4.7 are small (a few percents in Xianghe).
- Unfortunately, no correlative data is available in the Southern Hemisphere.In a future, tests will be performed with the BIRA-IASB instrument in Bujumbura, were the DirectSun capability was implemented in the beginning of 2015, but could no be used yet, due to instrumental issues.

F. CONCLUSION AND PERSPECTIVES

This document reports on the validation of O3M-SAF GOME-2 A and B reprocessed NO_2 column data products retrieved at DLR with versions 4.8 of the GOME Data Processor (GDP).

The following main conclusions can be drawn:

- The two version of NO_2 slant columns from DOAS retrievals have a very good agreement. The standard deviation of NO_2 columns and the RMS of DOAS are very similar between the two processor as well. Compared to the previous version, the GDP 4.8 NO_2 slant columns are slightly larger over the Southern Hemisphere, with slightly smaller RMS, thanks to the improvement of NO_2 cross section in the DOAS fits, and this effect is more significant for GOME-2B than GOME-2A. The difference is zonally homogeneous, with slightly larger differences found for GOME-2B results over the very polluted area of Eastern China region. This is probably linked to the different temperature of the used cross sections (240 K for Vandaele in GDP 4.8 vs. 243 K for GOME-2 FM cross section in GDP 4.7).
- The maps of the stratospheric SCD difference between the two processor versions is highly consistent with the maps of the SCD differences. The systematic bias on the slant columns is almost transferred to the stratospheric vertical columns.
- GDP 4.8 tropospheric NO_2 VCD are slightly smaller than previous GDP 4.7 for most regions (significant differences can be found over East Asia, North America, and Europe). The main change in the GDP 4.8 tropospheric NO_2 retrieval is due to the cloud product, that affects the calculation of the tropospheric AMF. Cloud free AMFs are identical between GDP 4.7 and GDP 4.8, since albedo, a-prioir profiles, and surface elevation maps have not been updated. Comparing the difference between AMF_{tropo} and AMF_{clear}, we highlighted the limitations of the previous version (no significant effect on AMF due to cloud correction for GDP 4.7, the cloud algorithm was not sensitive to cloud in the nearly cloudy-free scenes). The new cloud correction used in the GDP 4.8 (Lutz et al., 2015) leads to about ±20% difference in AMF. Positive and negative effect are found over the polluted regions over North Hemisphere, while a positive effect is fond over tropical biomass burning regions, where high clouds are present (and that were not seen in GDP 4.7). A better consistency of the cloud correction effect on NO_2 retrieval is found for GDP 4.8 between GOME-2A 2013 and GOME-2B 2013.
- The stratospheric NO_2 differences (due to slant column changes) and tropospheric NO_2 differences (due to cloud correction changes) are combined and transferred to the total NO_2 GDP 4.8 columns.
- With respect to 20 NDACC ZLS-DOAS UV-visible spectrometers, the MetOp-A GOME-2A and MetOp-B GOME-2B NO_2 column data sets processed with both GDP 4.7 and GDP 4.8, offer the same level of consistency. Variations of the stratospheric NO_2 column, from day-to-day fluctuations and to the annual cycle, are captured consistently by all measurement systems.
- In most of the cases, and for both GDP 4.7 and 4.8 processors, GOME-2B reports NO_2 column values slightly lower than GOME-2A, by about $1\text{-}3{\cdot}10^{14}$ molec.cm^{-2}, which is close to the combined uncertainty of ground-based NDACC measurements and of the comparison method.
- In most of the cases, GDP 4.8 reports NO_2 column values slightly higher than GDP 4.7, by about $1\text{-}3{\cdot}10^{14}$ molec.cm^{-2}, which is again close to the combined uncertainty of ground-based NDACC measurements and of the comparison method.
- Over the middle latitudes of the Northern Hemisphere (Aberystwyth, Jungfraujoch, O.H.P.), at low latitude stations like Izaña (Tenerife) and Saint-Denis (Reunion Island), and at both Arctic and Antarctic stations when only twilight GOME-2 data are considered, both satellites and both processor versions offer, with respect to NDACC ZLS-DOAS data, a comparable good agreement of a few 10^{14} molec.cm^{-2} on a monthly median basis.

- Over the Southern Hemisphere both GOME-2 instruments and both GDP processor versions report lower values than NDACC ZLS-DOAS spectrometers, this systematic bias starting at the Brazilian station of Bauru (22°S), propagating at four contributing middle latitude stations in the Pacific (New Zealand, Kerguelen, Macquarie) and in Argentina (Rio Galegos), and vanishing at Antarctic stations: within combined uncertainties.
- GOME-2 GDP 4.8 data are able to measure total and tropospheric NO_2 columns and it temporal evolution very well, especially in sub-urban and remote conditions, while larger under-estimation is found with respect to ground-based MAXDOAS and DirectSun measurements performed in urban environment. This is partially inherent to the large GOME-2 pixel size (40 x 80 km²), not representative of the local urban NO_2 pattern sampled by the ground-based instruments (sensitivity within ~10 km in the pointing direction) and partially due to the a priori NO_2 profile shape used to calculate GOME-2 AMF.
- The use of GOME-2 GDP 4.8 averaging kernels to smooth the MAXDOAS NO_2 profiles (in order to take into account the different sensitivity of the two instruments) is generally giving better comparisons results. The bias is generally improved, but not the correlation coefficient.
- Validation results for GOME-2A and B are generally very similar, with comparable mean biases (with and without smoothing the MAXDOAS profiles), even if the regression parameters can be slightly different.
- Differences in the tropopsheric NO_2 validation results due to GOME-2 GDP 4.8 version instead of GDP 4.7 are minimal in locations such as OHP, Beijing or Bujumbura and can be up to a factor 10% to 20% smaller in Xianghe and Uccle. These differences are mostly due to change in the estimation of the cloud parameters themselves, that have a strong effect on tropospheric NO_2 columns estimation. Possibles compensating errors due to the cloud correction are likely to explain the better validation results with the previous version, that are now more visible thanks to the improved cloud estimation and the more homogeneous approach between GOME-2A and B in the DOAS fit.
- Except the large differences with the MAXDOAS instruments found in urban cases (Bujumbura, Beijing, Uccle), the validation results in sub-urban conditions (Xianghe) are within the target accuracy of 30% for tropospheric NO_2. Impact of the a-priori profile shape is of about 10% around Uccle, 20% to 26% in Xianghe and Beijing and up to 35% in Bujumbura.
- Differences in the total NO_2 validation results due to GOME-2 GDP 4.8 version instead of GDP 4.7 are small (a few percents in Xianghe).

In summary, the transition to the new GDP 4.8 algorithm is recommended as it is more homogeneous between GOME-2A and B DOAS settings, and as the cloud product seems to better handle the scenes only slightly contaminated by clouds. Further improvements on surface albedo, stratospheric content estimation and model for the a-priori profile shapes for AMF calculation are recommended for a future release.

G. REFERENCES

G.1. Applicable documents

[ATBD] Algorithm Theoretical Basis Document for GOME-2 Total Column Products of Ozone, NO_2, BrO, SO_2, H_2O, HCHO and Cloud Properties (GDP 4.8 for O3M-SAF OTO and NTO), DLR/GOME-2/ATBD/01, Rev. 3/A, Valks, P., et al., March 2015.

[PUM] Product User Manual for GOME-2 Total Column Products of Ozone, NO_2, BrO, SO_2, H_2O, HCHO and Cloud Properties, DLR/GOME-2/PUM/01, Rev. 3/A, Valks, P., et. al., 2015.

[PRD] Product Requirements Document, SAF/O3M/FMI/RQ/PRD/001/Rev. 1.7, D. Hovila, S. Hassinen, D. Loyola, P. Valks, J., S. Kiemle, O. Tuinder, H. Joench-Soerensen, F. Karcher, 2015.

[SESP] Service Specification Document, http://o3msaG.fmi.fi/docs/O3M_SAF_Service_Specification.pdf, 2011.

[VIM] Joint Committee for Guides in Metrology (JCGM/WG 2) 200:2008 & ISO/IEC Guide 99-12:2007, International Vocabulary of Metrology – Basic and General Concepts and Associated Terms (VIM), http://www.bipm.org/en/publications/guides/vim.html

[GUM] Joint Committee for Guides in Metrology (JCGM/WG 1) 100:2008, Evaluation of measurement data – Guide to the expression of uncertainty in a measurement (GUM), http://www.bipm.org/utils/common/documents/jcgm/JCGM_100_2008_E.pdf

[QA4EO] A Quality Assurance framework for Earth Observation, established by the CEOS. It consists of ten distinct key guidelines linked through an overarching document (the QA4EO Guidelines Framework) and more community-specific QA4EO procedures, all available on http://qa4eo.org/documentation.html A short QA4EO "user" guide has been produced to provide background into QA4EO and how one would start implementing it (http://qa4eo.org/docs/QA4EO_guide.pdf)

G.2 Peer-reviewed articles

Boersma, K. G., Eskes, H. J. and Brinksma, E. J.: Error analysis for tropospheric NO_2 retrieval from space, J. Geophys. Res., 109(D4), doi:10.1029/2003JD003962, 2004.

Boersma, K. G., Eskes, H. J., Dirksen, R. J., van der A, R. J., Veefkind, J. P., Stammes, P., Huijnen, V., Kleipool, Q. L., Sneep, M., Claas, J., Leitão, J., et al.: An improved tropospheric NO2 column retrieval algorithm for the Ozone Monitoring Instrument, Atmos. Meas. Tech., 4(9), 2329-2388, doi:10.5194/amt-4-1905-2011, 2011.

Brinksma, E. J., et al. (2008), The 2005 and 2006 DANDELIONS NO2 and aerosol intercomparison campaigns, J. Geophys. Res., 113, D16S46, doi:10.1029/2007JD008808.

Celarier, E. A., E. J. Brinksma, J. F. Gleason, J. P. Veefkind, A. Cede, J. R. Herman, D. Ionov, F. Goutail, J-P. Pommereau, J.-C. Lambert, M. van Roozendael, G. Pinardi, F. Wittrock, A. Schönhardt, A. Richter, O. W. Ibrahim, T. Wagner, B. Bojkov, G. Mount, E. Spinei, C. M. Chen, T. J. Pongetti, S. P. Sander, E. J. Bucsela, M. O. Wenig, D. P. J. Swart, H. Volten, M. Kroon, and P. F. Levelt (2008), Validation of Ozone Monitoring Instrument Nitrogen Dioxide Columns, Journal of Geophysical Research – Atmosphere, Vol. 113, doi:10.1029/2007JD008908.

Clémer K., Van Roozendael, M., Fayt, C., Hendrick, G., Hermans, C., Pinardi, G., Spurr, R., Wang, P., and De Mazière, M., (2010) Multiple wavelength retrieval of tropospheric aerosol optical properties from MAXDOAS measurements in Beijing. Atmos. Meas. Tech., **3**, pp 863–878, doi:10.5194/amt-3-863-2010.

Hains, J. C., et al. (2010) Testing and improving OMI DOMINO tropospheric NO2 using observations from the DANDELIONS and INTEX-B validation campaigns. J. Geophys. Res., 115, D05301, doi: 10.1029/2009JD012399.

Hendrick, F., Müller, J.-F., Clémer, K., Wang, P., De Mazière, M., Fayt, C., Gielen, C., Hermans, C., Ma, J. Z., Pinardi, G., Stavrakou, T., Vlemmix, T., and Van Roozendael, M. (2014), Four years of ground-based MAX-DOAS observations of HONO and NO2 in the Beijing area, Atmos. Chem. Phys., 14, 765-781, doi:10.5194/acp-14-765-2014.

Herman, J., A. Cede, E. Spinei, G. Mount, M. Tzortziou, and N. Abuhassan (2009), NO_2 column amounts from ground-based Pandora and MFDOAS spectrometers using the direct-sun DOAS technique: Inter-comparisons and application to OMI validation, J. Geophys. Res., 114 (D13307), 10.1029/2009JD011848.

Ionov, D. V., et al., (2008) Ground-based validation of EOS-Aura OMI NO2 vertical column data in the midlatitude mountain ranges of Tien Shan (Kyrgyzstan) and Alps (France). J. Geophys. Res., 113, D15S08, doi:10.1029/2007JD008659.

Irie, H., Kanaya, Y., Akimoto, H., Tanimoto, H., Wang, Z., Gleason, J. G., and Bucsela, E. J.: Validation of OMI tropospheric NO_2 column data using MAX-DOAS measurements deep inside the North China Plain in June 2006: Mount Tai Experiment 2006, Atmos. Chem. Phys., 8, 6577-6586, doi:10.5194/acp-8-6577-2008, 2008.

Irie, H., Takashima, H., Kanaya, Y., Boersma, K. F., Gast, L., Wittrock, F., Brunner, D., Zhou, Y., and Van Roozendael, M. (2011), Eight-component retrievals from ground-based MAX-DOAS observations, Atmos. Meas. Tech.., 4, 1027-1044 doi:10.5194/amt-4-1027-2011.

Irie, H., Boersma, K. F., Kanaya, Y., Takashima, H., Pan, X., and Wang, Z. F. (2012), Quantitative bias estimates for tropospheric NO_2 columns retrieved from SCIAMACHY, OMI, and GOME-2 using a common standard for East Asia, Atmos. Meas. Tech., 5, 2403-2411, doi:10.5194/amt-5-2403-2012.

Kanaya, Y., Irie, H., Takashima, H., Iwabuchi, H., Akimoto, H., Sudo, K., Gu, M., Chong, J., Kim, Y. J., Lee, H., Li, A., Si, F., Xu, J., Xie, P.-H., Liu, W.-Q., Dzhola, A., Postylyakov, O., Ivanov, V., Grechko, E., Terpugova, S., and Panchenko, M. (2014), Long-term MAX-DOAS network observations of NO2 in Russia and Asia (MADRAS) during the period 2007–2012: instrumentation, elucidation of climatology, and comparisons with OMI satellite observations and global model simulations, Atmos. Chem. Phys., 14, 7909-7927, doi:10.5194/acp-14-7909-2014.

Kouremeti, N., Bais, A. F., Balis, D., and Zyrichidou, I.: Phaethon (2013), A System for the Validation of Satellite Derived Atmospheric Columns of Trace Gases, in Advances in Meteorology, Climatology and Atmospheric Physics, edited by C. G. Helmis and P. T. Nastos, pp. 1081-1088, Springer Berlin Heidelberg.

Lutz, R., D. Loyola, S. Gimeno Garcia, and F. Romahn, OCRA radiometric cloud fractions for GOME-2A/B, Atmos. Meas. Tech., to be submitted, 2015.

Ma, J. Z., Beirle, S., Jin, J. L., Shaiganfar, R., Yan, P., and Wagner, T.: Tropospheric NO_2 vertical column densities over Beijing: results of the first three years of ground-based MAX-DOAS measurements (2008–2011) and satellite validation, Atmos. Chem. Phys., 13, 1547-1567, doi:10.5194/acp-13-1547-2013, 2013.

Peters, E., Wittrock, F., Großmann, K., Frieß, U., Richter, A., and Burrows, J. P.: Formaldehyde and nitrogen dioxide over the remote western Pacific Ocean: SCIAMACHY and GOME-2 validation using ship-based MAX-DOAS observations, Atmos. Chem. Phys., 12, 11179-11197, doi:10.5194/acp-12-11179-2012, 2012.

Piters, A. J. M., Boersma, K. F., Kroon, M., Hains, J. C., Van Roozendael, M., Wittrock, F., Abuhassan, N., Adams, C., Akrami, M., Allaart, M. A. F., Apituley, A., Beirle, S., Bergwerff, J. B., Berkhout, A. J. C., Brunner, D., Cede, A., Chong, J., Clémer, K., Fayt, C., Frieß, U., Gast, L. F. L., Gil-Ojeda, M., Goutail, F., Graves, R., Griesfeller, A., Großmann, K., Hemerijckx, G., Hendrick, F., Henzing, B., Herman, J., Hermans, C., Hoexum, M., van der Hoff, G. R., Irie, H., Johnston, P. V., Kanaya, Y., Kim, Y. J., Klein Baltink, H., Kreher, K., de Leeuw, G., Leigh, R., Merlaud, A., Moerman, M. M., Monks, P. S., Mount, G. H., Navarro-Comas, M., Oetjen, H., Pazmino, A., Perez-Camacho, M., Peters, E., du Piesanie, A., Pinardi, G., Puentedura, O., Richter, A., Roscoe, H. K., Schönhardt, A., Schwarzenbach, B., Shaiganfar, R., Sluis, W., Spinei, E., Stolk, A. P., Strong, K., Swart, D. P. J., Takashima, H., Vlemmix, T., Vrekoussis, M., Wagner, T., Whyte, C., Wilson, K. M., Yela, M., Yilmaz, S., Zieger, P., and Zhou, Y. (2012), The Cabauw Intercomparison campaign for Nitrogen Dioxide measuring Instruments (CINDI): design, execution, and early results, Atmos. Meas. Tech., 5, 457-485, doi:10.5194/amt-5-457-2012.

Richter, A., Begoin, M., Hilboll, A. and Burrows, J. P.: An improved NO2 retrieval for the GOME-2 satellite instrument, Atmos. Meas. Tech., 4(6), 213-246, doi:10.5194/amt-4-1147-2011, 2011.

Richter, A., M. Weber, J. P. Burrows, J.-C. Lambert, and A. van Gijsel (2013), Validation Strategy for Satellite Observations of Tropospheric Reactive Gases, Annals of Geophysics, Vol. 56, 10.4401/AG-6335.

Roscoe, H. K., Van Roozendael, M., Fayt, C., du Piesanie, A., Abuhassan, N., Adams, C., Akrami, M., Cede, A., Chong, J., Clémer, K., Friess, U., Gil Ojeda, M., Goutail, F., Graves, R., Griesfeller, A., Grossmann, K., Hemerijckx, G., Hendrick, F., Herman, J., Hermans, C., Irie, H., Johnston, P. V., Kanaya, Y., Kreher, K., Leigh, R., Merlaud, A., Mount, G. H., Navarro, M., Oetjen, H., Pazmino, A., Perez-Camacho, M., Peters, E., Pinardi, G., Puentedura, O., Richter, A., Schonhardt, A., Shaiganfar, R., Spinei, E., Strong, K., Takashima, H., Vlemmix, T., Vrekoussis, M., Wagner, T., Wittrock, F., Yela, M., Yilmaz, S., Boersma, F., Hains, J., Kroon, M., Piters, A., and Kim, Y. J. (2010), Intercomparison of slant column measurements of NO2 and O4 by MAX-DOAS and zenith-sky UV and visible spectrometers, Atmos. Meas. Tech., 3, 1629-1646, doi:10.5194/amt-3-1629-2010.

Tzortziou M., Herman, J.R., Cede, A., Loughner, C.P., Abuhassa, N., Naik, S. (2013), Spatial and temporal variability of ozone and nitrogen dioxide over a major urban estuarine ecosystem, J. Atmos. Chem., DOI 10.1007/s10874-013-9255-8.

Valks, P., Pinardi, G., Richter, A., Lambert, J.-C., Hao, N., Loyola, D., Van Roozendael, M. and Emmadi, S.: Operational total and tropospheric NO2 column retrieval for GOME-2, Atmos. Meas. Tech., 4(7), 1491-1514, doi:10.5194/amt-4-1491-2011, 2011.

Vandaele, A.C., et al.: High-resolution Fourier transform measurement of the NO_2 visible and near-infrared absorption cross-section: Temperature and pressure effects, J. Geophys. Res., 107, D18, 4348, doi:10.1029/2001JD000971, 2002.

Vlemmix, T., Piters, A. J. M., Stammes, P., Wang, P., and Levelt, P. F. (2010), Retrieval of tropospheric NO_2 using the MAX-DOAS method combined with relative intensity measurements for aerosol correction, Atmos. Meas. Tech., 3, 1287-1305, doi:10.5194/amt-3-1287-2010.

Vlemmix, T., Piters, A. J. M., Berkhout, A. J. C., Gast, L. F. L., Wang, P., and Levelt, P. F. (2011), Ability of the MAX-DOAS method to derive profile information for NO_2: can the boundary layer and free troposphere be separated?, Atmos. Meas. Tech., 4, 2659-2684, doi:10.5194/amt-4-2659-2011.

Vlemmix, T., Hendrick, F., Pinardi, G., De Smedt, I., Fayt, C., Hermans, C., Piters, A., Levelt, P., and Van Roozendael, M. (2014), MAX-DOAS observations of aerosols, formaldehyde and nitrogen dioxide in the Beijing area: comparison of two profile retrieval approaches, Atmos. Meas. Tech. Discuss., 7, 9673-9731, doi:10.5194/amtd-7-9673-2014.

Wagner, T., Beirle, S., Brauers, T., Deutschmann, T., Frieß, U., Hak, C., Halla, J. D., Heue, K. P., Junkermann, W., Li, X., Platt, U., and Pundt-Gruber, I. (2011), Inversion of tropospheric profiles of aerosol extinction and HCHO and NO2 mixing ratios from MAX-DOAS observations in Milano during the summer of 2003 and comparison with independent data sets, Atmos. Meas. Tech., 4, 2685-2715, doi:10.5194/amt-4-2685-2011.

Wittrock, F., Oetjen, H., Richter, A., Fietkau, S., Medeke, T., Rozanov, A., and Burrows, J.P. (2004), MAX-DOAS measurements of atmospheric trace gases in Ny-Alesund – Radiative transfer studies and their application, Atmos. Chem. Phys., 4, 955–966, doi:10.5194/acp-4-955-2004.

Yilmaz, S (2012), Retrieval of Atmospheric Aerosol and Trace Gas Vertical Profiles using Multi-Axis Differential Optical Absorption Spectroscopy, Dissertation, University of Heidelberg.

Frieß, U., P. S. Monks, J. J. Remedios, A. Rozanov, R. Sinreich, T. Wagner, and U. Platt (2006), MAX-DOAS O4 measurements: A new technique to derive information on atmospheric aerosols: 2. Modeling studies, J. Geophys. Res., 111, D14203, doi:10.1029/2005JD006618.

G.3 Technical notes

NO_2 O3MSAF GOME-2B Validation Report: Pinardi, G., Lambert, J.-C., Granville, J., Yu, H., De Smedt, I., van Roozendael, M. and Valks, P., (2013) Interim verification report of GOME-2 GDP 4.7 NO2 column data for MetOp-B Operational Readiness Review, Technical Note / Validation Report for the EUMETSAT O3MSAF, http://o3msaf.fmi.fi/docs/vr/Validation_Report_NTO_OTO_NO2_Jun_2013.pdf, (SAF/O3M/IASB/VR/NO2/095/TN-IASB-GOME2B-O3MSAF-NO2-2013), 30 June 2013.

NO_2 O3MSAF GOME-2A Validation Report: Pinardi, G., Lambert, J.C., Granville, J., Clemer, K., Delcloo, A., Hao, N., and P. Valks, (2011) MetOp-A GOME-2 GDP 4.3 / 4.4 total and tropospheric NO2 validation: 2007 – 2010, Technical Note/Validation Report for the EUMETSAT O3MSAF, http://o3msaG.fmi.fi/docs/vr/Validation_ Report_NTO_OTO_NO2_ Feb_2011.pdf

Beirle, S., and T. Wagner, The STRatospheric Estimation Algorithm from Mainz (STREAM): Implementation for GOME-2, O3M-SAF Visiting Scientist Activity, Final Report, October 30, 2015.

Haze, F, S. Godin-Beekmann, F. Hendrick, K. Hocke, M. Palm, M. Pastel, A. Richter (2013), NORS Uncertainty Budgets report,D4.3, rev 00- issue of 28/04/2013, http://nors.aeronomie.be/projectdir/PDF/NORS_D4.3_UB.pdf.

Lambert, J-C., et al., (2004) Geophysical Validation of SCIAMACHY NO2 Vertical columns: Overview of Early 2004 Results. Proc. Atmospheric Chemistry Validation of Envisat-2, ESA/ESRIN, 3-7 May 2004, Frascati, Italy.

Lambert, J.-C., (2006) Télédétection spatiale ultraviolette et visible de l'ozone et du dioxyde d'azote dans l'atmosphère globale. PhD Thesis, Faculté des sciences appliquées/Ecole polytechnique, Free University of Brussels, 291 pp.

Pinardi, G., Hendrick, G., Clémer, K., Lambert, J. C., Bai, J., and Van Roozendael, M.: On the use of the MAXDOAS technique for the validation of tropospheric NO2 column measurements from satellite, proceeding of the EUMETSAT Meteorological Satellite Conference, 9–12 September 2008, Darmstadt, Germany, 2008.

Pinardi, G., Lambert, J.C., Granville, J., Van Roozendael, M., Delcloo, A., De Backer, H., Valks, P., Hao, N., (2010) OVERVIEW OF THE VALIDATION OF GOME-2 TOTAL AND TROPOSPHERIC NO2 COLUMNS, proceeding of the EUMETSAT Meteorological Satellite Conference, 9-12 September 2010, Cordoba, Spain.

Pinardi, G., Van Roozendael, Lambert, J.C., Clemer, K., De Smedt, I., Hendrick, G., Lerot, C., Theys, N., van Gent, J., Vlemmix, T., De Maziere, M., De Backer, H., Delcloo, A., Yu, H., INTEGRATED TRACE GAS VALIDATION AND QUALITY ASSESSMENT SYSTEM FOR THE EUMETSAT POLAR SYSTEM, proceeding of the EUMETSAT Meteorological Satellite Conference, 3-7 September 2012, Sopot, Poland.

Pinardi, G., Van Roozendael, M., Lambert, J.-C., Granville, J., Hendrick, F., Tack, F., Yu, H., Cede, A., Kanaya, Y., Irie, I., Goutail, F., Pommereau, J.-P., Pazmino, A., Wittrock, F., Richter, A., Wagner, T., Gu, M., Remmers, J., Friess, U., Vlemmix, T., Piters, A., Hao, N., Tiefengraber, M., Herman, J., Abuhassan, N., Bais, A., Kouremeti, N., Hovila, J., Holla, R., Chong, J., Postylyakov, O., Ma, J., GOME-2 TOTAL AND TROPOSPHERIC NO2 VALIDATION BASED ON ZENITH-SKY, DIRECT-SUN AND MULTI-AXIS DOAS NETWORK OBSERVATIONS, proceeding of the EUMETSAT Meteorological Satellite Conference, 22-26 September 2014, Geneva, Switzerland.

H. ANNEXES

H.1: Tropospheric NO_2 comparisons

This section groups the specific figures for BIRA MAXDOAS stations for GOME-2 NO_2 tropospheric data from Metop-A and –B for both GDP 4.7 and GDP 4.8 products. Time-series of daily means, monthly means and corresponding scatter plots are shown in Figures H.1.Xa, while absolute and relative differences and the histogram of the SAT-GB differences are shown in Figures H.1.Xb. An overview table of the result for each specific station is given after the figures.

BIRA-IASB performs continuous MAX-DOAS measurements at OHP, Xianghe, Bujumbura and Uccle. OHP (south of France) is a clean/remote NDACC station alternating between clean air and pollution episodes. MAXDOAS measurements are performed since 2005 and this is the longest BIRA-IASB time-serie available for the NO_2 validation. During the period from June 2008 to April 2009 BIRA-IASB performed MAXDOAS measurements in Beijing city center, exploring very polluted conditions. Comparisons at this station show large differences between satellite and ground-based measurements. This is mainly due to the difference of sensitivity to the local pollution between the MAXDOAS, located in the city centre of Beijing and the satellite, sampling a larger area. Since March 2010 the MAXDOAS instrument has been moved to Xianghe, approximately 60 km south-east of the Beijing city center. This site is less directly affected by local urban sources of pollution and it is thus better suited for satellite comparisons since the sampled air masses are more representative of the satellite measurements. A mini-MAXDOAShas been measuring in Uccle (Belgium) since May 2011, while in November 2013, BIRA-IASB has installed a MAXDOAS instrument in central Africa, in Bujumbura (Burundi).

OHP

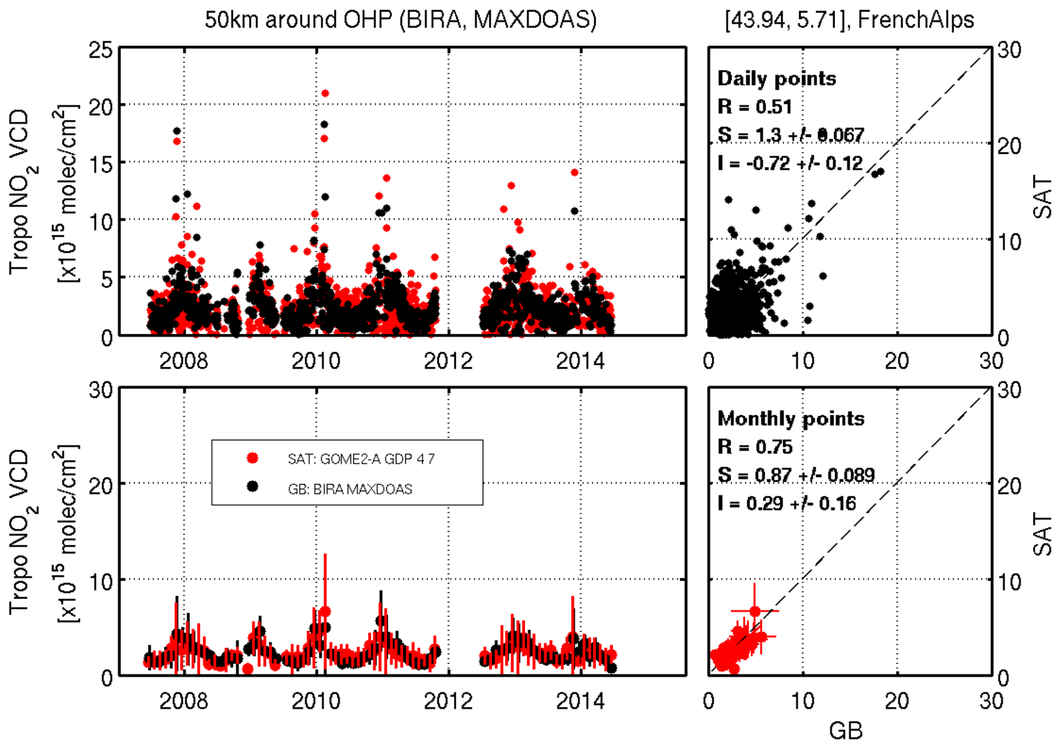

Figure H.1.1a Time series of MAXDOAS and GOME-2 A GDP 4.7 tropopsheric columns above OHP, from 2007 to June 2014. The first vertical panel presents the daily points and the second the monthly mean values. The right panels present the scatter plot and regression parameters.

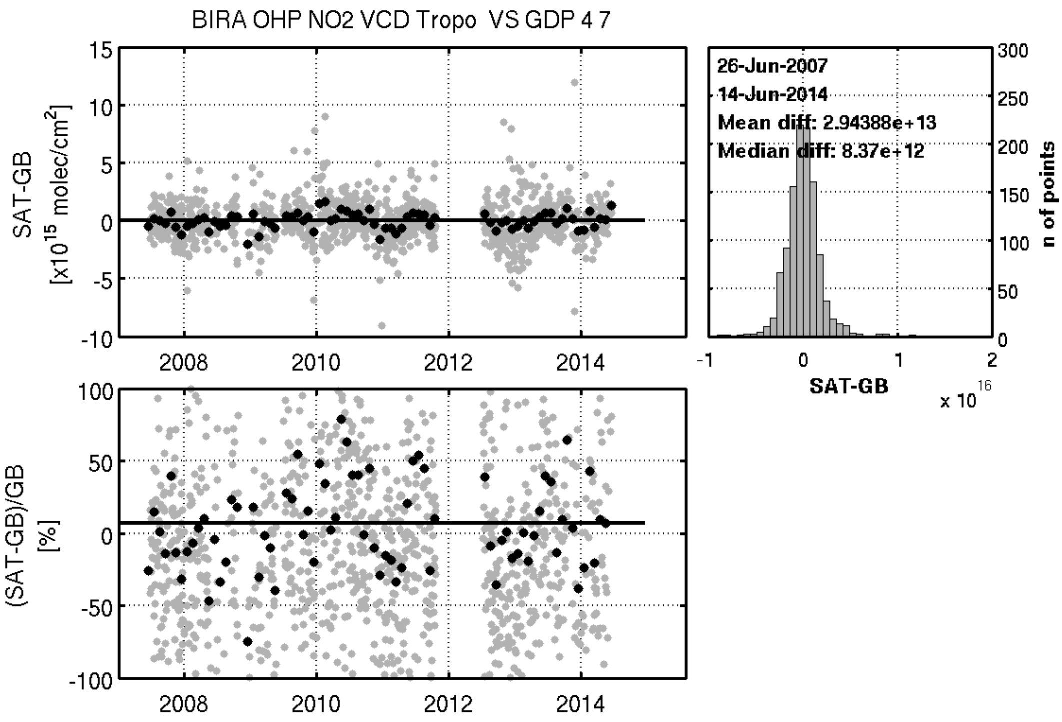

Figure H.1.1b Time series of GOME-2 A GDP 4.7 minus MAXDOAS tropopsheric columns above OHP, from 2007 to June 2014. The first vertical panel presents the absolute values (daily points in grey and monthly means in black) and the second the relative values. The right panels present the histogram of the absolute differences and the mean and median value.

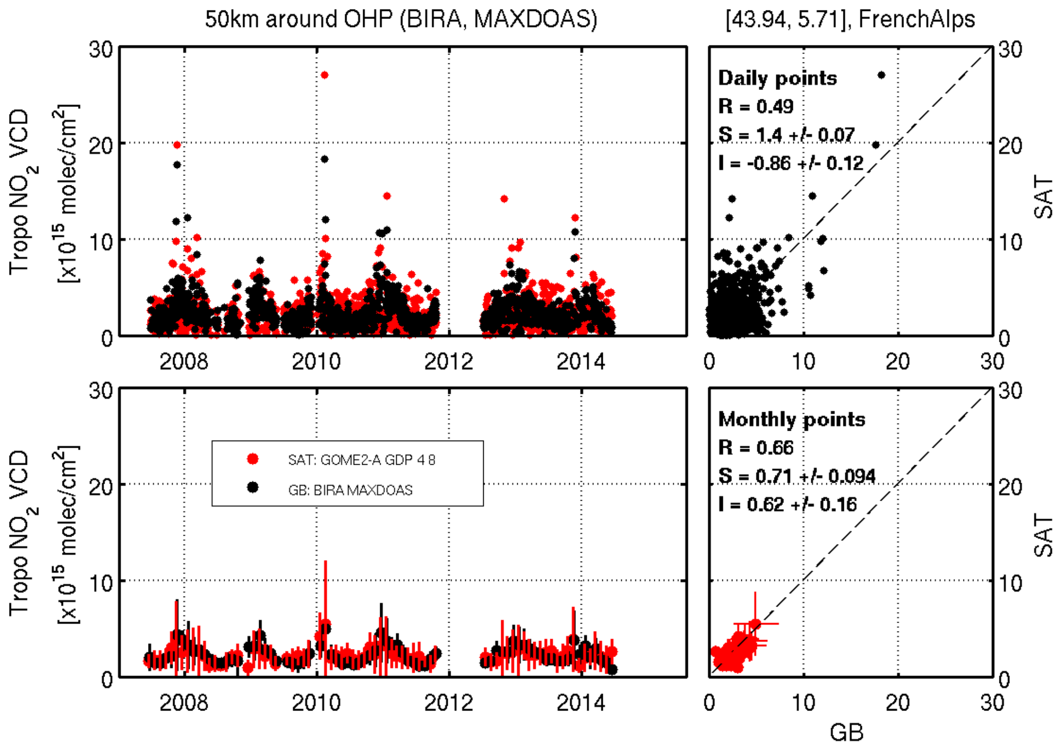

Figure H.1.2a Time series of MAXDOAS and GOME-2 A GDP 4.8 tropopsheric columns above OHP, from 2007 to June 2014. The first vertical panel presents the daily points and the second the monthly mean values. The right panels present the scatter plot and regression parameters.

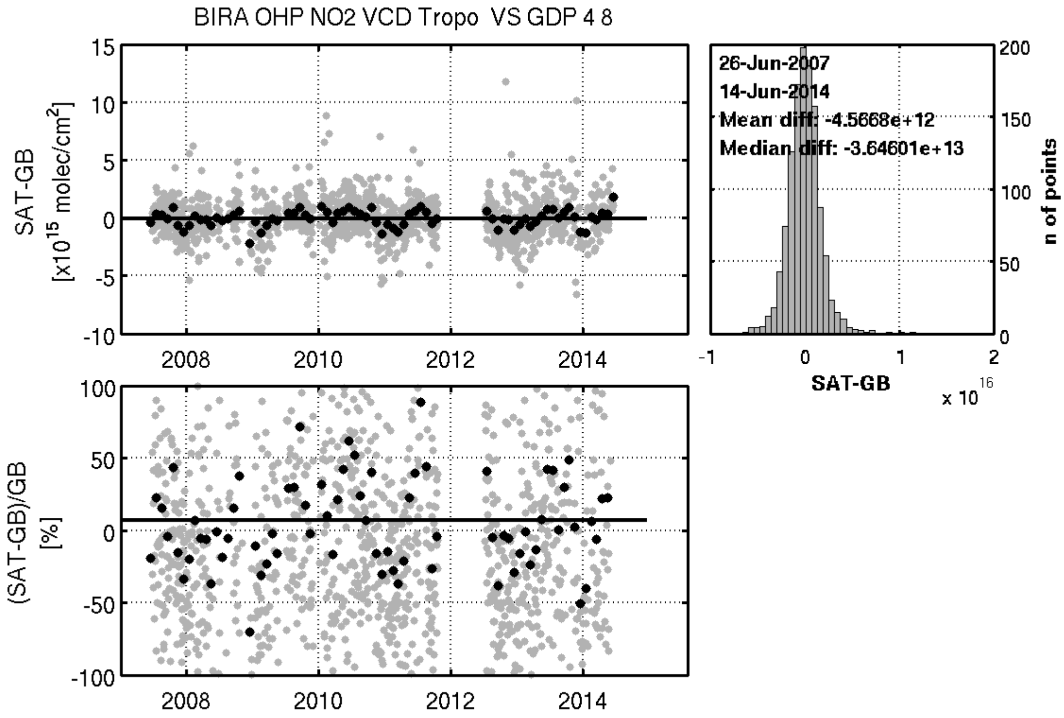

Figure H.1.2b Time series of GOME-2 A GDP 4.8 minus MAXDOAS tropopsheric columns above OHP, from 2007 to June 2014. The first vertical panel presents the absolute values (daily points in grey and monthly means in black) and the second the relative values. The right panels present the histogram of the absolute differences and the mean and median value.

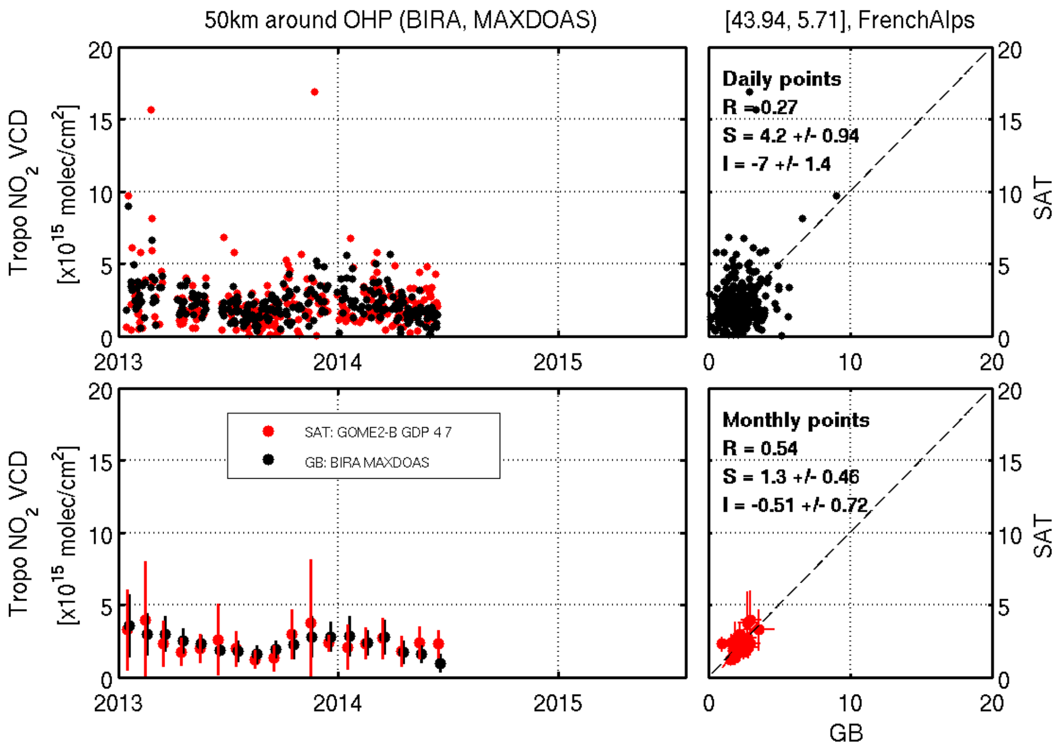

Figure H.1.3a Time series of MAXDOAS and GOME-2 B GDP 4.7 tropopsheric columns above OHP, from 2013 to June 2014. The first vertical panel presents the daily points and the second the monthly mean values. The right panels present the scatter plot and regression parameters.

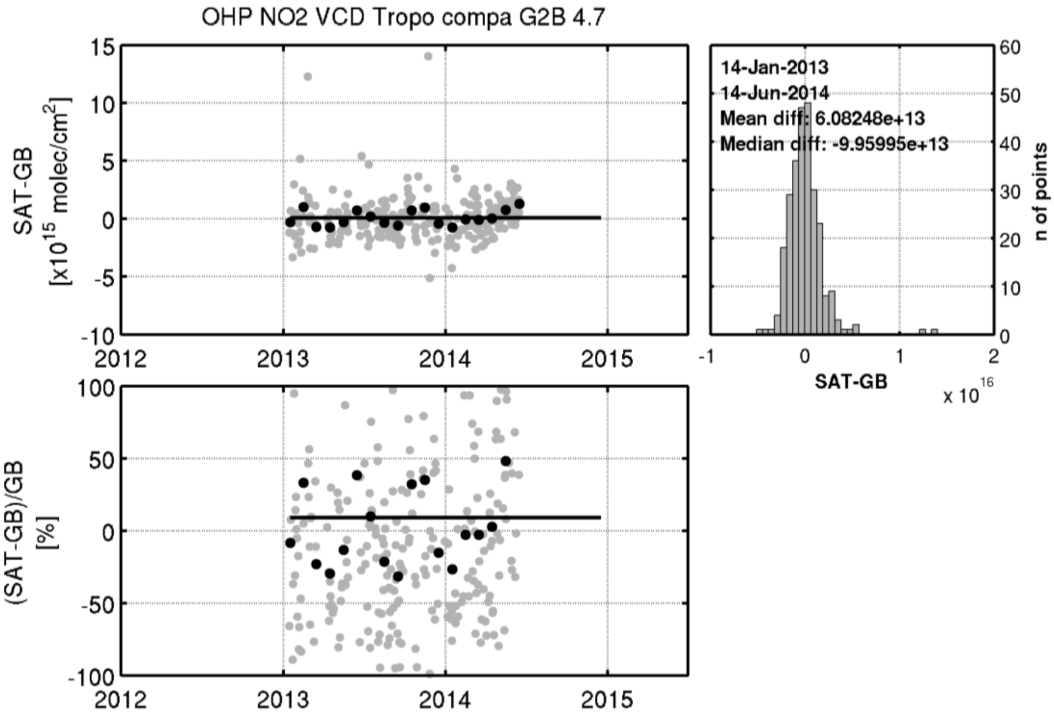

Figure H.1.3b Time series of GOME-2 B GDP 4.7 minus MAXDOAS tropopsheric columns above OHP, from 2013 to June 2014. The first vertical panel presents the absolute values (daily points in grey and monthly means in black) and the second the relative values. The right panels present the histogram of the absolute differences and the mean and median value.

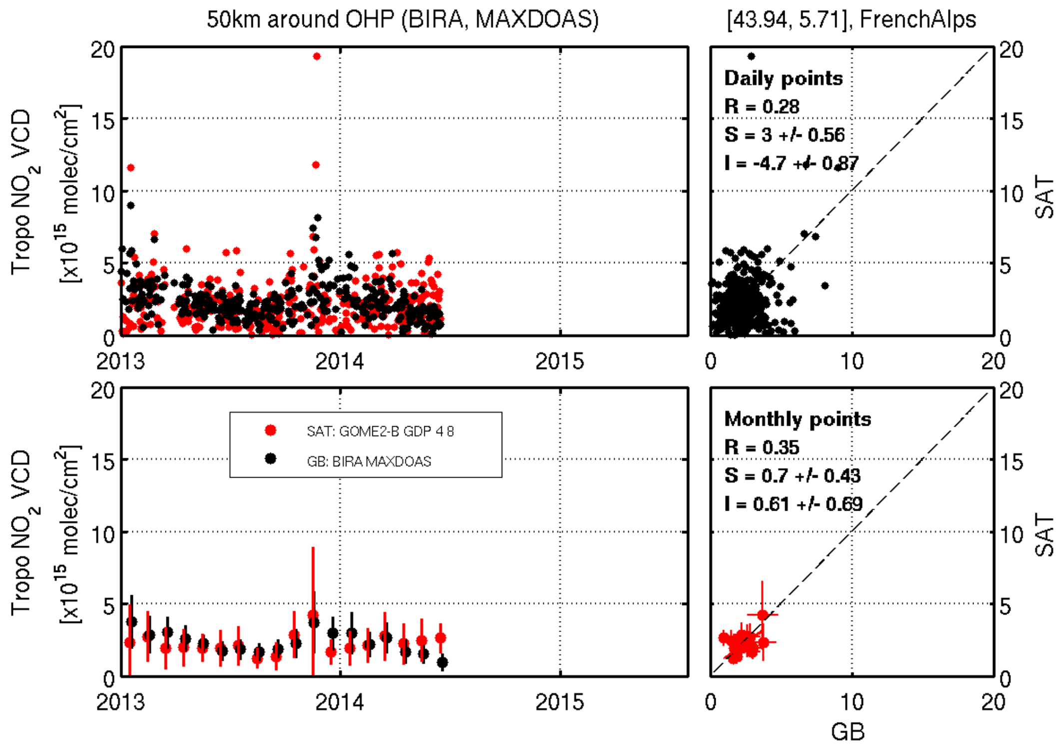

Figure H.1.4a Time series of MAXDOAS and GOME-2 B GDP 4.8 tropopsheric columns above OHP, from 2013 to June 2014. The first vertical panel presents the daily points and the second the monthly mean values. The right panels present the scatter plot and regression parameters.

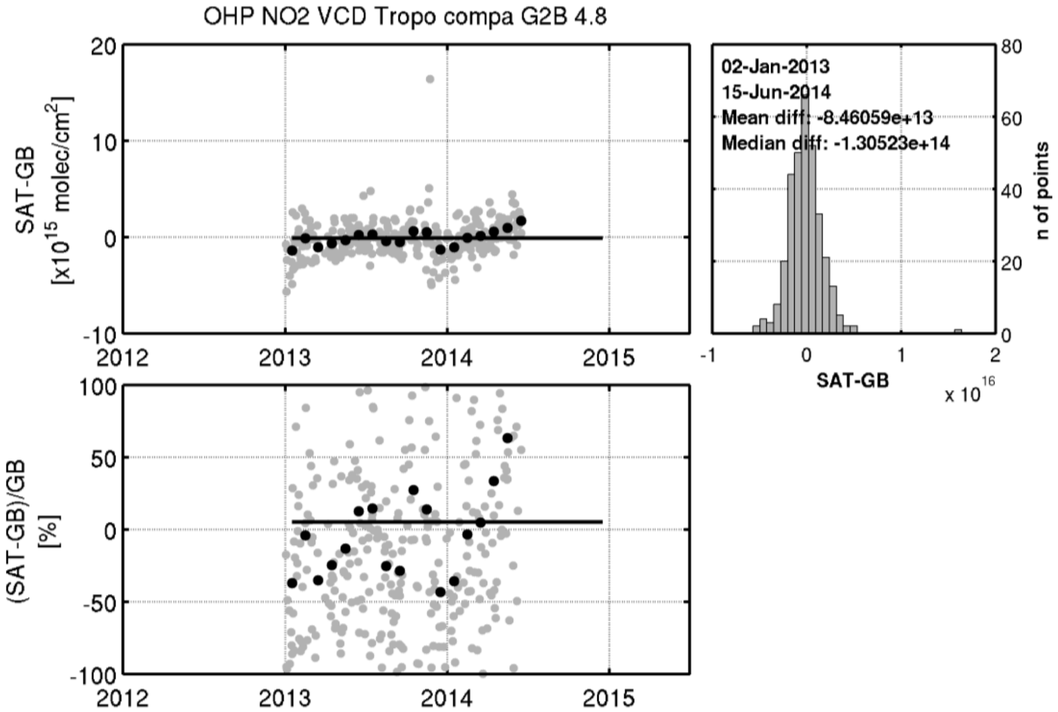

Figure H.1.4b Time series of GOME-2 B GDP 4.8 minus MAXDOAS tropopsheric columns above OHP, from 2013 to June 2014. The first vertical panel presents the absolute values (daily points in grey and monthly means in black) and the second the relative values. The right panels present the histogram of the absolute differences and the mean and median value.

Table H.1.1 Regression parameters (correlation coefficient R, slope S and intercept I of the regression) and differences (GDP – GB) of the monthly mean comparisons of GOME-2 A and B for both GDP 4.7 and GDP 4.8 at OHP.

Monthly means	MetOp-A GDP 4.7	MetOp-A GDP 4.8	MetOp-B GDP 4.7	MetOp-B GDP 4.8
Regression parameters	R = 0.75 S = 0.87±0.09 I = 0.29±0.16	R = 0.66 S = 0.71±0.09 I = 0.62±0.16	R = 0.54 S = 1.3±0.46 I = -0.51±0.72	R = 0.35 S = 0.7±0.43 I = 0.61±0.69
Differences [molec/cm²]	Mean: $2.9x10^{13}$ Median: $8.4x10^{14}$	Mean: $-0.46x10^{13}$ Median: $-0.36x10^{14}$	Mean: $6.1x10^{13}$ Median: $-0.99x10^{14}$	Mean: $-8.5x10^{13}$ Median: $-1.3x10^{14}$

Uccle

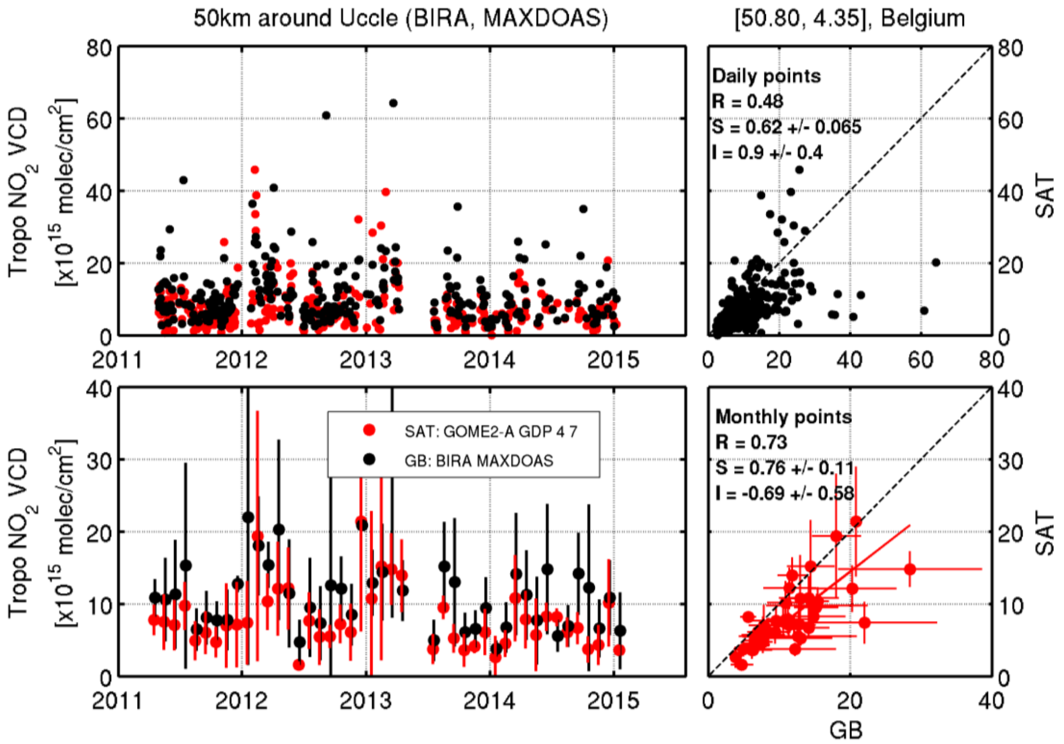

Figure H.1.5a Time series of MAXDOAS and GOME-2 A GDP 4.7 tropopsheric columns above Uccle, from April 2011 to January 2015. The first vertical panel presents the daily points and the second the monthly mean values. The right panels present the scatter plot and regression parameters.

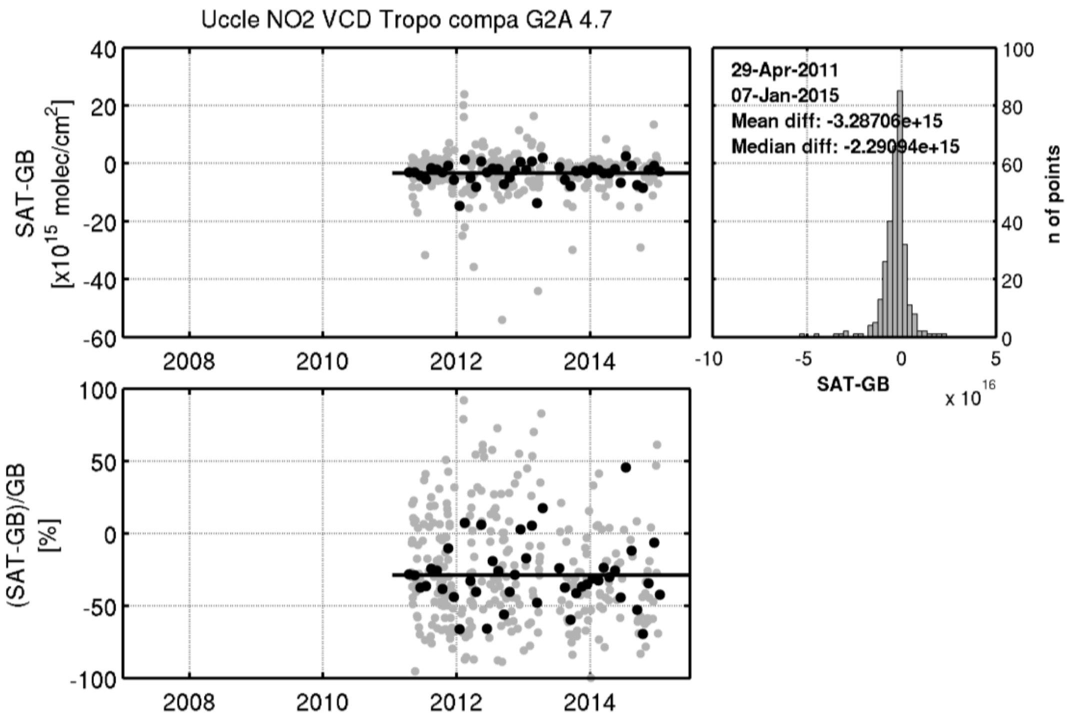

Figure H.1.5b Time series of GOME-2 A GDP 4.7 minus MAXDOAS tropopsheric columns above Uccle, from April 2011 to January 2015. The first vertical panel presents the absolute values (daily points in grey and monthly means in black) and the second the relative values. The right panels present the histogram of the absolute differences and the mean and median value.

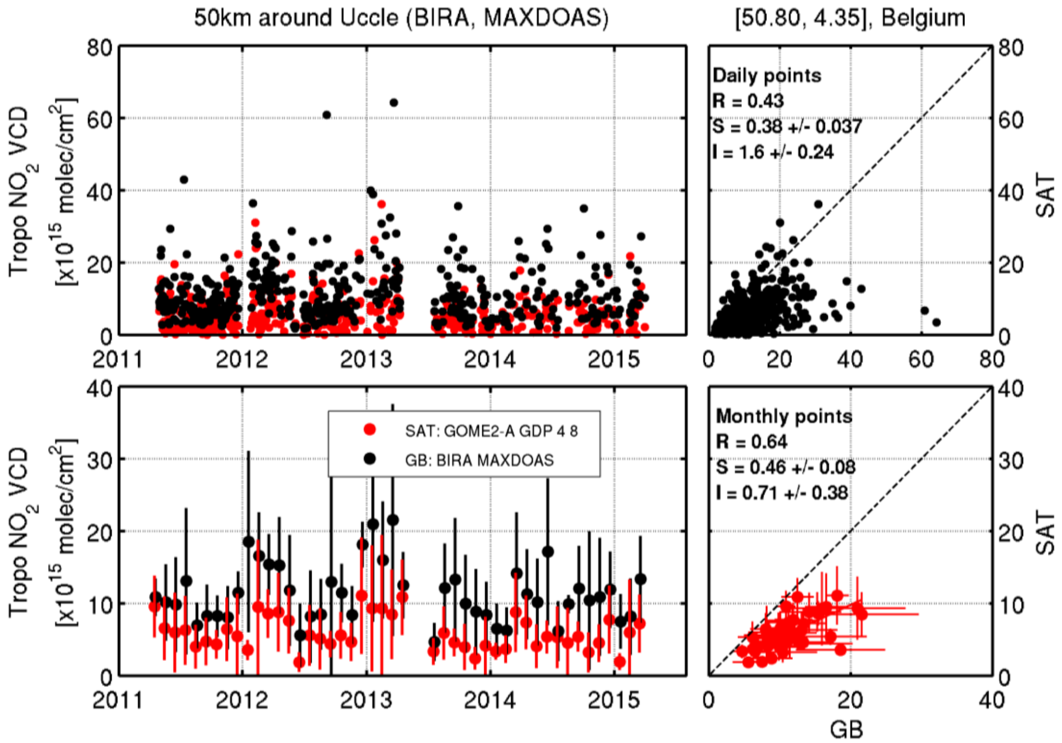

Figure H.1.6a Time series of MAXDOAS and GOME-2 A GDP 4.8 tropopsheric columns Uccle, from April 2011 to March 2015. The first vertical panel presents the daily points and the second the monthly mean values. The right panels present the scatter plot and regression parameters.

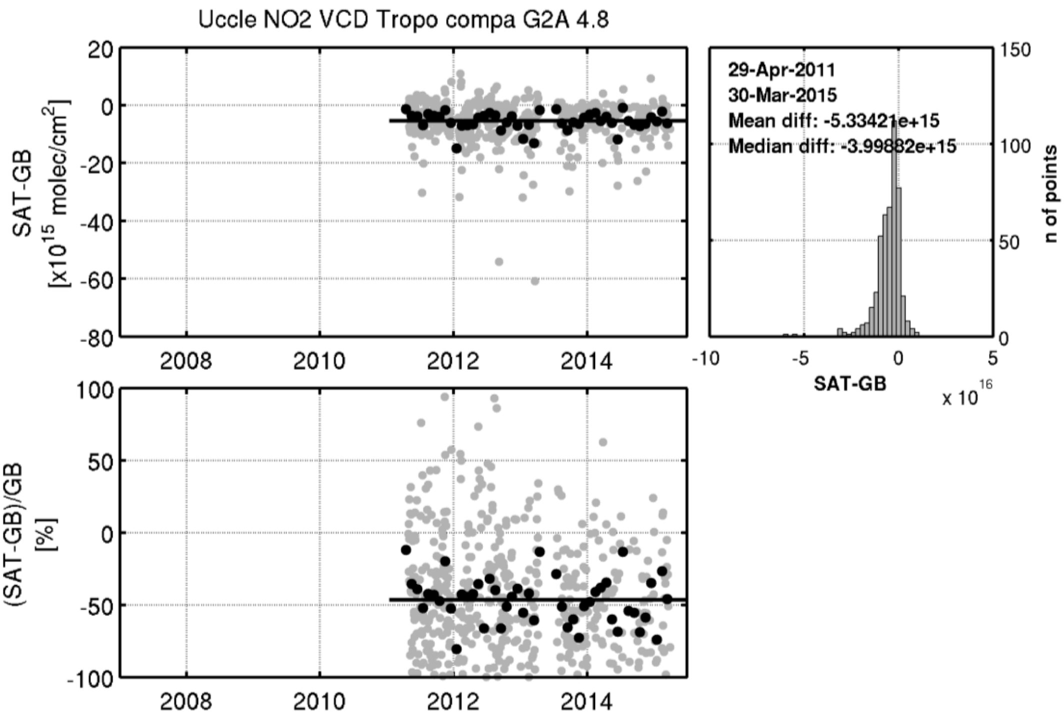

Figure H.1.6b Time series of GOME-2 A GDP 4.8 minus MAXDOAS tropopsheric columns above Uccle, from April 2011 to March 2015. The first vertical panel presents the absolute values (daily points in grey and monthly means in black) and the second the relative values. The right panels present the histogram of the absolute differences and the mean and median value.

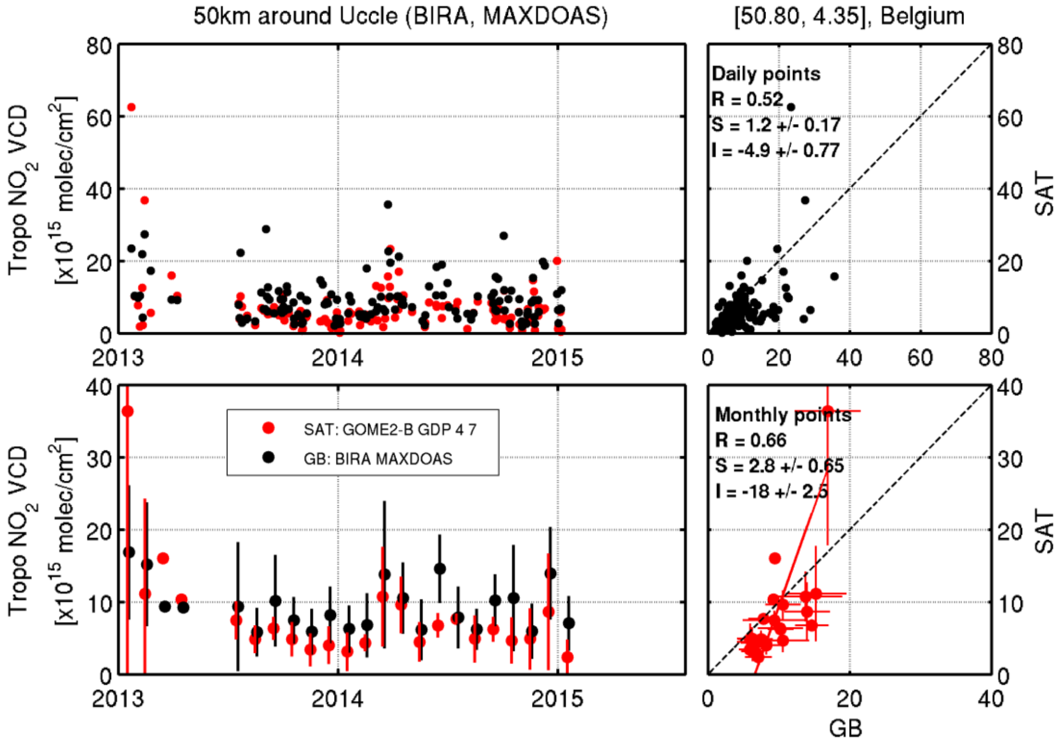

Figure H.1.7a Time series of MAXDOAS and GOME-2 B GDP 4.7 tropopsheric columns above Uccle, from January 2012 to January 2015. The first vertical panel presents the daily points and the second the monthly mean values. The right panels present the scatter plot and regression parameters.

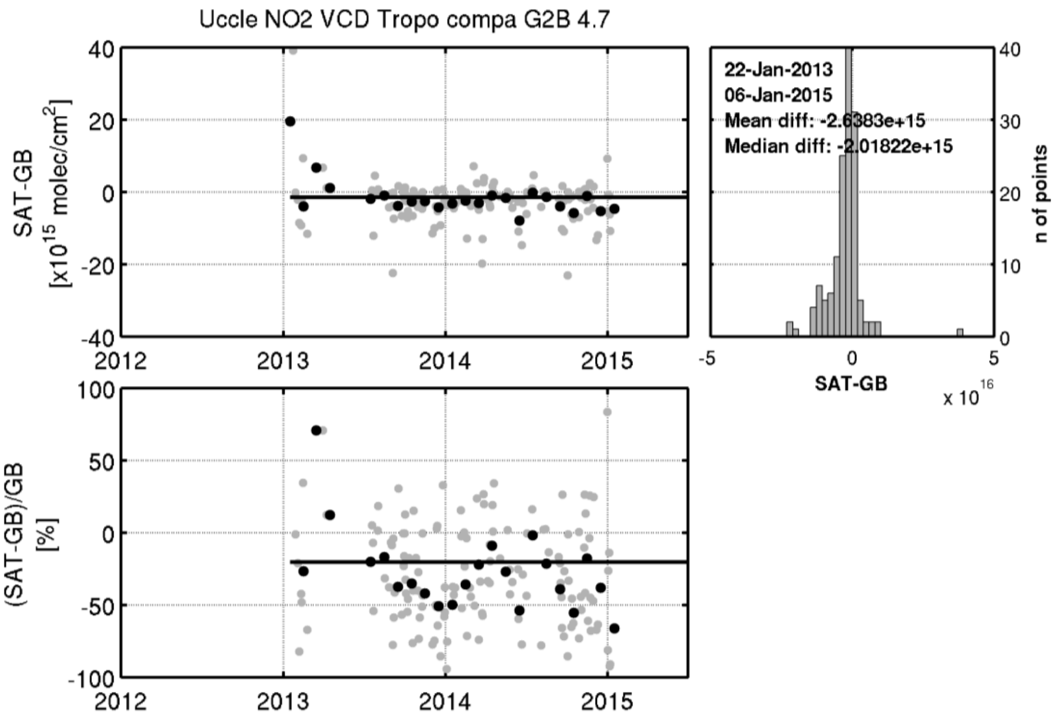

Figure H.1.7b Time series of GOME-2 B GDP 4.7 minus MAXDOAS tropopsheric columns above Uccle, from January 2012 to January 2015. The first vertical panel presents the absolute values (daily points in grey and monthly means in black) and the second the relative values. The right panels present the histogram of the absolute differences and the mean and median value.

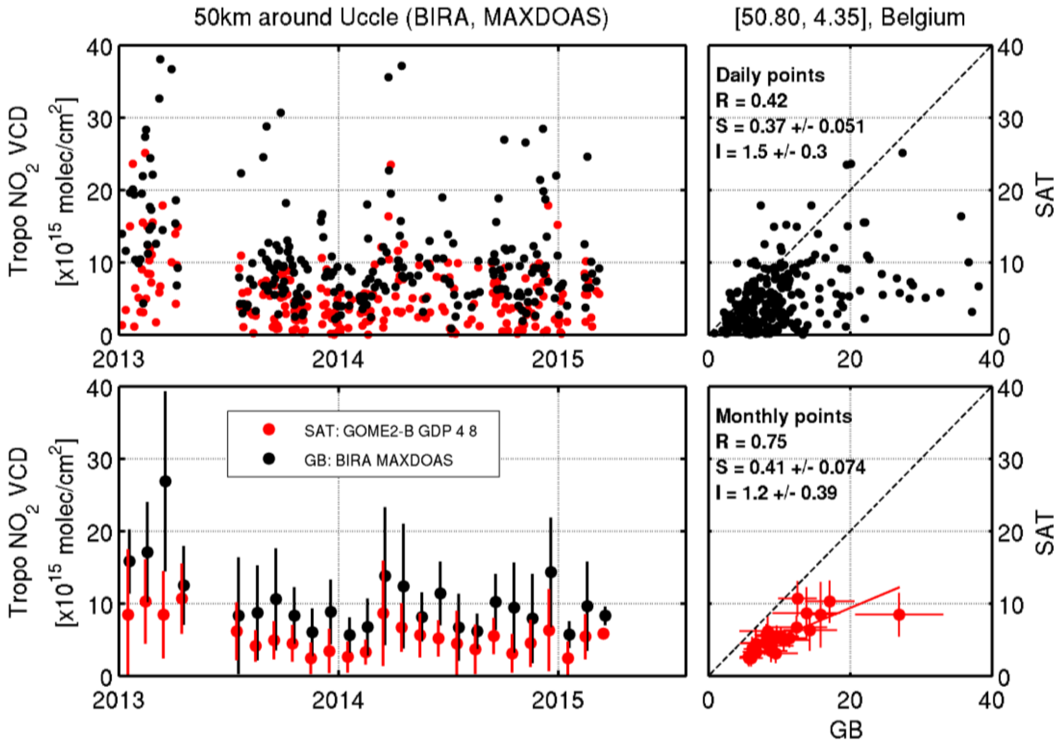

Figure H.1.8a Time series of MAXDOAS and GOME-2 B GDP 4.8 tropopsheric columns above Uccle, from January 2012 to March 2015. The first vertical panel presents the daily points and the second the monthly mean values. The right panels present the scatter plot and regression parameters.

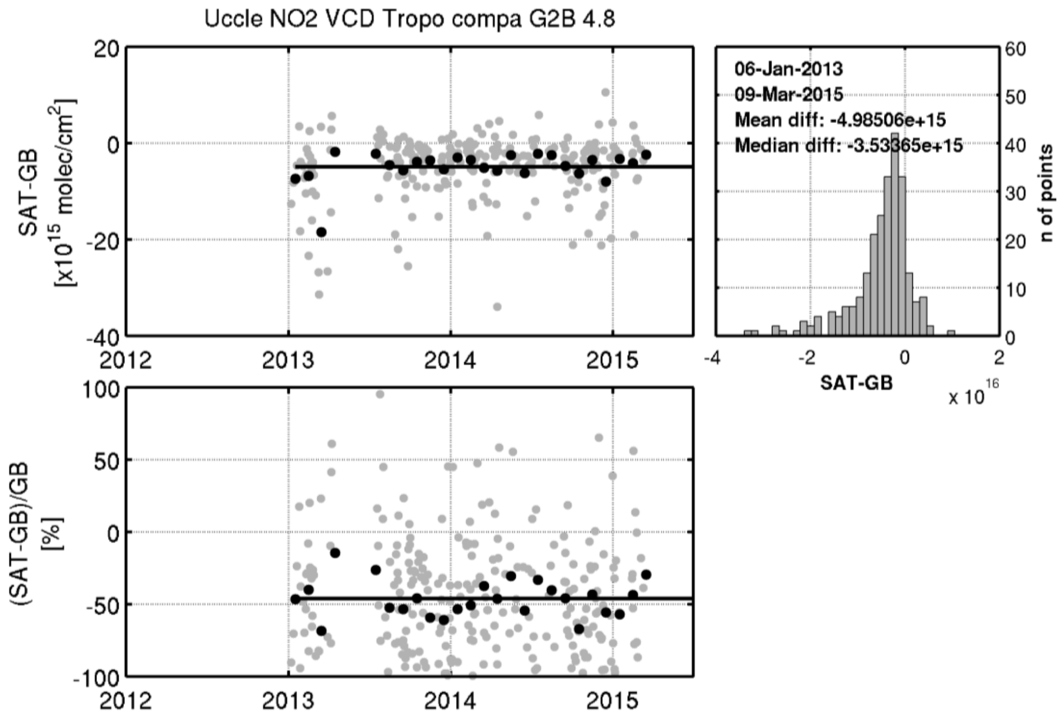

Figure H.1.8b Time series of GOME-2 B GDP 4.8 minus MAXDOAS tropopsheric columns above Uccle, from January 2012 to March 2015. The first vertical panel presents the absolute values (daily points in grey and monthly means in black) and the second the relative values. The right panels present the histogram of the absolute differences and the mean and median value.

Table H.1.2 Regression parameters (correlation coefficient R, slope S and intercept I of the regression) and differences (GDP – GB) of the monthly mean comparisons of GOME-2 A and B for both GDP 4.7 and GDP 4.8 at Uccle.

Monthly means	MetOp-A GDP 4.7	MetOp-A GDP 4.8	MetOp-B GDP 4.7	MetOp-B GDP 4.8
Regression parameters	R = 0.73 S = 0.76±0.11 I = -0.69±0.58	R = 0.64 S = 0.46±0.08 I = 0.71±0.4	R = 0.66 S = 2.8±0.65 I = -18 ± 2.5	R = 0.75 S = 0.41±0.07 I = 1.2 ±0.4
Differences [molec/cm²]	Mean: -3.28×10^{15} Median: -2.3×10^{15}	Mean: -5.33×10^{15} Median: $- 4\times10^{15}$	Mean: -2.6×10^{15} Median: -2.02×10^{15}	Mean: -4.9×10^{15} Median: -3.53×10^{15}

Xianghe

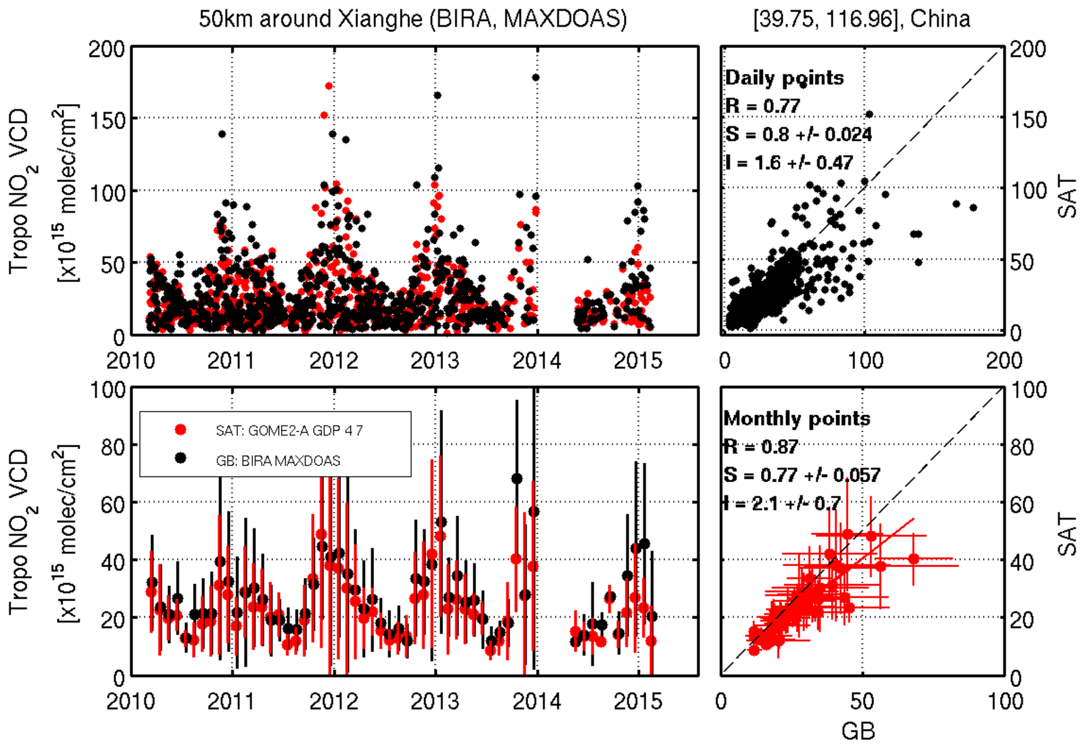

Figure H.1.9a Time series of MAXDOAS and GOME-2 A GDP 4.7 tropopsheric columns above Xianghe, from March 2010 to end February 2015. The first vertical panel presents the daily points and the second the monthly mean values. The right panels present the scatter plot and regression parameters.

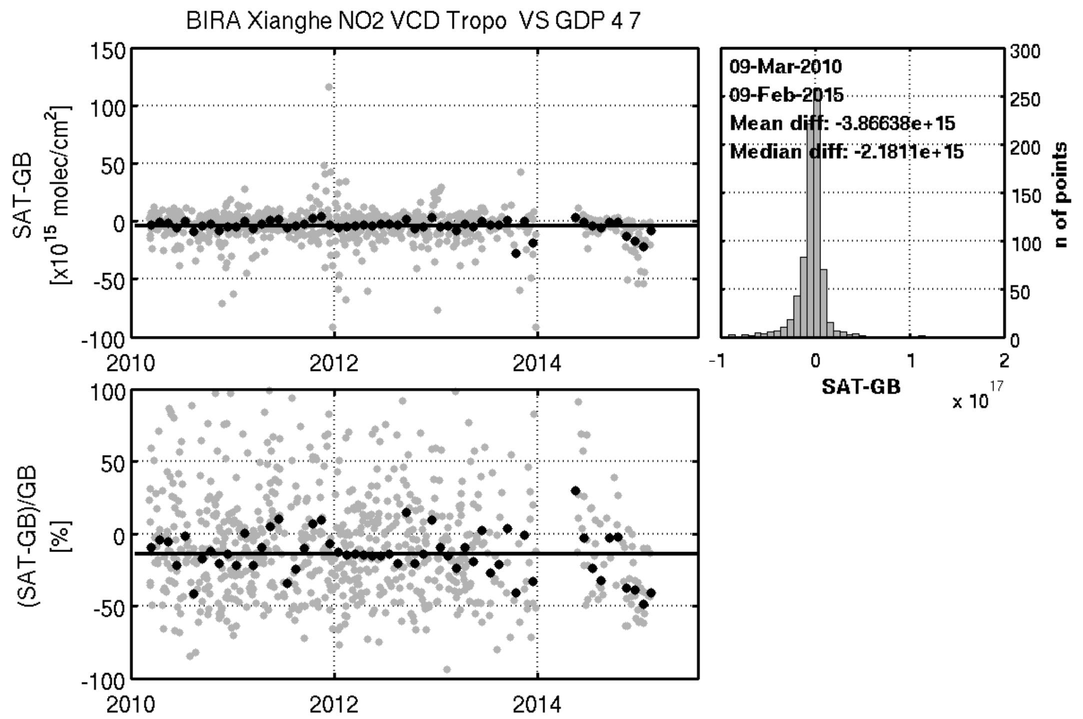

Figure H.1.9b Time series of GOME-2 A GDP 4.7 minus MAXDOAS tropopsheric columns above Xianghe, from March 2010 to end February 2015. The first vertical panel presents the absolute values (daily points in grey and monthly means in black) and the second the relative values. The right panels present the histogram of the absolute differences and the mean and median value.

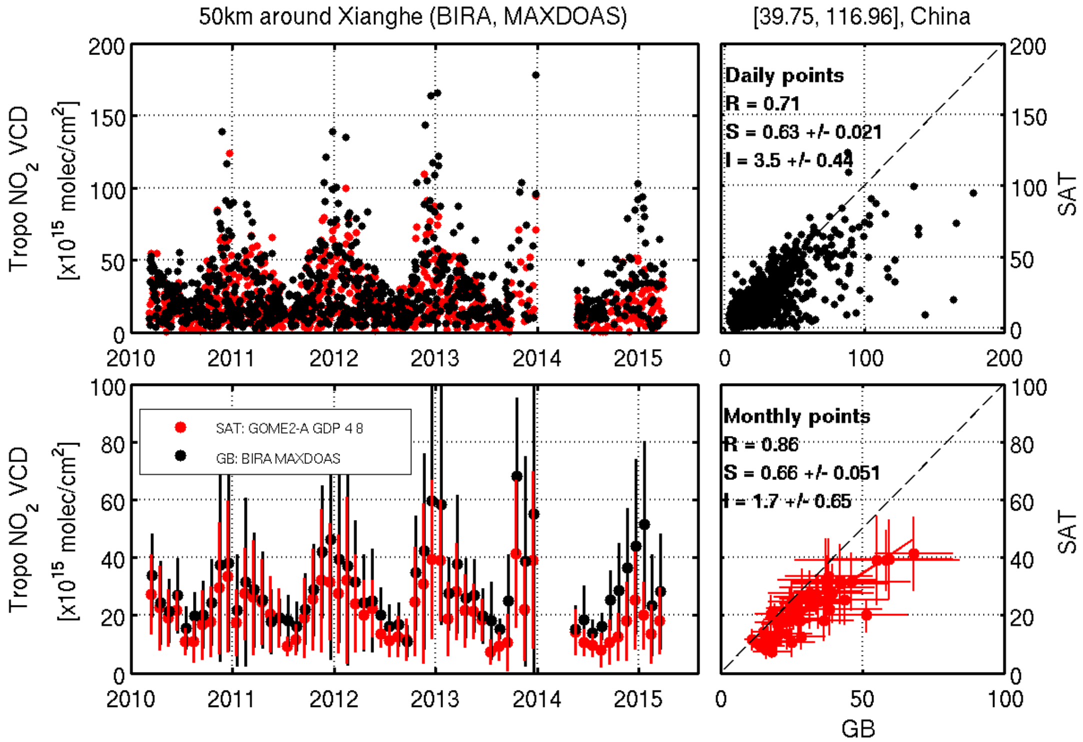

Figure H.1.10a Time series of MAXDOAS and GOME-2 A GDP 4.8 tropopsheric columns above Xianghe, from March 2010 to end March 2015. The first vertical panel presents the daily points and the second the monthly mean values. The right panels present the scatter plot and regression parameters.

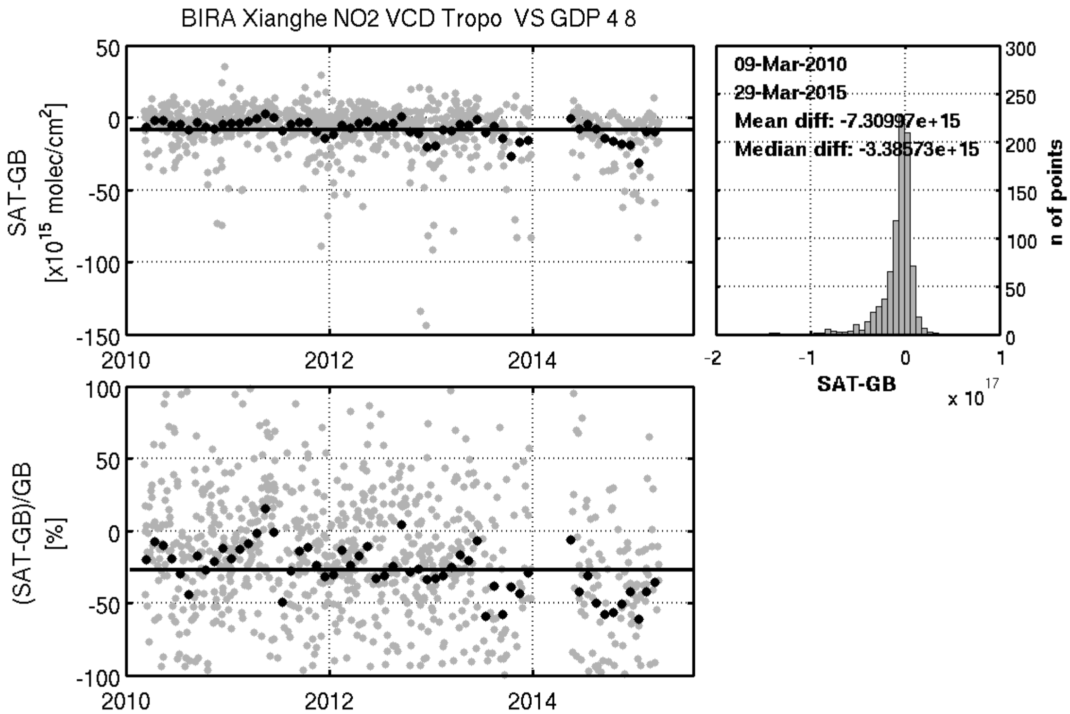

Figure H.1.10b Time series of GOME-2 A GDP 4.8 minus MAXDOAS tropopsheric columns above Xianghe, from March 2010 to end March 2015. The first vertical panel presents the absolute values (daily points in grey and monthly means in black) and the second the relative values. The right panels present the histogram of the absolute differences and the mean and median value.

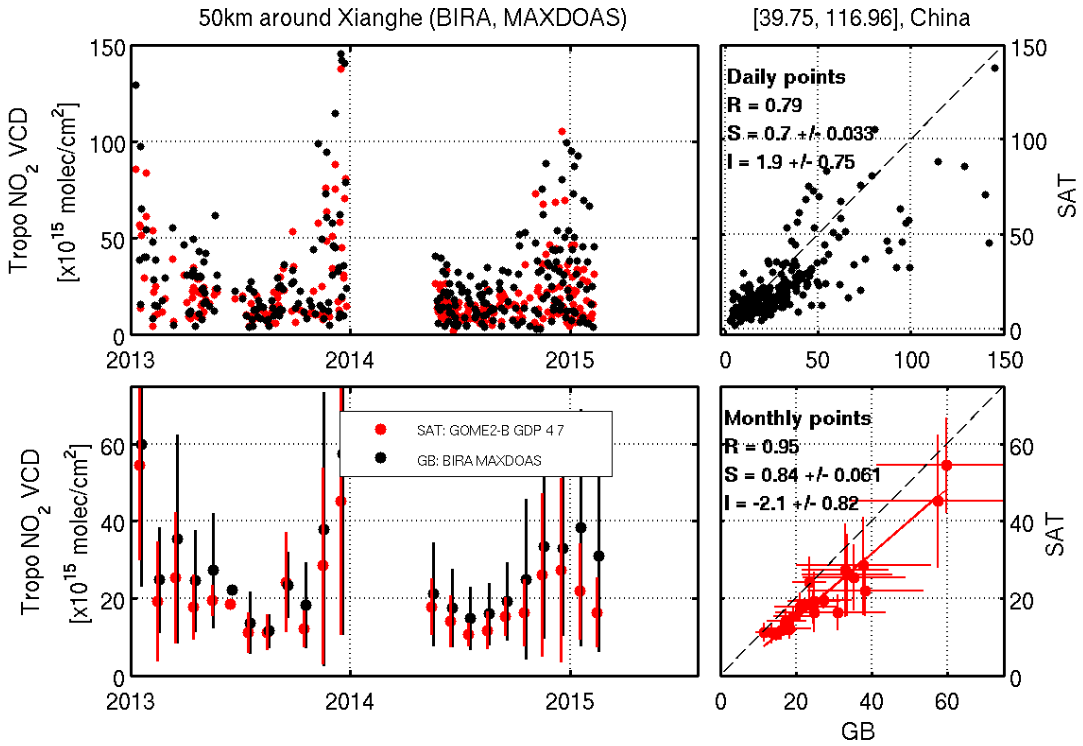

Figure H.1.11a Time series of MAXDOAS and GOME-2 B GDP 4.7 tropopsheric columns above Xianghe, from 2013 to February 2015. The first vertical panel presents the daily points and the second the monthly mean values. The right panels present the scatter plot and regression parameters.

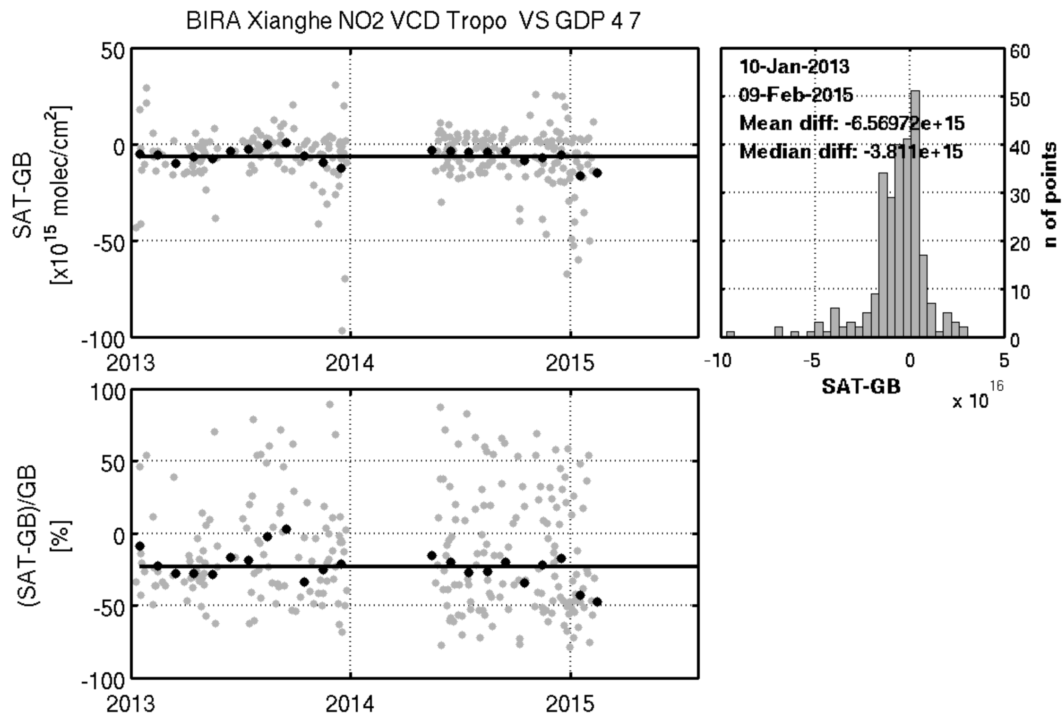

Figure H.1.11b Time series of GOME-2 B GDP 4.7 minus MAXDOAS tropopsheric columns above Xianghe, from 2013 to February 2015. The first vertical panel presents the absolute values (daily points in grey and monthly means in black) and the second the relative values. The right panels present the histogram of the absolute differences and the mean and median value.

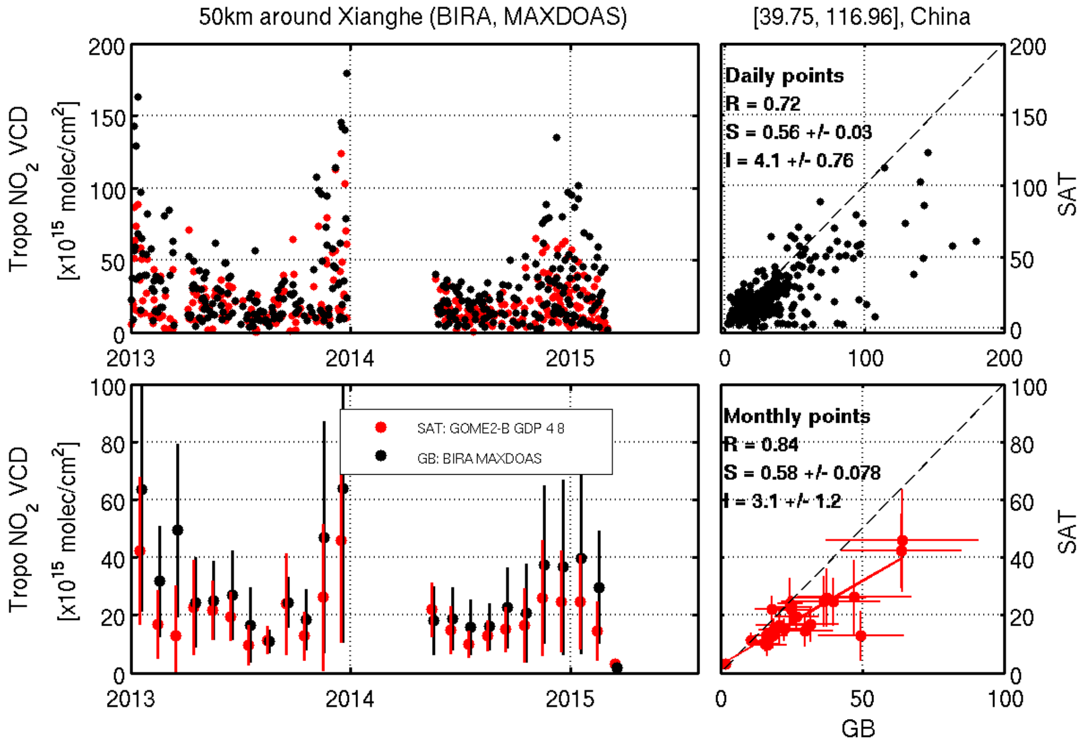

Figure H.1.12a Time series of MAXDOAS and GOME-2 B GDP 4.8 tropopsheric columns above Xianghe, from 2013 to March 2015. The first vertical panel presents the daily points and the second the monthly mean values. The right panels present the scatter plot and regression parameters.

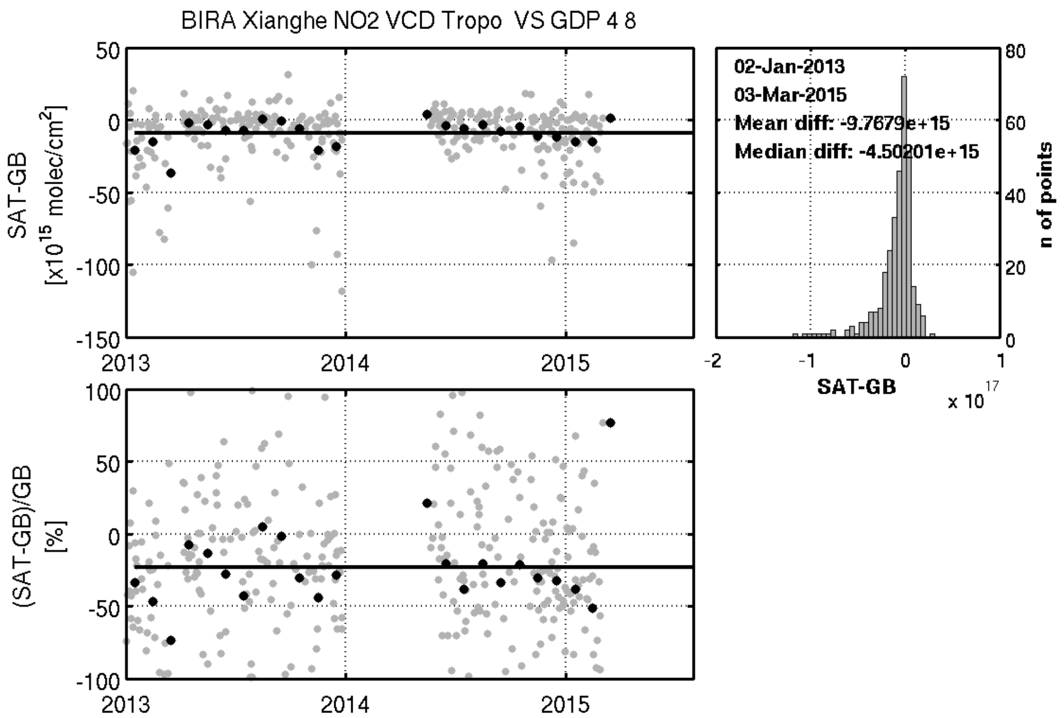

Figure H.1.12b Time series of GOME-2 B GDP 4.8 minus MAXDOAS tropopsheric columns above Xianghe, from 2013 to March 2015. The first vertical panel presents the absolute values (daily points in grey and monthly means in black) and the second the relative values. The right panels present the histogram of the absolute differences and the mean and median value.

Table H.1.3 Regression parameters (correlation coefficient R, slope of the regression S, intercept of the regression I) and differences (GDP – GB) of the monthly mean comparisons of GOME-2 A and B for both GDP 4.7 and GDP 4.8 at Xianghe.

Monthly means	MetOp-A GDP 4.7	MetOp-A GDP 4.8	MetOp-B GDP 4.7	MetOp-B GDP 4.8
Regression parameters	R = 0.87 S = 0.77±0.06 I = 2.1±0.7	R = 0.86 S = 0.66±0.06 I = 1.7 ±0.65	R = 0.95 S = 0.84 ±0.06 I = -2.1±0.82	R = 0.84 S = 0.58 ±0.08 I = 3.1±1.2
Differences [molec/cm^2]	Mean: -3.9×10^{15} Median: -2.18×10^{15}	Mean: -7.3×10^{15} Median: -3.4×10^{15}	Mean: -6.6×10^{15} Median: -3.8×10^{15}	Mean: -9.8×10^{15} Median: -4.5×10^{15}

Beijing

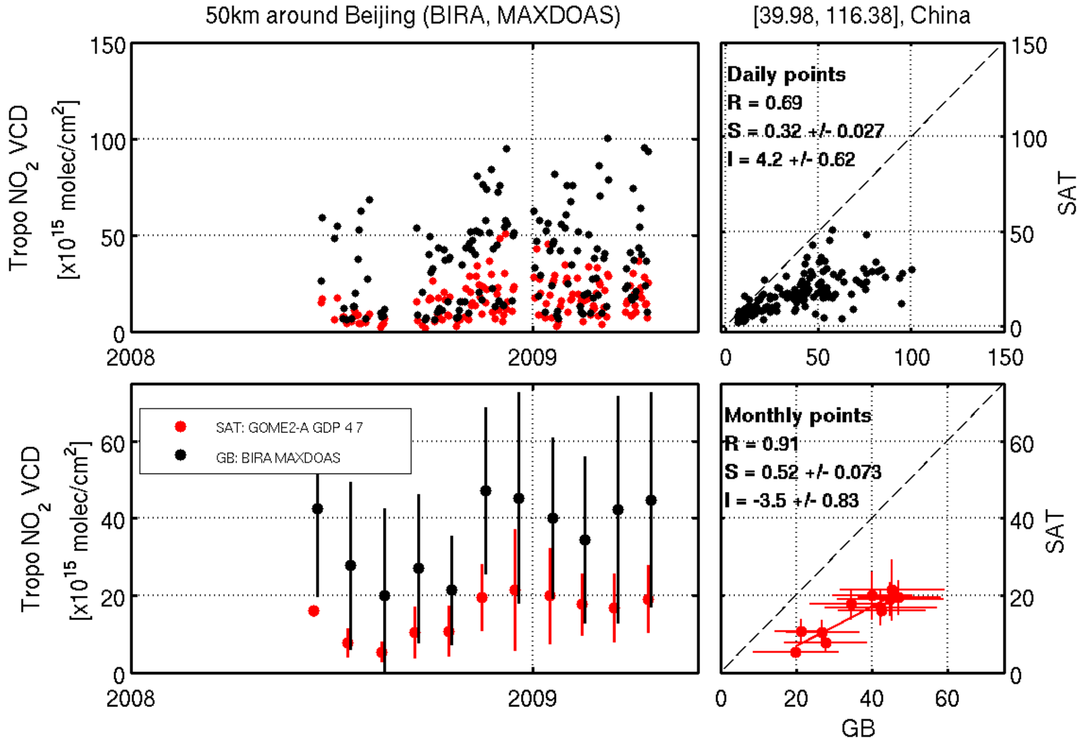

Figure H.1.13a Time series of MAXDOAS and GOME-2 A GDP 4.7 tropopsheric columns above Beijing, from June 2008 to April 2009. The first vertical panel presents the daily points and the second the monthly mean values. The right panels present the scatter plot and regression parameters.

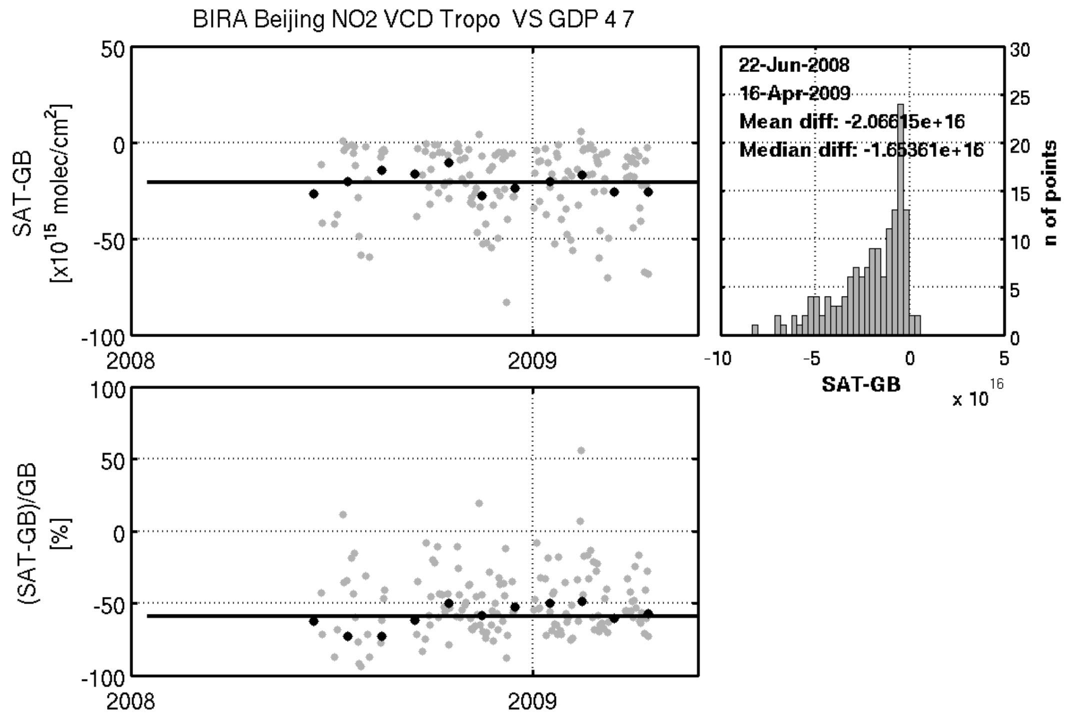

Figure H.1.13b Time series of GOME-2 A GDP 4.7 minus MAXDOAS tropopsheric columns above Beijing, from June 2008 to April 2009. The first vertical panel presents the absolute values (daily points in grey and monthly means in black) and the second the relative values. The right panels present the histogram of the absolute differences and the mean and median value.

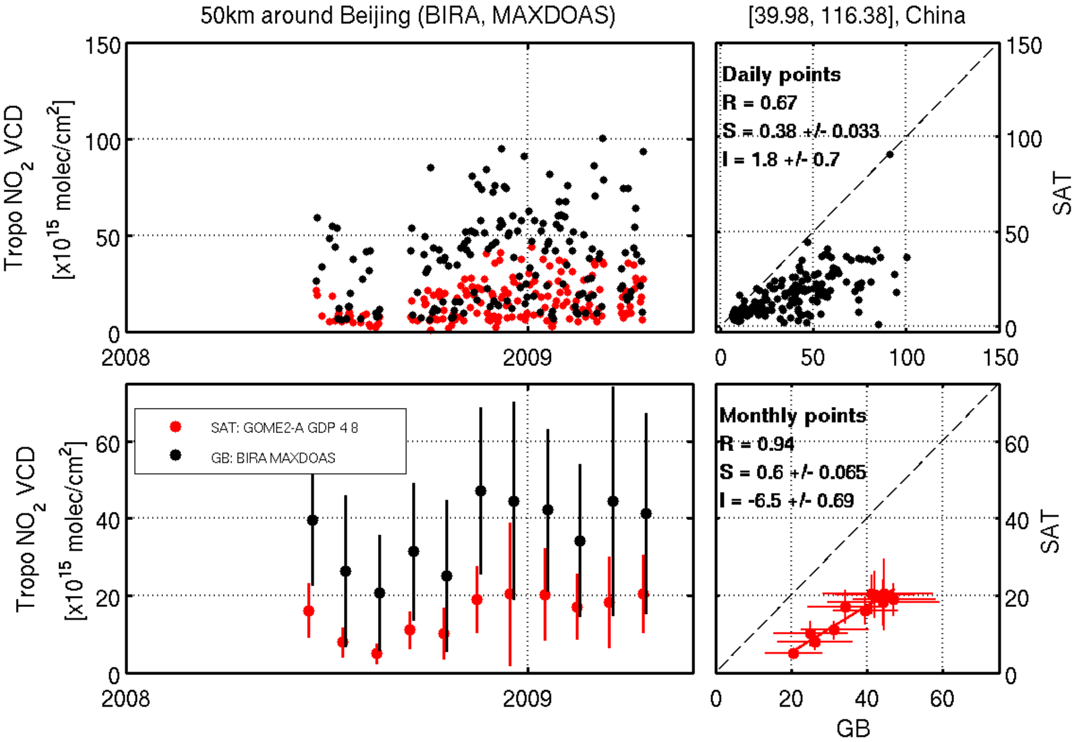

Figure H.1.14a Time series of MAXDOAS and GOME-2 A GDP 4.8 tropopsheric columns above Beijing, from June 2008 to April 2009. The first vertical panel presents the daily points and the second the monthly mean values. The right panels present the scatter plot and regression parameters.

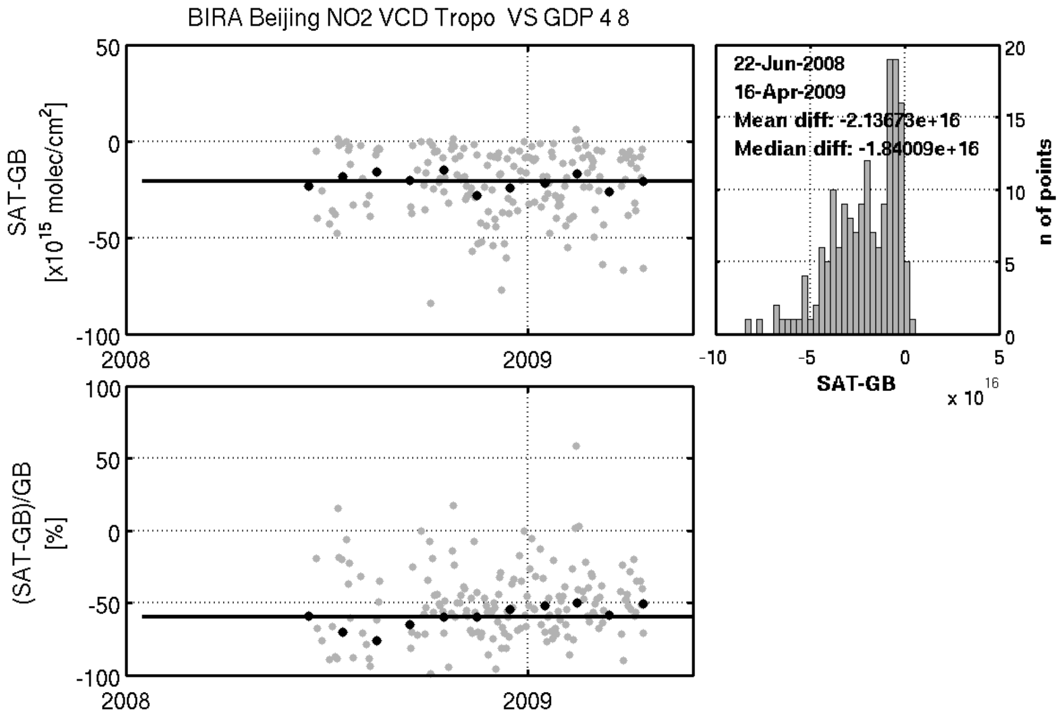

Figure H.1.14b Time series of GOME-2 A GDP 4.8 minus MAXDOAS tropopsheric columns above Beijing, from June 2008 to April 2009. The first vertical panel presents the absolute values (daily points in grey and monthly means in black) and the second the relative values. The right panels present the histogram of the absolute differences and the mean and median value.

Table H.1.4 Regression parameters (correlation coefficient R, slope S and intercept I of the regression) and differences (GDP – GB) of the monthly mean comparisons of GOME-2 A and B for both GDP 4.7 and GDP 4.8 at Beijing.

Monthly means	MetOp-A GDP 4.7	MetOp-A GDP 4.8	MetOp-B GDP 4.7	MetOp-B GDP 4.8
Regression parameters	R = 0.91 S = 0.52±0.07 I = -3.5±0.8	R = 0.94 S = 0.6±0.065 I = -6.5±0.69	na	na
Differences [molec/cm²]	Mean: -2.1×10^{16} Median: -1.6×10^{16}	Mean: -2.1×10^{16} Median: -1.8×10^{16}	na	na

No Metop-B comparisons for the Beijing stations because this station was operational only during 2008-2009.

Bujumbura

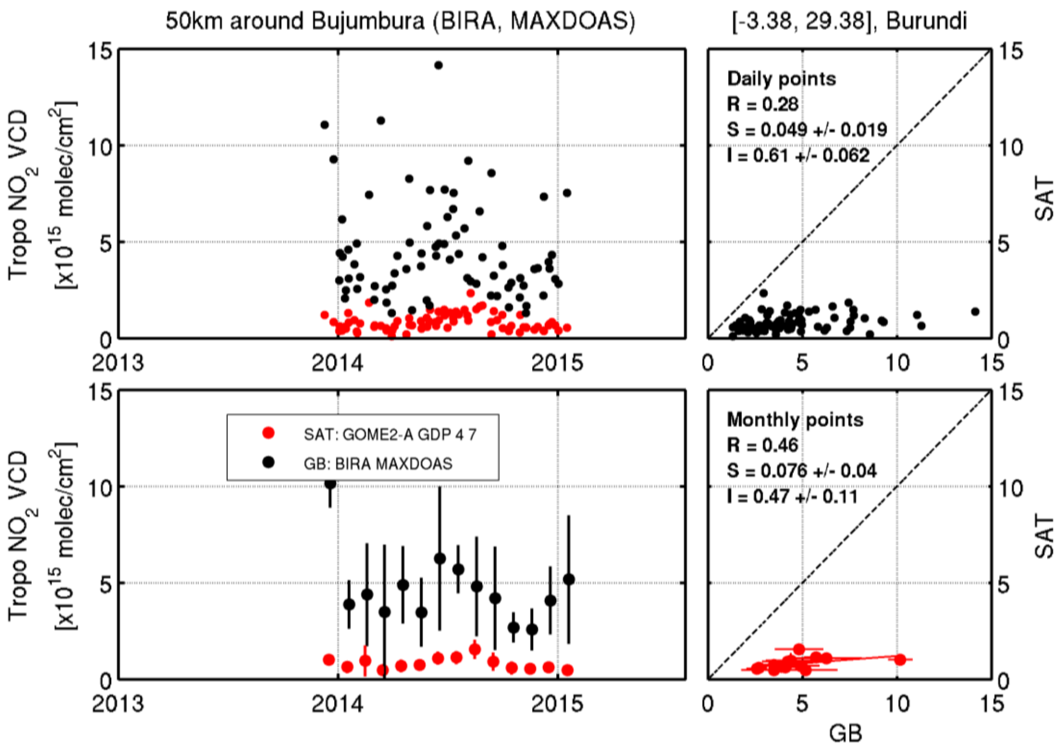

Figure H.1.15a Time series of MAXDOAS and GOME-2 A GDP 4.7 tropopsheric columns above Bujumbura, from Decmber 2013 to January 2015. The first vertical panel presents the daily points and the second the monthly mean values. The right panels present the scatter plot and regression parameters.

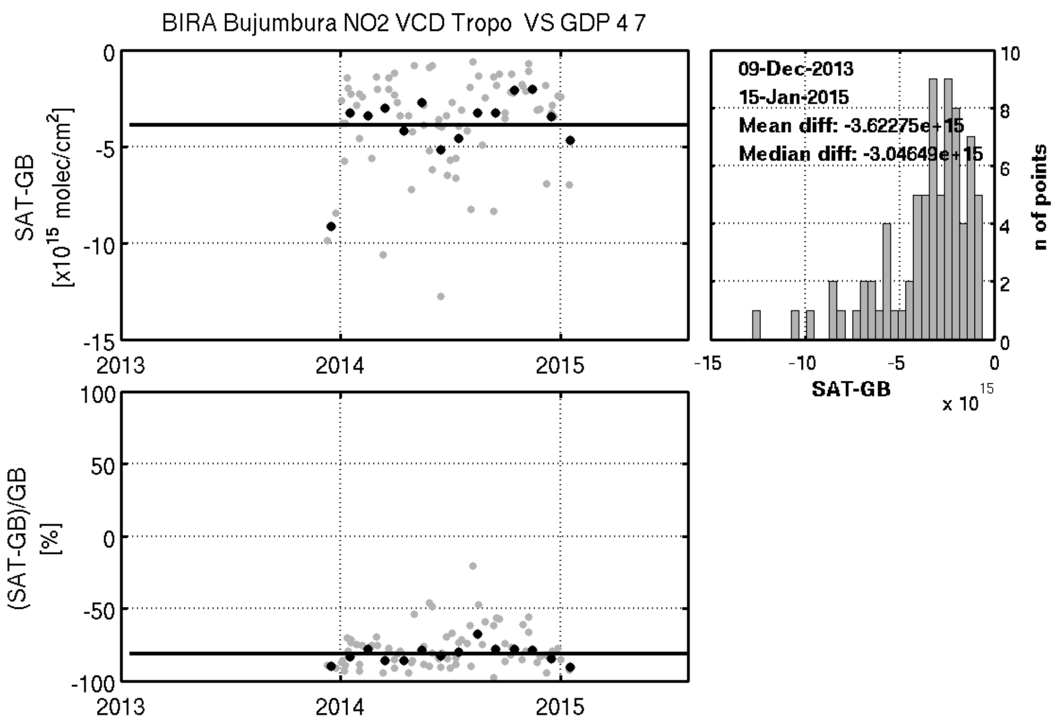

Figure H.1.15b Time series of GOME-2 A GDP 4.7 minus MAXDOAS tropopsheric columns above Bujumbura, from Decmber 2013 to January 2015. The first vertical panel presents the absolute values (daily points in grey and monthly means in black) and the second the relative values. The right panels present the histogram of the absolute differences and the mean and median value.

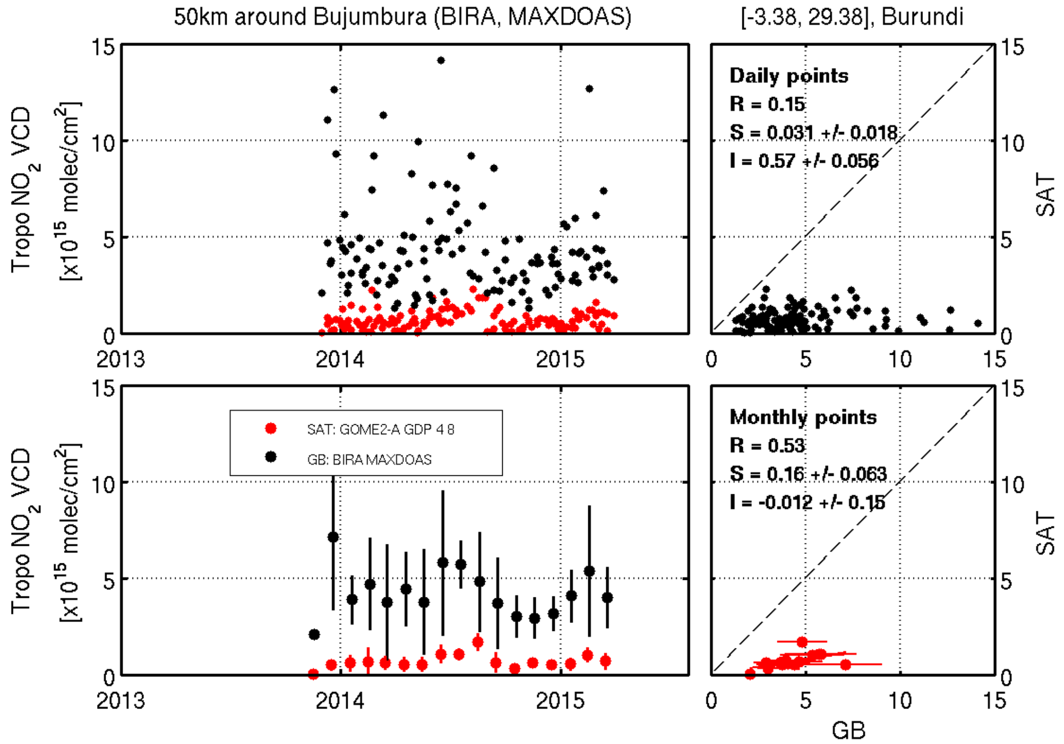

Figure H.1.16a Time series of MAXDOAS and GOME-2 A GDP 4.8 tropopsheric columns above Bujumbura, from Decmber 2013 to January 2015. The first vertical panel presents the daily points and the second the monthly mean values. The right panels present the scatter plot and regression parameters.

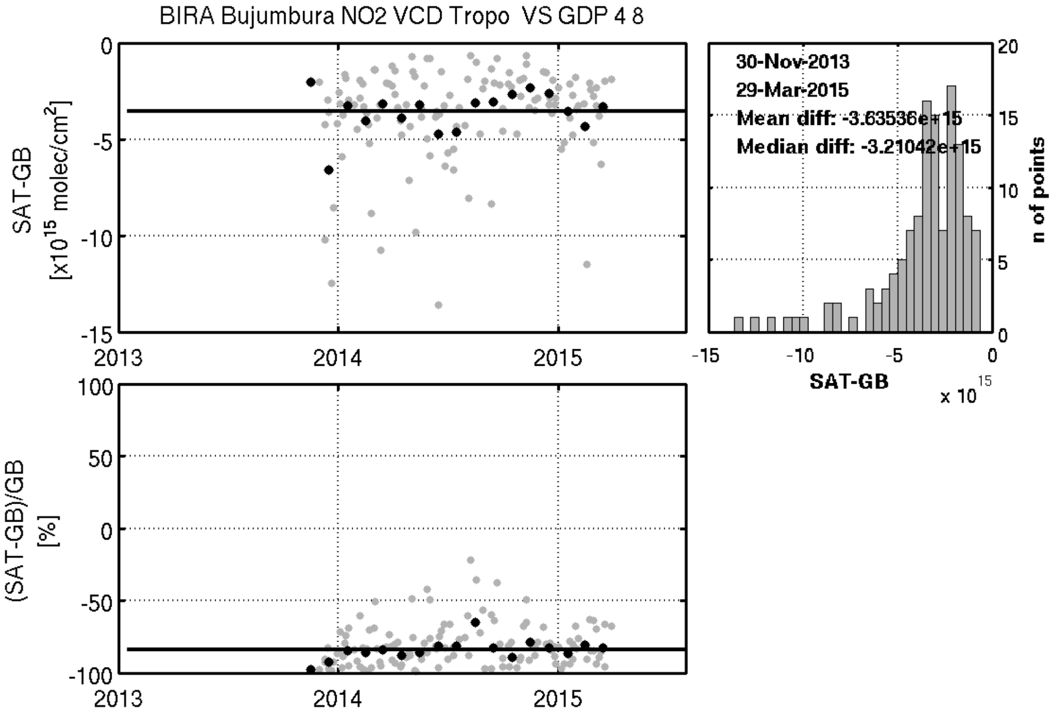

Figure H.1.16b Time series of GOME-2 A GDP 4.8 minus MAXDOAS tropopsheric columns above Bujumbura, from Decmber 2013 to January 2015. The first vertical panel presents the absolute values (daily points in grey and monthly means in black) and the second the relative values. The right panels present the histogram of the absolute differences and the mean and median value.

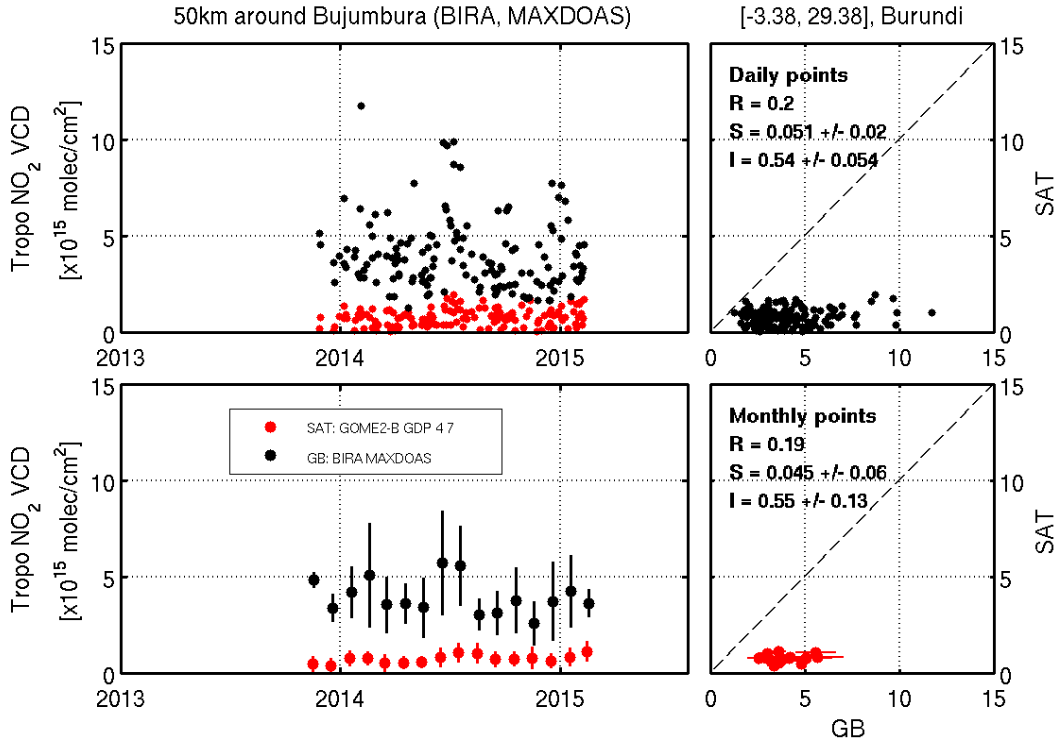

Figure H.1.17a Time series of MAXDOAS and GOME-2 B GDP 4.7 tropopsheric columns above Bujumbura, from Decmber 2013 to January 2015. The first vertical panel presents the daily points and the second the monthly mean values. The right panels present the scatter plot and regression parameters.

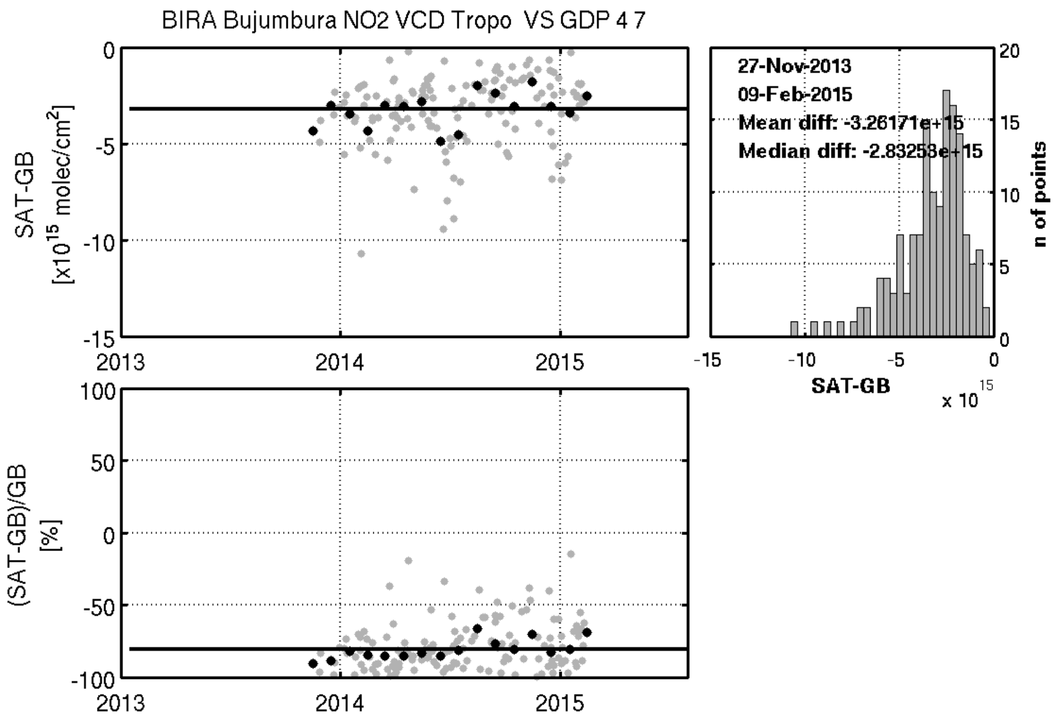

Figure H.1.17b Time series of GOME-2 B GDP 4.7 minus MAXDOAS tropopsheric columns above Bujumbura, from Decmber 2013 to January 2015. The first vertical panel presents the absolute values (daily points in grey and monthly means in black) and the second the relative values. The right panels present the histogram of the absolute differences and the mean and median value.

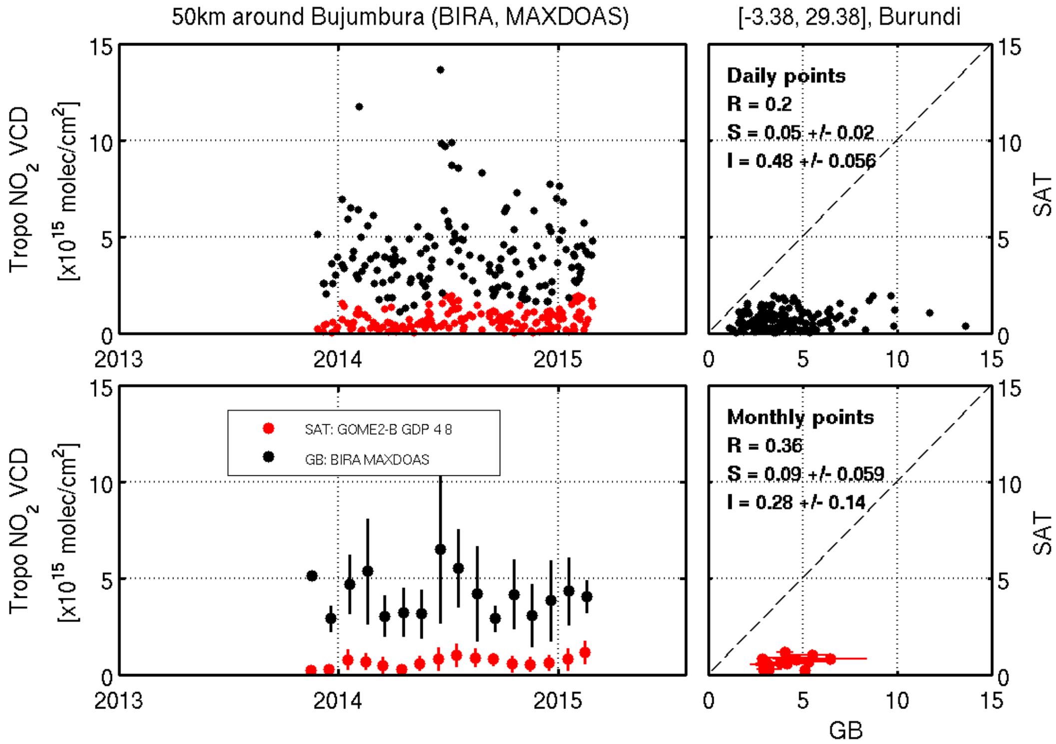

Figure H.1.18a Time series of MAXDOAS and GOME-2 B GDP 4.8 tropopsheric columns above Bujumbura, from Decmber 2013 to January 2015. The first vertical panel presents the daily points and the second the monthly mean values. The right panels present the scatter plot and regression parameters.

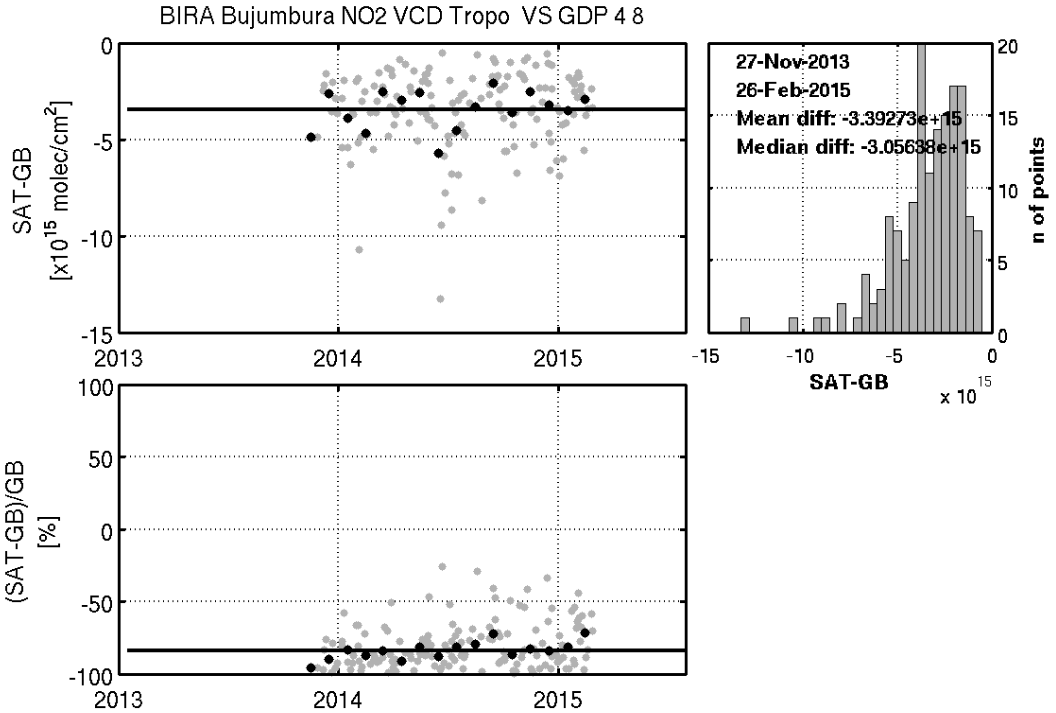

Figure H.1.18b Time series of GOME-2 B GDP 4.8 minus MAXDOAS tropopsheric columns above Bujumbura, from Decmber 2013 to January 2015. The first vertical panel presents the absolute values (daily points in grey and monthly means in black) and the second the relative values. The right panels present the histogram of the absolute differences and the mean and median value.

Table H.1.5 Regression parameters (correlation coefficient R, slope S and intercept I of the regression) and differences (GDP – GB) of the monthly mean comparisons of GOME-2 A and B for both GDP 4.7 and GDP 4.8 at Bujumbura.

Monthly means	MetOp-A GDP 4.7	MetOp-A GDP 4.8	MetOp-B GDP 4.7	MetOp-B GDP 4.8
Regression parameters	R = 0.46 S = 0.07±0.04 I = 0.47±0.11	R = 0.53 S = 0.16±0.06 I = -0.01±0.15	R = 0.19 S = 0.05±0.06 I = 0.55±0.13	R = 0.36 S = 0.09±0.06 I = 0.28±0.14
Differences [molec/cm²]	Mean: -3.6×10^{15} Median: -3×10^{15}	Mean: -3.6×10^{15} Median: -3.2×10^{15}	Mean: -3.26×10^{15} Median: -2.8×10^{15}	Mean: -3.4×10^{15} Median: -3.05×10^{15}

H.2 Total NO_2 comparisons

This section groups the specific figures for BIRA DirectSun stations (Beijing and Xianghe) for GOME-2 NO_2 total data from Metop-A and –B for both GDP 4.7 and GDP 4.8 products. Time-series of daily means, monthly means and corresponding scatter plots are shown in Figures H.2.Xa, while absolute and relative differences and the histogram of the SAT-GB differences are shown in Figures H.2.Xb. An overview table of the result for each specific station is given after the figures.

Beijing

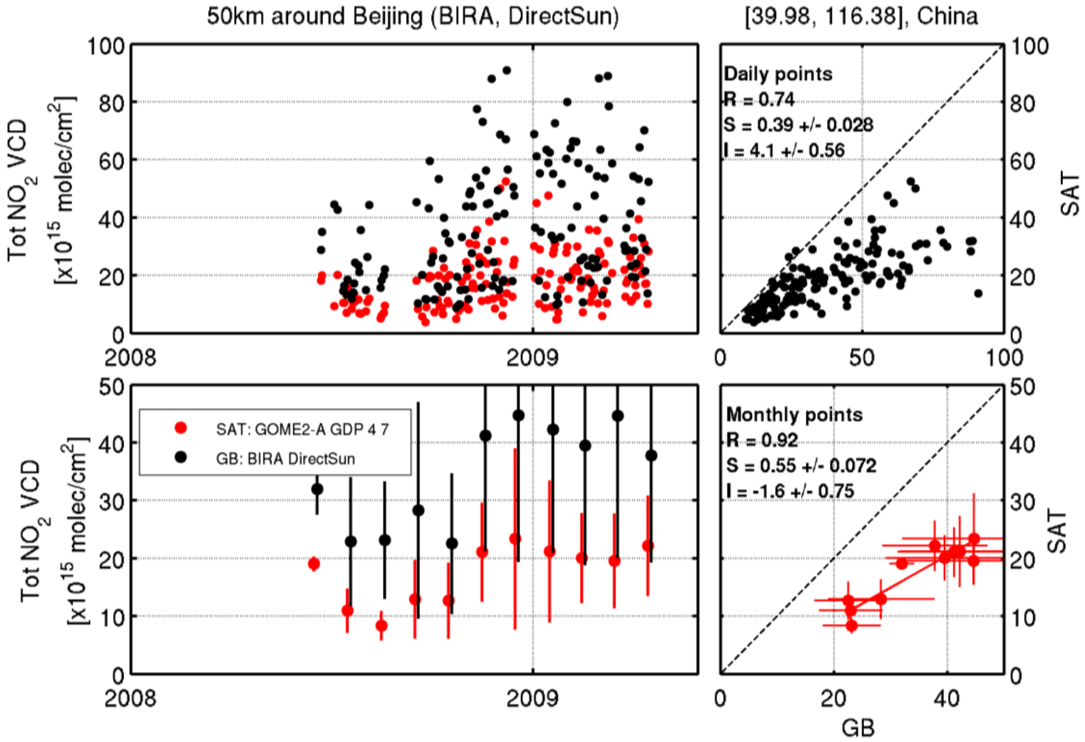

Figure H.2.1a Time series of DirectSun and GOME-2 A GDP 4.7 total columns above Beijing, from June 2008 to April 2009. The first vertical panel presents the daily points and the second the monthly mean values. The right panels present the scatter plot and regression parameters

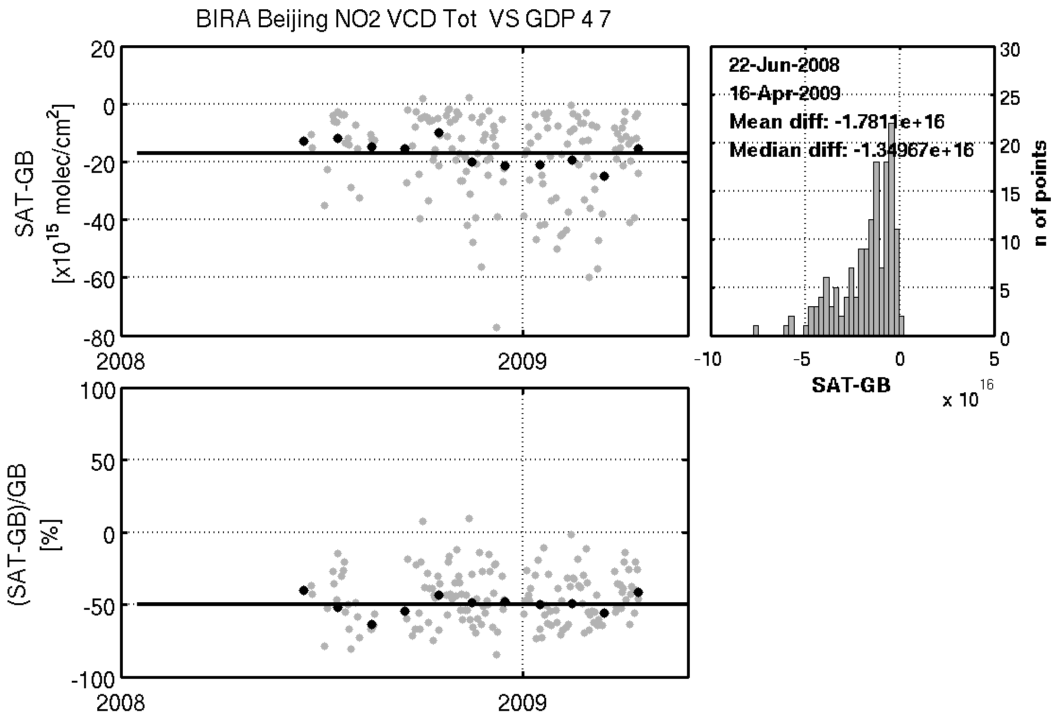

Figure H.2.1b Time series of GOME-2 A GDP 4.7 minus DirectSun total NO_2 columns above Beijing, from June 2008 to April 2009. The first vertical panel presents the absolute values (daily points in grey and monthly means in black) and the second the relative values. The right panels present the histogram of the absolute differences and the mean and median value.

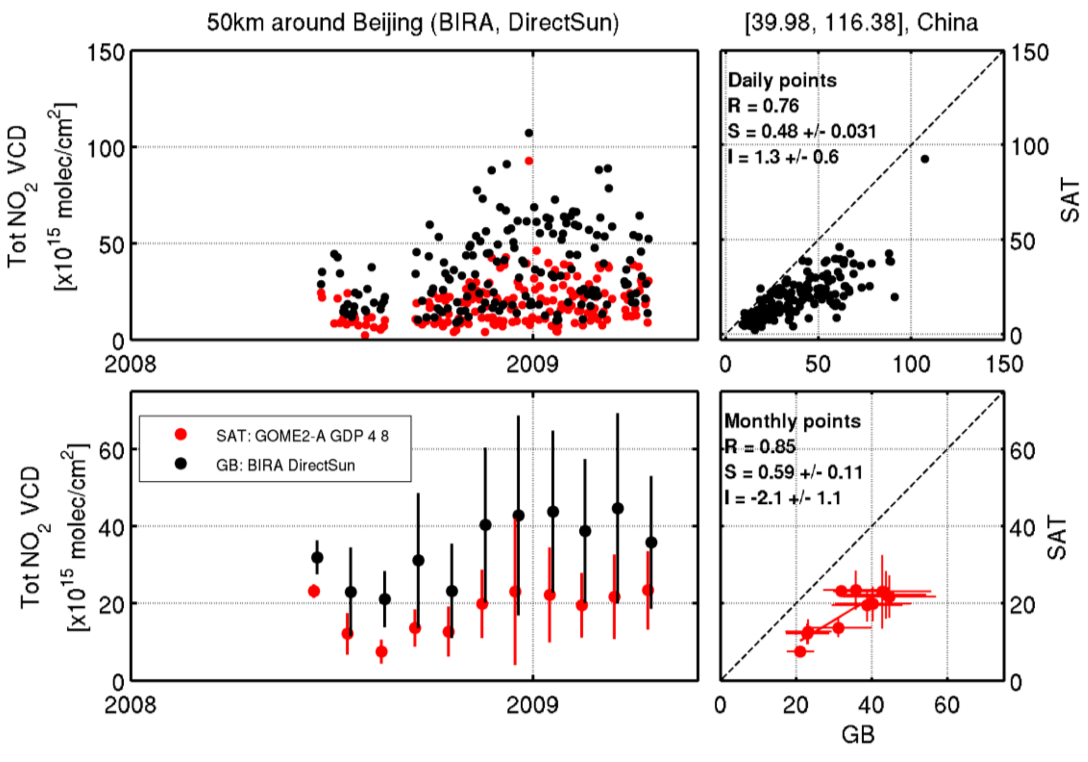

Figure H.2.2a Time series of DirectSun and GOME-2 A GDP 4.8 total columns above Beijing, from June 2008 to April 2009. The first vertical panel presents the daily points and the second the monthly mean values. The right panels present the scatter plot and regression parameters.

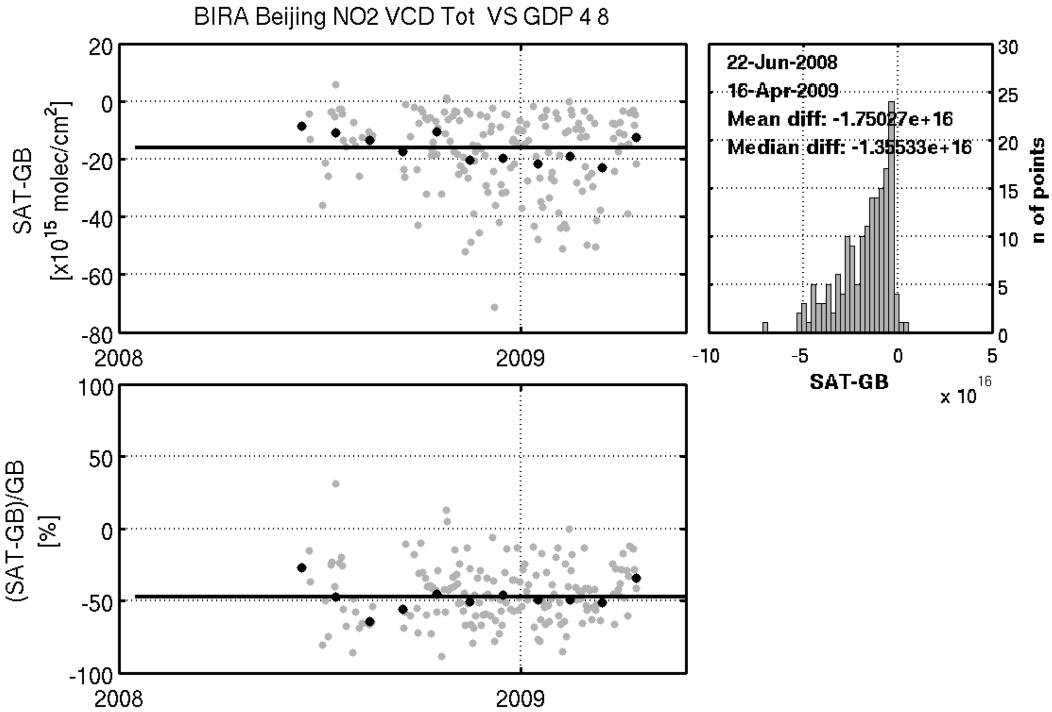

Figure H.2.2b Time series of GOME-2 A GDP 4.8 minus DirectSun total NO_2 columns above Beijing, from June 2008 to April 2009. The first vertical panel presents the absolute values (daily points in grey and monthly means in black) and the second the relative values. The right panels present the histogram of the absolute differences and the mean and median value.

Table H.2.1 Regression parameters (correlation coefficient R, slope S and intercept I of the regression) and differences (GDP – GB) of the monthly mean comparisons of GOME-2 A for both GDP 4.7 and GDP 4.8 at Beijing.

Monthly means	MetOp-A GDP 4.7	MetOp-A GDP 4.8	MetOp-B GDP 4.7	MetOp-B GDP 4.8
Regression parameters	R = 0.92 S = 0.55±0.07 I = -1.6±0.75	R = 0.85 S = 0.59±0.11 I = -2.1±1.1	na	na
Differences [molec/cm²]	Mean: -17.8×10^{15} Median: -13.5×10^{15}	Mean: -17.5×10^{15} Median: -13.5×10^{15}	na	na

Xianghe

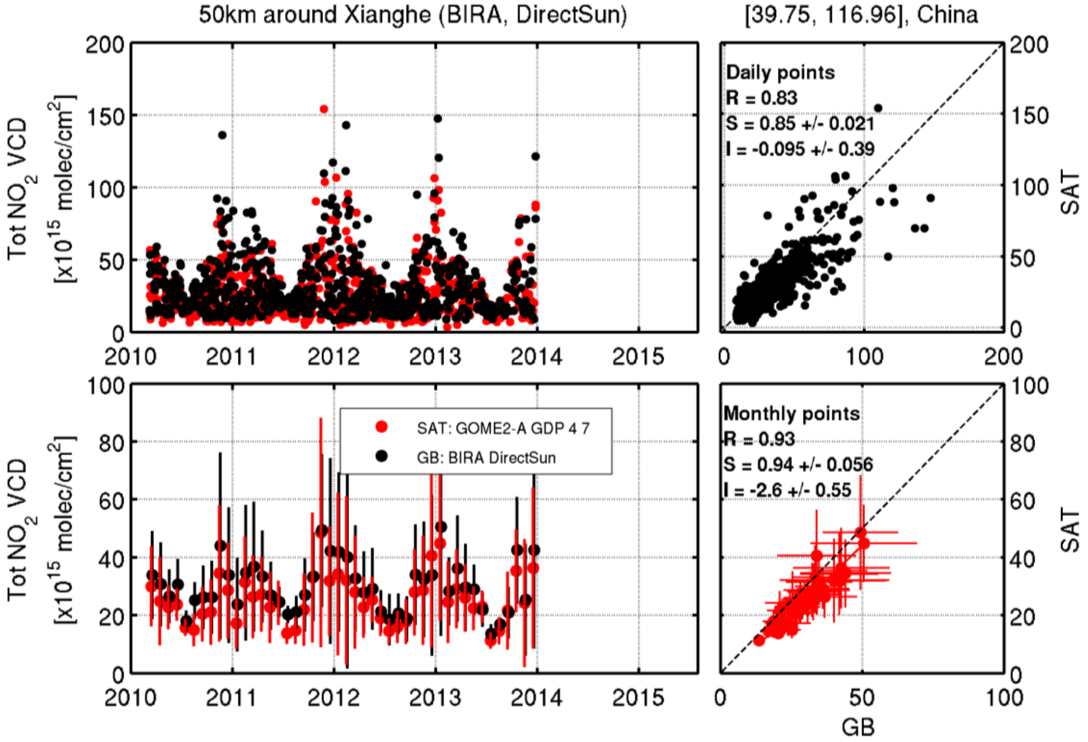

Figure H.2.3a Time series of DirectSun and GOME-2 A GDP 4.7 total columns above Xianghe, from March 2010 to December 2013. The first vertical panel presents the daily points and the second the monthly mean values. The right panels present the scatter plot and regression parameters.

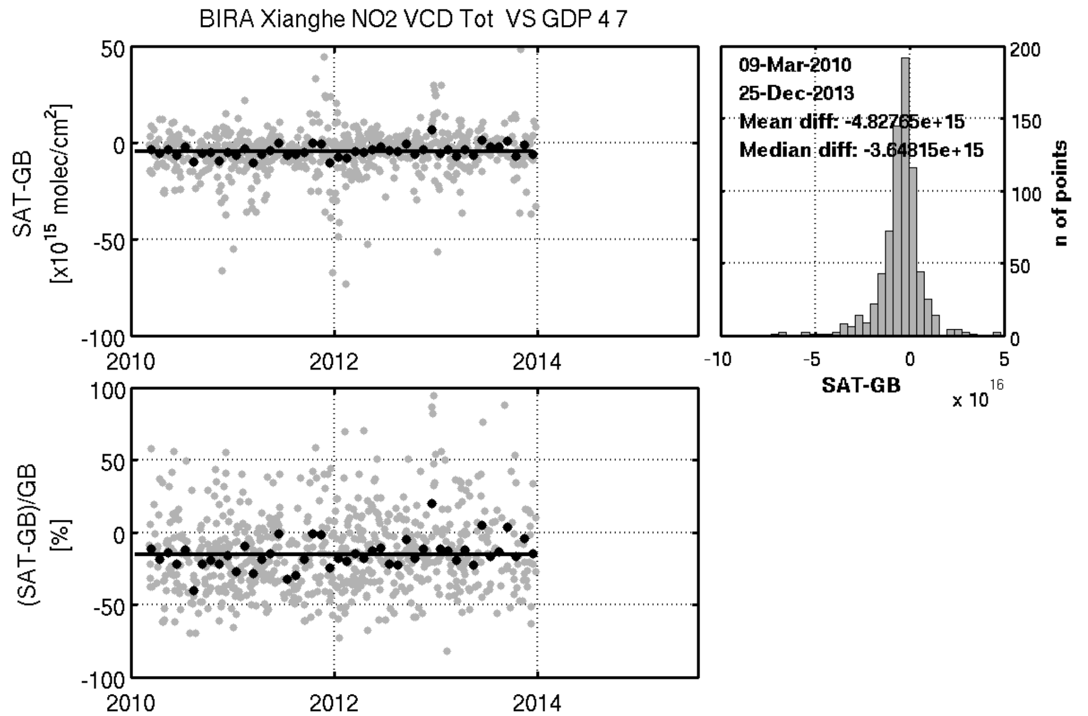

Figure H.2.3b Time series of GOME-2 A GDP 4.7 minus DirectSun total NO_2 columns above Xianghe, from March 2010 to December 2013. The first vertical panel presents the absolute values (daily points in grey and monthly means in black) and the second the relative values. The right panels present the histogram of the absolute differences and the mean and median value.

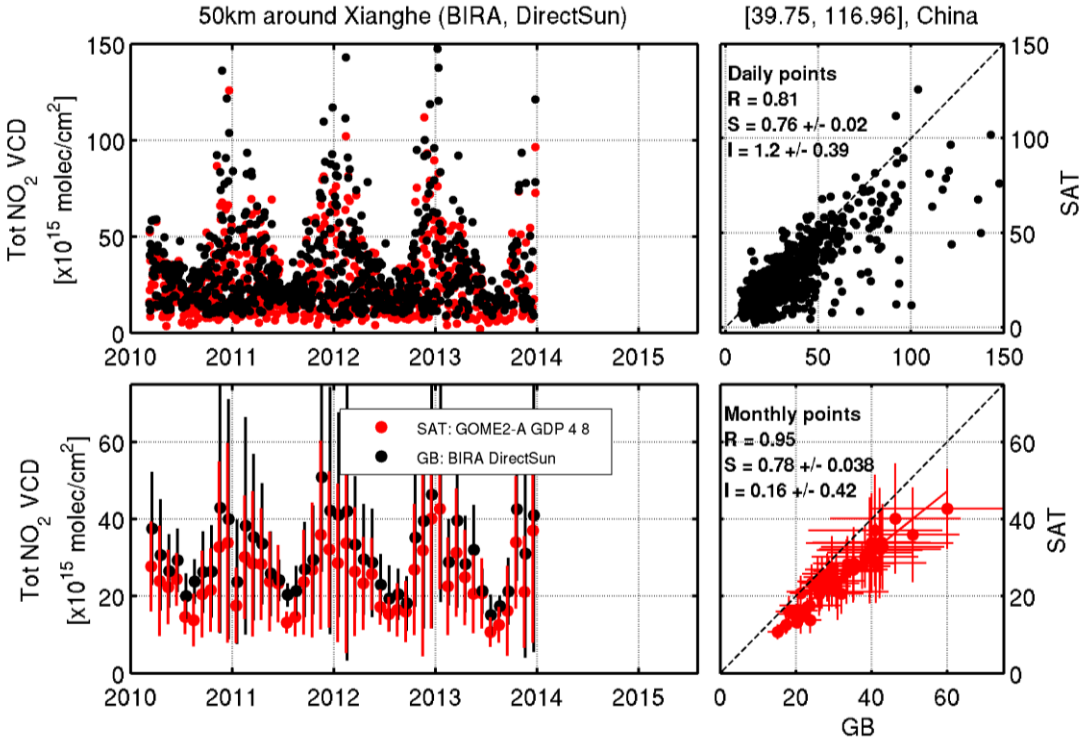

Figure H.2.4a Time series of DirectSun and GOME-2 A GDP 4.8 total columns above Xianghe, from March 2010 to December 2013. The first vertical panel presents the daily points and the second the monthly mean values. The right panels present the scatter plot and regression parameters

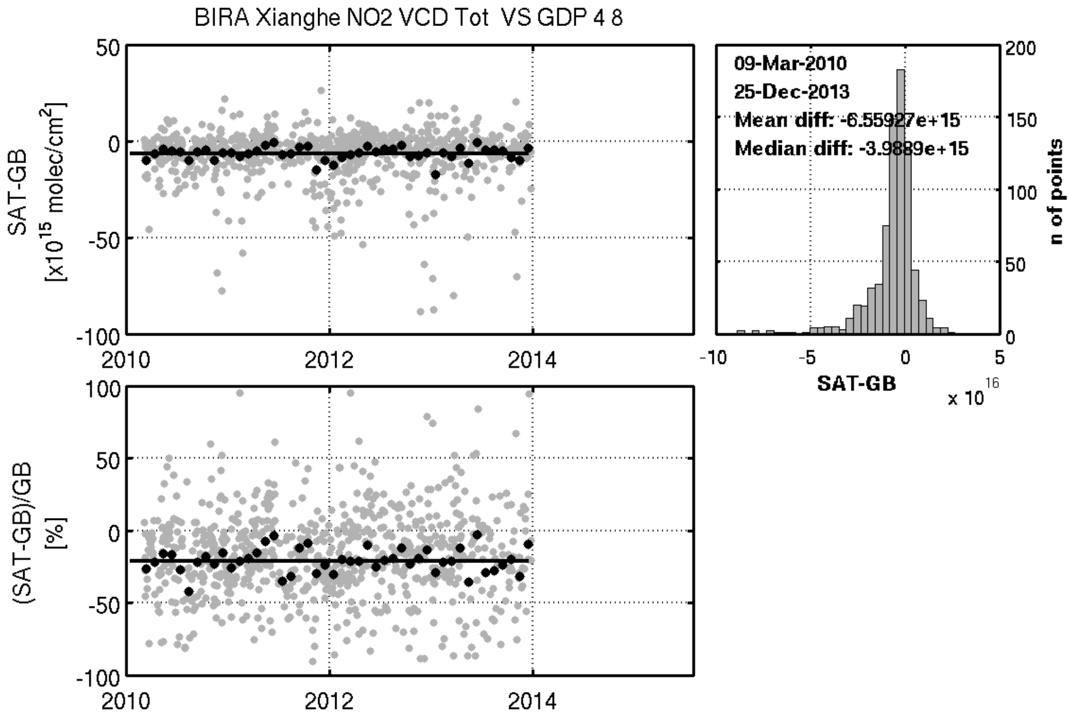

Figure H.2.4b Time series of GOME-2 A GDP 4.8 minus DirectSun total NO_2 columns above Xianghe, from March 2010 to December 2013. The first vertical panel presents the absolute values (daily points in grey and monthly means in black) and the second the relative values. The right panels present the histogram of the absolute differences and the mean and median value.

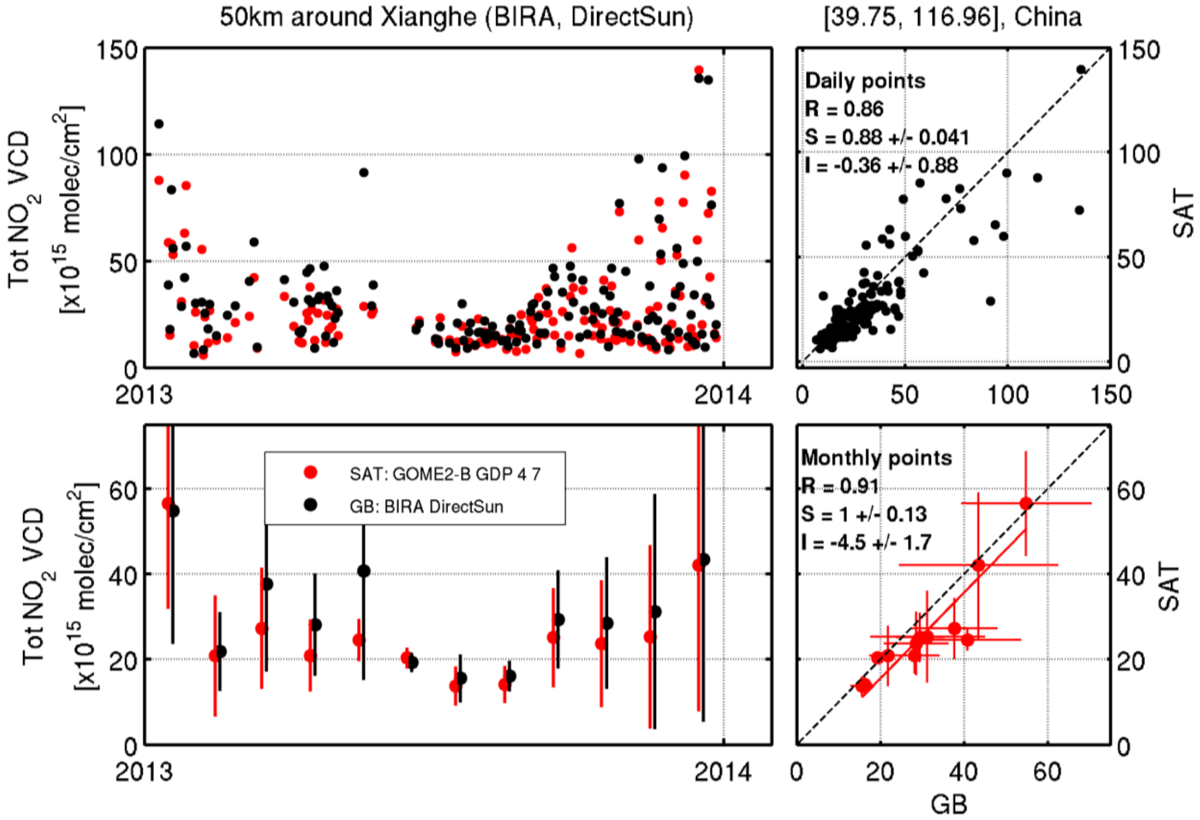

Figure H.2.5a Time series of DirectSun and GOME-2 B GDP 4.7 total columns above Xianghe, from 2013 to December 2013. The first vertical panel presents the daily points and the second the monthly mean values. The right panels present the scatter plot and regression parameters

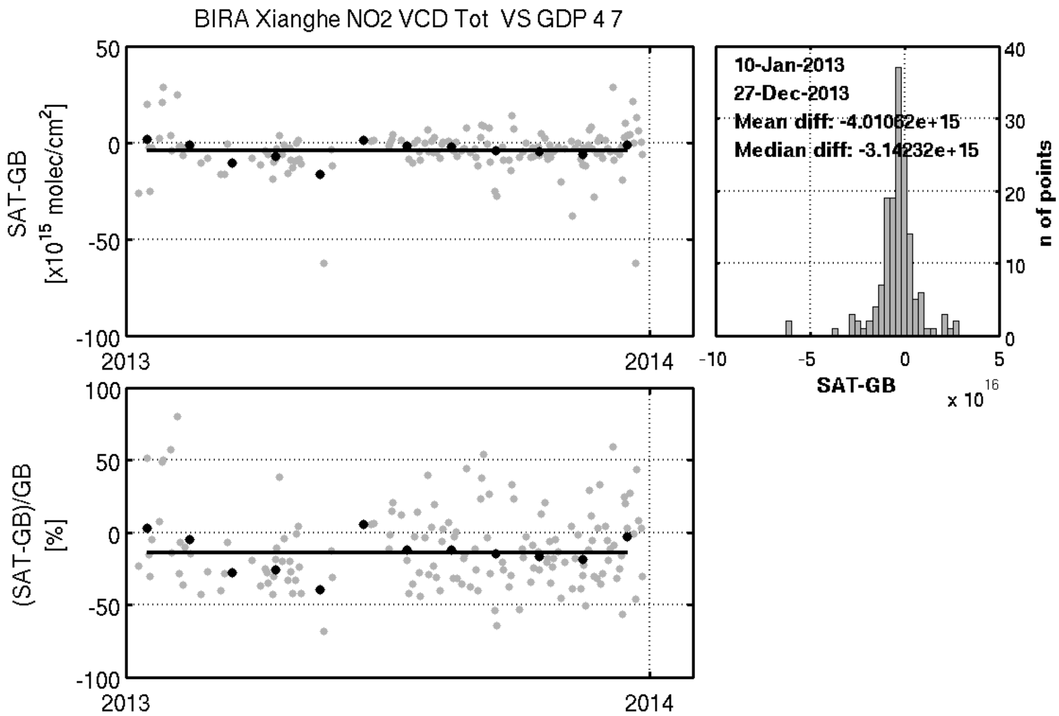

Figure H.2.5b Time series of GOME-2 B GDP 4.7 minus DirectSun total NO_2 columns above Xianghe, from 2013 to December 2013. The first vertical panel presents the absolute values (daily points in grey and monthly means in black) and the second the relative values. The right panels present the histogram of the absolute differences and the mean and median value.

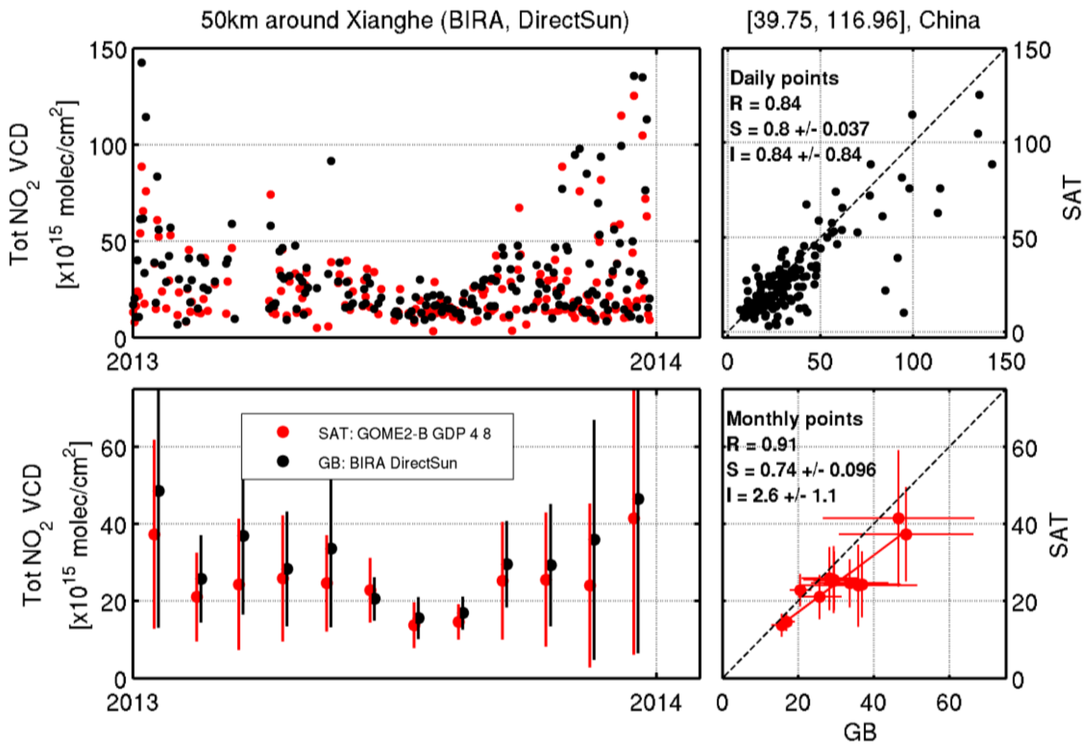

Figure H.2.6a Time series of DirectSun and GOME-2 B GDP 4.8 total columns above Xianghe, from 2013 to December 2013. The first vertical panel presents the daily points and the second the monthly mean values. The right panels present the scatter plot and regression parameters

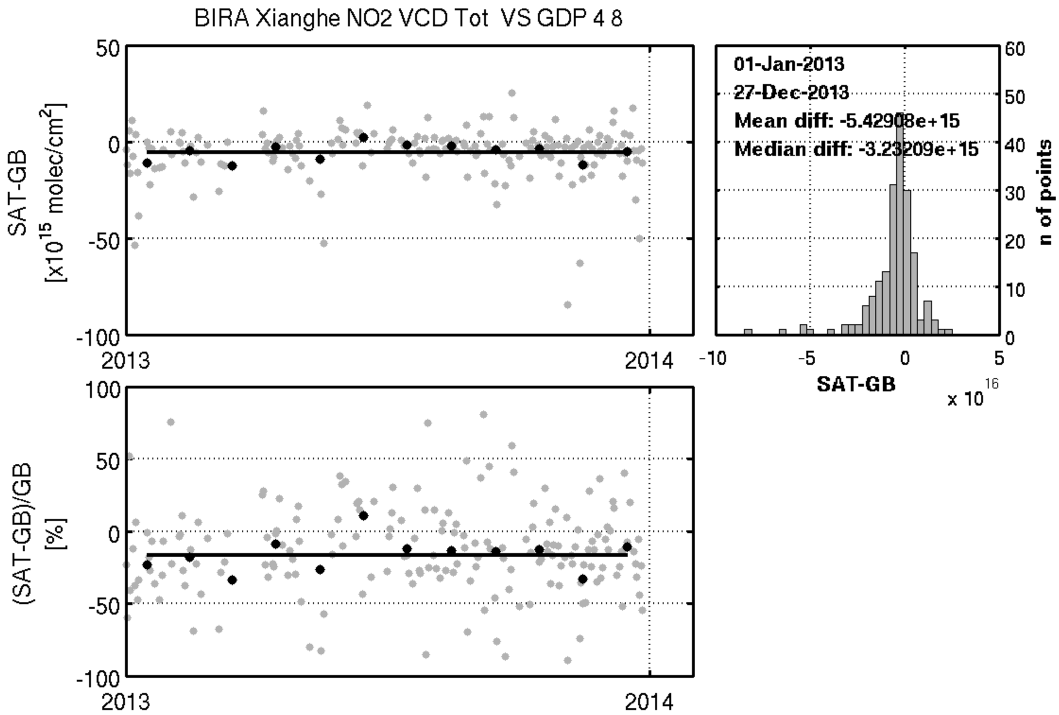

Figure H.2.6b Time series of GOME-2 B GDP 4.8 minus DirectSun total NO_2 columns above Xianghe, from 2013 to December 2013. The first vertical panel presents the absolute values (daily points in grey and monthly means in black) and the second the relative values. The right panels present the histogram of the absolute differences and the mean and median value.

Table H.2.2 Regression parameters (correlation coefficient R, slope S and intercept I of the regression) and differences (GDP – GB) of the monthly mean comparisons of GOME-2 A and B for both GDP 4.7 and GDP 4.8 at Xianghe.

Monthly means	MetOp-A GDP 4.7	MetOp-A GDP 4.8	MetOp-B GDP 4.7	MetOp-B GDP 4.8
Regression parameters	R = 0.93 S = 0.94±0.06 I = -2.6±0.55	R = 0.95 S = 0.78±0.04 I = 0.16±0.42	R = 0.91 S = 1±0.13 I = -4.5±1.7	R = 0.91 S = 0.74±0.09 I = 2.6±1.1
Differences [molec/cm²]	Mean: -4.8×10^{15} Median: -3.65×10^{15}	Mean: -6.6×10^{15} Median: -3.9×10^{15}	Mean: -4.01×10^{15} Median: -3.14×10^{15}	Mean: -5.43×10^{15} Median: -3.2×10^{15}